Aspects of climate change in the Northwest Atlantic off Canada

John W. Loder, Guoqi Han, Peter S. Galbraith, Joël Chassé,
and Augustine van der Baaren (Editors)

Ocean and Ecosystem Sciences Division,
Fisheries and Oceans Canada
Bedford Institute of Oceanography
P.O. Box 1006
Dartmouth, Nova Scotia
Canada B2Y 4A2

2013

Canadian Technical Report of
Fisheries and Aquatic Sciences 3045

Fisheries and Oceans Canada | Pêches et Océans Canada

Canada

Canadian Technical Report of Fisheries and Aquatic Sciences

Technical reports contain scientific and technical information that contributes to existing knowledge but which is not normally appropriate for the primary literature. Technical reports are directed primarily toward a worldwide audience and have an international distribution. No restriction is placed on subject matter and the series reflects the broad interests and policies of Fisheries and Oceans Canada, namely, fisheries and aquatic sciences.

Technical reports may be cited as full publications. The correct citation appears above the abstract of each report. Each report is abstracted in the data base *Aquatic Sciences and Fisheries Abstracts.*

Technical reports are produced regionally but are numbered nationally. Requests for individual reports will be filled by the issuing establishment listed on the front cover and title page.

Numbers 1-456 in this series were issued as Technical Reports of the Fisheries Research Board of Canada. Numbers 457-714 were issued as Department of the Environment, Fisheries and Marine Service, Research and Development Directorate Technical Reports. Numbera 715-924 were issued as Department of Fisheries and Environment, Fisheries and Marine Service Technical Reports. The current series name was changed with report number 925.

Rapport technique canadien des sciences halieutiques et aquatiques

Les rapports techniques contiennent des renseignements scientifiques et techniques qui constituent une contribution aux connaissances actuelles, mais qui ne sont pas normalement appropriés pour la publication dans un journal scientifique. Les rapports techniques sont destinés essentiellement à un public international et ils sont distribués à cet échelon. II n'y a aucune restriction quant au sujet; de fait, la série reflète la vaste gamme des intérêts et des politiques de Pêches et Océans Canada, c'est-à-dire les sciences halieutiques et aquatiques.

Les rapports techniques peuvent être cités comme des publications à part entière. Le titre exact figure au-dessus du résumé de chaque rapport. Les rapports techniques sont résumés dans la base de données *Résumés des sciences aquatiques et halieutiques.*

Les rapports techniques sont produits à l'échelon régional, mais numérotés à l'échelon national. Les demandes de rapports seront satisfaites par l'établissement auteur dont le nom figure sur la couverture et la page du titre.

Les numéros 1 à 456 de cette série ont été publiés à titre de Rapports techniques de l'Office des recherches sur les pêcheries du Canada. Les numéros 457 à 714 sont parus à titre de Rapports techniques de la Direction générale de la recherche et du développement, Service des pêches et de la mer, ministère de l'Environnement. Les numéros 715 à 924 ont été publiés à titre de Rapports techniques du Service des pêches et de la mer, ministère des Pêches et de l'Environnement. Le nom actuel de la série a été établi lors de la parution du numéro 925.

Canadian Technical Report of
Fisheries and Aquatic Sciences 3045

2013

Aspects of climate change in the Northwest Atlantic off Canada

by

John W. Loder [1], Guoqi Han[2], Peter S. Galbraith[3], Joël Chassé[4] and Augustine van der Baaren[5] (Editors)

Ecosystems and Oceans Science Sector
Fisheries and Oceans Canada

---

[1] **Bedford Institute of Oceanography**
P. O. Box 1006, Dartmouth, Nova Scotia B2Y 4A2
John.Loder@dfo-mpo.gc.ca

[2] **Northwest Atlantic Fisheries Centre**
P.O. Box 5667, St. John's, Newfoundland and Labrador A1C 5X1

[3] **Institut Maurice Lamontagne**
850 Route de la Mer, C. P. 1000, Mont-Joli, Québec G5H 3Z4

[4] **Gulf Fisheries Centre**
343 University Avenue, P.O. Box 5030, Moncton, New Brunswick E1C 9B6

[5] **8 Toye Lane, Wolfville, Nova Scotia B4P 2C8**

Cat. No. Fs 97-6/3045E ISSN 0706-6457 (print version)

Cat. No. Fs 97-6/3045E-PDF ISSN 1488-5379 (on-line version)

Correct Citation for this publication:

Loder, J.W., G. Han, P.S. Galbraith, J. Chassé, and A. van der Baaren (Eds.). 2013. Aspects of climate change in the Northwest Atlantic off Canada. Can. Tech. Rep. Fish. Aquat. Sci. 3045: x + 190 p.

TABLE OF CONTENTS

Abstract

Loder, J.W., G. Han, P.S. Galbraith, J. Chassé, and A. van der Baaren. (Eds.). 2013. Aspects of climate change in the Northwest Atlantic off Canada. Can. Tech. Rep. Fish. Aquat. Sci. 3045: x + 190 p.

This report is a collection of thirteen technical articles on observed trends and variability, and projected future changes, in different physical and chemical climate variables of importance to the activities and responsibilities of Fisheries and Oceans Canada (DFO) in the Atlantic Large Aquatic Basin (LAB). They were prepared as part of DFO's Aquatic Climate Change Adaptation Services Program (ACCASP). The articles deal with a wide range of important aspects of the coupled atmosphere-ice-aquatic/ocean climate system affecting the Atlantic LAB. Aspects covered include air temperature and wind, river temperature, sea ice, and key physical and chemical ocean variables. The ocean variables include surface and subsurface ocean temperature and salinity, upper-ocean stratification and mixed-layer depths, nutrients, Labrador Current transport, and mean and extreme coastal sea level. The thirteen articles, together with ten complementary stand-alone technical reports also prepared as part of ACCASP, provide background material to a separate, more synthetic summary of climate change trends and projections, for input to a climate change impacts risk assessment for the Atlantic LAB.

Résumé

Loder, J.W., G. Han, P.S. Galbraith, J. Chassé, and A. van der Baaren, (Eds.). 2013. Aspects des changements climatiques dans l'Atlantique Nord-Ouest au large du Canada. Can. Tech. Rep. Fish. Aquat. Sci.. 3045: x + 190 p.

Le présent rapport regroupe treize articles techniques sur la variabilité et les tendances observées ainsi que les changements prévus dans différentes variables physiques et chimiques du climat qui sont importantes pour les activités et les responsabilités de Pêches et Océans Canada dans le grand bassin aquatique de l'Atlantique. Ils ont été préparés dans le cadre du Programme des services d'adaptation aux changements climatiques en milieu aquatique (PSACCMA) de Pêches et Océans Canada. Les articles traitent d'un large éventail d'aspects importants du système climatique couplé atmosphère-glace-eau/océans touchant le grand bassin aquatique de l'Atlantique. Les aspects traités comprennent la température de l'air et le vent, la température des rivières, la glace de mer et les principales variables physiques et chimiques des océans. Les variables des océans comprennent la température et la salinité à la surface et sous la surface de l'océan, la stratification de la couche supérieure de l'océan et la profondeur de la couche de mélange, les nutriments, le transport du courant du Labrador ainsi que les niveaux moyens et extrêmes de la mer sur le littoral. Les treize articles, ainsi que les dix rapports techniques complémentaires distincts aussi préparés dans le cadre du PSACCMA, fournissent des documents de référence pour un sommaire séparé des tendances et des prévisions relatives aux changements climatiques aux fins d'intégration à une évaluation des risques des répercussions des changements climatiques pour le grand bassin aquatique de l'Atlantique.

Preface

This report comprises thirteen independent chapters (technical articles) on different aspects of observed and projected climate change affecting the aquatic and marine environment of Atlantic Canada. They were prepared as part of the "trends and projections" inputs to a climate change impacts risk assessment carried out by Fisheries and Oceans Canada (DFO) for the Atlantic Large Aquatic Basin (LAB), under its Aquatic Climate Change Adaptation Services Program (ACCASP). The articles are complementary to ten stand-alone technical reports (listed under References at the end of this preface) on related aspects of observed and projected climate change relevant to the Atlantic LAB, also prepared under ACCASP. These twenty-three contributions, focused on physical and chemical variables, provide a major portion of the background material for the trends and projections information provided to a companion report on climate change impacts, vulnerabilities and opportunities in the Atlantic LAB (Shackell *et al.*, 2013), and to DFO's risk assessment of climate change impacts in the LAB (DFO, 2013). A more synthetic summary report on physical and chemical climate change trends and projections for the Atlantic LAB, drawing on these contributions and the wider literature, is also being published (Loder *et al.*, 2013b).

The physical and chemical climate of the Atlantic LAB is affected by coupled atmosphere-ice aquatic/ocean interactions extending from Baffin Bay in the north to the Gulf of Maine in the south, and across the Atlantic Canadian shelf and slope from the offshore Northwest (NW) Atlantic to coastal watersheds. The chapters in this report, and the companion stand-alone reports, cover a mix of spatial scales ranging from the larger-scale atmospheric setting of the Atlantic LAB, to distinct oceanographic regions such as the Gulf of St. Lawrence and Scotian Shelf, to sub-regional features such as rivers and the St. Lawrence Estuary.

Nine of the chapters and reports describe observed variability in air temperature, sea ice, ocean temperature and salinity, and related variables such as stratification. Galbraith and Larouche (2013; Ch. 1) discuss the relation of trends in air temperature and sea surface temperature (SST) over the Atlantic Canadian shelf, while Thistle and Caissie (2013) discuss trends in air temperature, precipitation and streamflow in eastern Canada, and Peterson and Pettipas (2013) discuss the relation of trends in air temperature and sea ice in eastern Canada. Han *et al.* (2013b; Ch. 2) present trends in upper-ocean (≤700 m) temperature, salinity, stratification and mixed-layer depth in the off-shelf NW Atlantic, and Hebert (2013a, 2013b; Chs. 3 and 4) presents trends in near-surface (≤50 m) temperature, salinity and stratification off Atlantic Canada and over the Scotian Shelf, while Loder *et al.* (2013c) describe trends and variability in SST across the NW Atlantic. Galbraith *et al.* (2013; Ch. 5) describe trends and variability in subsurface temperature on the Atlantic Canadian shelf, and relations with air temperature and sea ice, while Han *et al.* (2013c; Ch. 6) describe the relations with air temperature of surface and subsurface temperature, sea ice extent, and iceberg numbers on the Newfoundland and Labrador Shelf. Both Galbraith and Larouche (2013; Ch.1) and Galbraith *et al.* (2013; Ch. 5) use their statistical relations with air temperature to discuss future changes in ice and/or ocean variables, while Han *et al.* (2013c; Ch. 6) use their statistical relationships and model projections of air temperature changes to provide projected changes in regional sea ice and ocean temperature.

Another six of the chapters and reports describe the observed variability of other important aspects of the climate system in the Atlantic LAB. Han *et al.* (2013a; Ch. 7) describe recent variability in the transport of the Labrador Current and its apparent relation to atmospheric forcing. Two chapters discuss variability in coastal sea level in the Atlantic LAB. Xu *et al.* (2013; Ch. 8) describe the seasonal variation of sea level, long-term changes in mean sea level, and changes in extreme sea level (storm surges) in the Gulf of St. Lawrence and its vicinity, while Han *et al.* (2013d; Ch. 9) examine mean sea level trends over a broader domain and provide future projections of mean sea level along the Canadian east coast using observations and results from climate models. Pepin *et al.* (2013; Ch. 10) describe trends and variability in nutrient concentrations over the NW Atlantic shelf and slope from the Gulf of Maine to the Labrador Sea, while Caissie (2013; Ch. 13) shows the relation between air temperature and summertime temperature in New Brunswick rivers, and points out the implications of increasing river temperature for Atlantic salmon. Hamilton and Wu (2013) describe trends and variability in the physical environment of Baffin Bay, relevant to both the Arctic and Atlantic LABs.

The final group of eight chapters and reports present information on projected changes in physical and chemical variables based on climate model simulations. Three of these present results from the downscaling of global General Circulation Models (GCMs) used in the Fourth Assessment (AR4) of the Intergovernmental Panel on Climate Change (IPCC), using Regional Climate Models (RCMs). Loder *et al.* (2013a; Ch. 11) discuss projected air temperature changes for Canada from eight model combinations from the North American Regional Climate Change Assessment Program (NARCCAP). Brickman *et al.* (2013; Ch. 12) present "emergence times" and other statistics for projected air temperature and wind from a version of the Canadian RCM (CRCM), while Chassé *et al.* (2013b) present ice-ocean projections for the Gulf of St. Lawrence from downscaling a CRCM+GCM projection using a regional ice-ocean model. Five reports describe projections from GCM simulations for the IPCC's Fifth Assessment Report (AR5). Chassé *et al.* (2013b) present projections of precipitation, evaporation and freshwater flux over Canada from six GCMs. Loder and van der Baaren (2013) present projections of air temperature, sea ice and selected physical ocean variables for the NW Atlantic from six Earth System Models (ESMs), while Lavoie *et al.* (2013a, 2013b) present projections of physical and chemical ocean variables for four areas of the NW Atlantic and Eastern Arctic from the same ESMs. Lambert *et al.* (2013) present projections of river run-off in Atlantic Canada from two RCMs using AR4 GCM forcing and three AR5 GCMs.

The preparation of this collections report and the stand-alone reports has involved a coordinated effort among the four DFO Regions (Gulf, Maritimes, Newfoundland and Labrador, Quebec) in the Atlantic LAB, in the planning, development and peer review of the articles and reports. We thank the various authors for their contributions, the reviewers for their valuable comments, the ACCASP leaders and ocean science managers of the four Atlantic Regions for their support, and the many others who have contributed to the overall effort.

A recommendation for the full citation of each chapter is provided on its first page.

- John Loder, Guoqi Han, Peter Galbraith, and Joël Chassé *26 November 2013*

References:

Brickman, D., B. DeTracey, Z. Long, L. Guo, and W. Perrie. 2013. Analyses of CRCM output for emergence times of climate changes in air temperature and wind speed. Ch. 12 (p. 171-182) *In:* This report.

Caissie, D. 2013. Impact of climate change on water temperatures for selected rivers in New Brunswick and potential implications on Atlantic salmon. Ch. 13 (p.183-190) *In:* This report.

Chassé, J., N. Lambert and D. Lavoie. 2013a. Precipitation, evaporation and freshwater flux over Canada from six Global Climate Models. Can. Tech. Rep. Hydrogr. Ocean Sci. 287: viii + 47 p. http://www.dfo-mpo.gc.ca/Library/349263.pdf

Chassé, J., W. Perrie, Z. Long, D. Brickman, L. Guo and N. Lambert. 2103b. Regional atmosphere-ocean-ice climate downscaling results for the Gulf of St. Lawrence using the DFO Regional Climate Downscaling System. Can. Tech. Rep. Hydrogr. Ocean Sci. (under revision)

DFO (2013). Risk-based assessment of climate change impacts and risks on the biological resources and infrastructure within Fisheries and Oceans Canada's mandate – Atlantic Large Aquatic Basin. Fisheries and Oceans Canada, Can. Sci. Sec. Sci. Resp. 2012/044. 40 p. http://www.dfo-mpo.gc.ca/csas-sccs/Publications/ScR-RS/2012/2012_044-eng.html

Galbraith, P. S. and P.. Larouche. 2013. Trends and variability in eastern Canada sea-surface ocean temperatures. Ch. 1 (p. 1-18) *In:* This report.

Galbraith, P. S., D. Hebert, E. Colbourne, and R. Pettipas. 2013. Trends and variability in eastern Canada sub-surface ocean temperatures and implications for sea-ice. Ch. 5 (p. 57-72) *In*: This report.

Hamilton, J. and Y. Wu. 2013. Synopsis and trends in the physical environment of Baffin Bay and Davis Strait. Can. Tech. Rep. Hydrogr. Ocean Sci. 282: vi + 39 p. http://www.dfo-mpo.gc.ca/Library/348087.pdf

Han, G., N. Chen and Z. Ma. 2013a. Interannual-to-decadal variations of the Labrador Current. Ch.7 (p. 85-94) *In:* This report.

Han, G., Z. Ma, and H. Bao. 2013b. Trends of temperature, salinity, stratification and mixed-layer depth in the Northwest Atlantic. Ch. 2 (p. 19-32) *In:* This report.

Han, G. E. Colbourne, P. Pepin, and R. Tang. 2013c. Statistical projections of physical oceanographic variables over the Newfoundland and Labrador Shelf. Ch. 6 (p. 73-84) *In:* This report.

Han, G., Z. Ma, J. Loder, H. Bao and A. van der Baaren. 2013d. Mean sea level trends in the Northwest Atlantic: Historical estimates and future projections. Ch. 9 (p. 113-126) *In:* This report.

Hebert, D. 2013a. Trends in temperature, salinity, density and stratification for different regions in the Atlantic Canadian shelf. Ch. 3 (p. 33-42) *In:* This report.

Hebert, D. 2013b. Trends in temperature, salinity, density and stratification in the upper ocean for the Scotian Shelf. Ch. 4 (p. 43-56) *In:* This report.

Lambert, N., J. Chassé, W. Perrie, Z. Long, L. Guo and J. Morrison. 2013. Projection of future river runoffs in Eastern Atlantic Canada from Global and Regional climate models. Can. Tech. Rep. Hydrogr. Ocean Sci. 288: viii+34 p. http://www.dfo-mpo.gc.ca/Library/349262.pdf

Lavoie, D., N. Lambert. S. ben Mustapha and A. van der Baaren. 2013a. Projections of future physical and biogeochemical conditions in the Northwest Atlantic from CMIP5 Global Climate Models. Can. Tech. Rep. Hydrog. Ocean Sci. 285: xiv + 156 p. http://www.dfo-mpo.gc.ca/Library/349066.pdf

Lavoie, D., N. Lambert and A. van der Baaren. 2013b. Projections of future physical and biogeochemical conditions in Hudson and Baffin Bays from CMIP5 Global Climate Models. Can. Tech. Rep. Hydrog. Ocean Sci. 289: xiii + 129 p. http://www.dfo-mpo.gc.ca/library/349552.pdf

Loder, J.W. and A. van der Baaren. 2013. Climate change projections for the Northwest Atlantic from six CMIP5 Earth System Models. Can. Tech. Rep. Hydrogr. Ocean Sci. 286: xiv + 112 p. http://www.dfo-mpo.gc.ca/library/349550.pdf

Loder, J.W., Z. Wang and J. Morrison. 2013a. Projected air temperature changes for Canada from eight NARCCAP model combinations. Ch. 11 (p. 151-172) *In:* This report.

Loder, J.W., J. Chassé, P. Galbraith, G. Han, D. Lavoie and others. 2013b. Summary of climate change trends and projections for the Atlantic Large Aquatic Basin off Canada. Can. Tech. Rep. Fish. Aquat. Sci. 3051 (under revision)

Loder, J.W., Z. Wang, A. van der Baaren and R. Pettipas. 2013c. Trends and variability of sea surface temperature (SST) in the North Atlantic from the HadISST, ERSST and COBE datasets. Can. Tech. Rep. Hydrogr. Ocean Sci. 292: viii + 36 p. http://www.dfo-mpo.gc.ca/Library/350066.pdf

Pepin, P., G.L. Maillet, D. Lavoie and C. Johnson. 2013. Temporal trends in nutrient concentrations in the northwest Atlantic basin. Ch. 10 (p. 127-150) *In:* This report.

Peterson, I.K. and R. Pettipas. 2013. Trends in air temperature and sea ice in the Atlantic Large Aquatic Basin and adjoining areas. Can. Tech. Rep. Hydrogr. Ocean Sci. 290: v + 59 p. http://www.dfo-mpo.gc.ca/Library/350061.pdf

Thistle, M.E. and Caissie, D. 2013. Trends in air temperature, total precipitation and streamflow characteristics in eastern Canada. Can. Tech. Rep. Fish. Aquat. Sci. 3018: xi + 97 p. http://www.dfo-mpo.gc.ca/Library/347639.pdf

Shackell, N.L., B.J.W. Greenan, P. Pepin and A. Warburton. (Eds.) 2013. Climate change impacts, vulnerabilities and opportunities analysis of the marine Atlantic Basin. Can. Man. Rep. Fish. Aquat. Sci. 3012: iv + 345 p.

Xu, Z., D. Lefaivre and M. Beaulieu. 2013. Sea levels and storm surges in the Gulf of St. Lawrence and its vicinity. Ch. 8 (p. 95-112) *In:* This report.

1 Trends and variability in air and sea surface temperatures in eastern Canada

Peter S. Galbraith * and Pierre Larouche

Fisheries and Oceans Canada, Maurice Lamontagne Institute
P.O. Box 1000, Mont-Joli, Québec G5H 3Z4

* Correspondence: Peter.Galbraith@dfo-mpo.gc.ca

Suggested Citation:

Galbraith, P.S. and P. Larouche. 2013. Trends and variability in eastern Canada sea-surface temperatures. Ch. 1 (p. 1-18) *In:* Aspects of climate change in the Northwest Atlantic off Canada [Loder, J.W., G. Han, P.S. Galbraith, J. Chassé and A. van der Baaren (Eds.)]. Can. Tech. Rep. Fish. Aquat. Sci. 3045: x + 190 p.

Abstract

This study assesses long term trends and seasonal variability in sea surface temperatures (SST) in eastern Canada since the early 20th century. It extends the work of Galbraith *et al.* (2012b) that examined decadal variability and long term trends in relation to air temperature forcing for the Gulf of St. Lawrence. Squared correlation coefficients (R^2) between seasonal averages of SST show that neighbour regions are highly correlated (R^2 = 0.70 to 0.92) but that correlations between the extremities of the zone are much weaker. Air temperature appears to be a reliable proxy for SST when averaged over ice-free seasonal time scales from the Labrador Shelf to the Newfoundland Shelf, the Gulf of St. Lawrence, and the eastern portion of the Scotian Shelf. April-November air temperature warming trends at AHCCD stations are 1.4 to 3°C per century since 1950 but are 0.7 to 1.3°C per century over the last century (except for two stations where trends are not statistically different from zero at the 95% confidence level). Trends since the 1870s at various stations are mostly consistent with a prior result of 0.9°C per century (1873-2011), with 8 of 12 stations having trends between 0.9 and 1.1°C per century. Trends since 1950 are higher, between 1.1 to 3.0°C per century for the April-November average with an average of 1.9°C per century over all stations. Trends since 1985 are much higher still, but coincide with a cool period from 1985 to 1993 that accentuate the trends. Seasonality trends in relation to air temperature show that onset of summer has occurred from 0.9 to 1.4 weeks earlier for each degree of air temperature anomaly over the past three decades, for all regions examined. In spite of there being few regions with overall trends in the timing of fall cooling of water temperatures over this period, some regions do exhibit interannual variability that is consistent with air temperature anomalies. These regions could see summertime conditions (i.e. warmer than the spring and fall selected thresholds) extended by as much as 2 weeks for each increase of seasonal-average air temperature of 1°C, if recent trends and relationships continue.

1.1 Introduction

Fisheries and Oceans Canada (DFO) is carrying out the Aquatic Climate Change Adaptation Services Program (ACCASP) designed to improve our understanding of aquatic climate change

and to help Canadians prepare for climate-related impacts. This study assesses long term trends and seasonal variability in sea surface temperatures (SST) in eastern Canada (Fig. 1-1) since the early 20th century as part of the Atlantic Large Aquatic Basin Risk Assessment component of ACCASP. It extends the work of Galbraith *et al.* (2012b) that examined decadal variability and long term trends in relation to air temperature (AT) forcing for the Gulf of St. Lawrence (GSL), establishing an AT proxy for SST that had a trend of 0.9°C per century (1873-2011) based on weather station data, and 0.6°C per century based on AT data from the NCEP 20th century reanalysis version 2 (Compo *et al.*, 2011). Complementing this study, long term sea surface temperature trends are also examined in Han *et al.* (2013a) and Loder *et al.* (2013), the Labrador and Newfoundland Shelf water temperatures and sea-ice extent in relation to atmospheric forcing in Han *et al.* (2013b), upper ocean temperature, salinity, and stratification in Hebert (2013a, 2013b), and CIL and deeper ocean temperature in Galbraith *et al.* (2013). AT trends are also examined in Thistle and Caissie (2013) and in Peterson and Pettipas (2013).

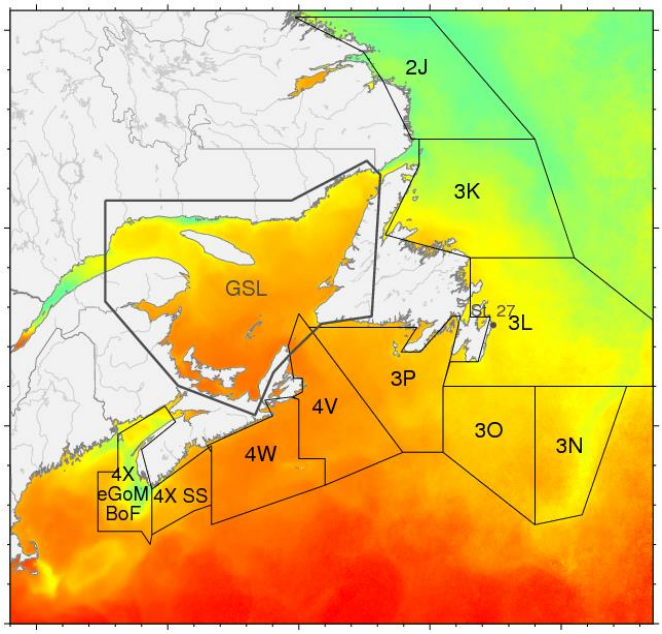

Figure 1-1 Study area. SST averaging is done for the Gulf of St. Lawrence (GSL) as delimited, and for Northwest Atlantic Fisheries Organization (NAFO) areas that are further limited to the shelf break.

The water column in the study area consists of three distinct layers: the surface layer, a cold intermediate layer, and a deeper layer. Only the first two exhibit strong seasonal variability (e.g. Galbraith *et al.*, 2012a and Fig. 2 of Galbraith *et al.*, 2012b, for the GSL). Surface temperatures typically reach maximum values from mid-July to mid-August; gradual cooling occurs thereafter. Wind mixing during the fall leads to a progressively deeper and cooler mixed layer, attaining maximum depth in winter prior to the onset of renewed stratification in spring due to ice melt, spring freshet, and surface warming. The SST is, therefore, representative of a mixed layer of varying thickness that is at minimum in spring and maximum in fall and winter.

1.2 Seasonally-Averaged Sea Surface Temperature

For this work, we used weekly average SST composites (1985-2011) calculated using a product based on National Oceanic and Atmospheric Administration (NOAA) Advanced Very High

Resolution Radiometer (AVHRR) satellite images. It is a 1 km resolution dataset available from the DFO Maurice Lamontagne Institute (MLI) remote sensing laboratory (see Galbraith and Larouche, 2011, for details of the processing). Analysis of this dataset for the GSL by Galbraith *et al.* (2012b) gave similar results to those using the Pathfinder 5 Version 5.2 dataset (Casey *et al.*, 2010), so only the former dataset will be shown here.

Figure 1-2 shows the 1985-2012 time series of SST averaged over the areas defined in Figure 1-1 from June to November, corresponding to the longest common ice-free period of the year over all areas. To facilitate comparison, each time series is standardized with respect to its mean and standard deviation (i.e. (T–<T>)/SD, where <T> is the mean of each time series and SD is its standard deviation). The latitudinal ocean climate gradient is seen in the mean June-November temperature, increasing from 4°C on the Labrador Shelf (Region 2J) to 14°C on the Scotian Shelf (Region 4W). Interannual variance is higher on the east coast of Newfoundland and Labrador and on the Grand Banks (2J, 3K, 3L, 3N, 3O) than on the Scotian Shelf. At first glance, a shift from cooler to warmer conditions is seen to have occurred over all regions between 1993 and 1994; thus at the decadal time scale the entire zone has similar variability. At interannual scales, squared correlation coefficients (R^2) between all the regional time series (Table 1-1) show that neighbouring regions are highly correlated (R^2 = 0.70 to 0.92) but that correlations between the extremities are much weaker (eastern Gulf of Maine and Bay of Fundy compared to Labrador and Newfoundland Shelf, R^2 = 0.26 to 0.31, p<0.05). Because Galbraith *et al.* (2012b) showed that May-November SST in the GSL was highly correlated to April-November AT, it is, therefore, reasonable to assume that local atmospheric forcing will be slightly different from one end of the zone to the other and relations to local weather stations should be attempted for various parts of the zone rather than attempting to identify a single mean forcing.

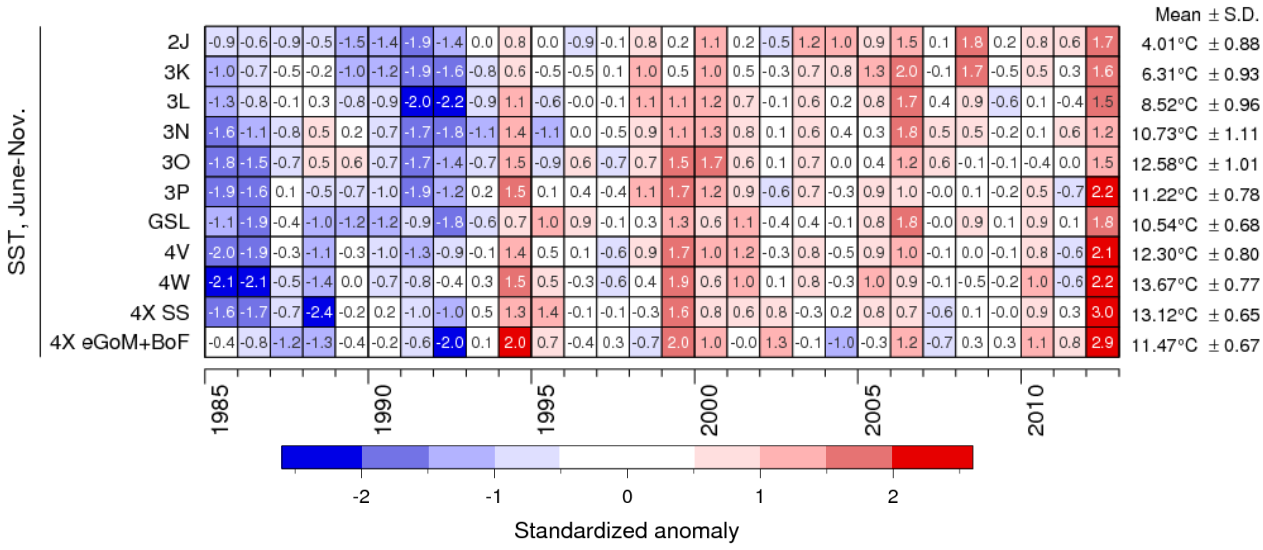

Figure 1-2 Time series of June to November SST standardized anomalies over areas defined in Figure 1-1, 1985–2012. A white cell indicates a value within 0.5 standard deviation of the long-term mean based on data from 1985–2010, a red cell indicates warmer than normal conditions and smaller volumes and areas, a blue cell indicates colder than normal. More intense colours indicate larger anomalies. The mean and standard deviation of each time series are displayed on the right and were used to standardize each of the time series [(T–mean)/SD].

Table 1-1 Correlation coefficients (R^2) for regressions between time series shown in Figure 1-2. All are statistically significant ($p<0.05$; auto-correlation of the time series is not considered to reduce the number of degrees of freedom).

R^2	3K	3L	3N	3O	3P	GSL	4V	4W	4X SS	eGoM + BoF
2J	0.88	0.67	0.55	0.37	0.53	0.57	0.47	0.33	0.31	0.29
3K		0.86	0.71	0.50	0.59	0.63	0.51	0.34	0.28	0.26
3L			0.86	0.75	0.75	0.63	0.62	0.42	0.27	0.30
3N				0.88	0.62	0.51	0.55	0.41	0.25	0.31
3O					0.71	0.45	0.64	0.53	0.29	0.30
3P						0.72	0.94	0.79	0.55	0.40
GSL							0.75	0.60	0.58	0.47
4V								0.92	0.65	0.44
4W									0.73	0.47
4X SS										0.70

1.3 SST Relation to Air Temperature

The monthly ATs used in Galbraith *et al.* (2012b) were climate summaries from Environment Canada's National Climate Data and Information Archive (henceforth labelled as 'Climate' in figures). However, Environment Canada has since released the Second Generation of Homogenized Surface Air Temperature Data as part of the Adjusted and Homogenized Canadian Climate Data (AHCCD), which accounts for shifts due to the relocation of stations, changes in observing practices and automation (Vincent *et al.*, 2012). Thus, it is worthwhile to compare these two data sets to determine if prior interpretations should be altered in view of the enhanced data set.

In Galbraith *et al.* (2012b), an AT index was created for the GSL using stations from eight locations, sometimes combining multiples stations at a single location to increase temporal coverage. All these locations are found within AHCCD except for Blanc Sablon and comparisons of anomalies relative to the 1981-2010 means are shown for each station (Figs. 1-3 and 1-4). Data and trends are similar at Port aux Basques and Daniels Harbour. Older data from the 1890s were removed for Îles-de-la-Madeleine in AHCCD leading to a higher trend with overlapping 95% confidence intervals (Fig. 1-4). Large corrections on data prior to the early 1970s introduced increased trends at Gaspé, Natashquan, and Sept-Îles, although confidence intervals still overlap such that the differences are not statistically significant. Charlottetown is the only location where corrections introduced a decreased trend. But because it is now the only location of the Galbraith *et al.* (2012b) index with coverage prior to 1909, the combined index time series for the GSL also has a slightly lesser trend in AHCCD (0.6±0.3°C per century) than when using the Climate dataset (0.9±0.3°C per century) although confidence intervals overlap. Note that the 0.6°C per century trend matches that extracted from the NCEP 20th century reanalysis (V2) shown in Galbraith *et al.* (2012b). The two average time series shown here are nevertheless nearly identical from 1970 onwards such that the correlations with SST that permit the use of April-November AT as an May-November SST proxy in Galbraith *et al.* (2012b) are not affected.

Furthermore, Figure 1-5 shows that the trend in average April-November AT is lower at Charlottetown than at other long-spanning AHCCD stations around the Gulf, and there are warming trends at various stations of 1.4 to 3°C per century since 1950 but of only 0.7 to 1.3°C per century over the last 100 years (except for two stations where trends are not statistically different from zero). Trends since the 1870s at various stations are mostly consistent with the 0.9°C per century (1873-2011) result of Galbraith *et al.* (2012b), with 8 of 12 stations having trends between 0.9 and 1.1°C per century (Fig. 1-6). Adding the stations Tête à la Baleine (available since 1911), Chatham (since 1873), and Stephenville (since 1895) to the Gulf of St. Lawrence April-November AT index increases its trend to 0.8±0.3°C per century (Fig. 1-4; top panel, black line), close to the results of Galbraith *et al.* (2012b).

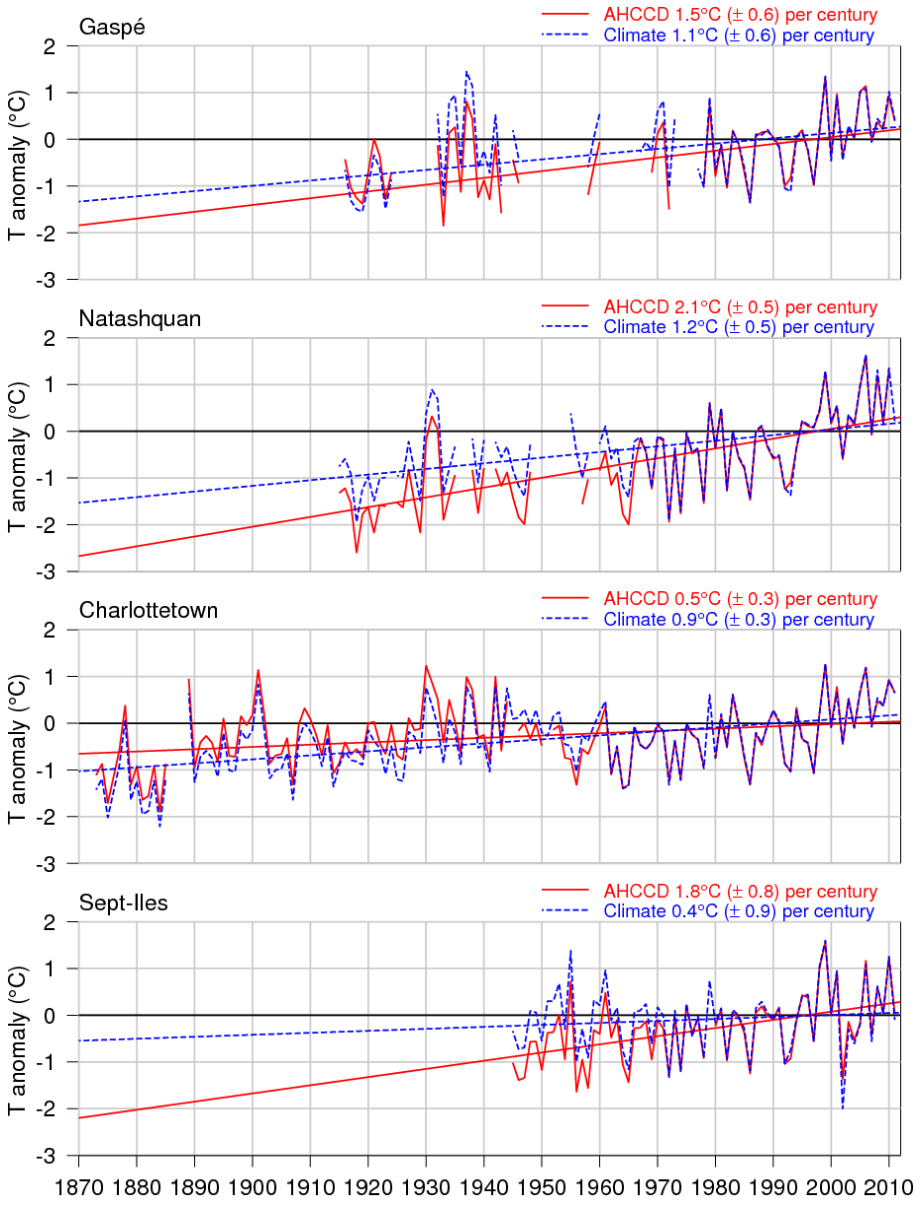

Figure 1-3 April-November temperature anomaly (1981-2010 climatology) for stations around the western Gulf, showing both Environment Canada's National Climate Data and AHCCD. Trends (with ±95% confidence intervals) are computed using all available data.

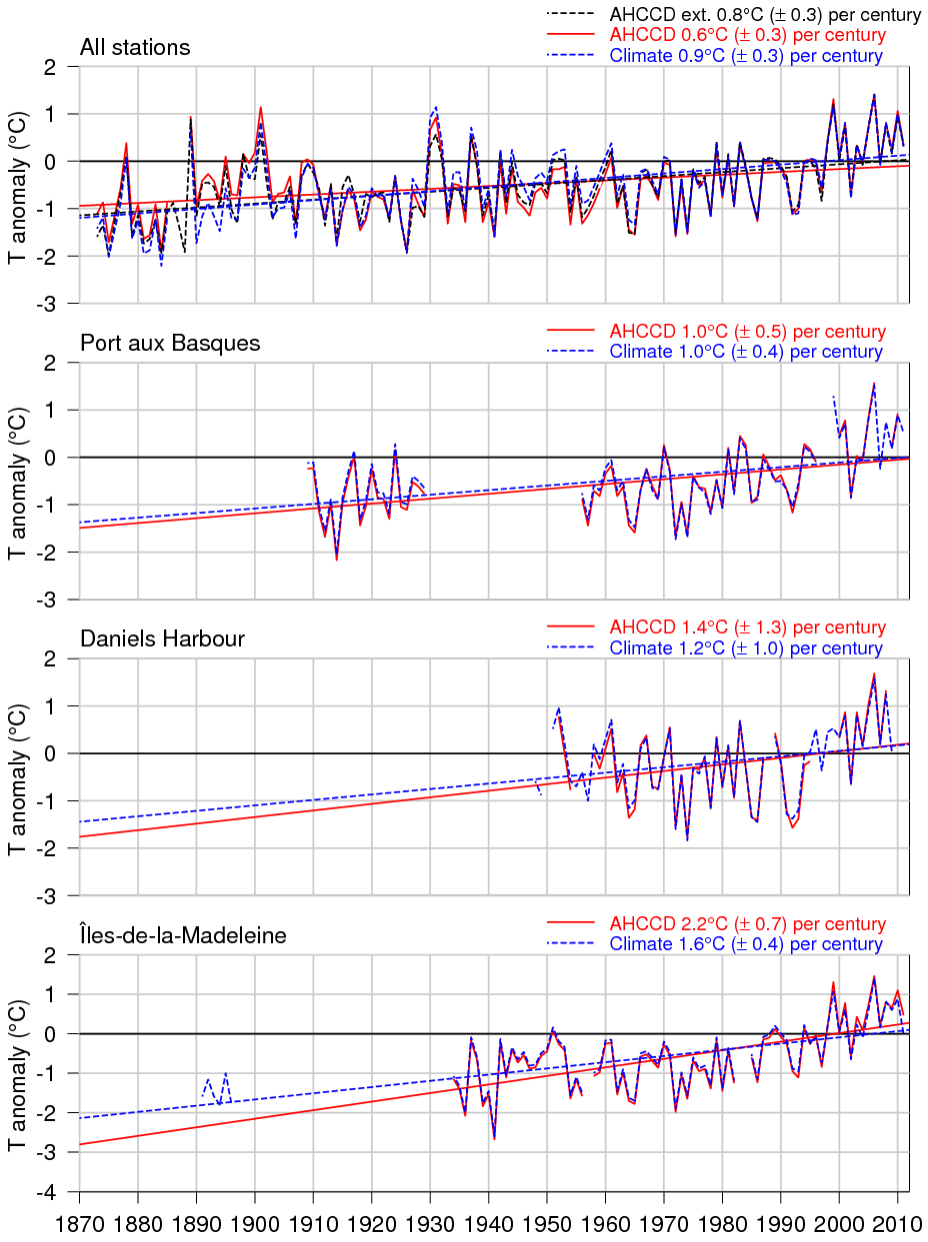

Figure 1-4 April-November temperature anomaly (1981-2010 climatology) for stations around the eastern Gulf, showing both Environment Canada's National Climate Data and AHCCD. Trends (with ±95% confidence intervals) are computed using all available data. The top panel shows the average for 7 stations using AHCCD, an extended average using 10 AHCCD stations, as well as the average computed using Climate data and including Blanc Sablon, as published by Galbraith *et al.* (2012b).

Similar to the work done for the GSL, AHCCD station AT anomalies can be compared to anomalies of SST spatially-averaged over neighbouring Northwest Atlantic Fisheries Organization (NAFO) regions of Figure 1-1. This is shown in Figure 1-7 for Cartwright AT compared with SST within NAFO 2J, St. John's compared with NAFO 3L, and Sable Island compared with NAFO 4W SST, and in Figure 1-8 for Halifax AT compared again with NAFO 4W SST, as well as both Yarmouth and Saint John AT compared with NAFO 4X eastern Gulf of Maine and Bay of Fundy SST. The seasonal averaging period varies from region to region to

cover only ice-free months. Because SST is limited by the freezing point, including the ice-covered months reduces correlations with AT. A comparison is also made in Figures 1-7 and 1-8 with *in situ* SST annually-averaged observations at AZMP stations at Station 27 (Colbourne *et al.*, 2011), Halifax Harbour, St. Andrews, and Prince 5 (Hebert *et al.*, 2011). Note that AHCCD data include temperatures up to 2011 while SST averages are provided up to 2012 when record maxima occurred in southwestern regions.

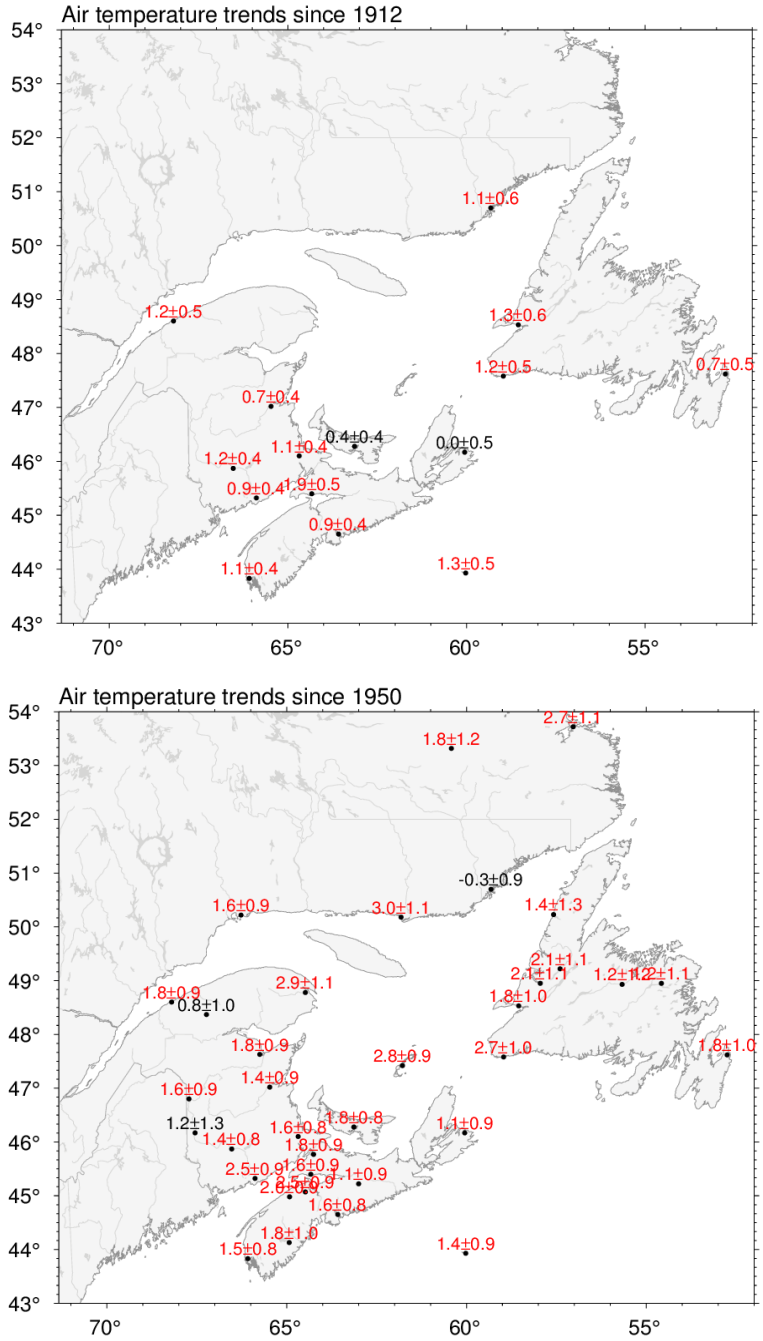

Figure 1-5 Medium-term (1950-2011) and 100-year (1912-2011) April-November AT trends at AHCCD stations (°C per century ±95% confidence intervals). Trends significantly different from zero are indicated in red.

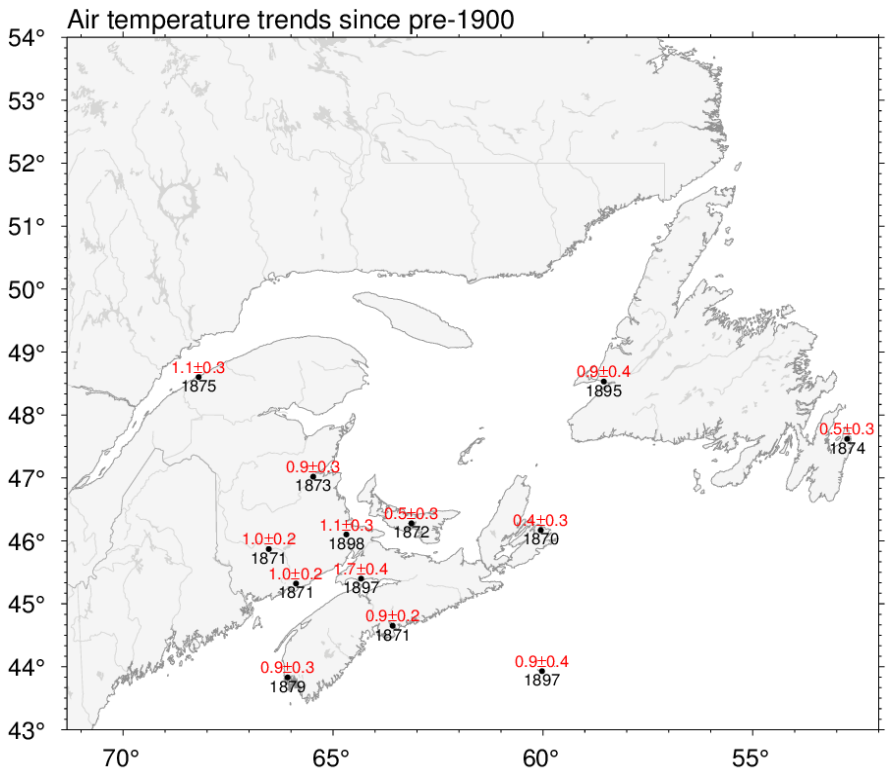

Figure 1-6 Long-term (pre-1900) April-November AT trends (°C per century ±95% confidence intervals) at AHCCD stations since the beginning of the time series at each station (indicated below each station).

Most AT time series show a pattern similar to that over the GSL (Fig. 1-4) with the coolest years of the records prior to 1889, small and sometimes cooling trends between 1945 and 1993, followed by higher warming trends in recent years. Trends over the last 100 years are in the range of 0.7 to 1.9°C per century for the April-November average (Fig. 1-5, top panel), with 11 of 13 stations showing trends between 0.9 and 1.3°C per century. Trends since 1950 are higher, between 1.1 to 3.0°C per century for the April-November average (Fig. 1-5, bottom panel) with an average of 1.9°C per century over all stations. Trends since 1985 are much higher still, but coincide with a cool period from 1985 to 1993 that accentuate the trends (Figs. 1-7 and 1-8).

From the Labrador Shelf in 2J down to Sable Island (Fig. 1-7), the correlations between spatial seasonal averages of SST and neighbouring station AT are high, with R^2 ranging from 0.65 to 0.75. All slopes of correlations between AT and SST (representing the fraction of the AT variance, or increase, that is carried over to SST) vary between 0.8 and 0.9, but the only slope that is statistically different from unity is between AT at St. John's and *in situ* SST at Station 27. Correlations between seasonal AVHRR SST and AT are weaker from Halifax to the eastern Gulf of Maine (Fig. 1-8) with $R^2 = 0.5$ and, not surprisingly, weakest in the Bay of Fundy ($R^2 = 0.37$) where strong vertical mixing buffers SST. The high correlations between seasonally-averaged SST and AT, combined with the much higher trends in the AVHRR period since 1985 compared with longer time scales, indicate that these high trends since 1985 are partly caused by the coincidental cool period between 1985 and 1993, as Galbraith el al. (2012b) found for the Gulf of St. Lawrence. However, many of the warmest years on record for AT across the zone have occurred during the last decade or so (Figs. 1-7 and 1-8).

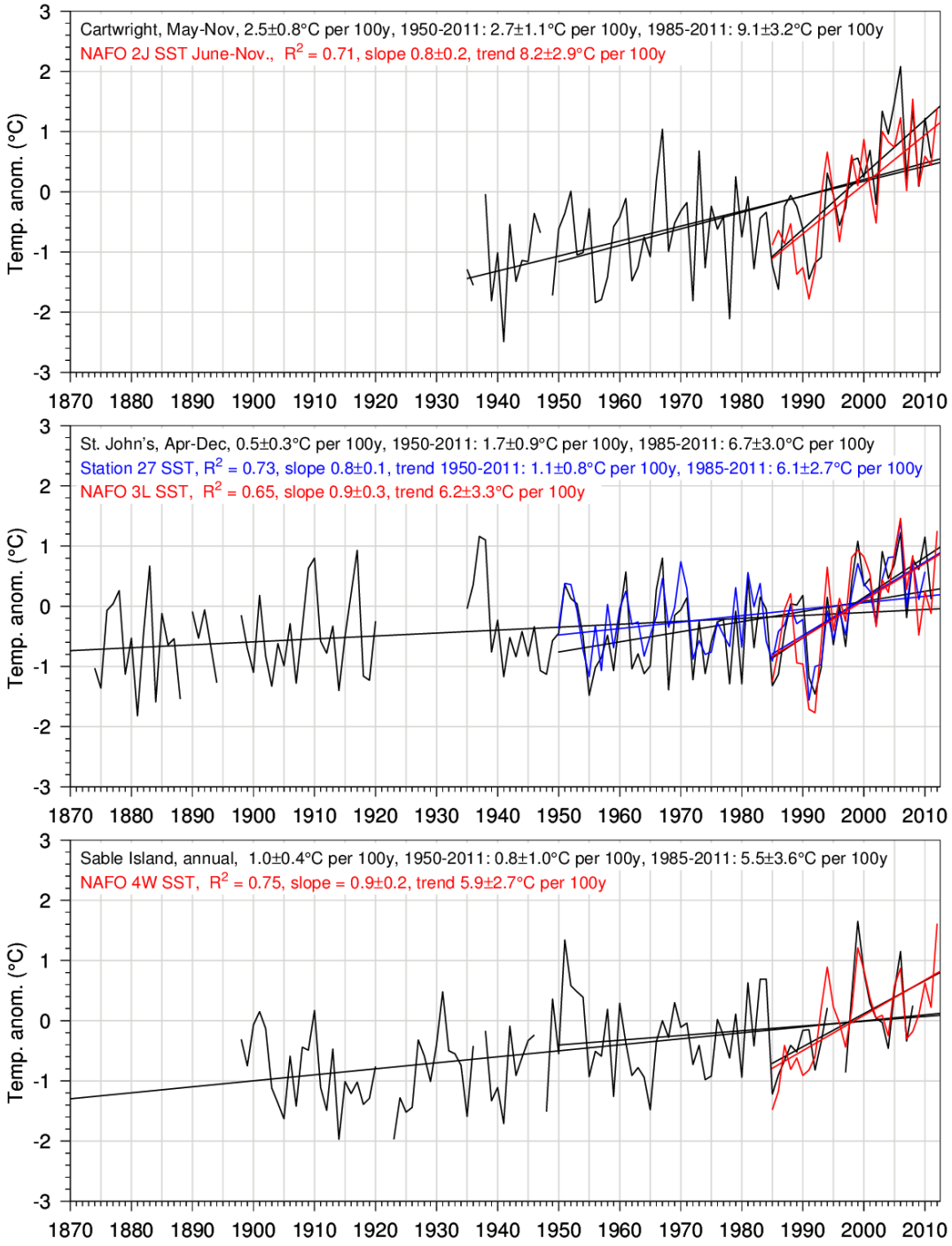

Figure 1-7 AHCCD station air temperature anomalies, yearly averaged for indicated month spans (e.g. May-Nov used at Cartwright), compared with anomalies of AVHRR SST averaged over the same period and spatially over the indicated NAFO region (Fig. 1-1). The St. John's panel also shows anomalies of annual average SST measured at AZMP Station 27. Correlation coefficients and regression slopes are for comparisons with the AT time series. Statistically significant trends (±95% confidence intervals) are shown for the entire time series, as well as for 1950- and 1985-2011. All anomalies are referenced to the 1981-2010 period.

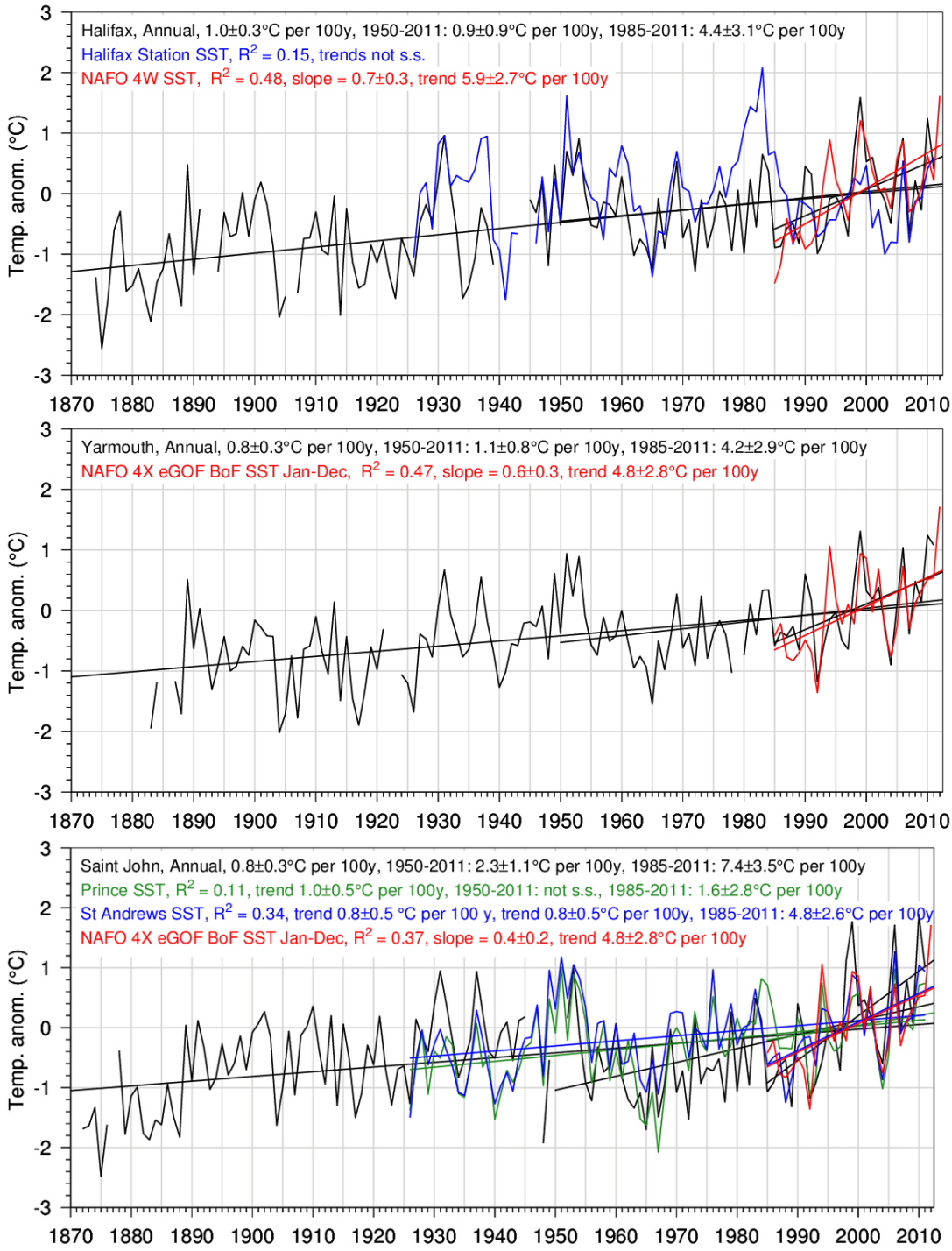

Figure 1-8 AHCCD station AT, yearly averaged for indicated month spans, compared with AVHRR SST averaged over the same period and spatially over the indicated NAFO region (Fig. 1-1). The Halifax panel also shows annual average SST measured at Halifax Harbour, while the St. John panel shows annual average SST measured at AZMP Stations St. Andrews and Prince 5. Correlation coefficients and regression slopes are for comparisons with the AT time series. Statistically significant trends (±95% confidence intervals) are shown for the entire time series, as well as for 1950- and 1985-2011. All anomalies are referenced to the 1981-2010 period.

The *in situ* SST time series at Halifax Harbour does not correlate very well with AT, displaying very warm temperatures in the early 1980s that are not observed in the AT record, nor does it compare well with offshore SST AVHRR observations. On the other hand, the *in situ* SST time series at St. Andrews and Prince 5 stations show a good correspondence with AVHRR SST, so its lack of correlation with AT is assumed to be associated with tidal mixing and other ocean influences dominating over the AT forcing.

In summary, just as it was found to be for the GSL by Galbraith *et al.* (2012b), AT appears to be a useful proxy for SST when averaged over seasonal timescales from the Labrador Shelf, down the Newfoundland Shelf, but limited to the eastern portion of the Scotian Shelf. The extrapolation of these relations to future ocean conditions, based on projected AT increases, requires that factors affecting SST and atmospheric exchanges such as the mixed layer depth, itself affected by wind stress and stratification, will be similar in the future as in the 26-year period that the statistics are based on.

1.4 Seasonality trends

Seasonality trends in relation to AT are examined by first displaying weekly averaged AVHRR SST in the GSL and in each NAFO region for all years between 1985 and 2012 (Figs. 1-9 to 1-11) with years on the x-axis and week of the year on the y-axis. Isotherms show the first and last occurrences of weekly temperatures of 8, 12, and 14°C over the years. These temperatures are chosen to be representative of spring (and fall) transitions to (and from) typical summer temperatures. Although arbitrary, the surface mixed layer tends to warm (cool) linearly in spring (fall) (e.g. Galbraith *et al.*, 2012b) such that the results that follow are not particularly sensitive to the exact temperature chosen. The weeks of the last and first occurrences of selected isotherms are tabulated in Tables 1-2 and 1-3, respectively, and colour-coded according to their normalized anomalies. All regions have experienced earlier spring warming between 1985 and 2012, with trends varying between -0.6 weeks per decade on the Scotian Shelf to -1.6 weeks per decade on the Labrador Shelf (Table 1-2). However, only three regions have experienced trends statistically different from zero for changes in the timing of fall cooling, with rates of +0.5 to +0.7 weeks per decade of later cooling (Table 1-3).

Because the beginning of the AVHRR SST record corresponds to an unusually cool period, and the last decade has been unusually warm, the apparent trends towards earlier springs are not surprising. But perhaps of more use for assessing the impact of climate change is relating this change and interannual variability to changes in AT during spring and summer months. These results are shown in Tables 1-4 and 1-5, showing the correlation between the week of the year when average SST first (last) reaches a suitable summer (fall) threshold and AHCCD AT at the closest ground station averaged over the previous month, or a combination of months (the AHCCD ten-station average was used for the GSL).

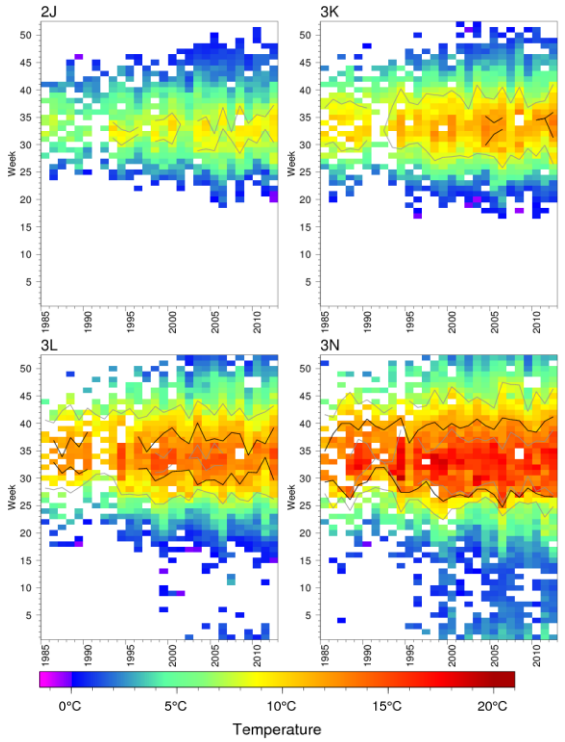

Figure 1-9 Weekly average SST (1985-2012) matrices for NAFO regions 2J, 3K, 3L, and 3N. Isotherms show the first and last occurrences of 8, 12, and 14°C.

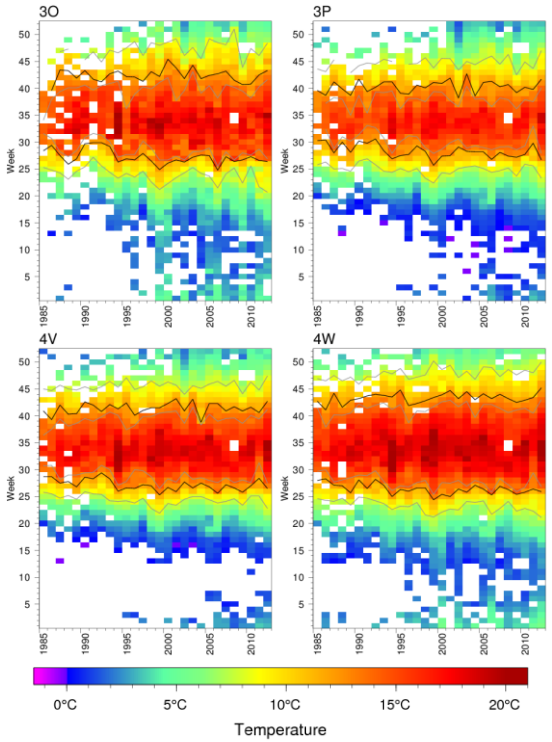

Figure 1-10 Weekly average SST (1985-2012) matrices for NAFO regions 3O, 3P, 4V, and 4W.

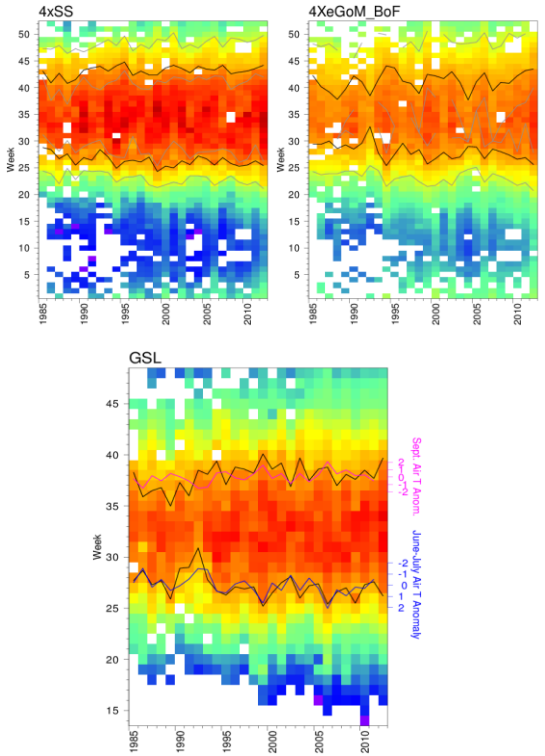

Figure 1-11 Weekly average SST (1985-2012) matrices for NAFO regions 4X SS (Scotian Shelf), 4X eGOM, BoF (east Gulf of Maine and Bay of Fundy), and the Gulf of St. Lawrence. Temperature anomaly proxies for the first and last occurrence of the 12°C isotherm based on June-July and September average air temperature are shown for the Gulf of St. Lawrence (axes on right).

Table 1-2 First seasonal occurrence of a given mean temperature in NAFO regions, 1985-2012, expressed as week of the year. The mean and standard deviations are provided on the right, as well as the trend over the period expressed as week per decade (± 95% confidence intervals).

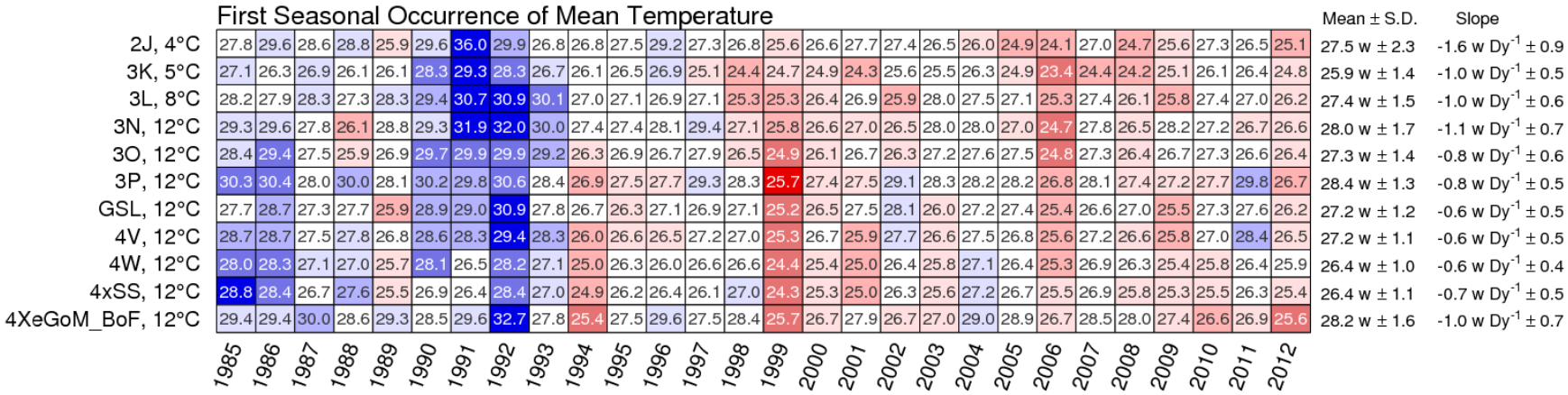

Table 1-3 Last seasonal occurrence of a given mean temperature in NAFO regions, 1985-2012, expressed as week of the year. The mean and standard deviations are provided on the right.

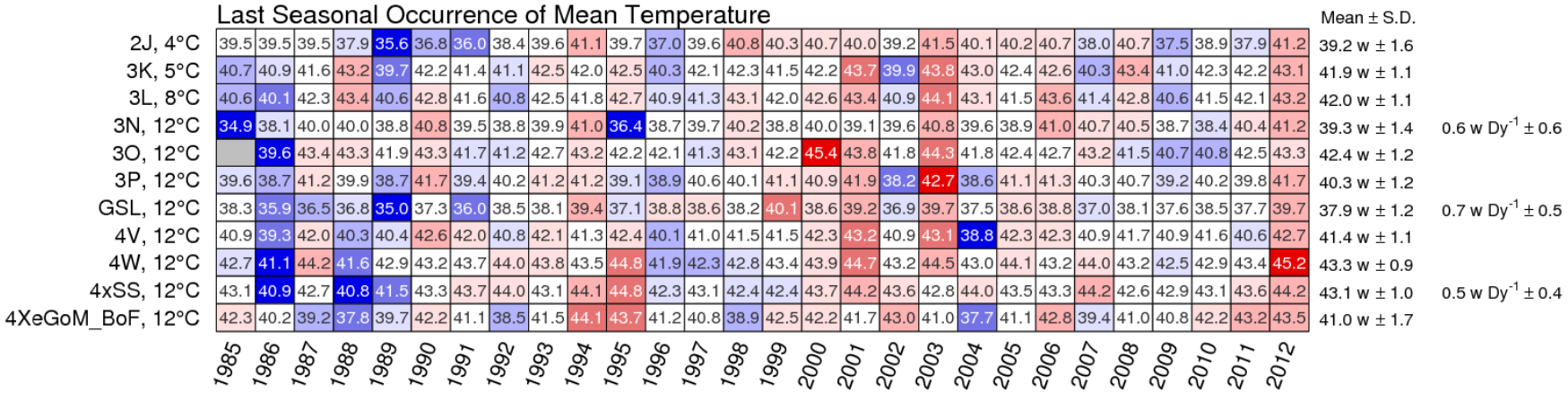

For the onset of summer, all regions examined show strong correlations, including eastern Gulf of Maine and Bay of Fundy. The highest correlations (R^2 = 0.59 to 0.65) are with AT for the month of July at eastern Gulf of Maine and Bay of Fundy, with the May-June-July AT average at regions 2J and 3L, and with the June-July Sable Island AT average at region 4W. The slopes indicate that onset of summer occurs from 0.9 to 1.4 weeks earlier for each degree of AT anomaly. The correlation between the onset of summer date and the spring AT anomaly is illustrated for the Gulf of St. Lawrence on the last panel of Figure 1-10 with overlays of the 12°C isotherm and of its AT proxy.

Table 1-4 Correlation table between week of year when average SST in various regions first reaches a given threshold (indicated on left) and station AT averaged over one or several months (different columns). The correlation coefficient R^2 is provided along with the slope of the linear regression (weeks per °C). All correlations are statistically significant (p<0.05).

	July R^2 / slope	June-July R^2 / slope	May-July R^2 / slope	Apr-July R^2 / slope	Apr-June R^2 / slope
2J, 4°C *vs* Cartwright	**0.50 / -0.9**	**0.64 / -1.2**	**0.64 / -1.4**	**0.58 / -1.3**	**0.44 / -1.1**
3L, 8°C *vs* St. John's	**0.43 / -0.6**	**0.53 / -1.0**	**0.65 / -1.3**	**0.64 / -1.4**	**0.37 / -0.9**
4W, 12°C *vs* Sable Island	**0.53 / -0.8**	**0.61 / -0.9**	**0.60 / -1.0**	**0.56 / -1.0**	**0.41 / -0.8**
eGOF BoF, 12°C *vs* Yarmouth	**0.59 / -1.2**	**0.54 / -1.5**	**0.44 / -1.5**	**0.39 / -1.4**	**0.19 / -0.9**
GSL, 12°C *vs* ten-station index	**0.46 / -0.9**	**0.56 / -1.1**	**0.45 / -1.0**	**0.39 / -0.9**	**0.25 / -0.7**

Table 1-5 Correlation table between week of year when average SST last reaches a given threshold with station AT averaged over one or several months. The correlation coefficient R^2 is provided along with the slope of the linear regression (weeks per °C). Statistically significant correlations (p<0.05) are in black type.

	October R^2 / slope	September R^2 / slope	Sep-Oct R^2 / slope	Aug-Oct R^2 / slope	Jul-Sep R^2 / slope
2J, 4°C *vs* Cartwright	**0.15 / 0.5**	**0.25 / 0.7**	**0.26 / 0.8**	**0.27 / 1.0**	**0.35 / 1.0**
3L, 8°C *vs* St. John's	**0.57 / 0.6**	**0.21 / 0.4**	**0.51 / 0.7**	**0.42 / 0.8**	**0.15 / 0.4**
4W, 12°C *vs* Sable Island	**0.63 / 0.6**	**0.28 / 0.4**	**0.58 / 0.7**	**0.46 / 0.8**	0.13 / 0.4
eGOF BoF, 12°C *vs* Yarmouth	0.12 / 0.5	0.14 / 0.7	**0.23 / 1.0**	**0.24 / 1.2**	**0.30 / 1.5**
GSL, 12°C *vs* ten-station index	0.04 / 0.2	**0.43 / 0.7**	**0.29 / 0.7**	**0.26 / 0.9**	**0.28 / 1.0**

In spite of there being few regions with overall trends in the timing of fall cooling water temperatures, some regions do exhibit interannual variability that is consistent with AT anomalies (Table 1-5). This was found to be the case at NAFO regions 3L and 4W, where the timing of the fall cooling was highly correlated with October ATs (R^2 = 0.57 and 0.63), with slopes of 0.6 weeks delay per degree of AT anomaly. Combining these results with the earlier onset of summer, it is concluded that these regions as well as the GSL could see their summertime conditions extended by as much as 2 weeks for each overall 1°C increase of AT.

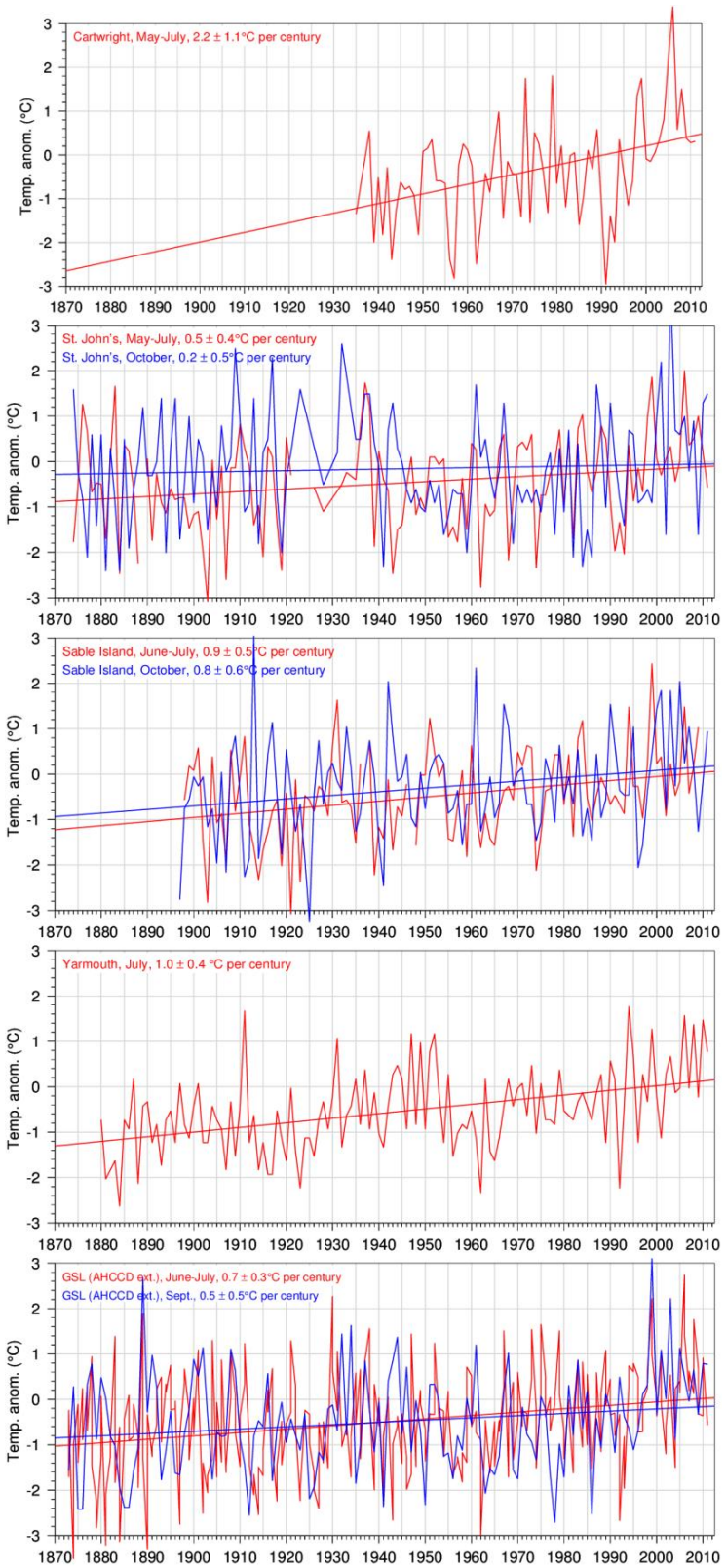

Figure 1-12 AHCCD station AT anomalies for selected spring month spans (e.g. May-July used at Cartwright) and fall month spans that were shown to be correlated with onset of summer and fall, respectively, at AZMP stations.

Past trends in AT for the month spans best representing the timing of spring warming and fall cooling are shown in Figure 1-12. Except for Cartwright, which has a relatively short AT record, trends in the spring period are positive in every region ranging from 0.5 to 1.0°C per century. Trends are generally comparable to the average trends of Figures 1-7 and 1-8. The fall period has experienced a warming trend in the Gulf of St. Lawrence (0.5°C per century) and at Sable Island (0.8°C per century), but no significant trend was found at St. John's for the month of October (contrary to the warming trend of 0.5°C per century observed in the April-November average). These trends can be combined with slopes in Tables 1-4 and 1-5 to estimate trends on longer timescales than those of Table 1-2 and 1-3 (1985-2012). For example, region 2J, off Cartwright, has possibly experienced a trend towards earlier spring water temperatures at the rate of 0.3 weeks per decade for the period 1935-2011, much less than the 1.6 weeks per decade observed during 1985-2012.

1.5 Conclusions

Although SST climatologies vary greatly across eastern Canada, seasonally-averaged anomalies were found to exhibit a very consistent shift from cool to warm occurring in 1994. Interannual correlations are high between neighbouring regions (R^2 = 0.70 to 0.92) but are much weaker between the extremities. Since Galbraith et al (2012b) found that May-November SST in the GSL was highly correlated to April-November AT, we first verified this result using the newer AHCCD AT data set, which accounts for shifts due to the relocation of stations as well as changes in observing practices and automation. The AHCCD data showed a warming trend in the GSL of 0.8±0.3°C per century (1873-2011) that is similar to the result of Galbraith et al (2012b). Since the interannual SST correlations are low between end points of the zone, we then looked for similar local AT-SST relations across the larger area. From the Labrador Shelf in 2J down to Sable Island (Fig. 1-7), the correlations between seasonal averages of SST and neighbouring station AT are high, with R^2 ranging from 0.65 to 0.75. Correlations between seasonal AVHRR SST and AT are weaker from Halifax to the eastern Gulf of Maine (Fig. 1-8) with R^2 = 0.5 and, not surprisingly, weakest in the Bay of Fundy (R^2 = 0.37) where strong vertical mixing buffers SST. AT thus appears to be a useful proxy for SST when averaged over seasonal timescales from the Labrador Shelf, down the Newfoundland Shelf and the western portion of the Scotian Shelf.

Seasonality trends were explored by determining when threshold spring- and fall-like temperatures were reached each year in the various areas. All regions have experienced earlier spring warming between 1985 and 2011, with trends varying between -0.6 weeks per decade on the Scotian Shelf to -1.6 weeks per decade on the Labrador Shelf (Table 1-2). However, only three regions have experienced trends statistically different from zero for changes in the timing of fall cooling, with rates of +0.5 to +0.7 weeks per decade of later cooling. The interannual variability was compared with air temperature at neighbouring coastal stations. For the onset of summer, all regions examined show strong correlations, including eastern Gulf of Maine and Bay of Fundy. For the onset of fall, only some regions (NAFO regions 3L and 4W, and the GSL) exhibited interannual variability that is consistent with AT anomalies (Table 1-5). Combining these results with the earlier onset of summer, it is concluded that these regions could see their summertime conditions extended by as much as 2 weeks for each overall 1°C increase of AT.

1.6 Acknowledgements

This work was supported by DFO's Aquatic Climate Change Adaptation Services Program (ACCASP). SST data from selected Atlantic Zone Monitoring Program stations were provided by Roger Pettipas and David Hebert (Halifax Harbour, St. Andrews, and Prince 5) and by Eugene Colbourne (Station 27) who was also the first to correlate them with air temperature at St. John's. The authors thank Ingrid Peterson and John Loder for their useful and constructive comments.

1.7 References

Casey, K. S., T. Brandon, P. Cornillon, and R. Evans. 2010. Oceanography from Space: revisited. In: *The Past, Present, and Future of the AVHRR Pathfinder SST Program* [V. Barale, J. F. R. Gower, and L. Alberotanza (Eds.)]. Springer.

Colbourne, E., J. Craig, C. Fitzpatrick, D. Senciall, P. Stead, and W. Bailey. 2011. An assessment of the physical oceanographic environment on the Newfoundland and Labrador Shelf during 2010. DFO Can. Sci. Advis. Sec. Res. Doc. 2011/089. iv + 31p. http://www.dfo-mpo.gc.ca/Csas-sccs/publications/resdocs-docrech/2011/2011_089-eng.pdf

Compo, G. P., J. S. Whitaker, P. D. Sardeshmukh, N. Matsui, R. J. Allan, X. Yin, B. E. Gleason, R. S. Vose, G. Rutledge, P. Bessemoulin, S. Brnnimann, M. Brunet, R. I. Crouthamel, A. N. Grant, P. Y. Groisman, P. D. Jones, M. C. Kruk, A. C. Kruger, G. J. Marshall, M. Maugeri, H. Y. Mok, Ø Nordli, T. F. Ross, R. M. Trigo, X. L. Wang, S. D. Woodruff, and S. J. Worley. 2011. The twentieth century reanalysis project. *Q. J. R. Meteorol. Soc.*, 137(654), 1–28, doi:10.1002/qj.776.

Galbraith, P. S. and P. Larouche. 2011. Sea-surface temperature in Hudson Bay and Hudson Strait in relation to air temperature and ice cover breakup, 1985-2009. *J. Mar. Systems*, 87, 66-78.

Galbraith, P. S., J. Chassé, D. Gilbert, P. Larouche, D. Brickman, B. Pettigrew, L. Devine, A. Gosselin, R. G. Pettipas, and C. Lafleur. 2012a. Physical oceanographic conditions in the Gulf of St. Lawrence in 2011. DFO Can. Sci. Advis. Sec. Res. Doc. 2012/023. iii + 85 p. http://www.dfo-mpo.gc.ca/Csas-sccs/publications/resdocs-docrech/2012/2012_023-eng.pdf

Galbraith P. S., P. Larouche, J. Chassé, and B. Petrie. 2012b. Sea surface temperature in relation to air temperature in the Gulf of St. Lawrence: interdecadal variability and long term trends. *Deep Sea Res. II*, http://dx.doi.org/10.1016/j.dsr2.2012.04.001.

Galbraith, P. S., D. Hebert, E. Colbourne, and R. Pettipas. 2013. Trends and variability in eastern Canada sub-surface ocean temperatures and implications for sea-ice. Ch. 5 (p. 57-72) *In*: This report.

Han, G., E. Colbourne, P. Pepin, and R. Tang. 2013a. Statistical projections of physical oceanographic variables over the Newfoundland and Labrador Shelf. Ch. 6 (p. 73-84) *In:* This report.

Han, G., Z. Ma, and H. Bao. 2013b. Trends of temperature, salinity, stratification and mixed-layer depth in the Northwest Atlantic. Ch. 2 (p. 19-32) *In:* This report.

Hebert, D. 2013a. Trends in temperature, salinity, density and stratification for different regions in the Atlantic Canadian shelf. Ch. 3 (p. 33-42) *In:* This report.

Hebert, D. 2013b. Trends in temperature, salinity, density and stratification in the upper ocean for the Scotian Shelf. Ch. 4 (p. 43-56) *In:* This report.

Hebert, D., R. Pettipas, and B. Petrie. 2011. Meteorological, sea ice and physical oceanographic conditions on the Scotian Shelf and in the Gulf of Maine during 2009 and 2010. DFO Can. Sci. Advis. Sec. Res. Doc. 2011/094: vi + 32 p. http://www.dfo-mpo.gc.ca/Csas-sccs/publications/resdocs-docrech/2011/2011_094-eng.pdf

Loder, J. W., Z. Wang, A. van der Baaren and R. Pettipas. 2013. Trends and variability of sea surface temperature in the North Atlantic, from the HadISST, ERSST and COBE datasets. Can. Tech. Rep. Hydrogr. Ocean Sci. 292: viii + 36 p. http://www.dfo-mpo.gc.ca/Library/350066.pdf

Peterson, I. K. and R. Pettipas. 2013. Trends in air temperature and sea ice in the Atlantic Large Aquatic Basin and adjoining areas. Can. Tech. Rep. Hydrogr, Ocean Sci. 290: v + 59 p. http://www.dfo-mpo.gc.ca/Library/350061.pdf

Thistle, M. E. and Caissie, D. 2013. Trends in air temperature, total precipitation and streamflow characteristics in eastern Canada. Can. Tech. Rep. Fish. Aquat. Sci. 3018: xi + 97 p. http://www.dfo-mpo.gc.ca/Library/347639.pdf

Vincent, L. A., X. L. Wang, E. J. Milewska, H. Wan, F. Yang, and V. Swail. 2012. A second generation of homogenized Canadian monthly surface air temperature for climate trend analysis. *J. Geophys. Res.* 117, D18110, doi:10.1029/2012JD017859.

2 Trends of temperature, salinity, stratification and mixed-layer depth in the Northwest Atlantic

Guoqi Han *, Zhimin Ma and Huizhi Bao

Fisheries and Oceans Canada, Northwest Atlantic Fisheries Centre
P.O. Box 5667, St. John's, Newfoundland and Labrador A1C 5X1

* Correspondence: Guoqi.Han@dfo-mpo.gc.ca

Suggested Citation:

Han, G., Z. Ma and H. Bao. 2013. Trends of temperature, salinity, stratification and mixed-layer depth in the Northwest Atlantic. Ch.2 (p. 19-32) *In:* Aspects of climate change in the Northwest Atlantic off Canada [Loder, J.W., G. Han, P.S. Galbraith, J. Chassé and A. van der Baaren (Eds.)]. Can. Tech. Rep. Fish. Aquat. Sci. 3045: x + 190 p.

Abstract

Monthly-mean temperature and salinity data sets were used to examine trends in the surface temperature, surface salinity, vertical density difference, and mixed-layer depth in waters with depths greater than 1000m in the Northwest Atlantic. The surface temperature had an average rate of warming of 0.05±0.04°C/decade (± two standard errors) in the Northwest Atlantic from 1945-2010, but cooling southwest of Nova Scotia. It increased at the much larger rate of 0.38±0.07°C/decade from 1981-2010 and warming was largest in the Labrador Sea. From 1945-2010, the subsurface temperature (averaged from 100 to 700 m) increased at 0.06±0.02°C/decade in the Northwest Atlantic, except in the vicinity of the Flemish Cap and southwest of Nova Scotia. Although the surface salinity increased at a rate of 0.01±0.01 psu/decade in the Northwest Atlantic from 1945-2010, it decreased over the southern Grand Bank slope and over the slope southwest of Nova Scotia. From 1981-2010 the surface salinity increased at a rate of 0.05±0.03 psu/decade in the Northwest Atlantic, but decreased off the southeastern Grand Banks and off Georges Bank. From 1945-2010, the subsurface salinity (averaged from 100 to 700 m) for the entire domain had no trend, but had positive trends along the Gulf Stream pathway and in the northern Labrador Sea. Subsurface salinity had negative trends in the vicinity of Flemish Cap, over the slope southwest of Nova Scotia and south of Greenland. Trends of the density difference between 50 m and the sea surface, as a whole, were statistically insignificant from zero from 1945-2010, but there were positive and negative trends in the Labrador Sea and along the Gulf Stream pathway, respectively. In contrast, the vertical density difference showed a widespread increase at an average rate of 0.04±0.02 kgm^{-3}/decade from 1981-2010. The mixed-layer depth increased along the Gulf Stream's path but decreased in the Labrador Sea from 1945-2010. It had a widespread decrease in the Northwest Atlantic from 1981-2010, except northwest of Flemish Cap.

2.1 Introduction

The Northwest Atlantic plays an important part in the global climate system because the Labrador Sea is among the few locations in the world's ocean that features wintertime deep convection. The surface water in the Labrador Sea can sink in extremely cold winters and subsequently flow

equatorward, at depth, as part of the Atlantic Meridional Overturning Circulation (AMOC) with the poleward flowing Gulf Stream near the surface. It has been suggested that on multi-decadal scales, the AMOC drives the Atlantic Multidecadal Oscillation (AMO), which is a natural variation in the North Atlantic's sea surface temperature on timescales of 30-80 years (e.g. Delworth and Mann, 2000). There is significant interannual and decadal variability in hydrographic properties (Petrie and Drinkwater, 1993; Petrie, 2007) and circulation strength (Häkkinen and Rhines, 2004; Han *et al.*, 2010) of the NW Atlantic subpolar and subtropical gyres off Atlantic Canada that appears to be related to the North Atlantic Oscillation which is the dominant atmospheric mode of variability over the North Atlantic.

From 1955-2010, the upper 2000 m of the world ocean had a volume mean warming of 0.09 ^{o}C (Levitus *et al.*, 2012). There was a general warming trend in the upper 2000 m North Atlantic over the last eighty years of the 20th century, with enhanced warming during the past couple decades (Polyakov *et al.*, 2009). Long-term trends of temperature and salinity have been analysed at fixed stations off eastern Canada. For example, there are substantial warming (small freshening) trends at the sea surface at Station 27 off St. John's (Colbourne, 2004). Remote sensing data have been used to assess the sea surface temperature trend in selected areas over the Atlantic Shelf (Hebert *et al.*, 2012). The upper-layer water stratification off Atlantic Canada has been quantified by calculating the density difference/gradient in the vertical (Hebert *et al.*, 2012). These studies have shown substantial spatial differences in the trends. The trends also depend on the periods over which they are estimated.

In this study, we have analysed linear trends in temperature, salinity, and stratification from 1945-2010 and 1981-2010 for water depths greater than 1000m in the Northwest Atlantic , based on a historical monthly-mean temperature and salinity dataset (Ishii *et al.*, 2006). Regional variations in these trends are briefly described. Hebert (2013) provides a complementary analysis for the Atlantic Canadian Shelf, Galbraith and Larouche (2013) a complementary analysis of sea surface temperature (SST) and Loder *et al.* (2013) an analysis of sea surface temperature variability in the North Atlantic using three historical datasets.

2.2 Data and Methods

We used an updated version of Ishii *et al.*'s (2006) monthly-mean temperature and salinity dataset. Their temperature and salinity fields were objectively analysed on a 1°×1° grid at the upper 16 standard levels (0, 10, 20, 30, 50, 75, 100, 125, 150, 200, 250, 300, 400, 500, 600, 700 m) from 1945-2010. Various historical hydrographic datasets were used in the objective analysis, including the latest version of the observational data, climatology and standard deviations compiled by the National Oceanic and Atmospheric Administration/National Oceanographic Data Center (NODC). Ishii *et al.* also used a tropical and subtropical Pacific Ocean sea surface salinity dataset for 1970-2001 and a global database archived by the Global Temperature-Salinity Profile Program of NODC from 1990-2010, and made the drop rate correction for the XBT data.

In this study, the Northwest Atlantic domain is defined from 72°W to 40°W and from 35°N to 66°N. We only considered areas where water depth is greater than 1000 m (Fig. 2-1) in consideration of potential degradation of the data quality over the coastal and shelf areas. In addition to the trends of the annual means for the temperature, salinity, density difference, and

mixed-layer depth, we also present those of the monthly means in August. The latter represents summer, when stratification is strong. A least squares fitting technique was used to extract linear trends over the periods 1945-2010 and 1981-2010 which are presented together with ±two standard errors. If we assume that the errors in the data are independent, any trend with magnitude equal or greater than twice the standard error is statistically significant at the 95% confidence level.

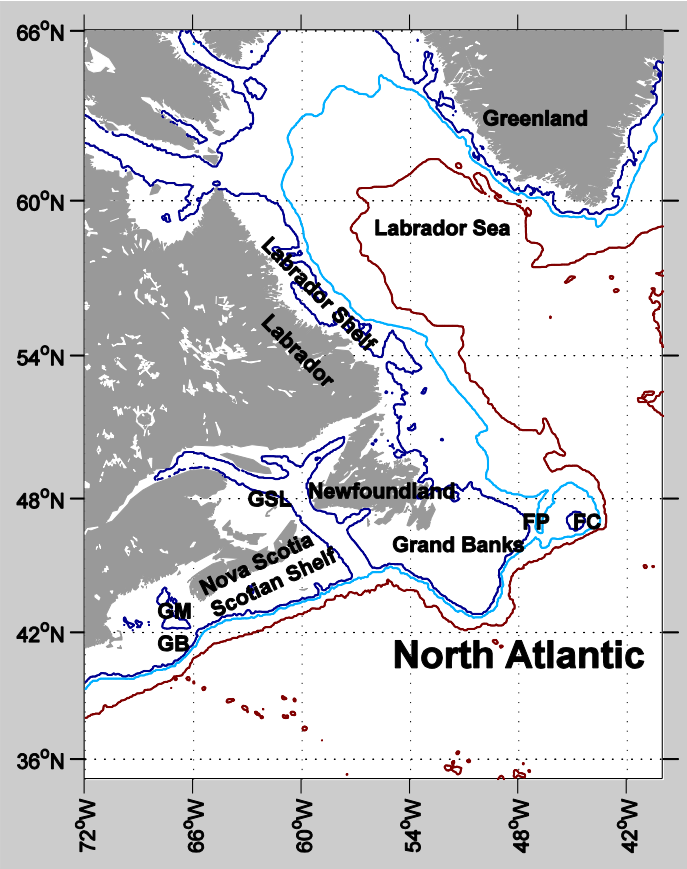

Figure 2-1 Map showing the Northwest Atlantic domain. FC: Flemish Cap; FP: Flemish Pass; GB: Georges Bank; GM: Gulf of Maine; GSL: Gulf of St. Lawrence. The 200 (blue), 1000 (light blue) and 3000 (red) m isobaths are also depicted.

The vertical density difference was calculated by subtracting the density at the sea surface from that at 50 m, as commonly used by the Atlantic Zone Monitoring Program (Hebert *et al.*, 2012). The mixed-layer depth was determined based on the 0.125 kgm^{-3} threshold criterion (Levitus, 1982) where the vertical density profile is a piecewise linear function of depth based on the density values at standard depths. Note that there is no standard criterion or method to determine the mixed layer depth. The calculated results are usually sensitive to the method and criterion used and to how the data are smoothed and decimated in the vertical (Thompson and Fine, 2003; Craig and Gilbert, 2008).

2.3 Results

Temperature

The surface temperature from 1945-2010 had a mean value of 13.0°C and a positive trend of 0.05±0.04°C/decade in the Northwest Atlantic as a whole (Fig. 2-2; Table 2-1). The largest increase occurred in the Labrador Sea. The trend is weakly negative in the deep waters southwest of the Scotian Shelf (west of 60°W and south of 42°N) (Fig. 2-3).

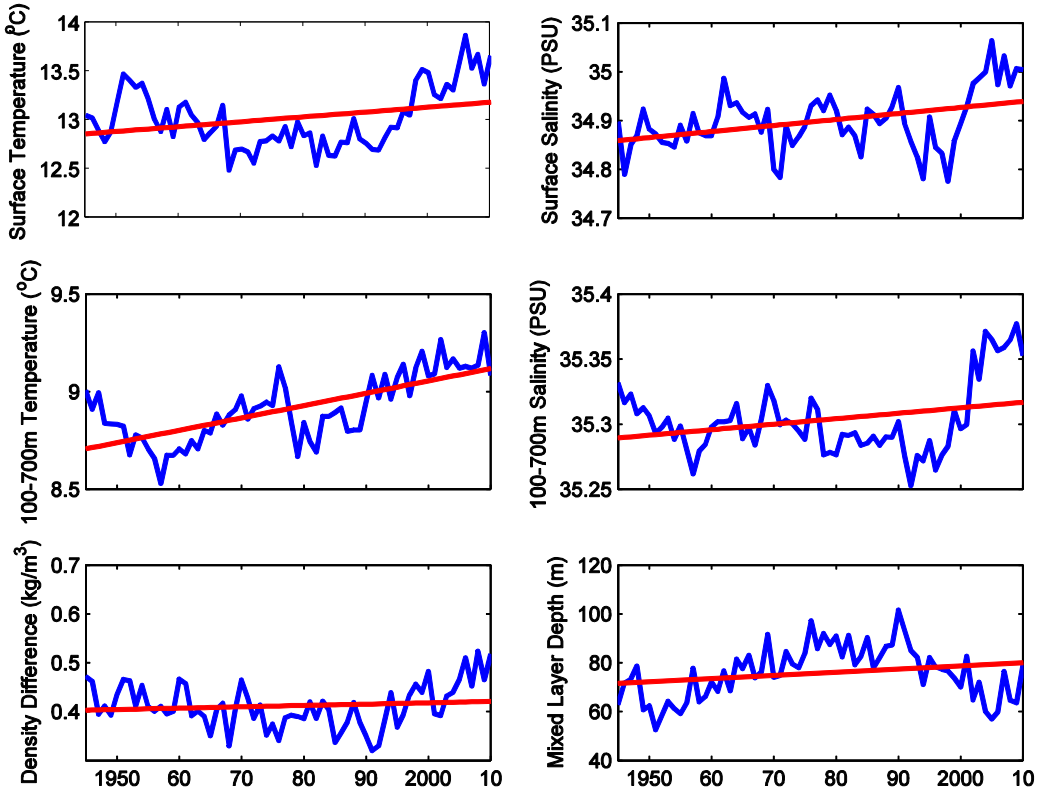

Figure 2-2 Time series of annual means (blue) and linearly fitted lines (red) in the Northwest Atlantic domain from 1945-2010.

From 1981-2010, the surface temperature had a much larger positive trend of 0.38±0.07 °C/decade in the Northwest Atlantic (Table 2-1), about 6 times larger than that from 1945-2010. The temperature increase encompassed the entire domain with the largest increase still being in the Labrador Sea (Fig. 2-4).

From 1945-2010, the subsurface temperature (averaged from 100 to 700 m) increased at a rate of 0.06±0.02°C/decade over the Northwest Atlantic (Fig. 2-2; Table 2-1), except in a couple of local areas: the vicinity of Flemish Cap and southwest of Nova Scotia (Fig. 2-5).

In August, the rate of the surface temperature increase was over 50% larger than that of the annual average for both periods while the difference was smaller for the subsurface temperature (Table 2-2).

Table 2-1 Averages and trends (±two standard errors) of the annual-mean temperature, salinity, vertical density difference, and mixed layer depth in the North Atlantic region (deep ocean >1000m). The density difference is calculated by subtracting the density at the surface from that at 50 m.

	1945-2010	**1981-2010**
Surface temperature (°C)	13.03	13.11
Surface salinity (psu)	34.90	34.91
Surface temperature rate (°C/decade)	0.05±0.04	0.38±0.07
Surface salinity rate (psu/decade)	0.01±0.01	0.05±0.03
Density difference (kg/m^3)	0.41	0.42
Mixed-layer depth (m)	74.3	76.1
Density difference rate (kg/m^3/decade)	0.00±0.01	0.04±0.02
Mixed-layer depth rate (m/decade)	1.3±1.4	-8.4±3.2
100-700 m temperature (°C)	8.91	9.02
100-700 m salinity (psu)	35.30	35.31
100-700 m temperature rate (°C/decade)	0.06±0.02	0.15±0.04
100-700 m salinity rate (psu/decade)	0.01±0.00	0.03±0.01

Table 2-2 Averages and trends (±two standard errors) of the August temperature, salinity, vertical density difference, and mixed layer depth in the North Atlantic region (deep ocean >1000m). The density difference is calculated by subtracting the density at the surface from that at 50 m

	1945-2010	**1981-2010**
Surface temperature (°C)	17.33	17.49
Surface salinity (psu)	34.64	34.66
Surface temperature rate (°C/decade)	0.10±0.06	0.65±0.15
Surface salinity rate (psu/decade)	0.02±0.01	0.05±0.03
Density difference (kg/m^3)	1.26	1.28
Mixed-layer depth (m)	16.2	15.7
Density difference rate (kg/m^3/decade)	0.01±0.01	0.13±0.05
Mixed-layer depth rate (m/decade)	-0.3±0.2	-1.3±0.7
100-700 m temperature (°C)	8.95	9.06
100-700 m salinity (psu)	35.32	35.33
100-700 m temperature rate (°C/decade)	0.07±0.02	0.17±0.04
100-700 m salinity rate (psu/decade)	0.01±0.00	0.03±0.01

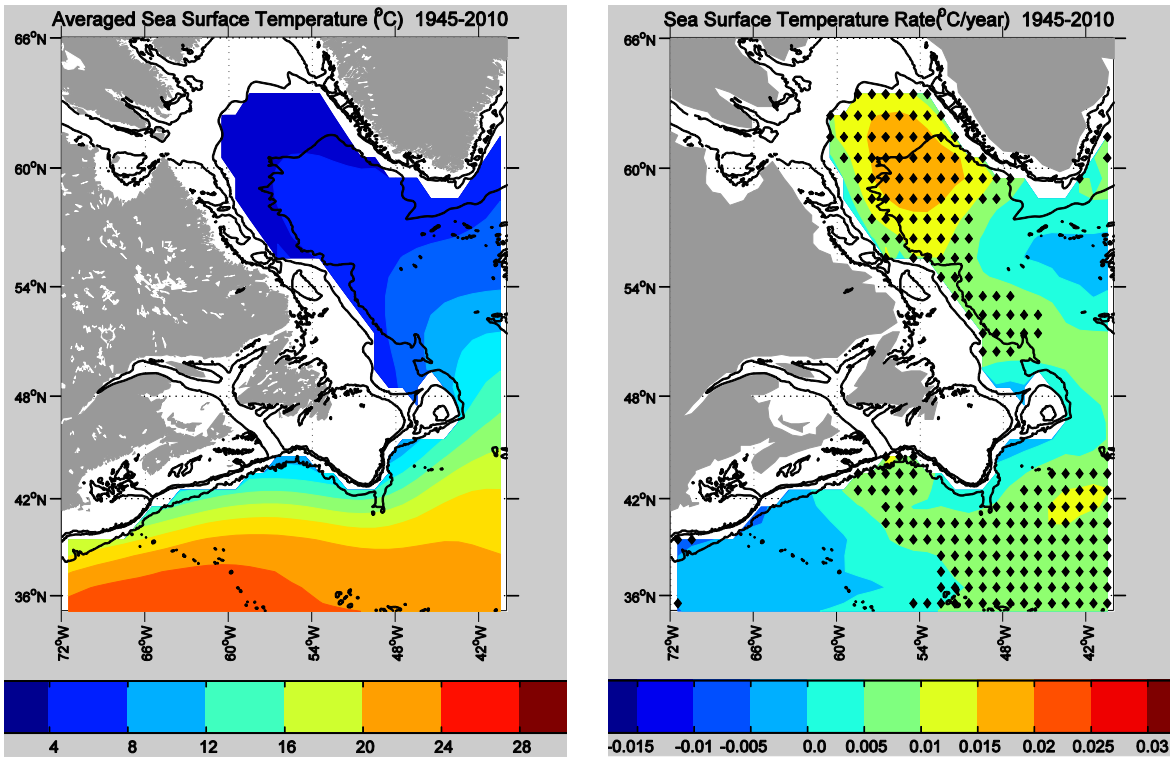

Figure 2-3 The mean surface temperature (top) and the linear trend (bottom) of the annual-mean surface temperature from 1945-2010. The diamonds indicate that the absolute value of the trend is equal or greater than two standard errors. The 200, 1000, and 3000 m isobaths are also depicted.

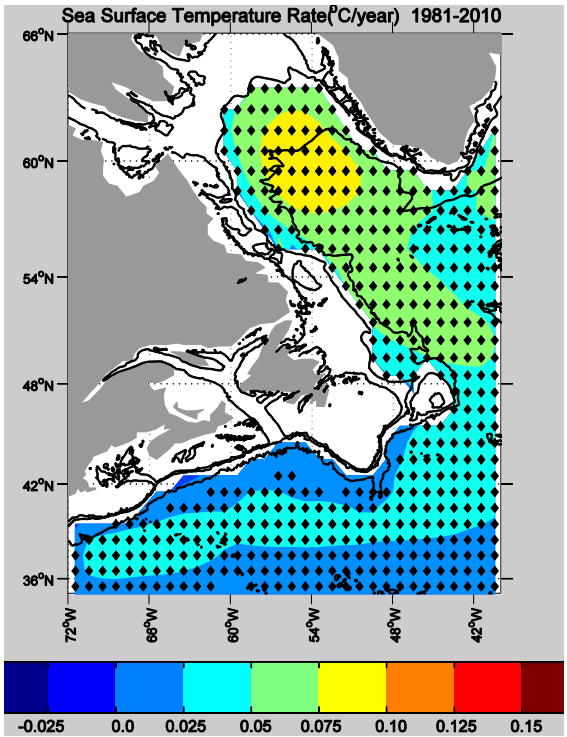

Figure 2-4 The linear trend of the annual-mean surface temperature from 1981-2010. The diamonds indicate that the absolute value of the trend is equal or greater than two standard errors. The 200, 1000, and 3000 m isobaths are also depicted.

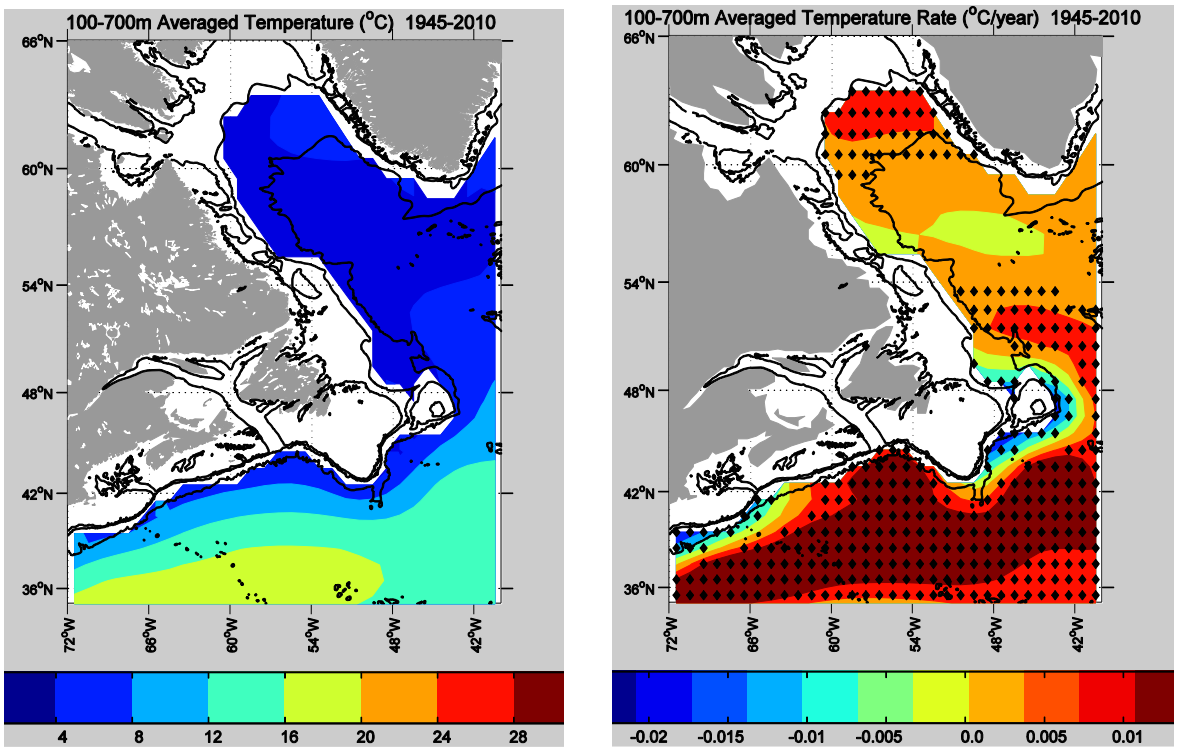

Figure 2-5 The mean subsurface (averaged from 100-700 m) temperature (top) and the linear trend (bottom) of the annual-mean subsurface temperature from 1945-2010. The diamonds indicate that the absolute value of the trend is equal or greater than two standard errors. The 200, 1000, and 3000 m isobaths are also depicted.

Salinity

From 1945-2010, the surface salinity had a mean value of 34.9 psu and an average positive trend of 0.01±0.01 psu/decade in the Northwest Atlantic (Fig. 2-2; Table 2-1). However, the trend is negative over the southern Grand Bank Slope and over the slope southwest of Nova Scotia (Fig. 2-6), which is also seen in Durack *et al.*'s (2012) results.

From 1981-2010, there is an average positive trend of 0.05±0.03 psu/decade in the Northwest Atlantic (Table 2-1). The trend is negative off the southeastern Grand Banks and off Georges Bank (Fig. 2-7).

From 1945-2010, the subsurface salinity (averaged from 100 to 700 m) shows little trend in the Northwest Atlantic (Fig. 2-2; Table 2-1). The trend is positive in the south along the Gulf Stream and in the Labrador Sea, north of 60°N, and negative near Flemish Cap, over the slope southwest of Nova Scotia, and south of Greenland (Fig. 2-8).

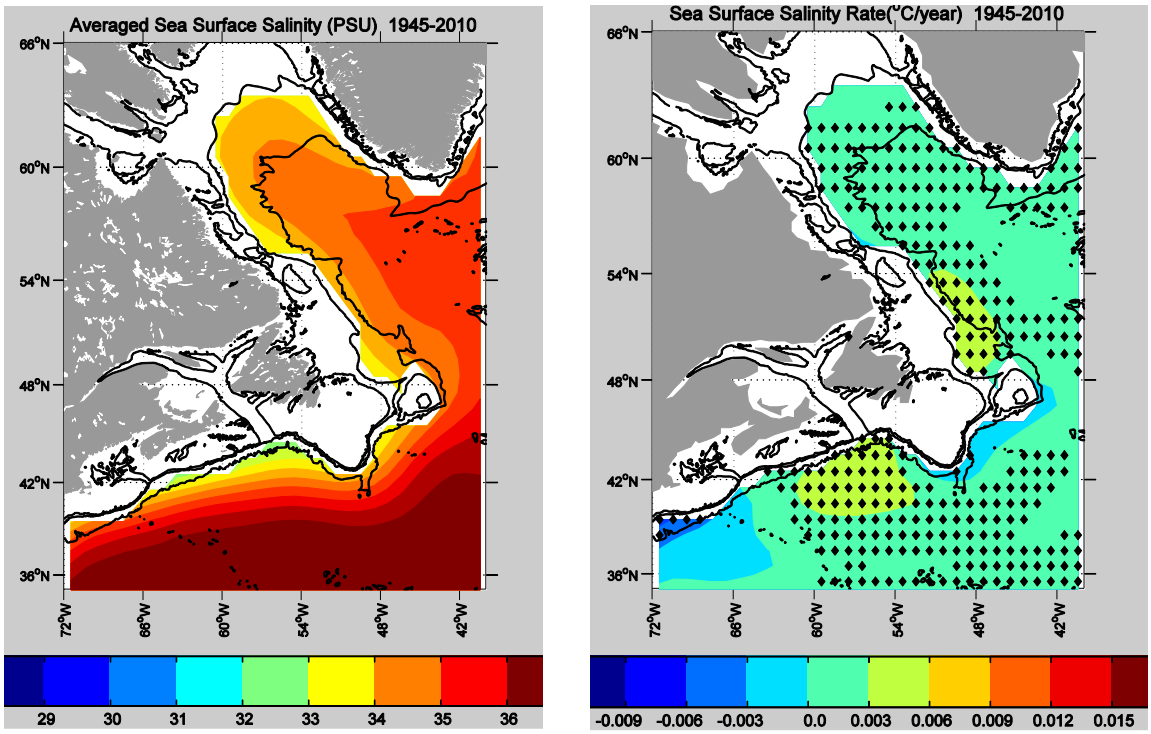

Figure 2-6 The mean surface salinity (top) and the linear trend (bottom) of the annual-mean surface salinity from 1945-2010. The diamonds indicate that the absolute value of the trend is equal or greater than two standard errors. The 200, 1000, and 3000 m isobaths are also depicted.

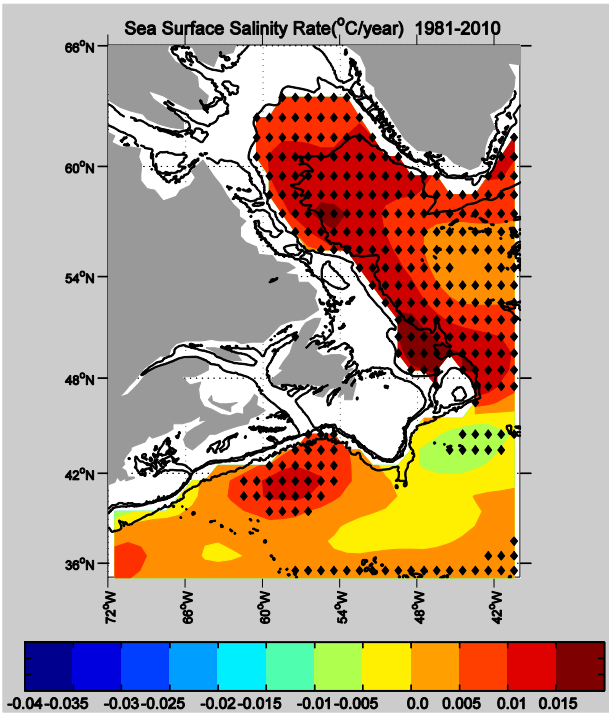

Figure 2-7 The linear trend of the annual-mean sea surface salinity from 1981-2010. The diamonds indicate that the absolute value of the trend is equal or greater than two standard errors. The 200, 1000, and 3000 m isobaths are also depicted.

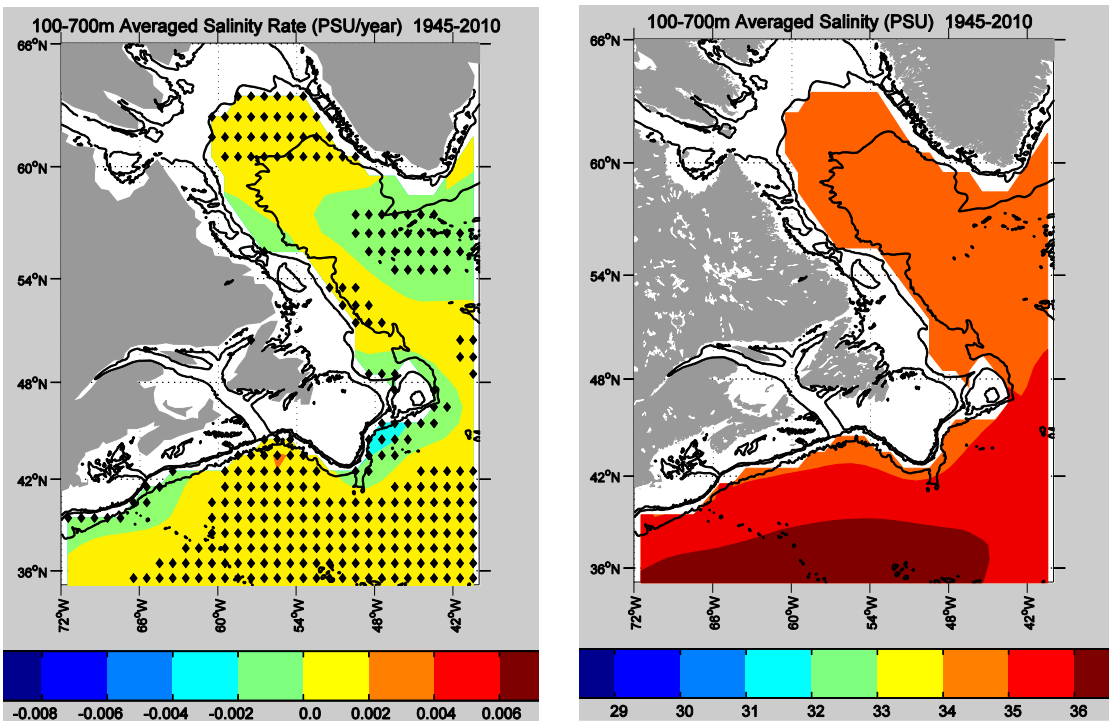

Figure 2-8 The mean subsurface (averaged from 100 to 700 m) salinity (top) and the linear trend (bottom) of the annual-mean subsurface salinity from 1945-2010. The diamonds indicate that the absolute value of the trend is equal or greater than two standard errors. The 200, 1000, and 3000 m isobaths are also depicted.

Density differences

The mean density difference between 50 m and the surface was 0.41 kg/m^3 in the Northwest Atlantic from 1945-2010 (Table 2-1). The difference was 1.26 kg/m^3 in August (Table 2-2). The mean differences were large over the Scotian Slope and Grand Banks Slope (Fig. 2-9).

The density difference shows little trend in the Northwest Atlantic, as a whole, from 1945-2010 (Fig. 2-2, Table 2-1), but positive trends in the Labrador Sea and negative ones along the Gulf Stream (Fig. 2-9). In contrast, there is an overall positive trend of the density difference at an average rate of 0.04±0.02 kg/m^3/decade in the Northwest Atlantic from 1981-2010 (Table 2-1), except northwest of Flemish Cap and off South Greenland (Fig. 2-10).

The density difference trend in August is statistically insignificant from 1945-2010 (Table 2-2). In contrast, the positive trend from 1981-2010 is about three times as large as that of the corresponding annual average.

Mixed-layer depth

The mean mixed-layer depth was 74.3 m in the Northwest Atlantic from 1945-2010 (Table 2-1). The spatial patterns are consistent with those of Zhao *et al.* (2013). The mixed-layer depth from 1945-2010 has a positive, but statistically insignificant, trend of 1.3±1.4 m/decade in the Northwest Atlantic (Fig. 2-2, Table 2-1). The largest increase was along the Gulf Stream. There are negative trends in the Labrador Sea (Fig. 2-11).

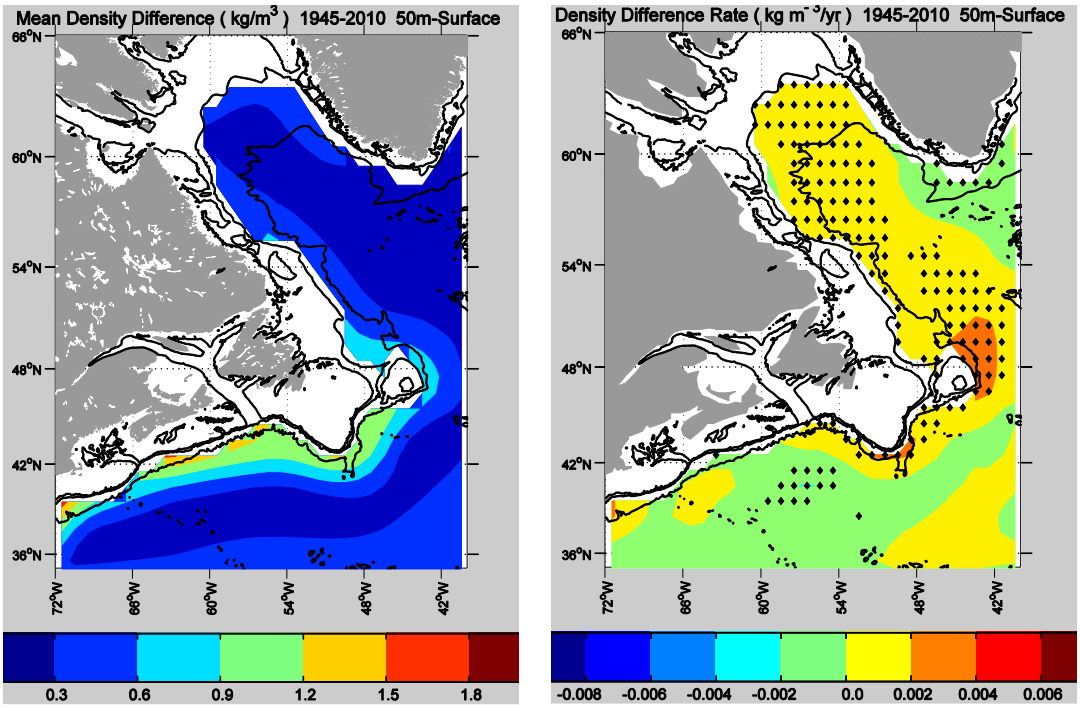

Figure 2-9 The mean density difference (50 m minus surface) (top) and the linear trend (bottom) of the annual-mean density difference from 1945-2010. The diamonds indicate that the absolute value of the trend is equal or greater than two standard errors. The 200, 1000, and 3000 m isobaths are also depicted.

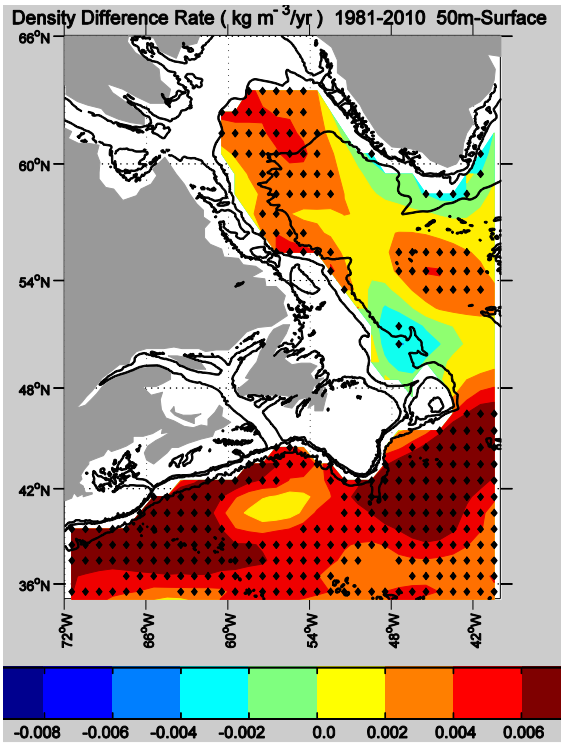

Figure 2-10 The linear trend of the annual-mean density difference (50 m minus surface) from 1981-2010. The diamonds indicate that the absolute value of the trend is equal or greater than two standard errors. The 200, 1000, and 3000 m isobaths are also depicted.

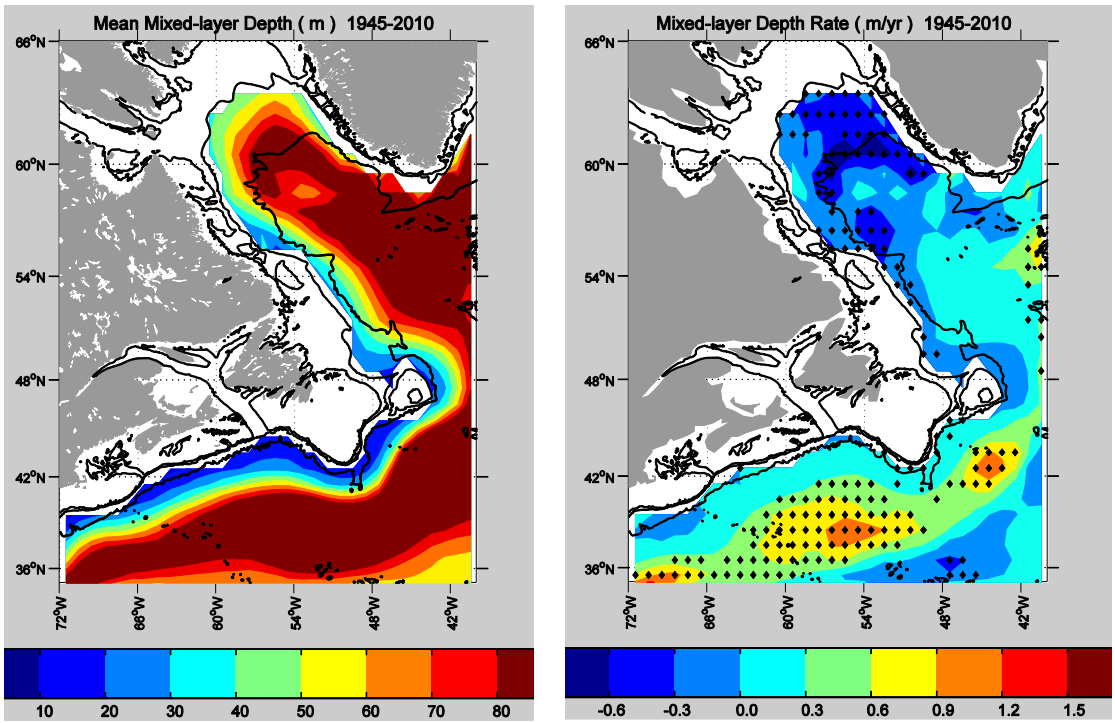

Figure 2-11 The mean mixed-layer depth (top) and the linear trend (bottom) of the annual-mean mixed-layer depth from 1945-2010. The diamonds indicate that the absolute value of the trend is equal or greater than two standard errors. The 200, 1000, and 3000 m isobaths are also depicted.

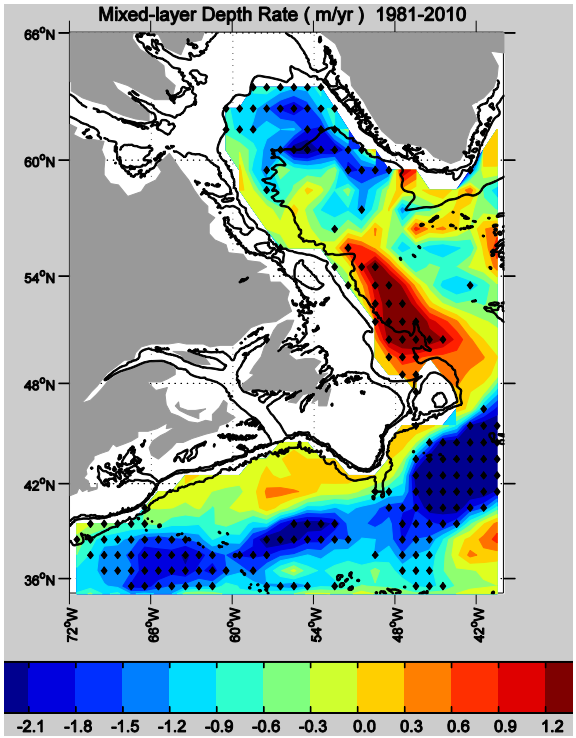

Figure 2-12 The linear trend of the annual-mean mixed-layer depth from 1981-2010. The diamonds indicate that the absolute value of the trend is equal or greater than two standard errors. The 200, 1000, and 3000 m isobaths are also depicted.

From 1981-2010, the mixed-layer depth has a large negative trend of -8.4±3.2 m/decade in the Northwest Atlantic (Table 2-1). The decrease was mainly in the Gulf Stream region and the Labrador Sea (Fig. 2-12). There are significant positive trends in an area northwest of Flemish Cap. There are weak positive trends over the Grand Bank Slope and the Scotian Slope.

The mixed-layer depth in August is about 16 m (Table 2-2). It has negative trends of -0.3±0.2 and -1.3±0.7 m/decade in the Northwest Atlantic for periods 1945-2010 and 1981-2010, respectively (Table 2-2).

2.4 Summary

We have used an updated version of Ishii *et al.*'s (2006) 1°×1° monthly-mean temperature and salinity dataset to examine linear trends of the surface temperature, surface salinity, vertical density difference, and mixed-layer depth over the Northwest Atlantic deep water (deeper than 1000 m).

The surface temperature in the deep Northwest Atlantic increased at an average rate of 0.05±0.04°C/decade from 1945-2010, but it shows cooling over the western Scotian Slope. There was an overwhelming increase of 0.38±0.07°C/decade from 1981-2010, with the largest being in the Labrador Sea. In August, the surface temperature rate is over 50% larger than that of the annual temperature.

The surface salinity increased at a positive rate of 0.01±0.01 psu/decade in the deep Northwest Atlantic from 1945-2010, while showing freshening over the southern Grand Bank Slope and over the slope southwest of Nova Scotia. From 1981-2010 the surface salinity increased at a rate of 0.05±0.03 psu/decade in the Northwest Atlantic, but decreased off the southeastern Grand Banks and off Georges Bank. From 1945-2010, the subsurface salinity (averaged from 100 to 700 m) for the entire domain has no trend, but increased in the south along the Gulf Stream and in the northern Labrador Sea and decreased in the vicinity of Flemish Cap, over the slope southwest of Nova Scotia, and south of Greenland.

There is no trend in the density difference between the 50 m and sea surface in the Northwest Atlantic as a whole, from 1945-2010, but there are positive trends in the Labrador Sea and negative ones along the Gulf Stream. In contrast, the vertical density difference shows a widespread increase at an average rate of 0.04±0.02 kgm^{-3}/decade from 1981-2010. The mixed-layer depth increased along the Gulf Stream but decreased in the Labrador Sea from 1945-2010. It shows an overwhelming decrease in the Northwest Atlantic from 1981-2010, except northwest of Flemish Cap.

Because of the decadal to multidecadal variability described in the Introduction and shown in Figure 4-2, the assumption of uncorrelated errors in the data may lead to the underestimation of the error associated with the trends. Trends identified over 3 or 6.5 decades do not necessarily represent long-term secular changes, but could possibly be part of the multi-decadal variability.

2.5 Acknowledgements

This work was funded by the Aquatic Climate Change and Adaptation Service Program (ACCASP) of Fisheries and Oceans Canada. We thank J. Loder and D. Hebert for providing useful comments and suggestions.

2.6 References

Colbourne, E. B. 2004. Decadal Changes in the Ocean Climate in Newfoundland Waters from the 1950s to the 1990s. *J. Northw. Atl. Fish. Sci.*, 34, 1-19.

Craig J. and D. Gilbert. 2008. Estimation of mixed layer depth at the AZMP fixed stations. Atlantic Zone Monitoring Program Bulletin, 7, 38-42. http://www.meds-sdmm.dfo-mpo.gc.ca/isdm-gdsi/azmp-pmza/docs/bulletin_7_06.pdf

Delworth T. L. and M. E. Mann. 2000. Observed and simulated multidecadal variability in the Northern Hemisphere. *Climate Dynamics*, 16, 661-676.

Durack, P. J., S. E. Wijffels, and R. J. Matear. 2012. Ocean salinities reveal strong global water cycle intensification during 1950 to 2000. *Science*, 336, 455-458.

Galbraith, P. S. and P.. Larouche. 2013. Trends and variability in eastern Canada sea-surface ocean temperatures. Ch. 1 (p. 1-18) *In:* This report.

Häkkinen, S. and P. B. Rhines. 2004. Decline of subpolar North Atlantic circulation during the 1990s. *Science*, 304, 555-559.

Han, G., K. Ohashi, N. Chen, P. G. Myers, N. Nunes, and J. Fischer. 2010. Decline and partial rebound of the Labrador Current 1993-2004: Monitoring ocean currents from altimetric and CTD data. *J. Geophys. Res.*, 115, C12012, doi:10.1029/2009JC006091.

Hebert, D. 2013. Trends in temperature, salinity, density and stratification for different regions in the Atlantic Canadian shelf. Ch. 3 (p. 33-42) *In:* This report.

Hebert, D., R. Pettipas., B. Petrie, and D. Brickman. 2012. Meteorological, Sea Ice and Physical Oceanographic Conditions on the Scotian Shelf and in the Gulf of Maine during 2011. DFO Can. Sci. Advis. Sec. Res. Doc. 2012/055. iv + 42 p. http://www.dfo-mpo.gc.ca/Csas-sccs/publications/resdocs-docrech/2012/2012_055-eng.pdf

Ishii, M., M. Kimoto, K. Sakamoto, and S. Iwasaki. 2006. Steric sea level changes estimated from historical ocean subsurface temperature and salinity analyses. *J. Oceanogr.*, 62, 155-170, doi: 10.1007/s10872-006-0041-y.

Levitus, S. 1982. Climatology atlas of the world ocean. NOAA Professional Paper 13. U. S. Department of Commerce.

Levitus, S., J. I. Antonov, T. P. Boyer, O. K. Baranova, H. E. Garcia, R. A. Locarnini, A. V. Mishonov, J. R. Reagan, D. Seidov, E. S. Yarosh, and M. M. Zweng. 2012. World ocean heat content and thermosteric sea level change (0-2000 m), 1955-2010. *Geophys. Res. Lett.*, 39(10), L10603, doi: 10.1029/2012GL051106

Loder, J. W., Z. Wang, A. van der Baaren and R. Pettipas. 2013. Trends and variability of sea surface temperature in the North Atlantic, from the HadISST, ERSST and COBE datasets. Can. Tech. Rep. Hydrogr. Ocean Sci. 292: viii + 36 p. http://www.dfo-mpo.gc.ca/Library/350066.pdf

Petrie, B. 2007. Does the North Atlantic Oscillation affect hydrographic properties on the Canadian Atlantic continental shelf? *Atmos.-Ocean*, 45, 141-151.

Petrie, B. and K. Drinkwater. 1993. Temperature and salinity variability on the Scotian Shelf and in the Gulf of Maine 1945-1990. *J. Geophys. Res.*, 98, 20709-20089.

Polykov, I. V., V. A. Alexeev, U. S. Bhatt, E. I. Polyakova, and X. Zhang. 2009. North Atlantic warming: patterns of long-term trends and multidecadal variability. *Climate Dynamics*, 34, 459, doi: 10.1007/s00382-008-0522-3.

Thomson, R. and I. V. Fine. 2003. Estimating mixed layer depth from oceanic profile data. *J. Atmos. Oceanic Tech.*, 20, 319-329.

Zhao H., G. Han, and D. Wang. 2013. Timing and magnitude of spring bloom and effects of physical environments over the Grand Banks of Newfoundland. *J. Geophys. Res.*, accepted.

3 Trends in temperature, salinity, and stratification in the upper ocean for different regions of the Atlantic Canadian shelf

Dave Hebert *

Fisheries and Oceans Canada, Bedford Institute of Oceanography
P.O. Box 1006, Dartmouth, Nova Scotia B2Y 4A2

* Correspondence: David.Hebert@dfo-mpo.gc.ca

Suggested Citation:

Hebert, D. 2013. Trends of temperature, salinity and stratification in the upper ocean for different regions of the Atlantic Canadian shelf. Ch. 3 (p. 33-42) *In:* Aspects of climate change in the Northwest Atlantic off Canada [Loder, J.W., G. Han, P.S. Galbraith, J. Chassé and A. van der Baaren (Eds.)]. Can. Tech. Rep. Fish. Aquat. Sci. 3045: x + 190 p.

Abstract

Linear trends in the near-surface and 50 m temperature, salinity, and density for 23 areas of the Atlantic Canadian shelf for the periods 1951-2011 and 1979-2011 were determined. Trends in the stratification, as defined by the difference in density at the surface and 50 m, were also calculated. The Gulf of Lawrence shows a consistent warming over the region for these periods. The surface salinity trend is generally negative over the Scotian Shelf and in the Gulf of St. Lawrence with the exception of the Magdalen region. These trends work in concert to reduce the surface density. Trends in temperature, salinity, and density at 50 m were more variable and less significantly different from zero.

3.1 Introduction

As part of DFO's Aquatic Climate Change Adaptation Services Program (ACCASP), historical trends in oceanographic conditions and predictions of future trends were investigated by multiple investigators, through the production of many reports, including this work in order to assess the magnitude of changes and their spatial variability, and their impacts.

Stratification of the near surface layer influences physical and biological processes in the ocean such as the extent of vertical mixing, the ocean's response to wind forcing, the timing of the spring bloom, vertical nutrient fluxes, and plankton distribution. Under increased stratification, there is a tendency for more primary production to be recycled within the upper mixed layer, and, hence, less available for the deeper layers. As part of the Atlantic Zone Monitoring Program (AZMP), historical variation of stratification, defined as the density difference between the surface and 50 m depth, on the Scotian Shelf has been reported (Hebert *et al.*, 2012). Since temperature and salinity affect density, variations in these quantities were also examined. This report is mainly focused on trends of upper ocean temperature, salinity, and density on the Atlantic Canadian Shelf. Companion reports have reported on trends in other regions on the Atlantic Canadian shelf (Galbraith and Larouche, 2013), Scotian Shelf (Hebert, 2013), and in the open ocean of the Northwest Atlantic (Han *et al.*, 2013; Loder *et al.*, 2013).

3.2 Methods

In order to determine if there are any trends in the upper ocean temperature, salinity, and upper ocean stratification in the shelf areas of the Atlantic Large Aquatic Basin, the hydrographic database 'Climate' was used (Gregory, 2004). The Ocean Science Hydrographic Climate Database (Climate) is a comprehensive, open access collection of temperature and salinity data for the Northwest Atlantic and Eastern Arctic, an area defined by 35°N-80°N and 42°W-100°W. The data come from a variety of sources including hydrographic bottles, Conductivity Temperature Depth (CTD) casts, profiling floats, spatially and temporally averaged Batfish tows, and expendable, digital or mechanical bathythermographs. Near real-time observations of temperature and salinity from the Global Telecommunications System (GTS) are also included. The database currently consists of approximately 850,000 profiles and 35 million individual observations from 1910 to 2009. As a first step, it was decided to look for trends for several previously defined boxes, the so-called AZMP 'Petrie' boxes (Figure 3-1). This report describes the results for these regions. A query was made to Climate to obtain the monthly averaged temperature, salinity, and density (sigma-t) at 0 m and 50 m for the period 1951-2009. Climate has not been updated since the end of 2009. These two depths were chosen since a stratification index used in AZMP reporting (e.g., Hebert *et al.*, 2012) uses the density difference between these two depths.

Determination of annual mean values is not straight-forward because of unequal temporal sampling from year to year. The following procedure was adopted. The monthly anomalies from the monthly 1951-2009 mean values were determined first and then averaged to estimate an annual anomaly. The number of monthly values used for each annual anomaly varies spatially and temporally. For example, the Hudson Strait, Nain, and Bravo regions (Figure 3-1) have an average of one month or less each year whereas the Avalon and Central Scotian Shelf regions average more than six months per year. The remainder of the regions usually have three or more monthly anomalies each year on average. Finally, the annual 1951-2009 mean based on the monthly means was added to these annual anomalies to determine an annual mean. These estimates could be biased if, in a particular year, most data were collected in months when anomalies are generally small, while in another year, sampling was in months when anomalies are generally large. For the stratification index, the difference between the surface and 50 m sigma-t divided by 50 m was determined for each profile first. The annual stratification was determined using the same procedure.

For the periods 1951-2009 and 1979-2009, linear trends were determined using the Matlab® routine 'regress'. The 1951-2009 period was chosen for the longest period with sufficient sampling. The 1979-2009 period approximately represents the last three decades. The p-value, a measure of how much the trend is significantly different from zero, was determined. The figures to follow show the trend (positive red; negative blue) for each region and parameter as bar graphs. For each region, the left bar is for 1951-2009 and the right bar for 1979-2009. The bar's height is proportional to the magnitude of the trend. A scale is provided at the bottom centre of the figure. The intensity of the red (blue) within each bar is an indication of the log of the p-value with higher intensities indicative of trends more significantly different from zero (e.g. significance levels of 0.1 and 0.01 correspond to log scale values of -1 and -2). It should be noted that the Matlab® routine assumes that the number of degrees of freedom is N-2. If the time series has a decorrelation scale greater than a year, the effective number of degrees of freedom would

be smaller and the confidence limited presented overestimated. A proper estimate of the significance of the trend of any autocorrelated series is beyond the scope of this paper.

Figure 3-1 Pre-defined polygons used to determine the monthly averaged hydrographic properties from the 'Climate' hydrographic database (Avalon: Avalon Channel; Bravo: Central Labrador Sea; Cabot: Cabot Strait; CSS: Central Scotian Shelf; ESS: Eastern Scotian Shelf; Estuary: St. Lawrence Estuary; Flemish: Flemish Pass; Fundy: Bay of Fundy; Georges: Georges Bank; Hamilton: Hamilton Bank; Hudson: Hudson Strait; Lurcher: Lurcher Shoals; Magdalen: Magdalen Shallows: NEGSL: Northeast Gulf of St. Lawrence; NENFS: Northeast Newfoundland Shelf; NWGSL: Northwest Gulf of St. Lawrence; SEShoal: Southeast Shoal; StAnth: St. Anthony; St. Pierre: St. Pierre Bank; WBank: Western Bank; WSS: Western Scotian Shelf).

3.3 Results

The linear trends in surface temperature vary over the Atlantic Basin and for the 1951-2009 and 1979-2009 periods (Fig. 3-2). The Gulf of Lawrence shows a consistent warming over the region for these periods. Flemish Pass shows a negative trend for the 1951-2009 period. In general, the Newfoundland and Labrador shelves show a positive trend. The surface salinity trend is generally negative over the Scotian Shelf and in the Gulf of St. Lawrence with the exception of the Magdalen Shallows. These temperature and salinity trends work in conjunction to reduce the surface density (Fig. 3-2). Tables 3-1 and 3-2 list those trends that are significantly different from zero at the 95% confidence limit.

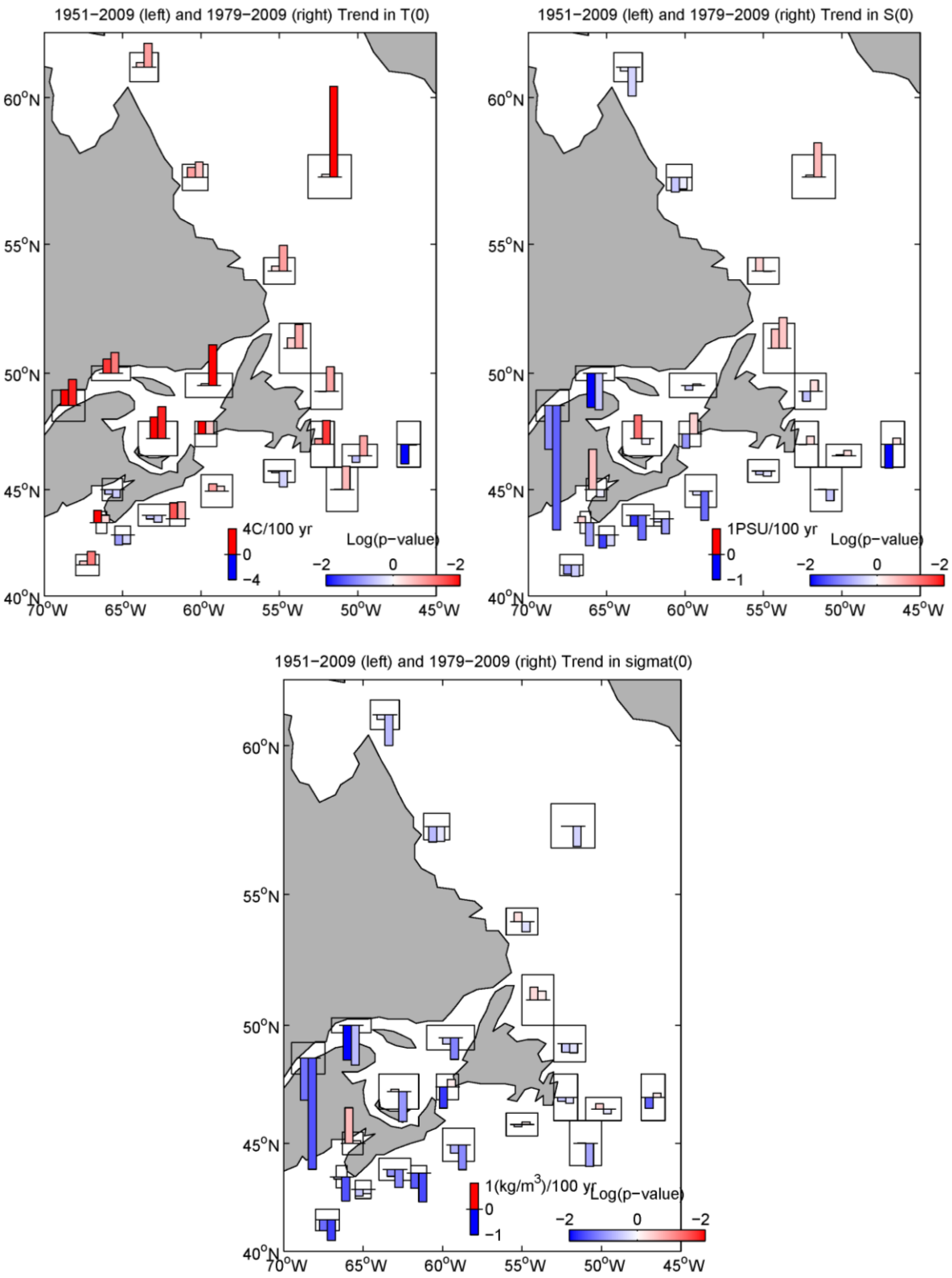

Figure 3-2 Surface temperature, salinity, and density trend for the 1951-2009 and 1979-2009 periods. The size of the bar is proportional to the trend. The intensity of the colour of the bar (red for increasing trend; blue for decreasing trend) indicates the p-value.

At 50 m depth, the trends are generally more variable and fewer are significantly different from zero (Fig. 3-3). The Labrador Sea (Bravo region) shows significant warming trends for both periods with the larger trend for the 1979-2009 period. For this period, there are also significant warming trends for Hudson Strait and St. Anthony regions (Table 3-2). There are general negative trends in the salinity at 50 m for the western Scotian Shelf, St. Lawrence Estuary, and Labrador coast. The Labrador Sea features an increase in salinity for the 1979-2009 period. There is a general decrease in density at 50 m across the zone but the significance level is low (Fig. 3-3).

Table 3-1 Trends in temperature (T in °C/decade), salinity (S in units/decade), density (D in (kg/m^3)/decade) at the surface and 50 m, and the density difference (ΔD in (kg/m^3)/decade) for regions which had trends significantly different from zero at the 95% confidence limit (p<0.05) for the 1951-2009 period.

Region	T(0m)	S(0m)	D(0m)	T(50m)	S(50m)	D(50m)	ΔD
Nain					-0.052	-0.039	
Central Labrador Sea (Bravo)				0.14		-0.015	
Avalon Channel							0.030
Flemish	-0.29	-0.087	-0.039	-0.41	-0.069	-0.024	0.078
Cabot Strait	0.18		-0.076				
Northeast Gulf of St. Lawrence				-0.19			
Northwest Gulf of St. Lawrence	0.19	-0.12	-0.12				-0.089
St. Lawrence Estuary	0.22		-0.15				-0.38
Magdalen Shallows	0.31	0.083					-0.14
Western Bank	0.24		-0.058				
Central Scotian Shelf		-0.042					-0.075
Western Scotian Shelf		-0.051		-0.28	-0.073		
Lurcher Shoals	0.18						0.15
Bay of Fundy							0.13
Georges Bank			-0.043				0.16

Table 3-2 Trends in temperature (T in °C/decade), salinity (S in units/decade), density (D in (kg/m^3)/decade) at the surface and 50 m, and the density difference (ΔD in (kg/m^3)/decade) for regions which had trends significantly different from zero at the 95% confidence limit (p<0.05) for the 1979-2009 period.

Region	T(0m)	S(0m)	D(0m)	T(50m)	S(50m)	D(50m)	ΔD
Hudson Strait				0.25			
Central Labrador Sea (Bravo)	0.99			0.59	0.076		
Hamilton Bank							0.078
St. Anthony				0.17			0.12
Northeast Newfoundland Shelf							0.14
Avalon Channel	0.34						
Flemish Pass							0.15
Southeast Shoal							0.16
Cabot Strait							0.16
Northeast Gulf of St. Lawrence	0.55						0.13
St. Lawrence Estuary	0.36	-0.46	-0.40		-0.18	-0.15	
Magdalen Shallows	0.45						
Eastern Scotian Shelf		-0.11					0.13
Western Bank			-0.11				0.10
Central Scotian Shelf		-0.096					
Western Scotian Shelf							0.094
Lurcher Shoals			-0.09				0.16
Bay of Fundy							0.14
Georges Bank			-0.08				0.17

The stratification index, based on the difference in density at the surface and 50 m, shows a significant trend over the eastern and western parts of our region (Fig. 3-4). A trend of 0.02 (kg/m^4)/century is equivalent to a density difference trend of 0.1 (kg/m^3)/decade. There is an increase in the stratification for both periods for the eastern Gulf of St. Lawrence, western Scotian Shelf, Gulf of Maine, Bay of Fundy, Newfoundland, and Labrador regions. For the St. Lawrence Estuary, central Scotian Shelf, and eastern Scotian Shelf, the trend in stratification for the 1951-2009 period was decreasing while it was increasing for the 1979-2009 period. This is indicative of the interdecadal variability in the surface density via the surface salinity (Fig.3-2). Even though the trend is generally decreasing for both periods, the amplitude of the trend is different.

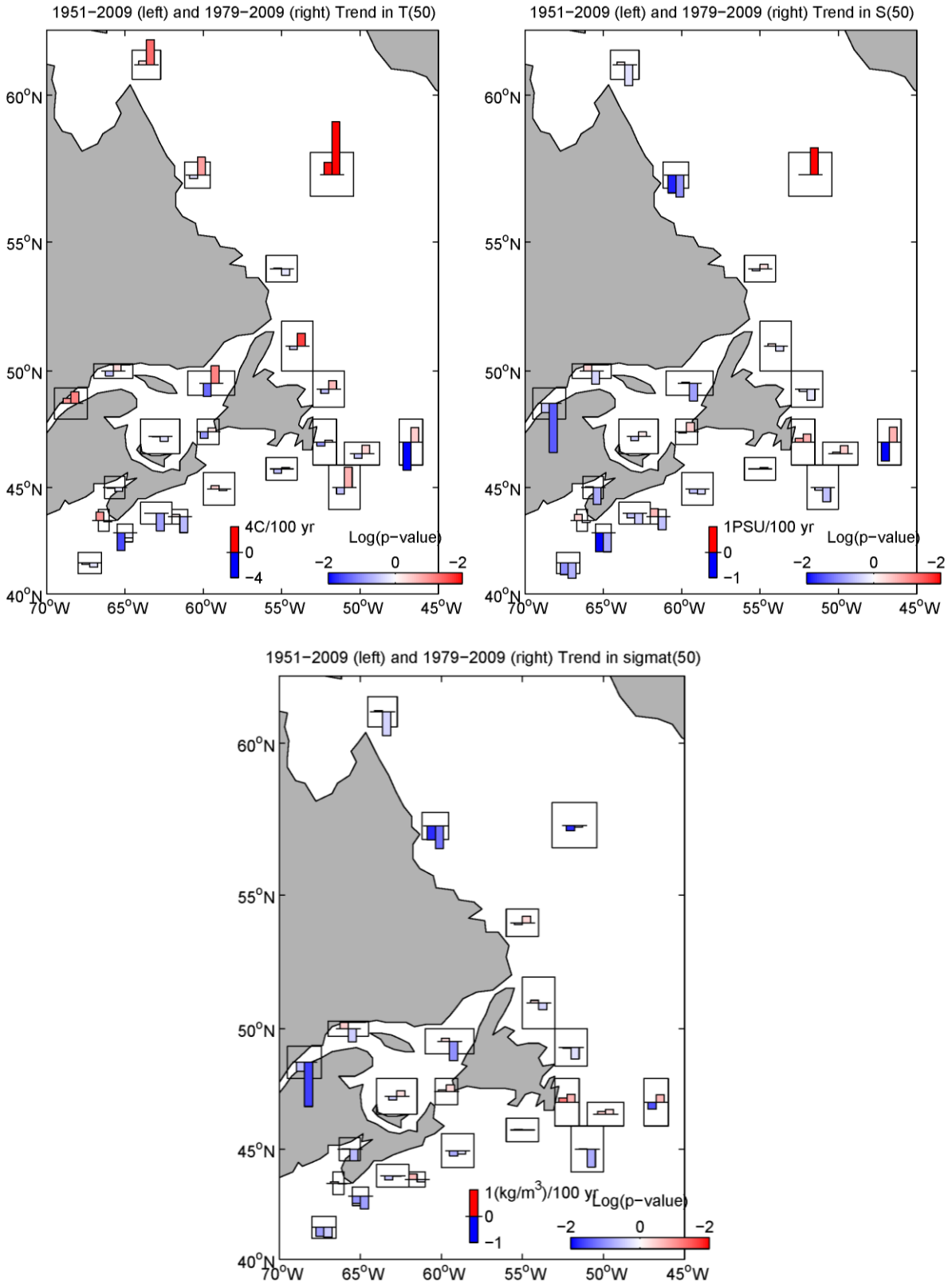

Figure 3-3 Temperature, salinity, and density trend at 50 m for the 1951-2009 and 1979-2009 periods. The size of the bar is proportional to the trend. The intensity of the colour of the bar (red for increasing trend; blue for decreasing trend) indicates the p-value.

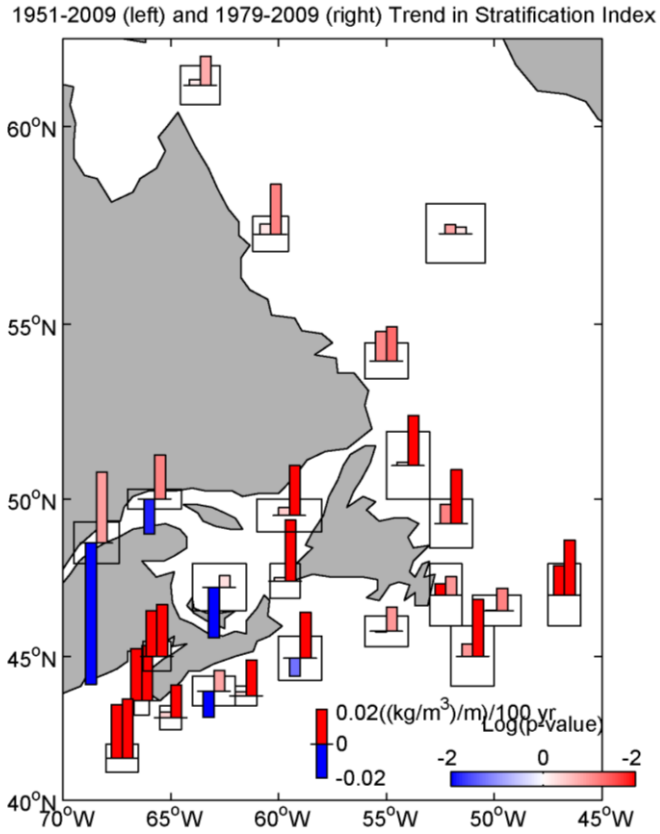

Figure 3-4 Stratification index trend ((kg/m^3)/century) for the 1951-2009 and 1979-2009 periods. The size of the bar is proportional to the trend. The intensity of the colour of the bar (red for increasing trend; blue for decreasing trend) indicates the p-value.

3.4 Summary

Linear trends in the near-surface and 50 m temperature, salinity, and density for several regions in the Atlantic Basin for the periods 1951-2009 and 1979-2009 were determined. Trends in the stratification, as defined by the difference in density at the surface and 50 m, were also calculated. The Gulf of Lawrence shows a consistent warming over the region for these periods. Avalon Channel and the central Labrador Sea (Bravo) have significant positive trends for the 1979-2009 period. The surface salinity trend is generally negative over the Scotian Shelf and in the Gulf of St. Lawrence with the exception of the Magdalen Shallows, Cabot Strait, and Flemish Pass (Table 3-1). These temperature and salinity trends work in conjunction to reduce the surface density. Trends in temperature, salinity and density at 50 m were more variable and less frequently significantly different from zero. Hudson Strait, central Labrador Sea and St. Anthony have large significant warming trends for the 1979-2009 period (Table 3-2). The central Labrador Sea also had a positive trend in salinity for this period. Flemish Pass and Western Scotian Shelf had negative trends in both temperature and salinity for this period that were not significant at the 95% confidence limit but produced a significant change in the stratification.

The trend in stratification was positive for the whole region for the 1979-2009 period. This was also positive for the 1951-2009 period except for the western Gulf of St. Lawrence, St. Lawrence estuary, and central Scotian Shelf where there was a significant decrease in stratification. In a companion report looking at areas on the Scotian Shelf (Hebert, 2013), there is general agreement with the trends here but not an exact correspondence. This is due to the differences in the amount of data and spatial variability used in determining the annual anomalies and the difference in the periods used for determining the trends.

There is significant interannual variability in the temperature, salinity, and density of the waters on the Atlantic Canadian Shelf by a wide range of processes. For the Scotian Shelf, Petrie and Drinkwater (1993) found that this variability was related to changes in the strength of the westward flow of the Labrador Current and inversely related to the temperature and salinity of the Labrador Current. In other words, when the Labrador Current transport increased, its salinity and temperature increased. The temperature and salinity of the Labrador Current were still less than the waters found on the Scotian Shelf. Using Empirical Orthogonal Function Analysis, Loder et al (2013) found that there is spatially-variable decadal variability in sea surface temperature off Atlantic Canada that appears to be related to each of the North Atlantic Oscillation and the Atlantic Multi-decadal Oscillation (AMO). Depending on the phase of this variability, the location and the length of the period used, the determined trends can vary significantly. The stratification in the Gulf of St. Lawrence and St. Lawrence Estuary is greatly influenced by freshwater discharges in the region. As well, the annual May-November average of the GSL surface water temperature was found to be well correlated with April-November average air temperature over the GSL by Galbraith et al (2012). Depending on the phase of this variability and the length of the period used, the determined trends can vary significantly.

3.5 Acknowledgements

Generation of the monthly anomalies of salinity, temperature, density, and stratification index was by Roger Pettipas as part of the Atlantic Zone Monitoring Program. Thanks to Guoqi Han, John Loder, and Brian Petrie for many comments and suggestions on this manuscript which greatly improved it.

3.6 References

Galbraith, P. S. and P.. Larouche. 2013. Trends and variability in eastern Canada sea-surface ocean temperatures. Ch. 1 (p. 1-18) *In:* This report.

Galbraith, P.S., P. Larouche, J. Chasse and B. Petrie, 2012. Sea-surface temperature in relation to air temperature in the Gulf of St. Lawrence: interdecadal variability and long term trends. *Deep Sea Res. II*, V77–80, 10–20.

Gregory, D. N. 2004. Climate: a database of temperature and salinity Ooservations for the Northwest Atlantic. DFO Can. Sci. Advis. Sec. Res. Doc. 2004/075. http://www.dfo-mpo.gc.ca/CSAS/Csas/DocREC/2004/RES2004_075_e.pdf

Han, G., Z. Ma, and H. Bao. 2013. Trends of temperature, salinity, stratification and mixed-layer depth in the Northwest Atlantic. Ch. 2 (p. 19-32) *In:* This report.

Hebert, D. 2013. Trends in temperature, salinity and stratification in the upper ocean for the Scotian Shelf. Ch. 4 (p. 43-56) *In:* This report.

Hebert, D., R. Pettipas, B. Petrie, and D. Brickman. 2012. Meteorological, Sea Ice and Physical Oceanographic Conditions on the Scotian Shelf and in the Gulf of Maine during 2011. DFO Can. Sci. Advis. Sec. Res. Doc. 2012/055. iv + 42 p. http://www.dfo-mpo.gc.ca/Csas-sccs/publications/resdocs-docrech/2012/2012_055-eng.pdf

Loder, J.W., Z. Wang, A. van der Baaren and R. Pettipas. 2013. Trends and variability of sea surface temperature in the Northwest Atlantic, from the HadISST1, ERSST and COBE datasets. Can. Tech. Rep. Hydrogr. Ocean Sci. 292: viii + 36 p. http://www.dfo-mpo.gc.ca/Library/350066.pdf

Petrie, B. and K. Drinkwater. 1993. Temperature and salinity variability on the Scotian Shelf and in the Gulf of Maine 1945-1990. *J. Geophys. Res.*, 98, 20079-20089.

4 Trends in temperature, salinity, density, and stratification in the upper ocean for the Scotian Shelf

Dave Hebert *

Fisheries and Oceans Canada, Bedford Institute of Oceanography
P.O. Box 1006, Dartmouth, Nova Scotia B2Y 4A2

* Correspondence: David.Hebert@dfo-mpo.gc.ca

Suggested Citation:

Hebert, D. 2013. Trends of temperature, salinity, density and stratification in the upper ocean for the Scotian Shelf. Ch. 4 (p. 43-56) *In:* Aspects of climate change in the Northwest Atlantic off Canada [Loder, J.W., G. Han, P.S. Galbraith, J. Chassé and A. van der Baaren (Eds.)]. Can. Tech. Rep. Fish. Aquat. Sci. 3045: x + 190 p.

Abstract

Trends in the near surface temperature, salinity, and density in twenty-nine subareas on the Scotian Shelf, for the periods 1951-2011 and 1979-2011, were determined. Similarly, the trends in these properties at 50 m depth were determined. Finally, trends in the stratification, as defined by the difference in density at the surface and 50 m, were calculated. For both periods, the trends in surface temperature are generally positive. The surface salinity trends are generally negative. These trends lead to a trend of decreasing surface density. Trends in temperature, salinity, and density at 50 m were more variable and less significantly different from zero. The trend in stratification was positive for the whole region.

4.1 Introduction

As part of DFO's Aquatic Climate Change Adaptation Services Program (ACCASP), historical trends in oceanographic conditions were investigated by multiple investigators, through the production of many reports, including this work in order to assess the magnitude of changes and their spatial variability, and their impacts.

Stratification of the near surface layer influences physical and biological processes in the ocean such as the extent of vertical mixing, the ocean's response to wind forcing, the timing of the spring bloom, vertical nutrient fluxes, and plankton distribution. Under increased stratification, there is a tendency for more primary production to be recycled within the upper mixed layer and hence less available for the deeper layers. As part of the Atlantic Zone Monitoring Program (AZMP), the historical variation of stratification, defined as the density difference between the surface and 50 m depth, on the Scotian Shelf has been reported (Hebert *et al.*, 2012). Because temperature and salinity affect density, variations in these quantities were also examined. This report is mainly focused on trends of upper ocean temperature, salinity, and density on the Scotian Shelf. Companion reports describe trends in other regions on the Atlantic Canadian shelf (Galbraith and Larouche, 2013; Hebert, 2013) and in the open ocean of the Northwest Atlantic (Han *et al.*, 2013; Loder *et al.*, 2013).

4.2 Methods

In order to determine if there are any trends in these variables, data from polygons defined by Drinkwater and Trites (1987) were analysed (Fig. 4-1). For data collected before 2010, the hydrographic database 'Climate' was used (Gregory, 2004). The Ocean Science Hydrographic Climate Database (Climate) is a comprehensive, open access collection of temperature and salinity data for the Northwest Atlantic and Eastern Arctic, an area defined by 35°N-80°N and 42°W-100°W. The data come from a variety of sources including hydrographic bottles, Conductivity Temperature Depth (CTD) casts, profiling floats, spatially and temporally averaged Batfish tows, and expendable, digital or mechanical bathythermographs. The database currently consists of approximately 850,000 profiles and 35 million individual observations from 1910 to 2009. Climate has not been updated since the end of 2009. For data from 2010 and later, a local database of hydrographic data is maintained using data from DFO's Integrated Science Data Management (ISDM) which is the Canadian National Ocean Data Centre, and other sources such as the U.S. National Marine Fisheries Service. Monthly averaged temperatures, salinities, and densities (sigma-t) at 0 m and 50 m were determined for each polygon from these data as well as the average for the Scotian Shelf (SS; region enclosed by the thick line in Fig. 4-2).

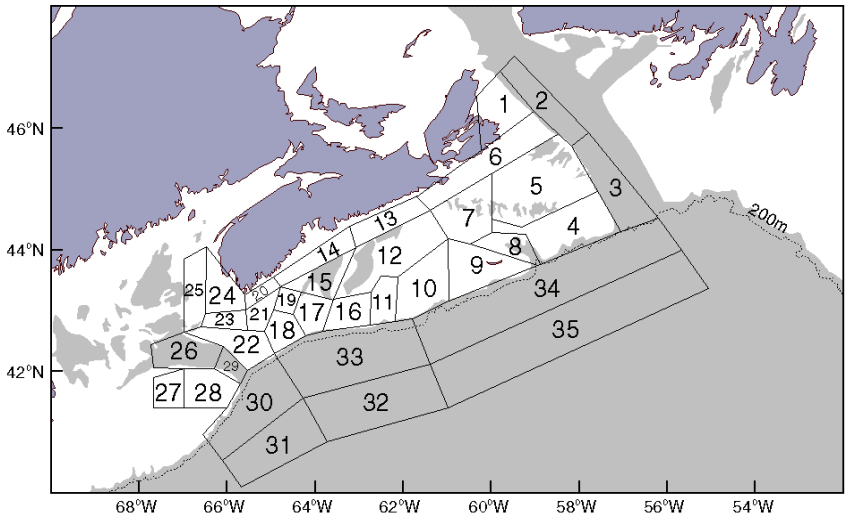

1. Sydney Bight
2. N. Laurentian Channel
3. S. Laurentian Channel
4. Banquereau
5. Misaine Bank
6. Canso
7. Middle Bank
8. The Gully
9. Sable Island
10. Western Bank
11. Emerald Bank
12. Emerald Basin
13. Eastern Shore
14. South Shore
15. Lahave Basin
16. Saddle
17. Lahave Bank
18. Baccaro Bank
19. Roseway Bank
20. Shelburne
21. Roseway Basin
22. Browns Bank
23. Roseway Channel
24. Lurcher Shoals
25. E. Gulf of Maine
26. Georges Basin
27. Georges Shoal
28. E. Georges Bank
29. N.E. Channel
30. Southern Slope
31. Southern Offshore
32. Central Offshore
33. Central Slope
34. Northern Slope
35. Northern Offshore

Figure 4-1 Areas on the Scotian Shelf (SS) and eastern Gulf of Maine from Drinkwater and Trites (1987).

Determination of annual mean values is not straight-forward because of unequal temporal sampling from year to year. The following procedure was adopted. The monthly anomalies from the monthly 1981-2010 mean values were determined first and then averaged to estimate an annual anomaly. The 1981-2010 period is the reference presently used by AZMP for determining anomalies. The number of monthly values used for each annual anomaly varies spatially and temporally. For example, the Sydney Bight, Laurentian Channel, LaHave Basin, and Baccaro Bank regions (Fig. 4-1) have an average of two months each year. The South Shore, Emerald Bank, and Emerald Basin regions have four to six months per year on average. Georges Bank and Georges Basin have five to six monthly anomalies on average from 1951-2011. The average increases to seven to eight monthly anomalies for 1979-2011. Finally, the annual 1981-2010 mean was added to these annual anomalies to determine an annual mean. These estimates could be biased if, in a particular year, most data were collected in months when anomalies are generally small, while in another year, sampling was in months when anomalies are generally large. For the stratification index, the difference between the surface and 50 m sigma-t divided by 50 m was determined for each profile first. The annual stratification was determined using the same procedure.

For the periods 1951-2011 and 1979-2011, linear trends were determined for each parameter using the Matlab® routine 'regress'. The 1951-2011 period was chosen for the longest period with sufficient sampling. The 1979-2011 period represents the last approximate three decades. The p-value, a measure of how much the trend is significantly different from zero, was determined. The following figures show the trend (positive is red; negative is blue) for each region and an area-weighted average of areas 4 to 23 as bar graphs. The height of the bar is proportional to the magnitude of the trend. A scale is provided at the bottom right of the figure. The intensity of the red (blue) within each bar is an indication of the log of the p-value with higher intensities indicative of trends more significantly different from zero (e.g. a significance level of 0.1 and 0.01 corresponds to a log value of -1 and -2). It should be noted that the Matlab® routine assumes that the number of degrees of freedom is N-2. If the time series have decorrelation scales greater than a year, the effective number of degrees of freedom would be smaller and the confidence limits presented overestimated. A proper estimate of the significance of the trend of any autocorrelated series is beyond the scope of this paper.

4.3 Results

1951-2011

The trend in surface temperature is generally positive over the 1951-2011 period with the largest changes in southwest Nova Scotia (e.g., Roseway Channel, Roseway Basin, Georges Basin and Georges Shoal, and the eastern Scotian Shelf (SS) (Fig. 4-2). The surface salinity trend is generally negative with significant trends in regions similar to the temperature trends (Fig. 4-3). These trends work in conjunction to provide a negative trend in the surface density (Fig. 4-4). The SS average (subareas 4-23) trend in surface temperature is 1.0°C/century (p=0.06); for surface salinity, it is -0.3 /century (p=0.03); and for density, -0.5 (kg/m^3)/century (p=0.004) Table 4-1 lists those trends that are significantly different from zero at the 95% confidence limit.

The trends in temperature, salinity and density at 50 m are more variable and less frequently significantly different from zero (Figs. 4-5, 4-6 and 4-7). The temperature trends are positive in

the western part of the domain and negative in the eastern part (Fig. 4-5). There are no significant trends in the SS average temperature (p=0.71), salinity (p=0.62), and density (p=0.48) at 50 m. The stratification index, based on the difference in density at the surface and 50 m, shows a significant trend over the eastern and western parts of our region (Fig. 4-8).

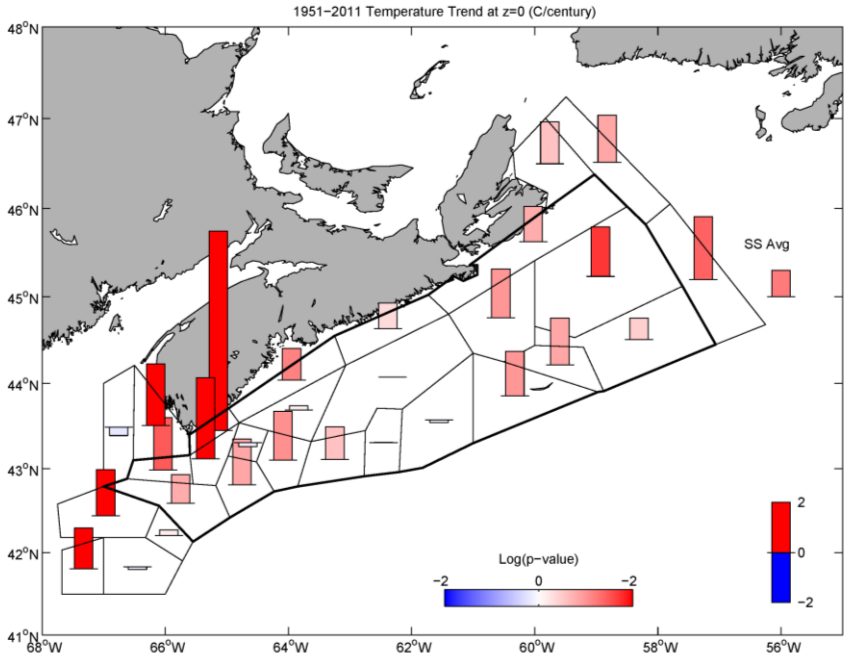

Figure 4-2 Surface temperature trend (°C/century) for 1951-2011. The size of the bar is proportional to the trend. The intensity of the colour of the bar (red for increasing trend; blue for decreasing trend) indicates the p-value. The Scotian Shelf (SS) average trend is shown to the right of the SS.

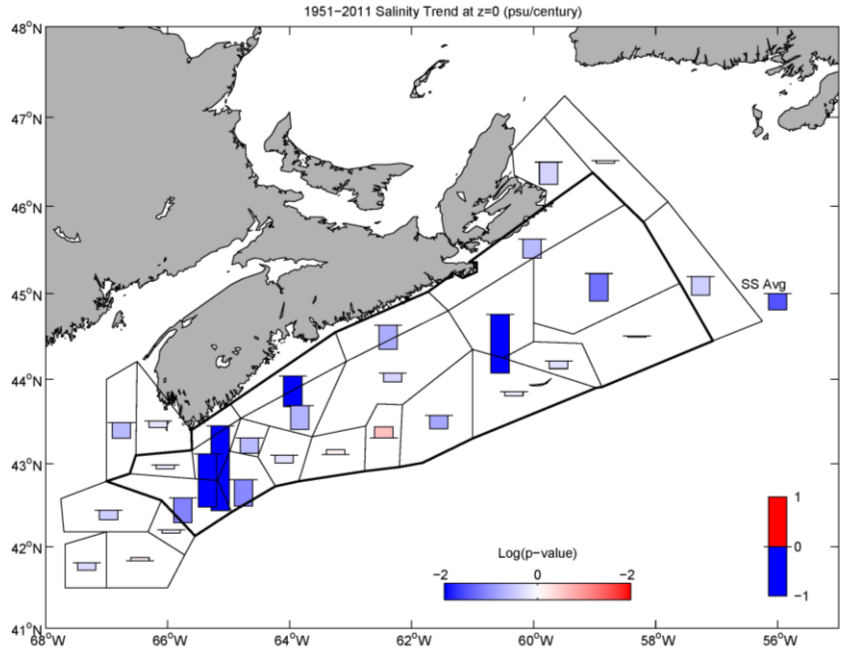

Figure 4-3 Surface salinity trend (/century) for 1951-2011, using the same display format as Fig. 4-2.

The SS average trend is 0.0123 (kg/m^4)/century (p=0.00022), which is equivalent to a change in density between 0 and 50 of 0.06 (kg/m^3)/decade, and is due to a decrease in surface density associated with approximately equal parts of the effects of temperature and salinity changes.

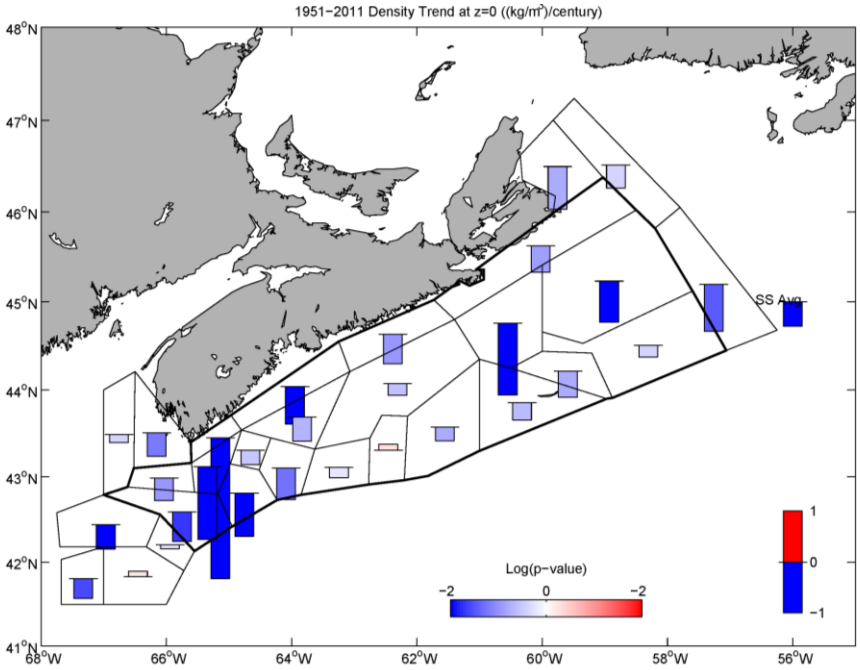

Figure 4-4 Surface density trend ((kg/m^3)/century) for 1951-2011. The size of the bar is proportional to the trend, and the intensity of its colour (red for increasing trend, blue for decreasing) indicates the p-value. The SS average trend is shown to the right of the SS.

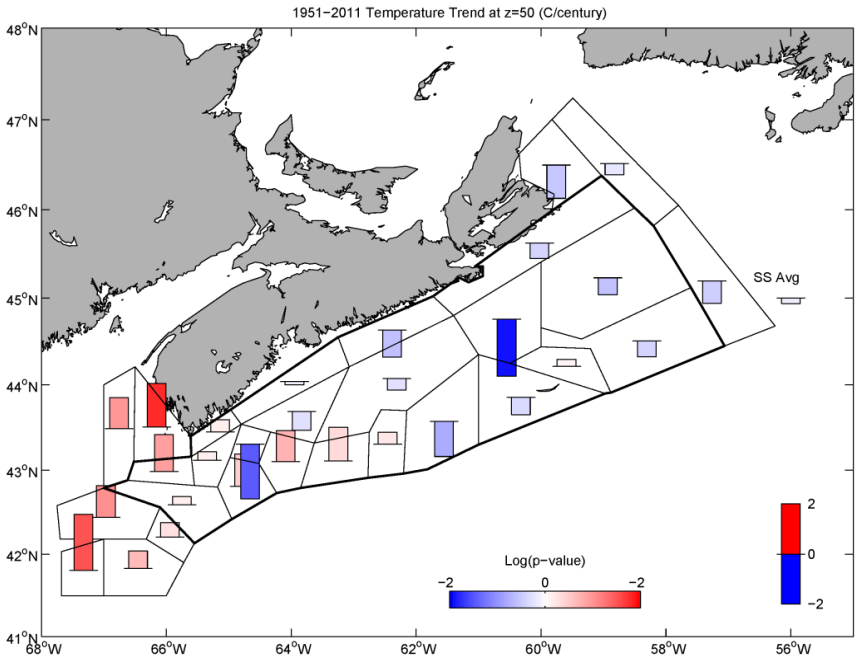

Figure 4-5 Temperature trend (°C/century) at 50 m for 1951-2011, using the same format as Fig. 4-4.

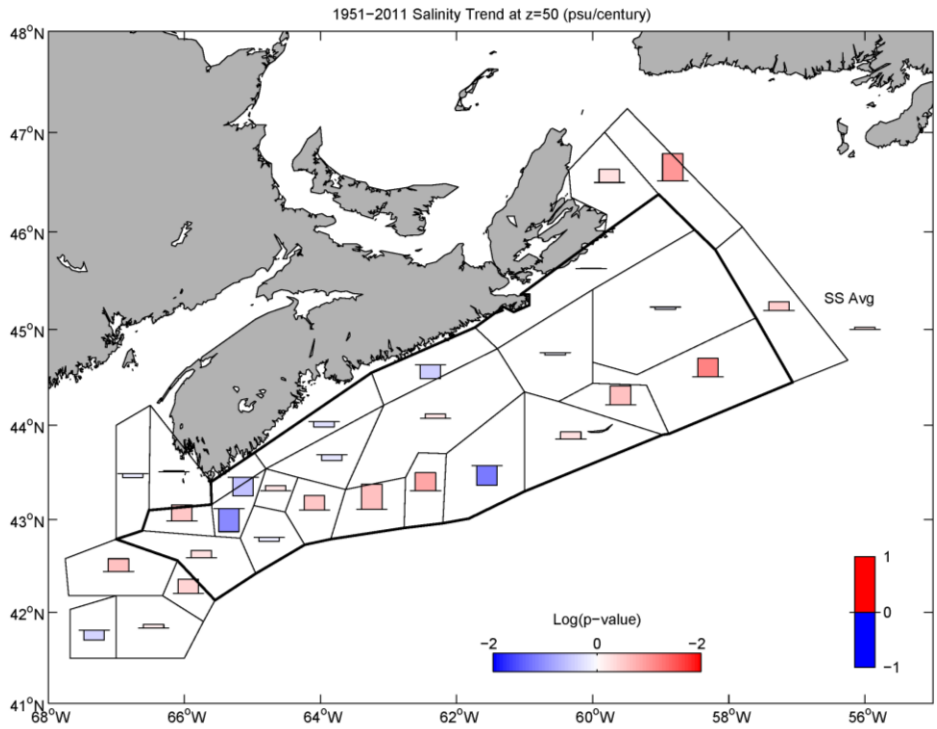

Figure 4-6 Salinity trend (/century) at 50 m for 1951-2011. The size of the bar is proportional to the trend, and the intensity of its colour (red for increasing trend, blue for decreasing) indicates the p-value. The SS average trend is shown to the right of the SS.

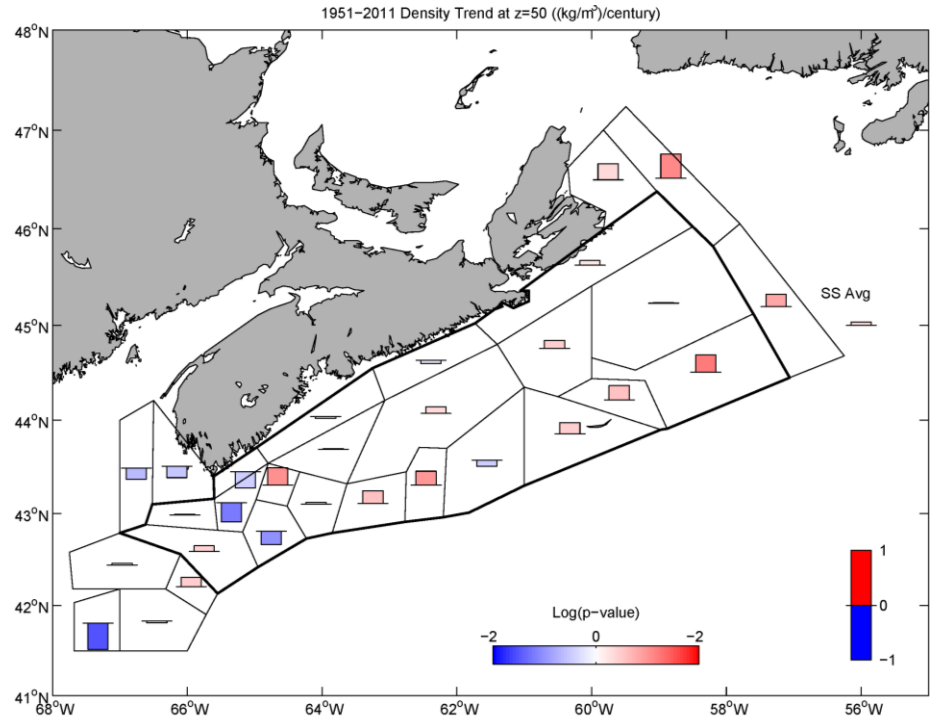

Figure 4-7 Density trend ((kg/m^3)/century) at 50 m for 1951-2011, using the same format as Fig. 4-6.

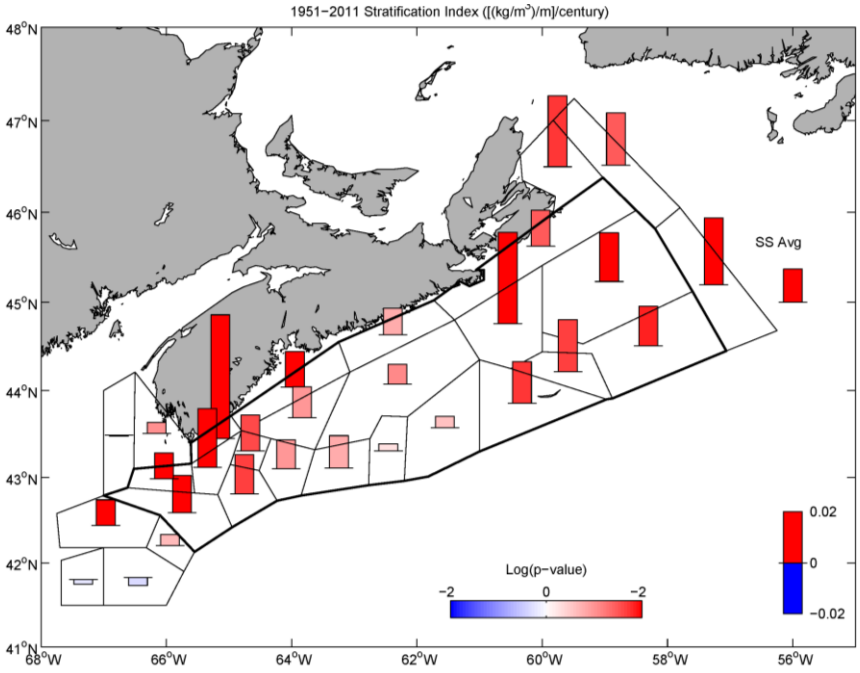

Figure 4-8 Stratification index trend ((kg/m^4)/century) for 1951-2011, using the same format as Fig. 4-6.

Table 4-1 Trends (1951-2011) in temperature (°C/decade), salinity (/decade), density (D in (kg/m3)/decade) at the surface and 50 m, and the density difference (ΔD in (kg/m3)/decade) for regions which had trends significantly different from zero at the 95% confidence limit (p<0.05).

Region	T(0m)	S(0m)	D(0m)	T(50m	S(50m)	D(50m)	ΔD
Sydney Bight							0.12
N. Laurentian Channel							0.095
S. Laurentian Channel	0.24		-0.088				0.12
Banquereau							0.074
Missaine Bank	0.19		-0.077				0.090
Canso							0.066
Middle Bank		-0.11	-0.14	-0.22			0.17
The Gully							0.098
Sable Island							0.080
South Shore		-0.06	-0.07				0.068
Lahave Bank			-0.06				
Baccaro Bank			-0.08				0.076
Roseway Bank				-0.22			0.068
Shelburne	0.77	-0.17	-0.27				0.24
Roseway Basin	0.32	-0.11	-0.14				0.11
Browns Bank			-0.058				0.072
Roseway Channel	0.21						0.050
Lurcher Shoals	0.24			0.17			
Georges Basin	0.18		-0.048				0.050
Georges Shoal	0.16		-0.039	0.22		-0.048	
Scotian Shelf		-0.03	-0.046				0.061

1979-2011

Over the period 1979-2011, the trend in surface temperature is generally larger than the 1951-2011 period but not as significantly different from zero as found for the longer period (Fig. 4-9; Table 4-2).The most significant and largest trends are in Sydney Bight and North Laurentian Channel. The surface salinity trend is mainly negative throughout the region (Fig. 4-10). These trends result in a decrease of surface density (Fig. 4-11). The Scotian Shelf average (subareas 4-23) trend is 1.9°C/century (p=0.13) for surface temperature; -0.4/century (p=0.24) for surface salinity; and -0.7 (kg/m^3)/century (p=0.06) for density. The trends in temperature, salinity, and density at 50 m are more variable and less significantly different from zero than at the surface, except for salinity in the eastern Gulf of Maine (Figs. 4-12, 4-13 and 4-14). There are no significant trends in the Scotian Shelf (SS) average temperature (p=0.84), salinity (p=0.97), and density (p=0.73) at 50 m. The stratification index shows a significant trend over the eastern and western parts of the region (Fig. 15). The SS average trend is 0.020 (kg/m^4)/century (p=0.014), equivalent to a density difference of 0.1 (kg/m^3)/decade. Table 4-2 lists those trends that are significantly different from zero at the 95% confidence limit.

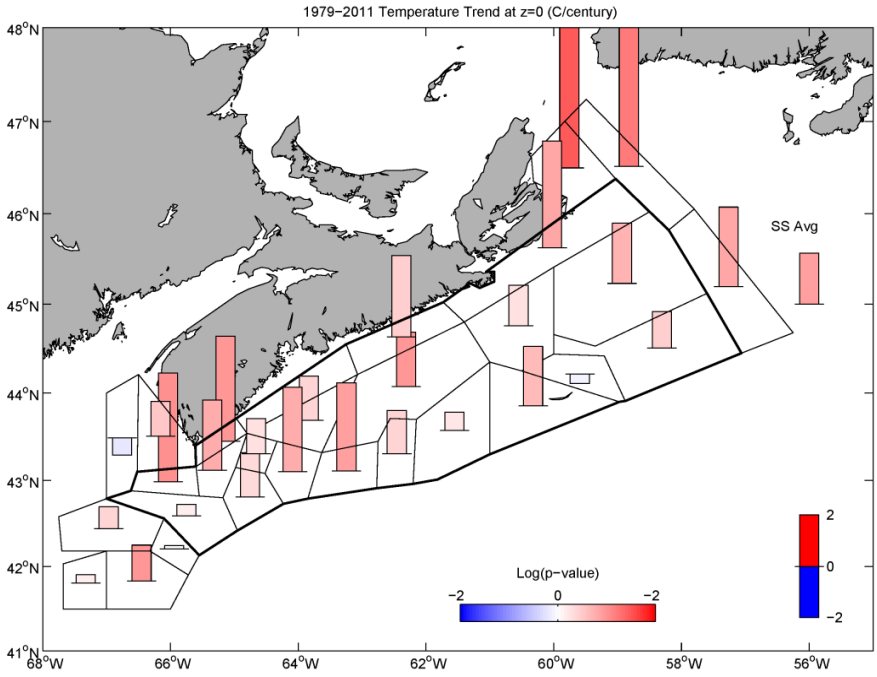

Figure 4-9 Surface temperature trend (°C/century) for 1979-2011. The size of the bar is proportional to the trend. The intensity of the colour of the bar (red for increasing trend; blue for decreasing trend) indicates the p-value. The Scotian Shelf (SS) average trend is shown to the right of the SS.

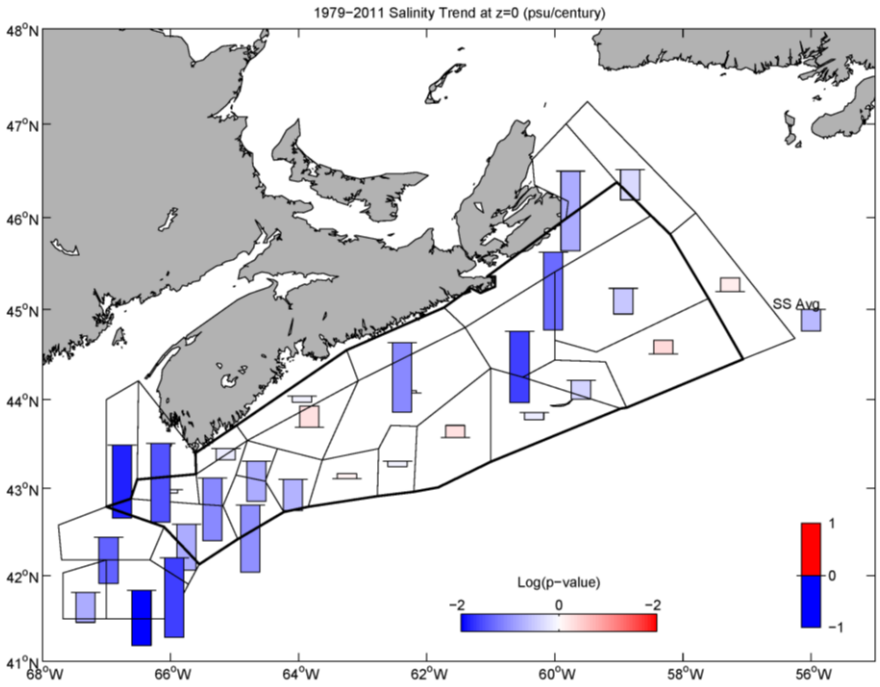

Figure 4-10 Surface salinity trend (/century) for 1979-2011. . The size of the bar is proportional to the trend, and the intensity of its colour (red for increasing trend, blue for decreasing) indicates the p-value. The SS average trend is shown to the right of the SS.

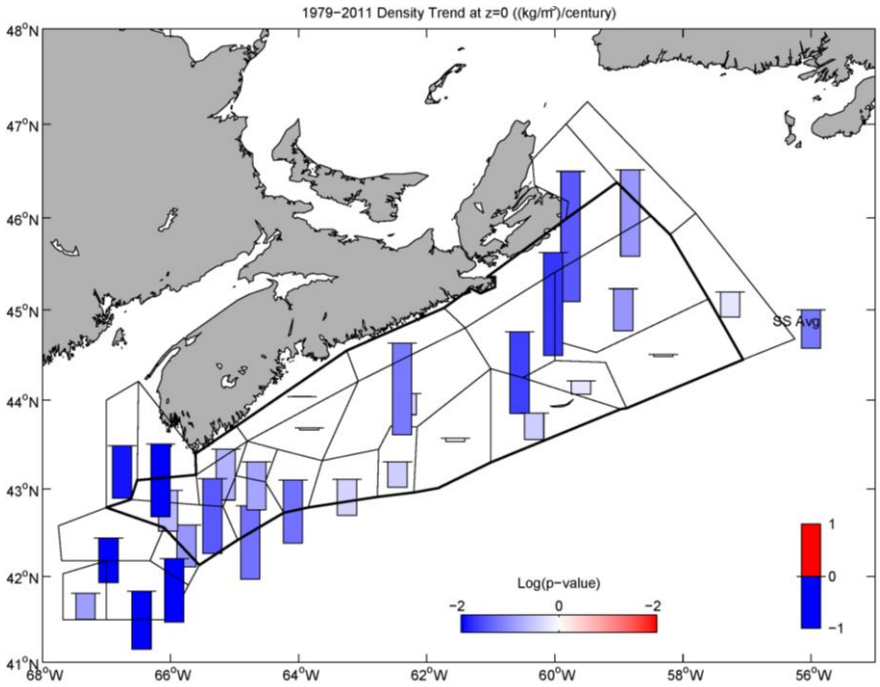

Figure 4-11 Surface density trend ((kg/m^3)/century) for 1979-2011, using the same presentation format as Fig. 4-10.

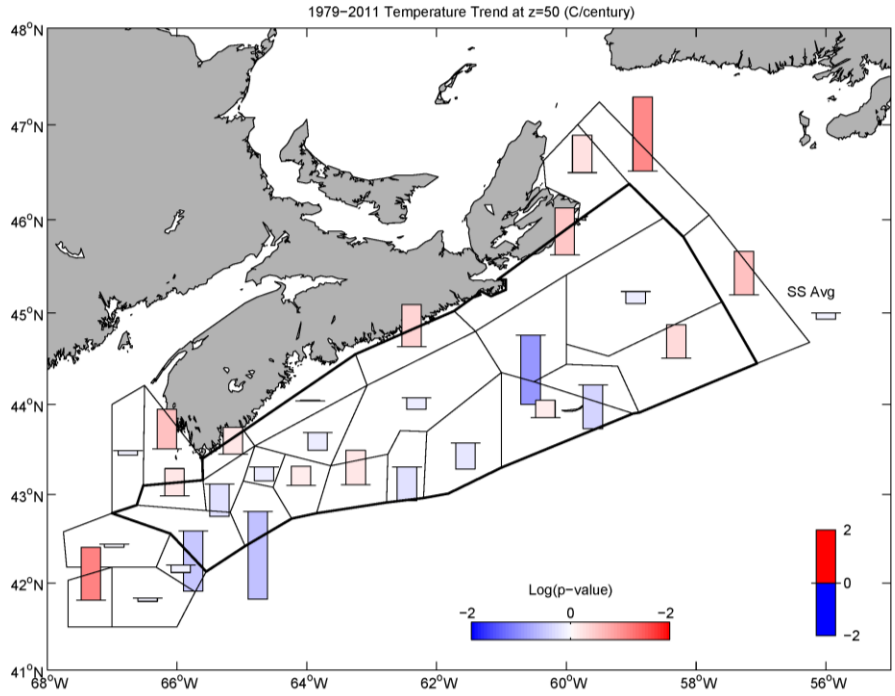

Figure 4-12 Temperature trend (°C/century) at 50 m for 1979-2011. The size of the bar is proportional to the trend, and the intensity of its colour (red for increasing trend, blue for decreasing) indicates the p-value. The SS average trend is shown to the right of the SS.

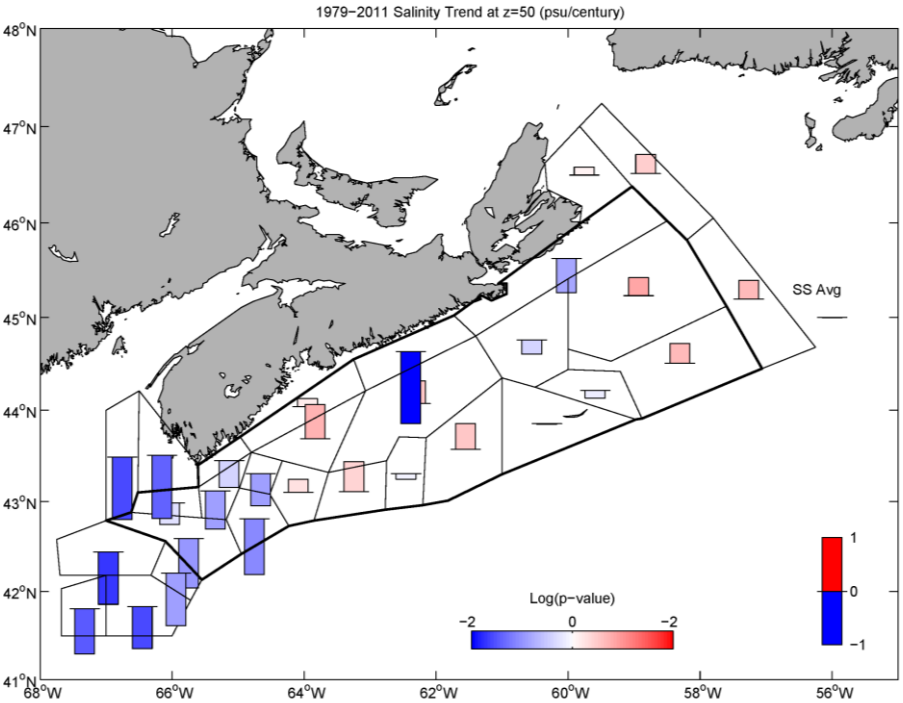

Figure 4-13 Salinity trend (/century) at 50 m for 1979-2011, using the same presentation format as Fig. 4-12.

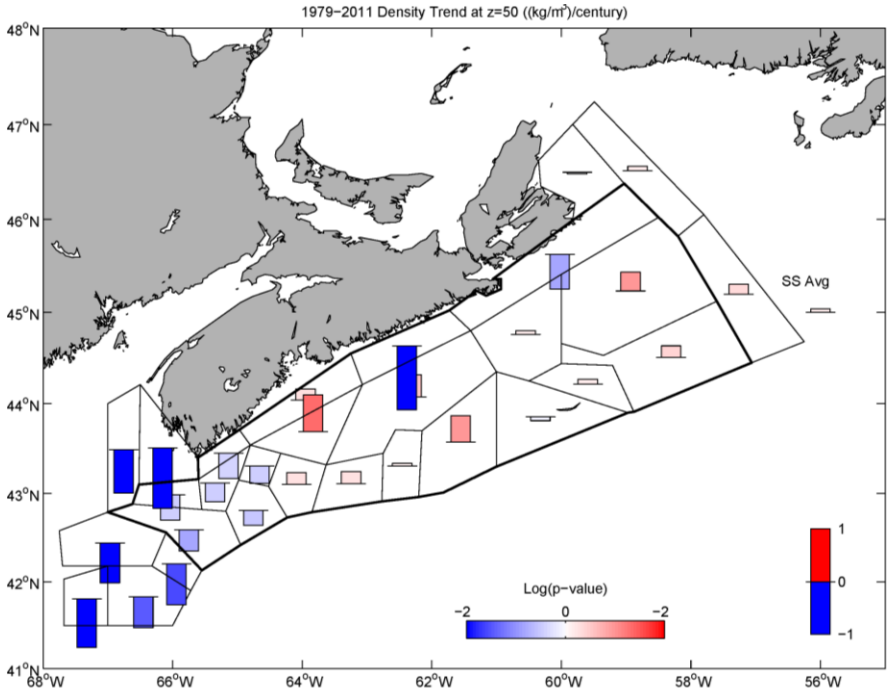

Figure 4-14 Density trend ((kg/m^3)/century) at 50 m for 1979-2011. The size of the bar is proportional to the trend, and the intensity of its colour (red for increasing trend, blue for decreasing) indicates the p-value. The SS average trend is shown to the right of the SS.

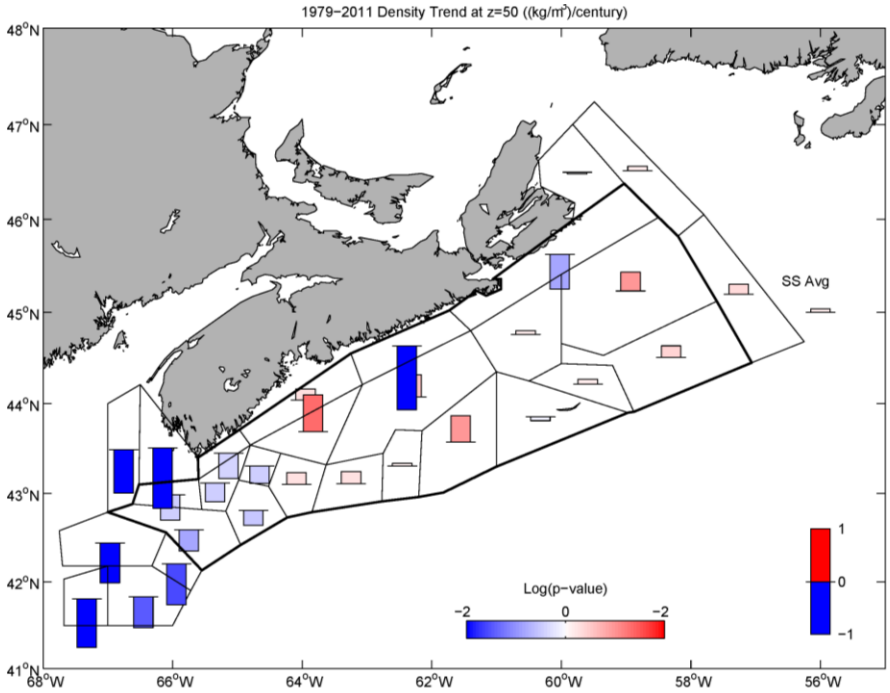

Figure 4-15 Stratification trend ((kg/m^4)/century) for 1979-2011, using the same format for presentation as Fig. 4-14.

Table 4-2 Trends (1979-2011) in temperature (°C/decade), salinity (/decade), density (D in (kg/m^3)/decade) at the surface and 50 m, and the density difference (ΔD in (kg/m^3)/decade) for regions which had trends significantly different from zero at the 95% confidence limit.

Region	T(0m)	S(0m)	D(0m)	T(50m)	S(50m)	D(50m)	ΔD
Sydney Bight	0.56		-0.24				0.29
Misaine Bank							0.14
Canso		-0.14	-0.19				
Middle Bank		-0.13	-0.15				0.21
Emerald Bank							0.10
Lahave Basin						0.068	
Lahave Bank			-0.12				0.16
Baccaro Bank			-0.14				
Roseway Bank			-0.14				
Lurcher Shoals		-0.15	-0.14		-0.12	-0.11	
E. Gulf of Maine		-0.14	-0.099		-0.12	-0.081	
Georges Basin		-0.089	-0.086		-0.098	-0.076	
Georges Shoal					-0.085	-0.093	
E. Georges Bank		-0.11	-0.11		-0.079	-0.059	0.054
N. E. Channel		-0.15	-0.12			-0.078	
E. Gulf of Maine		-0.14	-0.099		-0.12	-0.081	
Georges Basin		-0.089	-0.086		-0.098	-0.076	
Georges Shoal					-0.085	-0.093	
E. Georges Bank		-0.11	-0.11		-0.079	-0.059	0.054
N. E. Channel		-0.15	-0.12			-0.078	

4.4 Summary

Linear trends in the near-surface and 50 m temperature, salinity and density were determined for several regions of the Scotian Shelf and surrounding areas for the periods 1951-2011 and 1979-2011. Trends in the stratification, as defined by the difference in density between the surface and 50 m, were also calculated. For both periods, the trends in surface temperature are generally positive. Those that were significantly different than zero at the 95% confidence limit tended to be in southwest Nova Scotia for the 1951-2011 period; only the Sydney Bight area was significant at this level for the 1979-2011 period. The surface salinity trends are generally negative for both periods. Again, the 95% significant trends were on the western Scotian Shelf These trends lead to a trend of decreasing surface density. Trends in temperature, salinity, and density at 50 m were more variable and less significantly different from zero than at the surface. The trend in stratification was positive for the whole region. For the 1951-2011 period, there were significant trends at the 95% confidence limit over a significant portion of the Scotian Shelf. These trends were less significant for the 1979-2011 period. In a companion report looking at larger areas on the Atlantic Canada shelf (Hebert, 2013), there is general agreement

with the trends here but not an exact correspondence. This is due to the differences in the amount of data and spatial variability used in determining the annual anomalies and the difference in the periods used for determining the trends.

There is significant decadal variability in the temperature, salinity, and density of the waters on the Scotian Shelf. Petrie and Drinkwater (1993) found that this variability was related to changes in the strength of the westward flow of the Labrador Current and inversely related to the temperature and salinity of the Labrador Current. In other words, when the Labrador Current transport increased, its salinity and temperature increased. The temperature and salinity of the Labrador Current were still less than the waters found on the Scotian Shelf. Using Empirical Orthogonal Function Analysis, Loder *et al.* (2013) found that there is spatially-variable decadal variability in sea surface temperature off Atlantic Canada that appears to be related to each of the North Atlantic Oscillation and the Atlantic Multi-decadal Oscillation (AMO). Depending on the phase of this variability, the location and the length of the period used, the determined trends can vary significantly.

4.5 Acknowledgements

Generation of the monthly anomalies of salinity, temperature, density, and stratification index was by Roger Pettipas as part of the Atlantic Zone Monitoring Program. Thanks to Guoqi Han, John Loder, and Brian Petrie for many comments and suggestions on this manuscript which greatly improved it.

4.6 References

Drinkwater, K. . and R. W. Trites. 1987. Monthly means of temperature and salinity in the Scotian Shelf region. Can. Tech. Rep. Fish. Aquat. Sci. 1539, iv + 101p.

Galbraith, P. S. and D. Larouche. 2013. Trends and variability in eastern Canada sea-surface ocean temperatures. Ch. 1 (p. 1-18) *In:* This report.

Gregory, D. N. 2004. Climate: A database of temperature and salinity observations for the Northwest Atlantic. DFO Can. Sci. Advis. Sec. Res. Doc. 2004/075. http://www.dfo-mpo.gc.ca/CSAS/Csas/DocREC/2004/RES2004_075_e.pdf.

Han, G., Z. Ma, and H. Bao. 2013. Trends of temperature, salinity, stratification and mixed-layer depth in the Northwest Atlantic. Ch. 2 (p. 19-32) *In:* This report.

Hebert, D. 2013. Trends in temperature, salinity and stratification in the upper ocean for different regions of the Atlantic Canadian Shelf. Ch. 3 (p. 33-42) *In:* This report.

Hebert, D., R. Pettipas, B. Petrie, and D. Brickman. 2012. Meteorological, sea ice and physical oceanographic conditions on the Scotian Shelf and in the Gulf of Maine during 2011. DFO Can. Sci. Advis. Sec. Res. Doc. 2012/055. iv + 42 p. http://www.dfo-mpo.gc.ca/Csas-sccs/publications/resdocs-docrech/2012/2012_055-eng.pdf

Loder, J. W., Z. Wang, A. van der Baaren and R. Pettipas. 2013. Trends and variability of sea surface temperature in the Northwest Atlantic, from the HadISST1, ERSST and COBE datasets. Can. Tech. Rep. Hydrogr. Sci. 292: viii + 36 p. .
http://www.dfo-mpo.gc.ca/Library/350066.pdf

Petrie, B. and K. Drinkwater. 1993. Temperature and salinity variability on the Scotian Shelf and in the Gulf of Maine 1945-1990. *J. Geophys. Res.*, 98, 20079-20089.

5 Trends and variability in eastern Canada sub-surface ocean temperatures and implications for sea ice

Peter S. Galbraith [1] *, Dave Hebert [2], Eugene Colbourne [3], and Roger Pettipas [2]

[1] Fisheries and Oceans Canada, Maurice-Lamontagne Institute
P.O. Box 1000, Mont-Joli, Québec G5H 3Z4

[2] Fisheries and Oceans Canada, Bedford Institute of Oceanography
Dartmouth, Nova Scotia

[3] Fisheries and Oceans Canada, Northwest Atlantic Fisheries Centre
St. John's, Newfoundland and Labrador

* Correspondence: Peter.Galbraith@dfo-mpo.gc.ca

Suggested Citation:

Galbraith, P.S., D. Hebert, E. Colbourne and R. Pettipas. 2013. Trends and variability in eastern Canada sub-surface temperatures and implications for sea ice. Ch. 5 (p. 57-72) *In:* Aspects of climate change in the Northwest Atlantic off Canada [Loder, J.W., G. Han, P.S. Galbraith, J. Chassé and A. van der Baaren (Eds.)]. Can. Tech. Rep. Fish. Aquat. Sci. 3045: x + 190 p.

Abstract

The longest mid- and deep-water temperature time series available for the Labrador, Newfoundland, and Scotian Shelves, and the Gulf of St. Lawrence are analysed to determine the relationships among their decadal variability and long term trends. Cold Intermediate Layer (CIL) properties are well-correlated (R^2 = 0.33 to 0.59) along the Newfoundland-Labrador Shelf and between the Gulf of St. Lawrence (GSL) and the Scotian Shelf (R^2 = 0.62). Inter-decadal variability dominates over long term trends, however, prior work and new results presented here have identified correlations of CIL properties to ice and winter air temperatures. Updated comparisons show that all occurrences of winter air temperature anomalies of +2.5°C account for all three low-ice winters recorded in the Gulf of St. Lawrence (1969, 2010, and 2011), a situation that could become normal by the end of this century if air temperature warming trends are maintained. Deep and bottom water temperatures in the GSL and Scotian Shelf vary widely on decadal time scales depending on the proportions of warm, salty Slope Water and cold, relatively fresh Labrador Slope Water such that long term trends do not reflect changes that have occurred in recent decades. The highest inter-regional correlations (R^2 = 0.39) are found between bottom temperatures in NAFO regions 4W and 4Vs, between bottom temperature in 4Vs and waters at 150 m in Cabot Strait (R^2 = 0.37), and between temperature at Hamilton Bank and station 27 (R^2 = 0.29). While shifts in water temperature have been related to the winter North Atlantic Oscillation (NAO) Index, correlations between them are low.

5.1 Introduction

Fisheries and Oceans Canada (DFO) is carrying out the Aquatic Climate Change Adaptation Services Program (ACCASP) designed to improve our understanding of climate change and to help Canadians prepare for climate-related impacts. This study assesses long term trends and variability of ocean temperatures in eastern Canada (Fig. 5-1) since the early 20th century. It was conducted as part of the Atlantic Large Aquatic Basin Risk Assessment component of ACCASP, leveraging data consolidation and analyses done within the Atlantic Zone Monitoring Program (AZMP) (Colbourne *et al.*, 2012; Galbraith *et al.*, 2012b; Hebert *et al.*, 2012). Complementary with this study, the Labrador and Newfoundland shelf water temperatures and sea-ice extent in relation to atmospheric forcing are also examined in Han *et al.* (2013), upper ocean temperature, salinity, and stratification in Hebert (2013a, 2013b) and sea surface temperature in Galbraith and Larouche (2013).

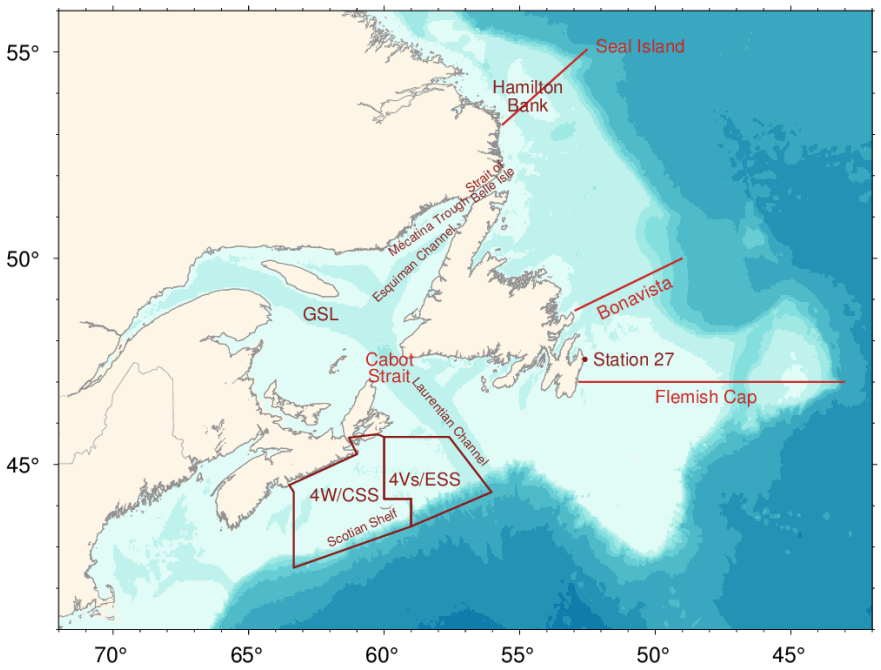

Figure 5-1 Atlantic Zone Monitoring Program (AZMP) sections and sites used in this report. The Newfoundland and Labrador Shelf extends from off-map northwest of Hamilton Bank to include the shallow bank south of Flemish Cap.

5.2 Cold Intermediate layer indices

The summertime temperature (T) structure in the Atlantic zone consists of three distinct layers: the warm surface layer, the cold intermediate layer (CIL), and the deeper water layer (e.g. Fig. 5-2 for the Gulf of St. Lawrence). During fall and winter, this surface layer deepens and cools, partly because of buoyancy loss (cooling and reduced runoff) and brine rejection associated with sea ice formation where it occurs, but mostly from wind-driven mixing prior to ice formation (Galbraith, 2006). The surface winter layer extends to an average depth of about 75 m on the Scotian Shelf and in the Gulf of St. Lawrence (GSL) by March, and can extend to the bottom (>150m) on the Labrador and Newfoundland Shelves. During spring, surface warming, sea-ice melt waters, and continental runoff lead to a lower salinity and higher temperature surface layer,

below which cold waters from the previous winter are partly isolated from the atmosphere and form the summer CIL. This layer persists until the next winter, gradually warming and deepening during summer (Gilbert and Pettigrew, 1997; Cyr *et al.*, 2011); more rapid deepening occurs during the fall as vertical mixing intensifies. The CIL is, for the most part, locally formed in winter on the Labrador Shelf, in the GSL (Galbraith, 2006), on the Scotian Shelf (Umoh and Thompson, 1994), as well as on the Newfoundland Shelf (Umoh *et al.*, 1995). However, advection from the Labrador Shelf to the GSL (Galbraith, 2006) and Newfoundland Shelf (Umoh *et al.*, 1995) and from the GSL to the St. Lawrence Estuary (Galbraith, 2006) and to the Scotian Shelf (Umoh and Thompson, 1994) are also contributing influences. The temperature minimum of the winter mixed layer occurs at about the same time in March both on the Scotian Shelf and in the GSL, reaching different minimum temperatures; this is an indication of local formation rather than advection from one region to the other.

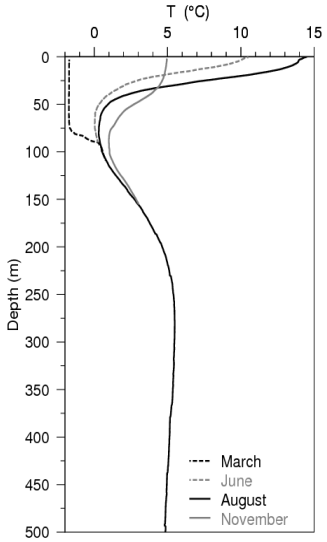

Figure 5-2 Typical seasonal progression of the depth profile of temperature observed in the Gulf of St. Lawrence. Profiles are averages of observations in August, June, and November 2007 in the northern Gulf. The dashed line at left shows a single winter temperature profile (March 2008), with near-freezing temperatures in the top 75 m. The CIL is defined as the layer contained by the 1°C isotherms, although some authors use a different temperature threshold. Figure from Galbraith *et al.* (2012a).

The CIL indices for the Newfoundland and Labrador Shelf are the cross sectional area of waters with T<0°C during summer along the Seal Island, Bonavista, and Flemish Cap AZMP sections (Fig. 5-1) (Colbourne *et al.*, 2012). For the GSL, the most commonly used CIL index is that of Gilbert and Pettigrew (1997), and is defined as the mean of the CIL minimum core temperatures observed between 1 May and 30 September of each year, adjusted to 15 July. It is updated annually using all available temperature profiles from the Gulf between May and September, inclusive, since 1947 (Fig. 5-3; Galbraith *et al.*, 2012b). A second GSL CIL index is the areal average of the CIL temperature minimum (interpolated to a standard grid) observed during the annual August-September multispecies survey beginning in 1994 (Galbraith *et al.*, 2012b). On the Scotian Shelf, the volume of water having T<4°C during the July ecosystem survey (1972 to present) is used as an index of the CIL (Hebert *et al.*, 2012). The survey covers the Scotian Shelf from Cabot Strait to the Bay of Fundy. Limited data prior to 1990 is compensated for by the use of a 5 year running mean to achieve extended temporal coverage; however, this results in a loss of high-frequency variability from that part of the time series. The CIL indices reported here are taken at about the same time within their respective annual cycles , although not simultaneously.

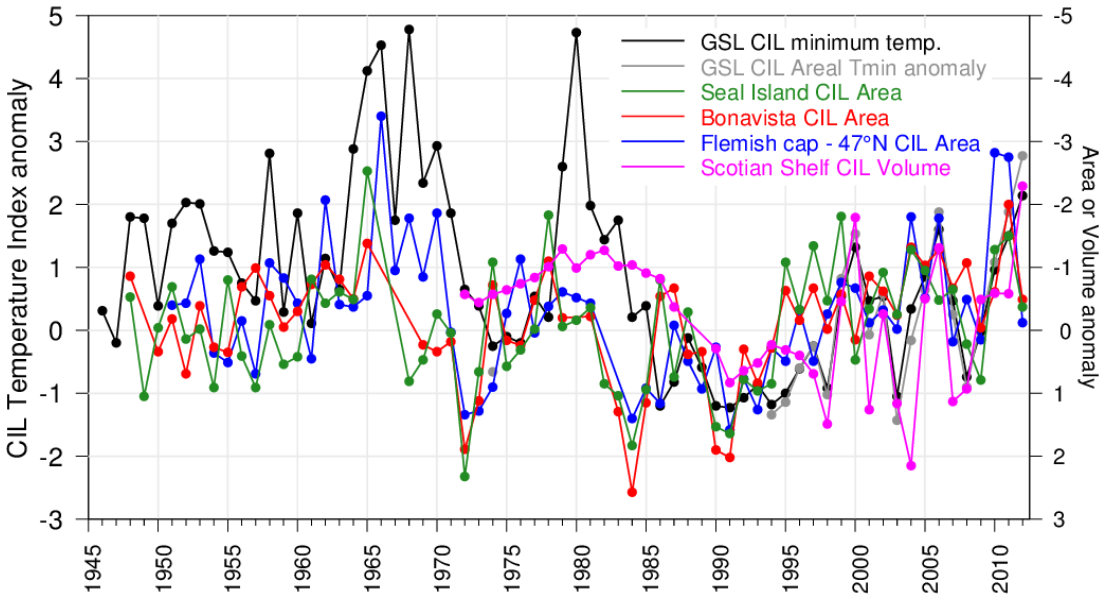

Figure 5-3 Cold Intermediate Layer normalized indices for the Gulf of St. Lawrence and various AZMP sections. The GSL indices are the Gilbert & Pettigrew (1997) minimum temperature index and the Galbraith et al (2012b) areal temperature minimum index. Areas are for T<0°C during summer along the Seal Island, Bonavista, and Flemish Cap AZMP sections (Colbourne *et al.*, 2012) and the volume is for T<4°C on the Scotian Shelf during the July ecosystem survey for which a running mean of 5 years is used prior to 1990 because of limited data. All time series are normalized relative to the 1981-2010 mean and standard deviation, e.g., [T(year)-T(mean)]/SD. Note the reversed scale for area and volume anomalies (less area indicates warmer conditions).

Figure 5-3 shows all CIL time series and Table 5-1 shows trends and squared cross-correlations among them. Statistically significant correlations ($p < 0.05$) are indicated but the numbers of degrees of freedom were not adjusted for autocorrelation of the time series in the calculation. The GSL Gilbert and Pettigrew (1997) CIL index is characterized by some very warm years prior to and in 1980, and some of these may be spurious because of sparse vertical resolution data that fail to capture real temperature minimums. However, the late 1960s was characterized by a warm period that was also observed along the Flemish Cap section. Data coverage is much more complete since 1994 in the GSL, leading to $R^2 = 0.96$ between the two GSL indices (Table 5-1).

Some connectivity is observed between the regions as seen from squared cross-correlation coefficients (Table 5-1). The highest correlations are between the GSL and Scotian Shelf ($R^2 = 0.62$ for the period 1994-2012) presumably caused by the similarity of atmospheric forcing in both areas followed by advection from the Gulf to the Shelf through Cabot Strait. The next highest correlation value is between the Seal Island and Bonavista time series ($R^2 = 0.59$) also presumably caused by the coherent large-scale atmospheric forcing and by the advective connection between the two areas.

Table 5-1 Trends and correlation coefficients for CIL time series. (Top) overall trends are shown for the entire time series (first line) and for 1980-2012 (second line). CIL area trends are expressed as percentage change per 100 years of the 1981-2010 mean. Temperature trends are expressed in °C per century. Trends significantly different from zero are in black type and plus and minus numbers are 95% confidence intervals. (Bottom) correlation coefficients (R^2) between the time series. Correlations with the Scotian Shelf CIL volume were limited to >1990 because prior data are 5-year averages. Statistically significant correlations ($p < 0.05$) are in black type.

Trends					
Seal Island	Bonavista	Flemish Cap	GSL T_{min}	GSL T_{min} areal	Scotian Shelf
-22% ± 34 (1948-2012)	-19% ± 45 (1948-2012)	0% ± 38 (1951-2012)	**-1.0 ± 0.7** (1946-2012)		2.8 ± 2.9 (1972-2012)
-140 ± 90 (1980-2012)	**-270 ± 120** (1981-2012)	**-170 ± 88** (1980-2012)	-0.2 ± 1.9 (1980-2012)	**4.5 ± 2.9** (1994-2012)	2.4 ± 4.6 (1980-2012)

R^2 Table CIL	Bonavista (1948-2012)	Flemish Cap (1951-2012)	GSL T_{min} (1946-2012)	GSL T_{min} areal (1994-2012)	Scotian Shelf (1990-2012)
Seal Island (1948-2012)	**0.59**	**0.18**	0.02	0.06	0.00
Bonavista (1948-2012)		**0.33**	0.05	0.14	0.01
Flemish Cap (1951-2012)			**0.31**	**0.27**	0.08
GSL T_{min} (1946-2012)				**0.96**	**0.46**
GSL T_{min} areal (1994-2012)					**0.62**

These relatively high values are followed by the correlation between the Flemish Cap and the Bonavista section ($R^2 = 0.33$; again coherent forcing, southerly advection), and, lastly, between Flemish Cap and the GSL ($R^2 = 0.29$-0.31), possibly because of similarities in winter atmospheric forcing, but also possibly because of the variable winter inflow of Labrador Shelf Water into the GSL (Galbraith, 2006).

Over the entire time series, the only significant trends are in the GSL indices for CIL minimum temperature, showing cooling since 1946 whereas the trend shows warming since 1994. These trends therefore depend on the length of period chosen. Since 1980, there are warming trends along the Flemish Cap, Bonavista and Seal Island AZMP sections associated with a near-record large CIL area in 1984 and more recent small areas (2004, 2006, 2010, and 2011). These trends are spuriously caused by strong inter decadal variability and the period selected for trend calculation. For example, the early 1970 and mid-1980s are cold periods characterized with large CIL areas, whereas some years in between were very warm (see also Colbourne, 2004).

5.3 Atmospheric Influences and Sea Ice Implications

Trends over specified periods are not very useful as predictive indicators when interdecadal variability is high and time series are relatively short, whereas links to environmental forcing and other oceanographic responses may be of more use. Colbourne *et al.* (1997) identified a correlation between the Bonavista CIL area and ice cover on the Newfoundland Shelf between the early 1970s and the early 1990s ($R^2 = 0.61$), both in response to winter atmospheric forcing. The 1980-2010 correlation between average seasonal ice volume on the Shelf with the CIL area along the various Newfoundland and Labrador sections varies between $R^2 = 0.51$ to 0.55. More information can be found in Han *et al.* (2013).

Galbraith *et al.* (2010) identified similar correlations between the maximum annual ice volume within the GSL and on the Scotian Shelf (since 1969), the winter cold-water volume (T<-1°C; since 1997), the August–September CIL volume (since 1985), and the winter (January-February-March) air temperature anomaly in the GSL (since 1969) up to 2009 ($R^2 = 0.55$ to 0.77). However, this was before the very warm winter of 2010 when very little of the winter mixed layer cooled below -1°C; including that year in the analysis reduced the high correlations with winter cold-water volume substantially in spite of the near-absence of sea-ice. However, with very low ice volumes recorded in winters 2010 and 2011 in the GSL, an updated correlation (Fig. 5-4) between the seasonal maximum ice volume and the December-January-February (instead of January through March) average air temperature in the western GSL (Mont-Joli, Sept-Îles, Gaspé, Charlottetown, and Îles-de-la-Madeleine) between 1969 and 2012 is very high ($R^2 = 0.72$). In addition, air temperature anomalies greater than +2.5°C account for all three low ice seasons with less than 20 km^3 of sea-ice (1969 and 2011 with +2.9°C, and 2010 with +4.1°C) in the GSL. The very low ice conditions during these three years (Fig. 5-5) were characterized by open water in the central GSL and off the coast of Newfoundland. However, there was some ice in the shallow Northumberland Strait, the *Baie des Chaleurs*, and the ice-producing northwest GSL and Estuary, as well as a tongue of ice in 2011 that was likely advected into the GSL through the Strait of Belle Isle.

The monthly air temperatures used in Galbraith *et al.* (2010) were climate summaries from Environment Canada's National Climate Data and Information Archive (NCDIA). However, Environment Canada has since released the Second Generation of Homogenized Surface Air Temperature Data as part of the Adjusted and Homogenized Canadian Climate Data (AHCCD), which accounts for shifts due to the relocation of stations, changes in observing practices, and automation (Vincent *et al.*, 2012). It is worthwhile to compare these two data sets to determine if prior interpretations should be altered in view of the enhanced data set, either caused by corrections or addition/removal of data. This is shown on Figure 5-6 for annual averages of December-January-February temperatures as well as on their trends up to 2011. The largest differences in trends occur for Sept-Îles, where data prior to the early 1960s were corrected downward in AHCCD, and for Mont-Joli, where data prior to 1943 were added to AHCDD. In both cases, the trend calculated based on AHCCD is much higher. Data and trends are very similar for Îles-de-la-Madeleine, and while there are larger differences in temperature averages for Gaspé between the two datasets, the overall trends are similar. Only at Charlottetown is the long term warming trend lower in AHCCD (1.2 vs 1.5°C per century). Overall, combining all five station anomalies into a single (straight average) index yields a greater trend of 2.0°C per

century in the December-January-February average in AHCCD (compared to the earlier estimate of 1.6°C per century based on NCDIA).

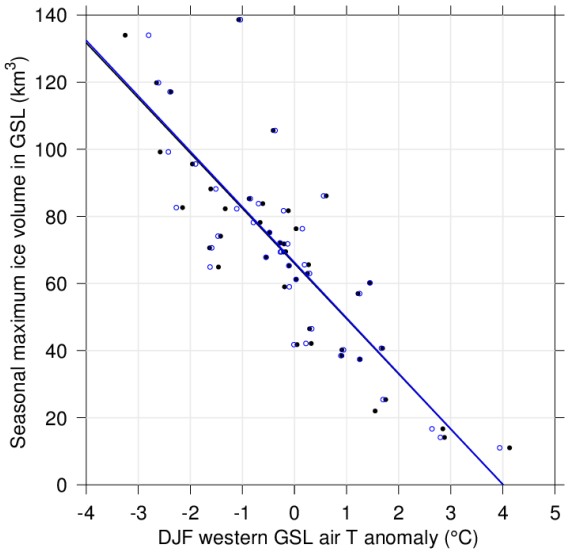

Figure 5-4 Relation between the seasonal maximum ice volume observed in the GSL and the December-January-February air temperature anomaly in the western GSL using both the air temperature data from the NCDIA database (black dots) and from AHCCD (blue circles). Linear regressions are shown for both the NCDIA and AHCCD datasets, but nearly overlap.

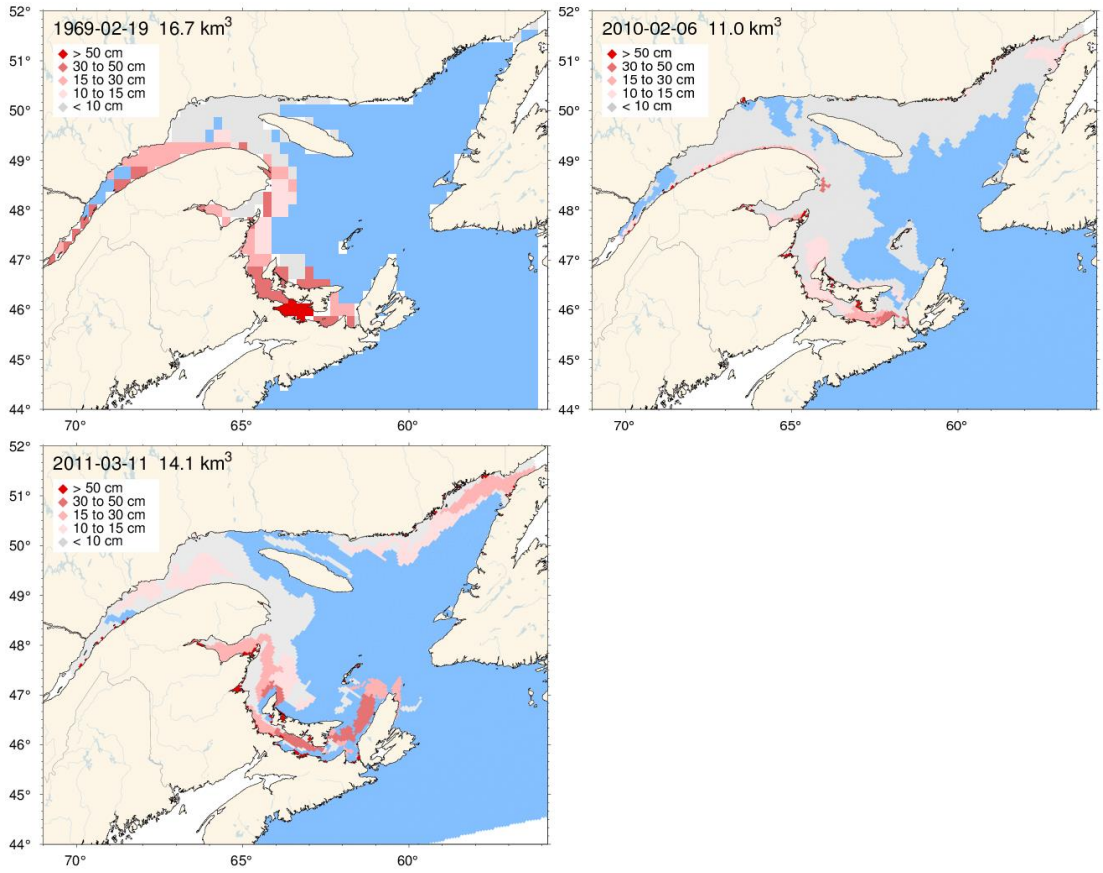

Figure 5-5 Seasonal maximum sea-ice cover for the three winters that had very low sea-ice maximum volumes since 1969: 1969, 2010, and 2011.

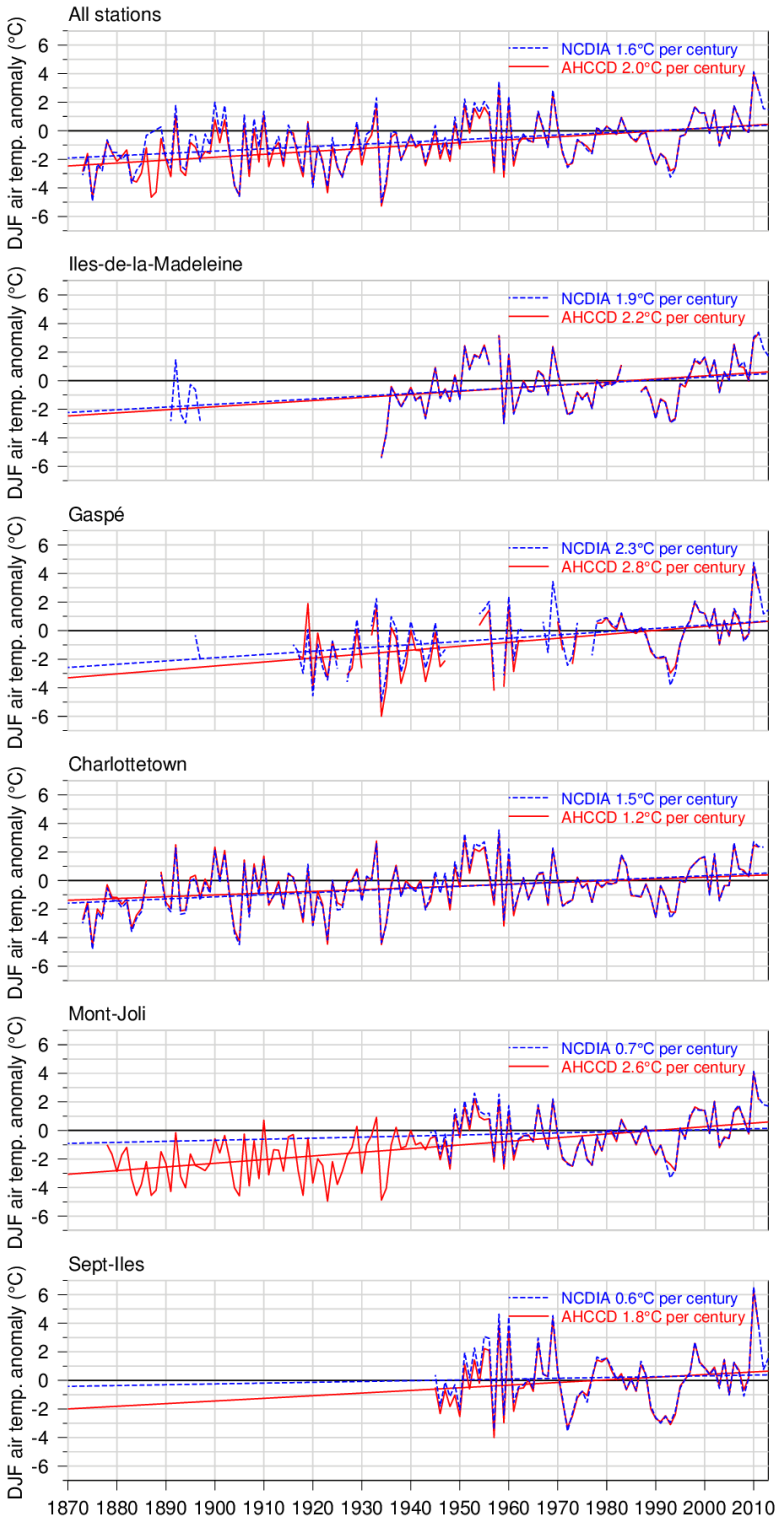

Figure 5-6 Comparison of December-January-February averages of air temperature using Environment Canada's AHCCD and NCDIA data sources. Five stations are compared as well as anomalies combined from all five stations (top). Trends are calculated based on all available data. NCDIA data are shown up to 2013 but trends are considered only with data up to 2011 for comparison with AHCCD.

For the temperature anomaly associated with winters with very low GSL ice cover, again only the December-January-February averages for 1969 (+2.6°C), 2010 (+3.9°C) and 2011 (+2.8°C) are greater than +2.5°C, the next highest since 1969 being for 2006 at +1.7°C (Fig. 5-4).

If the trend of 2.0°C per century were to continue, the above threshold suggests that, within 125 years, very low sea ice volumes will occur in the GSL during climatologically normal winters.. However, it is more likely that very-low-ice winters will become normal by the end of this century given the enhanced trend of 3.2°C per century observed during the last five decades. The climatology will have by then increased by 2.5°C similar to anomalies that occurred in 1969, 2010, and 2011 when sea ice was all but absent from the GSL (<20 km^3). The regression of air temperature anomaly against sea ice volume (Fig. 5-4) leads to zero sea ice volume with an air temperature anomaly of +4°C, much higher than +2.5°C. However this is an extrapolation past current minimum ice covers and extra dynamics will be at play to lead to a complete sea-ice cover disappearance (e.g. it is easier to withdraw heat from the water and lead to freezing in shallow bays than offshore). Indeed, such a temperature anomaly occurred in 2010 and some sea ice remained.

5.4 Scotian Shelf and Deep Layer temperatures

Interdecadal changes in temperature, salinity, and dissolved oxygen of the deep waters of the GSL, Scotian Shelf, and Gulf of Maine are related to the varying proportion of their source waters: cold–fresh/high-dissolved-oxygen Labrador Current water and warm–salty/low-dissolved-oxygen Slope Water (McLellan, 1957; Lauzier and Trites, 1958; Bugden, 1991, Gilbert *et al.,* 2005). The >150m water layer of the GSLbelow the CIL originates from an inflow at the entrance of the Laurentian Channel which circulates towards the heads of the Laurentian, Anticosti, and Esquiman Channels in up to roughly three to four years, with limited exchange with shallower upper layers (Bugden, 1991; Gilbert, 2004). The layer from 150 to 540 m is characterized by temperatures between 1 and 7°C and salinities between 32.5 and 35. Deeper portions of the Scotian Shelf and Gulf of Maine are similarly connected to the slope through deep channels that cut into the shelves from the shelf break. Petrie and Drinkwater (1993) showed that variations in the westward transport of Labrador Slope Water from the Newfoundland region along the shelf break had a strong effect on water masses of the Scotian Shelf deep basins. Increased transport through Flemish Pass was associated with below-normal deep temperatures and salinities on the Scotian Shelf and in the Gulf of Maine. Deep basins such as Emerald Basin undergo very large interannual and interdecadal variability of the bottom water temperature, but such changes are not necessarily appropriate for this study as they are associated with deep renewal events. Instead the average bottom water temperature over the central and eastern Scotian Shelf (NAFO regions 4W and 4Vs respectively) are used in this study. These are areal averages of spatial interpolations based on annual July survey data. Bathymetry in these areas is fairly evenly distributed between 30 m and 170 m, with 4Vs including some 400-450 m depths from the Laurentian Channel (Fig. 5-7). Both these areas are therefore affected somewhat by CIL waters as well as the waters underneath.

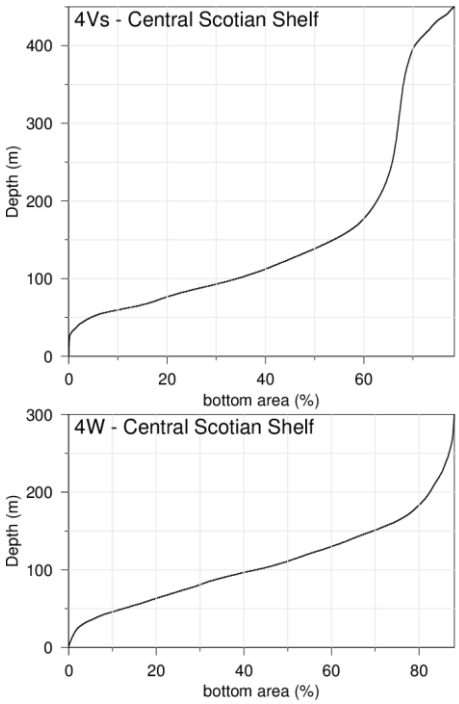

Figure 5-7 Cumulative depth distribution of the shallowest 78% and 88% bottom area in (top) eastern Scotian Shelf (NAFO region 4Vs) and (bottom) central Scotian Shelf (NAFO region 4W). Actual bathymetry extends to 2462 m in 4W and to 3060 m in 4V.

On the Newfoundland and Labrador Shelf, deep and bottom water properties also undergo large interannual and decadal variability exceeding 2°C. The water mass characteristics vary from sub-polar waters on the shelf to warmer-saltier Labrador Slope Water that flows along the shelf edge and into deeper troughs between the banks. Petrie (2007) showed a relationship between bottom temperature decadal anomalies and the North Atlantic Oscillation (NAO) atmospheric forcing in this region. The NAO Index as defined by Rogers (1984) is the difference in winter (December, January, and February) sea level atmospheric pressures between the Azores and Iceland and is a measure of the strength of the winter westerly and northwesterly winds over the Northwest Atlantic. A high NAO index results from an intensification of the Icelandic Low and Azores High. This favours strong northwest winds, cold air and sea temperatures, and heavy ice conditions on the NL Shelf regions (Colbourne et al, 1994; Drinkwater, 1996; Petrie, 2007). Petrie (2007) also showed that deep waters of the entire region had a bimodal response and were correlated with the NAO index. The NL Shelf and GSL deeper waters were negatively correlated with the NAO, while deep waters in areas west of the Halifax Section towards the Gulf of Maine had an opposite correlation.

Deep water temperature time series are shown in Figure 5-8 for many of the sites shown in Figure 5-1. The Labrador Shelf is represented by the Hamilton Bank time series while the Newfoundland Shelf is represented by the long time series at the AZMP station 27 (Colbourne *et al.*, 2012). The Scotian Shelf is represented by the aforementioned July bottom temperature averages in eastern and central Scotian Shelf, and the GSL by monitoring its only entry point of deep waters at Cabot Strait (Galbraith et al, 2012b).

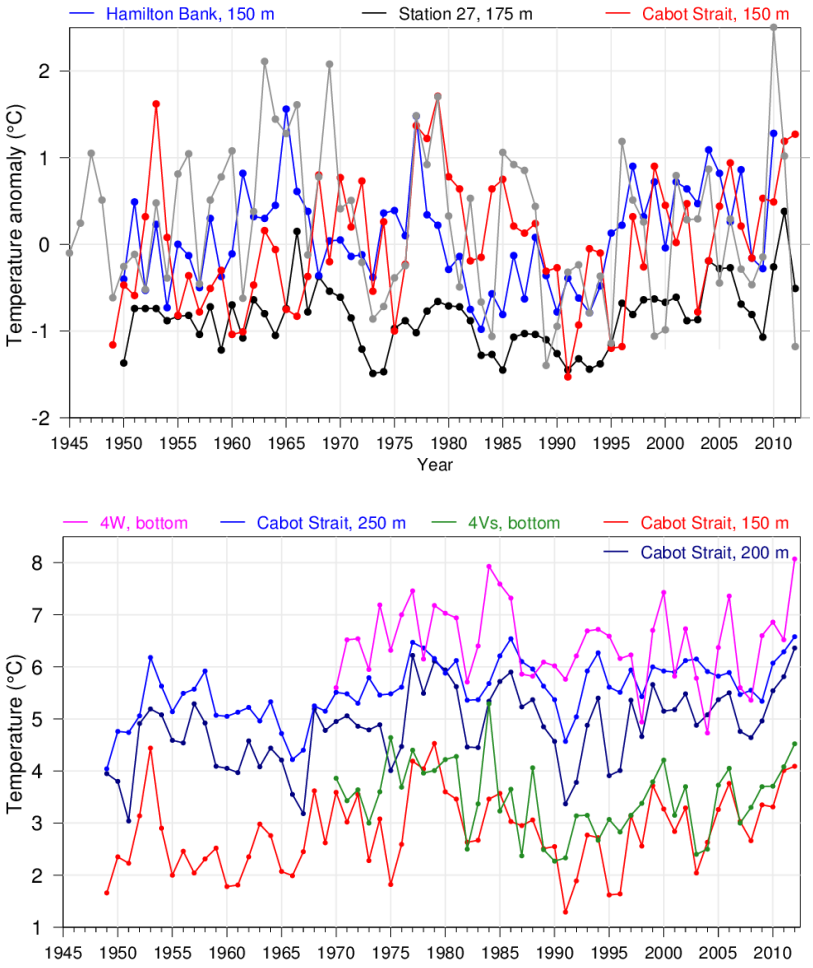

Figure 5-8 (top) Deep layer annual temperature anomalies for selected eastern sites and NAO December-January-February index (scale on right). (bottom) Annual temperatures for selected sites representing the Gulf of St. Lawrence (Cabot Strait; mean of all available monthly averages in a given year) and the Scotian Shelf in July (NAFO region 4Vs and 4W bottom temperatures for eastern and central Scotian Shelf, respectively).

Trends over various time scales (i.e. all the time series since 1950 and since 1980) and cross-correlations (R^2) are shown in Table 5-2. Figure 5-8 is divided into two parts, the first to compare Newfoundland-Labrador temperature anomalies with those of the GSL and the second to compare temperatures of Scotian Shelf bottom waters with those of the GSL. Bottom temperatures on the eastern Scotian Shelf (4Vs) are similar in range to those at 150 m in Cabot Strait, while central Scotian Shelf (4W) bottom temperatures are usually warmer than even the temperature maximum in Cabot Strait, found close to 250 m depth. There is much less coherence across the zone than for the CIL properties already discussed. Strongest correlations are found between bottom temperatures in NAFO regions 4W and 4Vs (R^2 = 0.39), between bottom temperature in 4Vs and the waters at 150 m in Cabot Strait (R^2 = 0.37), between Hamilton Bank and station 27 (R^2 = 0.29), and lastly between the 4W bottom temperature and Cabot Strait temperatures (R^2 = 0.23-0.27 at 150-200m). The highest correlations with the NAO index, albeit weak, are found on the Newfoundland and Labrador Shelf with station 27 bottom temperature (R^2 = 0.18; R^2 = 0.15 with NAO lagged by 1 year) and with Hamilton Bank temperature at 150 m (R^2 = 0.15; R^2 = 0.07 with NAO lagged by 1 year). The 200 m temperature in Cabot Strait has a long term trend of 3.0°C per century since 1915 associated with a water mass mixture shifting to higher Warm Slope Water content. However, the trend has dropped to 1.6°C per century since 1950, and there has not been a trend significantly different from zero since 1980 when

temperatures were some of the warmest of the record, followed by near-record lows in the early 1990s and ending with record highs in 2012. On the Newfoundland and Labrador Shelf, there are no significant trends since 1950 but positive trends since 1980 (4.9 and 2.7°C per century at Hamilton Bank and Station 27 respectively) while, on the Scotian Shelf, no statistically significant trends are found in 4W and 4Vs bottom temperatures since 1970.

Table 5-2 Trends and correlation coefficients for selected deep layer temperature time-series. (Top) Overall trends are shown for the entire span of the time series shown as well as for the period 1980-present. Trends not significantly different from zero at the 95% confidence limit are grayed out. The plus and minus numbers for the trends are 95% confidence intervals. Temperature trends are expressed in °C per century. (Bottom) Squared correlation coefficients (R^2) between all time-series. Statistically significant correlations ($p < 0.05$) are in black type.

Trends					
Hamilton Bank 150 m	St. 27 175 m	Cabot Strait 150 m	4Vs Bottom	Cabot Strait 200 m	4W Bottom
		2.1 ± 0.8 (1915-2011)		**3.0 ± 0.8** (1915-2011)	
0.5 ± 0.8 (1950-2010)	0.4 ± 0.5 (1950-2012)	0.8 ± 1.0 (1950-2011)	-0.7 ± 1.7 (1970-2012)	**1.4 ± 0.9** (1950-2011)	-0.6 ± 1.8 (1970-2012)
4.9 ± 1.9 (1980-2010)	**2.7 ± 1.3** (1980-2012)	0.8 ± 2.6 (1980-2011)	0.7 ± 2.7 (1980-2012)	0.7 ± 2.5 (1980-2011)	-0.8 ± 3.0 (1980-2012)

R^2 Table Deep T	St. 27 (1950-2012)	CS, 150 m (1915-2011)	4Vs (1970-2012)	CS, 200 m (1915-2011)	4W (1970-2012)
Hamilton Bank (1950-2010)	**0.29**	0.00	0.05	0.00	0.01
St. 27 (1950-2012)		0.04	0.07	0.02	0.01
CS, 150 m (1915-2011)			**0.37**	**0.72**	**0.27**
4Vs (1970-2012)				**0.20**	**0.39**
CS, 200 m (1915-2011)					**0.23**

5.5 Summary

A summary of the presented environmental and oceanographic variables is shown in Figure 5-9. CIL properties are only partly cross-correlated throughout the zone; they are well-correlated along the Newfoundland-Labrador Shelf, and, separately, well-correlated between the GSL and the Scotian Shelf, in both cases presumed to be mostly because of similar atmospheric forcing.

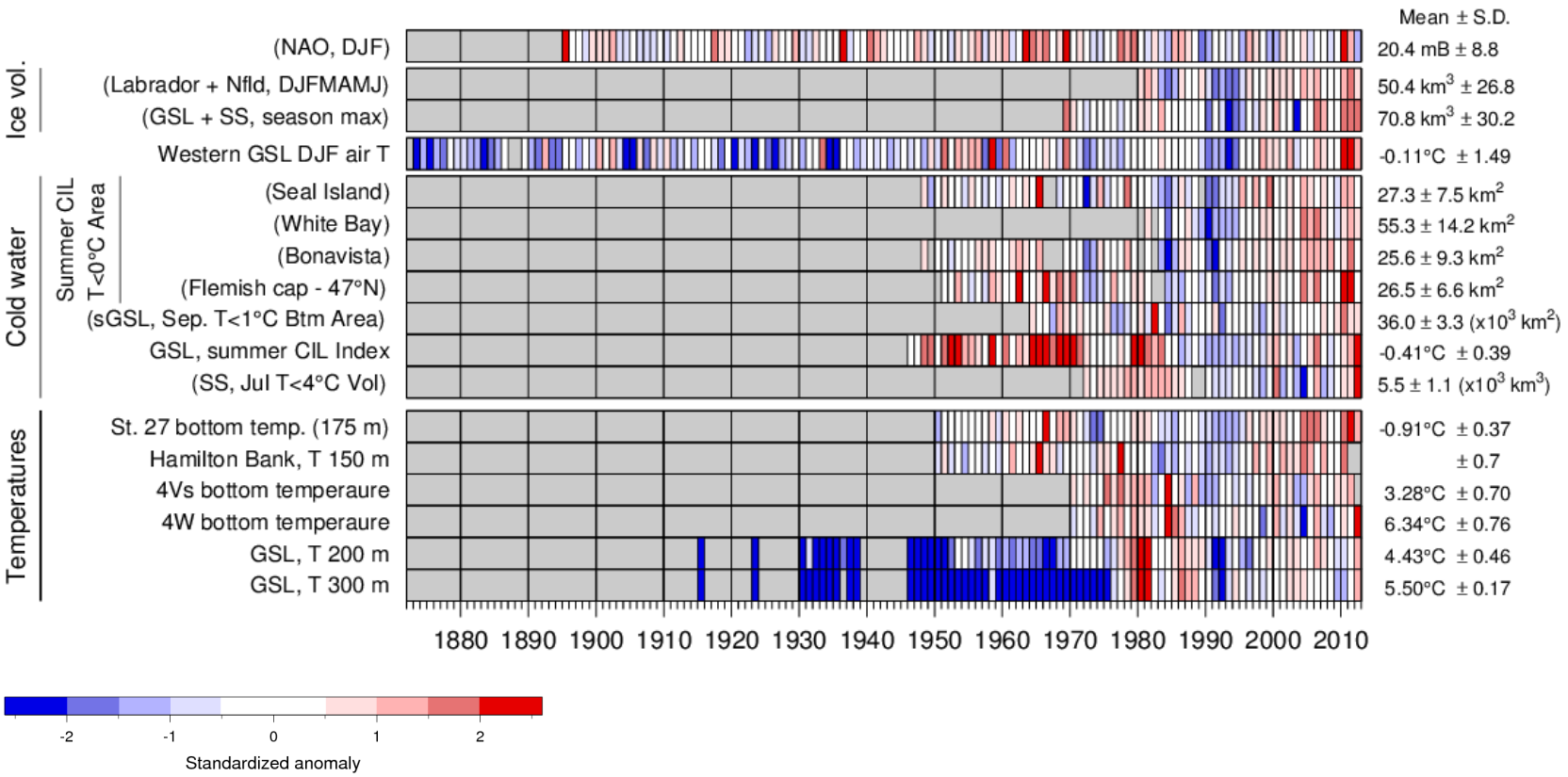

Figure 5-9 Summary of environmental and oceanographic variables. A grey cell indicates missing data, a white cell is a value within 0.5 standard deviations of the long-term mean based on data from 1981–2010 when possible; for the NAO index, ice volumes, cold-water volumes and areas, and bottom temperature, a red cell indicates warmer-than-normal conditions and smaller volumes and areas, a blue cell colder than normal. Long-term means and standard deviations are shown on the right-hand side of the figure. (North Atlantic Oscillation [NAO], GSL [Gulf of St. Lawrence], sGSL [southern Gulf of St. Lawrence], cold intermediate layer [CIL]).

Prior work and new results presented here have identified correlations with ice and winter air temperatures. The 1980-2010 correlation between average seasonal ice volume on the Shelf with the CIL area along the various Newfoundland and Labrador sections varies between $R^2 = 0.51$ to 0.55.

Previous work had identified a correlation between GSL summer CIL conditions, winter ice and mixed layer volumes, and air temperatures (using NCDIA). The updated relation between the seasonal maximum ice volume and the December-January-February average air temperature (using AHCCD) in the western GSL between 1969 and 2012 has a high correlation coefficient ($R^2 = 0.72$). Air temperature anomalies greater than +2.5°C account for all three very-low-ice winter seasons recorded by the Canadian Ice Service in the GSL (1969, 2010 and 2011; Figs. 5-4 and 5-5). The December-January-February average air temperature has increased at a mean rate of 2.0°C per century since the 1870s and 3.2°C per century over the last five decades. The same latter trend in coming decades would lead to very low sea-ice cover in the GSL (similar to 1969, 2010 and 2011) during a climatologically normal winter by the end of this century, with sea ice in larger quantities than during the winters of 2010 and 2011 present only during anomalously cold winters.

Sub-CIL and bottom water properties in the GSL and Scotian Shelf vary widely on decadal timescales depending on the mixture of warm and salty Warm Slope Water, and cold and relatively fresh Labrador Slope Water. Strongest correlations are found between bottom temperatures on the central and eastern Scotian Shelf (NAFO regions 4W and 4Vs, $R^2 = 0.39$), between bottom temperature in 4Vs and waters at 150 m in Cabot Strait ($R^2 = 0.37$), between Hamilton Bank and station 27 ($R^2 = 0.29$), and, lastly, between the 4W bottom temperature and Cabot Strait water temperatures ($R^2 = 0.23$-0.27 at 150-200m in Cabot Strait). While shifts have been related to the winter NAO Index, zero-lagged correlations are low ($R^2 = 0.15$ to 0.18). The long term trends observed at Cabot Strait do not reflect changes in recent decades; although the GSL deep waters remain rich in Slope Water content compared to pre-1975 values and waters have been warming since 1991, the mixing ratio was comparable in 2012 to that of the late 1970's.

5.6 Acknowledgements

This work was supported by DFO's Aquatic Climate Change Adaptation Services Program (ACCASP). The authors thank Brian Petrie, Ingrid Peterson, and John Loder for useful and constructive comments on a draft of this manuscript.

5.7 References

Bugden, G. L. 1991. Changes in the temperature-salinity characteristics of the deeper waters of the Gulf of St. Lawrence over the past several decades. p. 139-147. In J.-C. Therriault [Ed.] The Gulf of St. Lawrence: small ocean or big estuary? Can. Spec. Publ. Fish. Aquat. Sci. 113.

Colbourne, E. B. 2004. Decadal changes in the ocean climate in Newfoundland and Labrador waters from the 1950s to the 1990s. *J. Northw. Atl. Fish. Sci.*, 34, 43-61, doi:10.2960/J.v34.m478.

Colbourne, E., J. Craig, C. Fitzpatrick, D. Senciall, P. Stead, and W. Bailey. 2012. An assessment of the physical oceanographic environment on the Newfoundland and Labrador Shelf during 2011. DFO Can. Sci. Advis. Sec. Res. Doc. 2012/044: iv + 33 p. http://www.dfo-mpo.gc.ca/csas-sccs/Publications/ResDocs-DocRech/2012/2012_044-eng.pdf

Colbourne, E. B., S. Narayanan, and S. Prinsenberg. 1994. Climatic change and environmental conditions in the Northwest Atlantic during the period 1970-1993. *ICES Mar. Sci. Symp*., 198, 311-322.

Colbourne, E., B. deYoung, S. Narayanan, and J. Helbig. 1997. Comparison of hydrography and circulation on the Newfoundland Shelf during 1990–1993 with the long-term mean. *Can. J. Fish. Aquat. Sci.* 54 (Suppl. 1), 68–80.

Cyr, F., D. Bourgault and P. S. Galbraith, 2011. Interior versus boundary mixing of a cold intermediate layer. *J. Geophys. Res. (Oceans)*, 116, C12029, doi:10.1029/2011JC007359

Drinkwater, K. F. 1996. Climate and oceanographic variability in the Northwest Atlantic during the 1980s and early-1990s. *J. Northw. Atl. Fish. Sci*., 18, 77-97.

Galbraith, P.S., 2006. Winter water masses in the Gulf of St. Lawrence. *J. Geophys. Res. (Oceans)*, 111, C06022. doi: 10.1029/2005JC003159

Galbraith P. S., P. Larouche, J. Chassé, and B. Petrie. 2012a. Sea-surface temperature in relation to air temperature in the Gulf of St. Lawrence: interdecadal variability and long term trends. *Deep Sea Res. II*, http://dx.doi.org/10.1016/j.dsr2.2012.04.001

Galbraith, P. S., J. Chassé, D. Gilbert, P. Larouche, D. Brickman, B. Pettigrew, L. Devine, A. Gosselin, R. G. Pettipas, and C. Lafleur. 2012b. Physical Oceanographic Conditions in the Gulf of St. Lawrence in 2011. DFO Can. Sci. Advis. Sec. Res. Doc. 2012/023. iii + 85 p. http://www.dfo-mpo.gc.ca/csas-sccs/Publications/ResDocs-DocRech/2012/2012_044-eng.pdf

Galbraith, P. S., P. Larouche, D. Gilbert, J. Chassé, and B. Petrie. 2010. Trends in sea-surface and CIL temperatures in the Gulf of St. Lawrence in relation to air temperature. *Atlantic Zone Monitoring Program Bulletin*, 9: 20-23. http://www.meds-sdmm.dfo-mpo.gc.ca/isdm-gdsi/azmp-pmza/docs/bulletin_9_04.pdf

Galbraith, P. S. and P. Larouche. 2013. Trends and variability in eastern Canada sea-surface ocean temperatures. Ch. 1 (p. 1-18) *In:* This report.

Gilbert, D. 2004. Propagation of temperature signals from the northwest Atlantic continental shelf edge into the Laurentian Channel. *ICES CM*, 2004/N:7, 12 pp.

Gilbert, D. and B. Pettigrew. 1997. Interannual variability (1948-1994) of the CIL core temperature in the Gulf of St. Lawrence. *Can. J. Fish. Aquat. Sci.*, 54 (Suppl. 1), 57–67.

Gilbert, D., B. Sundby, C. Gobeil, A. Mucci, and G.-H. Tremblay. 2005. A seventy-two-year record of diminishing deep-water oxygen in the St. Lawrence estuary: The northwest Atlantic connection. *Limnol. Oceanogr.*, 50(5), 1654–1666.

Han, G. E. Colbourne, P. Pepin, and R. Tang. 2013. Statistical projections of physical oceanographic variables over the Newfoundland and Labrador Shelf. Ch. 6 (p. 73-84) *In:* This report.

Hebert, D., R. Pettipas, B. Petrie, and D. Brickman. 2012. Meteorological, Sea Ice and Physical Oceanographic Conditions on the Scotian Shelf and in the Gulf of Maine during 2011. DFO Can. Sci. Advis. Sec. Res. Doc. 2012/055. iv + 42 p.
http://www.dfo-mpo.gc.ca/Csas-sccs/publications/resdocs-docrech/2012/2012_055-eng.pdf

Hebert, D. 2013a. Trends in temperature, salinity and stratification in the upper ocean for different regions of the Atlantic Canadian Shelf. Ch. 3 (p. 33-42) *In:* This report.

Hebert, D. 2013b. Trends in temperature, salinity and stratification in the upper ocean for the Scotian Shelf. Ch. 4 (p. 43-56) *In:* This report.

Lauzier, L. M. and R. W. Trites. 1958. The deep waters of the Laurentian Channel. J. *Fish. Res. Board Can.*, 15, 1247–1257.

McLellan, H. J. 1957. On the distinctness and origin of the slope water off the Scotian Shelf and its easterly flow south of the Grand Banks. *J. Fish. Res. Board. Can.*, 14, 213–239.

Petrie, B. 2007. Does the North Atlantic Oscillation affect hydrographic properties on the Canadian Atlantic continental shelf? *Atmos.-Ocean*, 45(3), 141–151.

Petrie, B., and K. Drinkwater. 1993. Temperature and salinity variability on the Scotian Shelf and in the Gulf of Maine 1945–1990. *J. Geophys. Res.*, 98, 20,079–20,089.

Rogers, J. C. 1984. The association between the North Atlantic Oscillation and the Southern Oscillation in the Northern Hemisphere. *Mon. Wea. Rev*., 112, 1999-2015.

Umoh, J. U. and K. R. Thompson. 1994. Surface heat flux, horizontal advection, and the seasonal evolution of water temperature on the Scotian Shelf. *J. Geophys. Res.*, 99, 20403–20416.

Umoh, J. U., J. W. Loder, and B. Petrie. 1995. The role of air-sea heat fluxes in annual and interannual ocean temperature variability on the eastern Newfoundland Shelf. *Atmos.-Ocean*, 33(3), 531-568.

Vincent, L. A., X. L. Wang, E. J. Milewska, H. Wan, F. Yang, and V. Swail. 2012: A Second Generation of Homogenized Canadian Monthly Surface Air Temperature for Climate Trend Analysis. *J. Geophys. Res.*, 117, D18110, doi: 10.1029/2012JD017859.

6 Statistical projections of physical oceanographic variables over the Newfoundland and Labrador Shelf

Guoqi Han [1] *,Eugene Colbourne [1], Pierre Pepin [1], and Ruohan Tang [1, 2, 3]

[1] Fisheries and Oceans Canada, Northwest Atlantic Fisheries Centre
P.O. Box 5667, St. John's, Newfoundland and:Labrador A1C 5X1

[2] Memorial University of Newfoundland
St. John's, Newfoundland and Labrador

[3] Hohai Univeristy, Nanjing, China

* Correspondence: Guoqi.Han@dfo-mpo.gc.ca

Suggested Citation:

Han, G., E. Colbourne, P. Pepin and R. Tang. 2013. Statistical projections of physical oceanographic variables over the Newfoundland and Labrador Shelf. Ch.6 (p. 73-84) *In:* Aspects of climate change in the Northwest Atlantic off Canada [Loder, J.W., G. Han, P.S. Galbraith, J. Chassé and A. van der Baaren (Eds.)]. Can. Tech. Rep. Fish. Aquat. Sci. 3045: x + 190 p.

Abstract

Present global climate models (GCM) are unable to resolve many oceanic processes, and, thus, are unable to provide reasonable projections for coastal and shelf physical oceanographic properties. On the other hand, studies have shown that physical oceanographic properties over the Newfoundland and Labrador Shelf are closely linked to air temperatures. Here we first explore statistical relationships between shelf oceanographic properties and air temperature based on historical observations. Oceanographic properties include the sea surface temperature at Station 27, the fall bottom temperature over the Newfoundland Shelf, the area of the cold intermediate layer on the Flemish Cap (47°N) section, the winter sea ice extent off Newfoundland and Labrador, and the number of icebergs south of 48°N. Using the statistical relationships we then project future states of the physical oceanographic variables under two representative concentration pathways (RCP): RCPs 4.5 and 8.5, based on the projected air temperatures from two global climate models (GCM): CanESM2 and GFDL-ESM2M. Projections are also produced under the A1B emission scenario based on the model air temperatures from a Canadian regional climate model (CRCM). The CRCM or CanESM2 air temperatures at St. John's and Cartwright have stronger trends than the GFDL-ESM2M air temperature.

In the next 50 years, the projected sea surface temperature increases off eastern Newfoundland (Station 27) range from 0.4 to 2.0°C. The bottom temperature increases over the Newfoundland and Labrador Shelf range from 0.4 to 2.1°C. The area of the cold intermediate layer (<0°C) decreases on the Flemish Cap (47°N) section are in the range of 2 to 10 km^2 (8-38% of the 1981-2010 mean). The sea ice extent decreases off Labrador and Newfoundland range from 0.3 to 1.6×10^5 km^2 (15-80%), and the decrease in the number of icebergs at 48°N off Newfoundland

range from 245 (30%) to 1315 (almost no icebergs at this latitude). The differences between the CanESM2 and GFDL models are larger than those between the two RCPs. Despite differences among the models and scenarios, statistical projections indicate that conditions in this region will reach or exceed the upper range of conditions that were observed over the course of past monitoring activities, possibly as early as 2040. It is cautioned that the statistical relationships established are from historical data and may not hold for the future and that there are large uncertainties in the air temperatures projected by the climate models.

6.1 Introduction

Present global climate models (GCMs) are unable to resolve many oceanic processes (such as mesoscale and sub-mesoscale eddies) that are important to climate variability, and thus unable to provide reasonable projections of water properties in many parts of the world ocean, especially for coastal and shelf regions (e.g. Loder and van der Baaren, 2013). One solution is to develop dynamic downscaling based on regional climate models (RCMs) (e.g. Chassé *et al.*, 2011; Guo *et al.*, 2013). However, such downscaled RCMs are not always available or even if available they are still insufficient to resolve some important oceanic processes. An alternative, then, is to develop statistical downscaling based on historical observations.

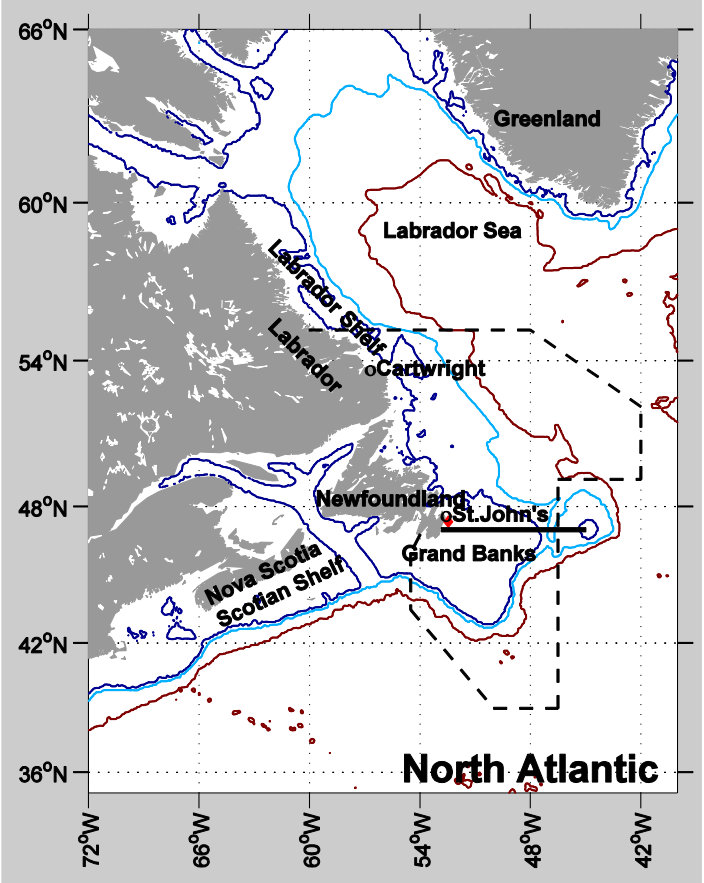

Figure 6-1 Map showing the study region. Station 27 (red diamond), the Flemish Cap transect (black line), and the area with the fall bottom temperature data (dashed lines) are indicated. The 200 (dark blue), 1000 (light blue), and 3000 (red) m isobaths are depicted.

The subpolar Northwest Atlantic (Fig. 6-1) is important and sensitive to climate variability and change. For the Labrador and Newfoundland Shelf, physical oceanographic variables in the shelf region exhibit significant interannual, decadal, and secular changes. Studies (e.g., Deser, 2002) have shown that physical oceanographic properties are closely linked to meteorological forcing, specifically air temperatures and the North Atlantic Oscillation (NAO), the dominant atmospheric mode in the North Atlantic (Hurrell, 1995). In addition, the proximity of the Labrador and Newfoundland Shelf to the North Atlantic subpolar gyre is subject to strong influences by the Labrador Current, the Gulf Stream, and the North Atlantic Current (Loder *et al.*, 1998), which are closely linked to the NAO (Han *et al.*, 2010).

In this study, we combine historical oceanographic and meteorological observations to establish their empirical linear relationships statistically. Based on the output of two GCMs and one RCM, and the established empirical relationships, we project linear trends of ocean variables over the Newfoundland and Labrador Shelf for the next 50 years. For sub-surface temperature trends in eastern Canada and implications for future sea ice in the Gulf of St. Lawrence, see Galbraith *et al.* (2013).

6.2 Data and Method

Historical oceanographic data along standard sections and at fixed sites are available from the Atlantic Zone Monitoring Program (AZMP) (http://www.meds-sdmm.dfo-mpo.gc.ca/isdm-gdsi/azmp-pmza/index-eng.html) and over broad spatial areas from regional fisheries assessment surveys. Anomalies in selected oceanographic variables are calculated relative to their means (Table 6-1) over the period 1981-2010 which is the standard climatological reference period. Linear regressions are carried out to establish statistical relationships between the anomalies of ocean variables of interest and those of air temperature at St. John's and Cartwright. The air temperatures at St. John's and Cartwright are from the Environment Canada (EC) website http://climate.weatheroffice.gc.ca/prods_servs/cdn_climate_summary_e.html, though those from the Adjusted and Homogenized Canada Climate Data would be more suitable. Sea Ice extent was available from Canadian Ice Service (CIS) of EC, and iceberg numbers were provided by the International Ice Patrol of the US Coast Guard.

Table 6-1 Means and standard deviations over 1981-2010. SST: sea surface temperature; CIL: cold intermediate layer; BT: bottom temperature. See Fig. 6-1 for locations.

Variable	1981-2010 Mean	Standard Deviation
SST (°C) at Station 27	5.18	0.82
CIL (km^2) at the Flemish Cap Transect	26.52	6.63
Fall BT (°C) over the Newfoundland and Labrador Shelf	1.61	0.50
Winter Sea Ice Extent (10^5 km^2)	1.96	0.81
Number of Iceberg at 48°N	813	648
NAO (mb)	20.44	8.77
St. John's Air Temperature (°C)	5.03	0.84
Cartwright Air Temperature (°C)	0.05	1.32

By using the statistical relationships, the outputs of CanESM2 (an ensemble of 5 members) and GFDL-ESM2M (1 member only) (Loder and van der Baaren, 2013), and of CRCM (2 members: Guo *et al.*, 2013; Brickman *et al.*, 2013) are used to produce projections for certain oceanographic variables. These include the sea surface temperature (SST) at a fixed monitoring site off eastern Newfoundland (Station 27, located approximately 8 km off St. John's), the fall bottom temperature (BT) over the Newfoundland and Labrador Shelf (the North Atlantic Fisheries Organization Divisions 2J3KLNO), the area of the cold intermediate layer of shelf water <0°C (CIL) along the Flemish Cap (47°N) section, the sea ice extent (SIE) off Labrador and Newfoundland south of 55°N, and the number of icebergs south of 48°N (Fig. 6-1). Two representative concentration pathways (RCPs), RCP4.5 and RCP8.5, are considered for CanESM2 and GFDL-ESM2M, corresponding to moderate and extreme emissions of CO_2, respectively. For CRCM, only a moderate emission scenario (A1B) is considered that was downscaled from the predecessor of CanESM2. Differences among members of a model represent the model's internal variability. The projected trends are essentially the same for the 5 members of CanESM2, therefore we show the ensemble results only. According to Loder and van der Barren (2013) GFDL and CanESM provide approximate lower and higher bounds for projected changes among 6 ESMs they considered.

Note that the values in all the figures are the anomalies relative to the means over the period 1981-2010 (Table 6-1). We linearly fit the statistically projected values over 2011-2100 (CanESM2 and GFDL-ESM2M) or 2011-2070 (CRCM). The linear changes over 2011-2060 are presented in the next section.

6.3 Results

SST at Station 27

There is a strong positive correlation ($R^2 = 0.72$) between the annual-mean SST at Station 27 and the annual-mean air temperature at St. John's (Fig. 6-2). The CanESM2 air temperature projections at St. John's predict a greater increase over time; while the GFDL-ESM2M output demonstrates greater variability and a weaker increase in temperature (Fig. 6-3). Based on the CanESM2 output, the projected annual-mean SST increase is about 1.0 and 2.0°C by 2060, under RCP4.5 and RCP8.5, respectively (Fig. 6-3). The GFDL-ESM2M projections indicate an increase of about 0.4 and 1.0°C, respectively. The CRCM projected increases are 1.2 to 1.6°C.

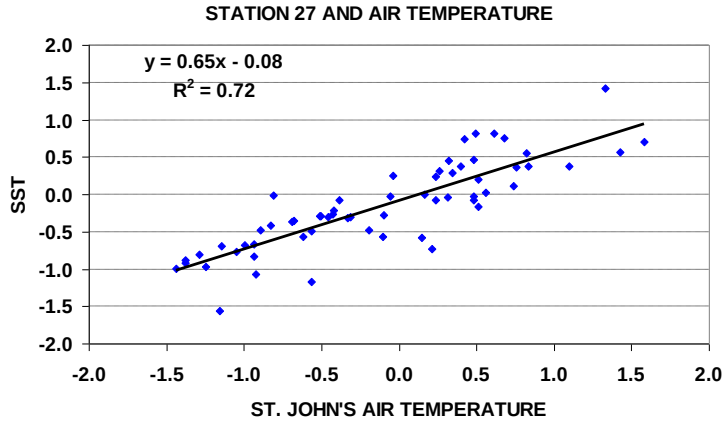

Figure 6-2 Scatter diagram between the observed sea surface temperature anomalies (SST, °C) at Station 27 and the observed air temperature anomalies (°C) at St. John's from 1950-2010. The line is the linear fit to the annual-mean observations

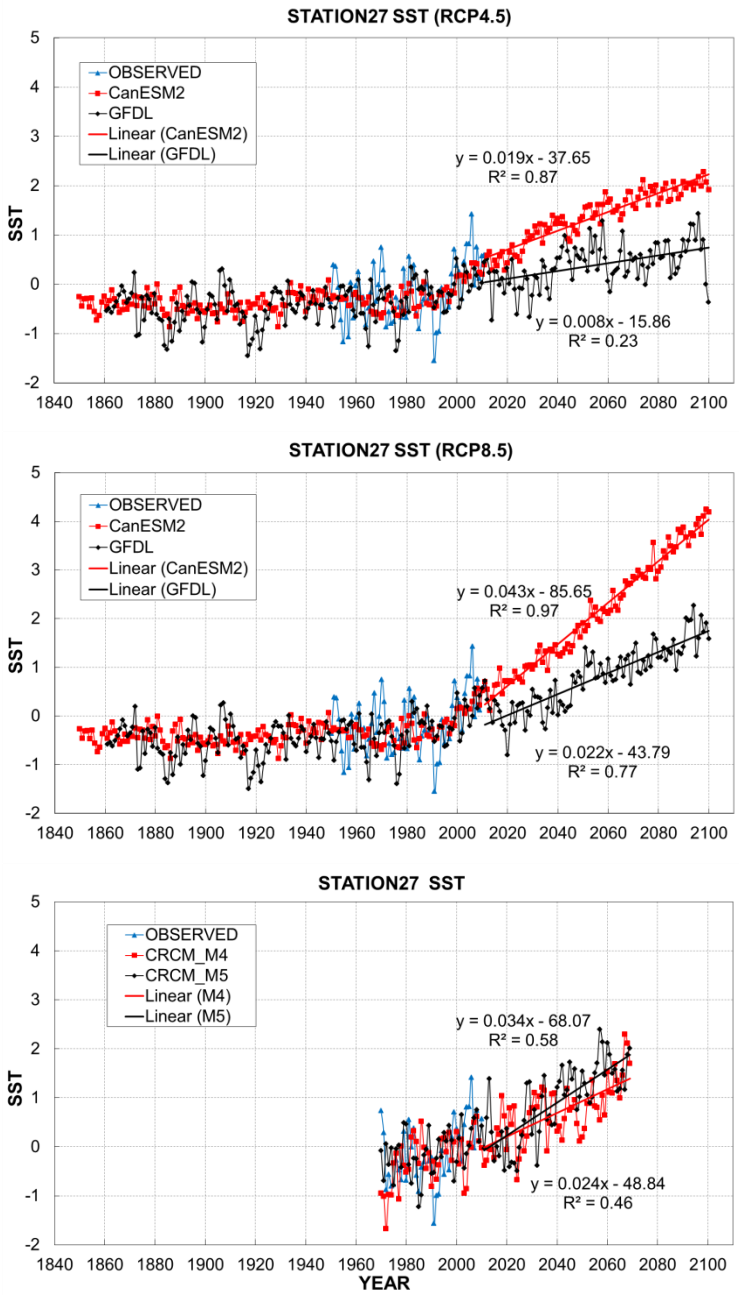

Figure 6-3 Reconstructed SST anomalies (°C) at Station 27 based on the simulated air temperature anomalies at St. John's. The air temperatures are the CanESM2 and GFDL-ESM2M output under RCP4.5 and RCP8.5 and the CRCM output under A1B. The straight lines are the linear fits to the SST projections over 2011-2100 or over 2011-2070.

BT over the Newfoundland and Labrador Shelf

The fall BT over the Newfoundland and Labrador Shelf shows a strong positive correlation (R^2 = 0.61) with the annual mean air temperature at Cartwright (Fig. 6-4). Based on the CanESM2 output, the projected BT increase is 1.0 and 2.1°C by 2060, under RCP4.5 and RCP8.5, respectively (Fig. 6-5). Based on the GFDL-ESM2M output, BT is projected to rise 0.4 and 1.0°C, respectively, under RCP4.5 and RCP8.5. The CRCM projected increases are 1.3 to 1.6°C.

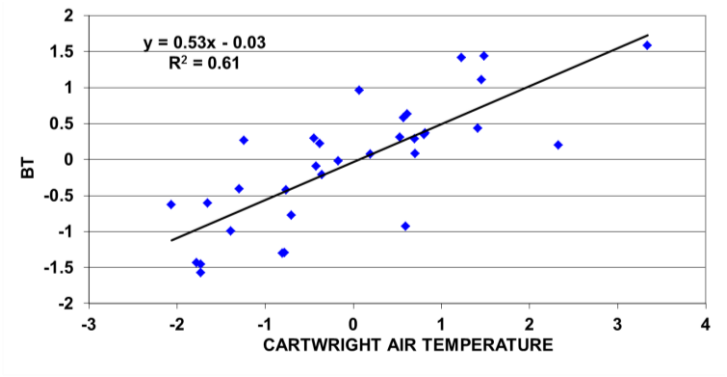

Figure 6-4 Scatter diagram between the observed fall bottom temperature anomalies (BT, °C) over the Newfoundland and Labrador Shelf and the observed air temperature anomalies (°C) at Cartwright from 1978-2010. The line is the linear fit to the observations.

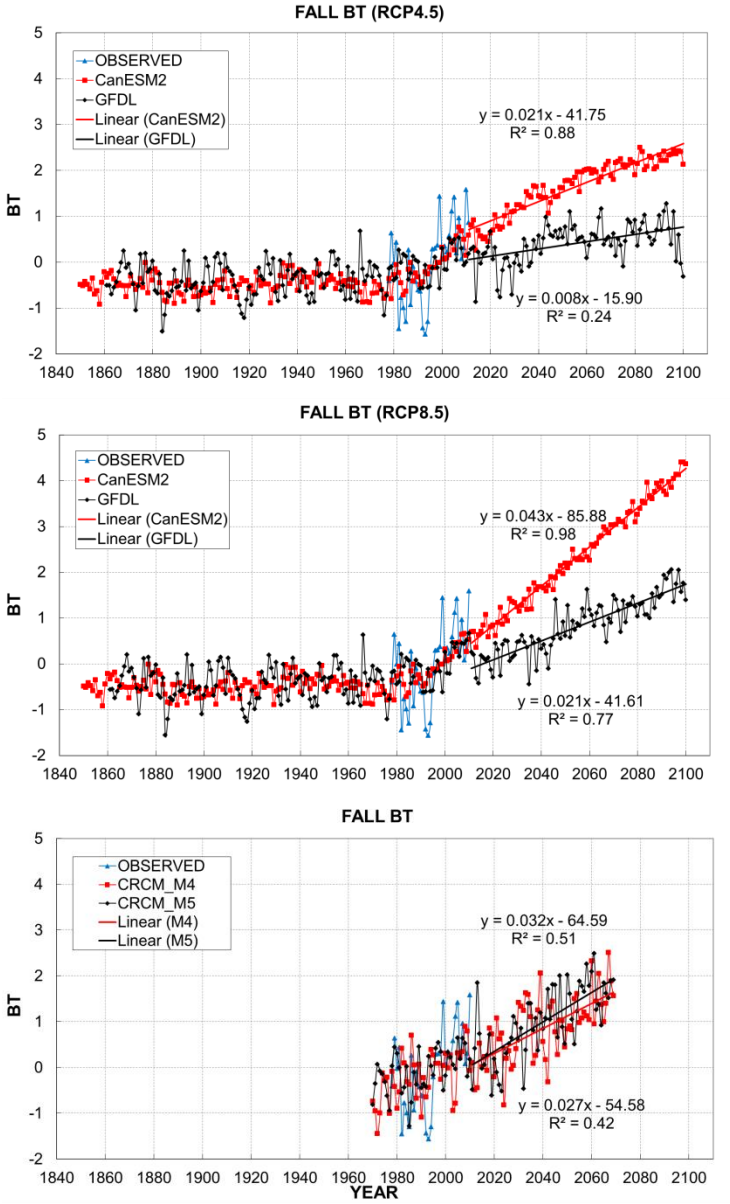

Figure 6-5 Reconstructed fall bottom temperature anomalies (BT, °C) over the Newfoundland and Labrador Shelf based on the simulated air temperature anomalies at Cartwright. The air temperatures are the CanESM2 and GFDL-ESM2M output under RCP4.5 and RCP8.5 and the CRCM output under A1B. The straight lines are the linear fit to the BT projections over 2011-2100 or over 2011-2070.

CIL area along the Flemish Cap (47ºN) Section

The summer CIL area on the Flemish Cap section is correlated (R^2 = 0.47) with the winter (January through March) mean air temperature upstream at Cartwright (Fig. 6-6) but represents the weakest of the statistical relationships explored in this analysis. By 2060, the projected CIL decreases by about 5 and 8 km^2 (19 and 30% of the 1981-2010 mean) under RCP4.5 and RCP8.5, respectively, based on CanESM2 output (Fig. 6-7). The CIL area decreases are 2 and 5 km^2 (8 and 19% of the 1981-2010 mean) under RCP4.5 and RCP8.5, respectively, based on the GFDL-ESM2M output. The CRCM projected decreases are 8-10 km^2 (30-38% of the 1981-2010 mean).

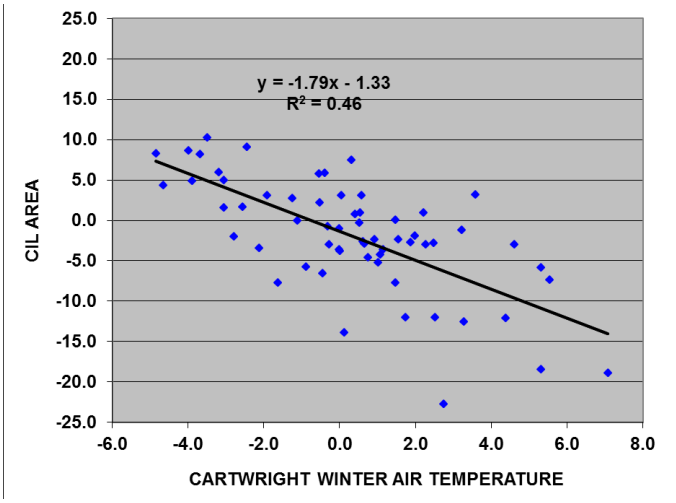

Figure 6-6 Scatter diagram between the observed cold intermediate layer (CIL) area anomalies (km^2) along the Flemish Cap transect and the observed winter air temperature anomalies (°C) at Cartwright from 1951-2011. The line is the linear fit to the observations.

Winter SIE off Labrador and Newfoundland

The winter SIE off Labrador and Newfoundland is highly correlated (R^2 = 0.80) with the winter mean air temperature at Cartwright (Fig. 6-8). The difference between the CanESM2 reconstructed and observed SIE has a standard deviation of 0.8×10^5 km^2 over 1963-2011. By 2060, the projected SIE decreases are approximately 0.8 and 1.3×10^5 km^2 (40 and 65% of the 1981-2010 mean) under RCP4.5 and RCP8.5, respectively, based on the CanESM2 output (Fig. 6-9). Projected decreases are of $0.3\text{-}0.7\times10^5$ km^2 (15-35% of the 1981-2010 mean) under RCP4.5 and RCP8.5, respectively, based on the GFDL-ESM2M output. The CRCM projected decreases are $1.3\text{-}1.6\times10^5$ km^2 (65-80% of the 1981-2010 mean).

Iceberg number at 48ºN off Newfoundland

The iceberg number at 48°N is correlated (R^2 = 0.40) with the winter mean air temperature at Cartwright (Fig. 6-10). By 2060, the projected decrease in the number of icebergs range, approximately, from 641-1315 (79-162% of the 1981-2010 mean) under RCP4.5 and RCP8.5, respectively, based on the CanESM2 output (Fig. 6-11). There are projected decreases of 245-630 icebergs (30-77% of the 1981-2010 mean) under RCP4.5 and RCP8.5, respectively, based on the GFDL-ESM2M output. The CRCM projected decreases are 831-955 (102-117% of the 1981-2010 mean).

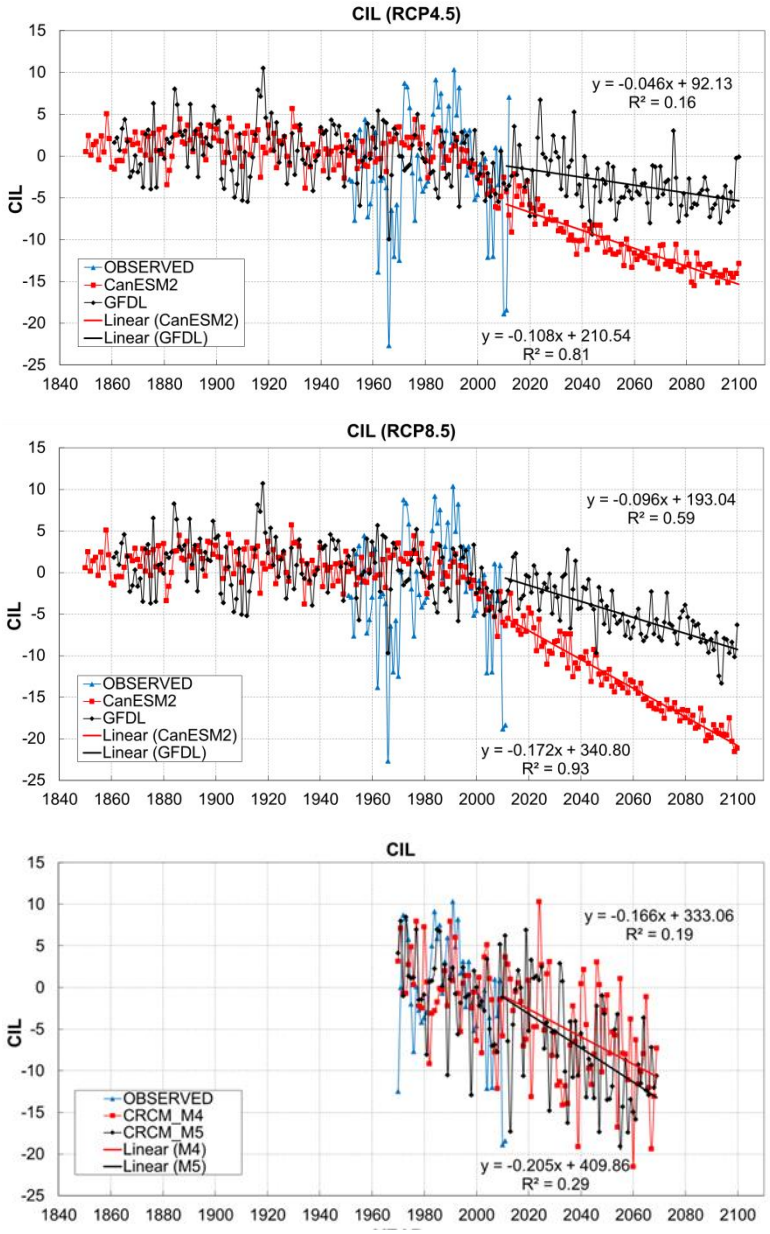

Figure 6-7 Reconstructed cold intermediate layer (CIL) area anomalies (km^2) along the Flemish Cap transect based on the simulated winter air temperature anomalies at Cartwright. The air temperatures are the CanESM2 and GFDL-ESM2M output under RCP4.5 and RCP8.5 and the CRCM output under A1B. The straight lines are the linear fit to the CIL projections over 2011-2100 or over 2011-2070.

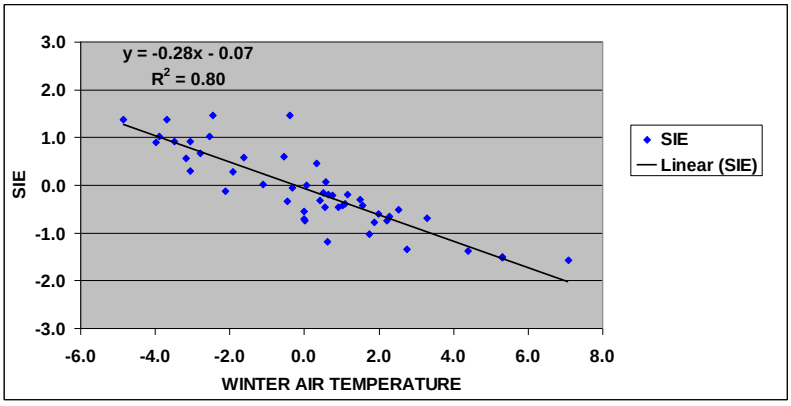

Figure 6-8 Scatter diagram between the observed sea ice extent (SIE) anomalies ($\times 10^5$ km^2) off Labrador and Newfoundland and the observed winter air temperature anomalies (°C) at Cartwright from 1963-2011. The line is the linear fit to the observations.

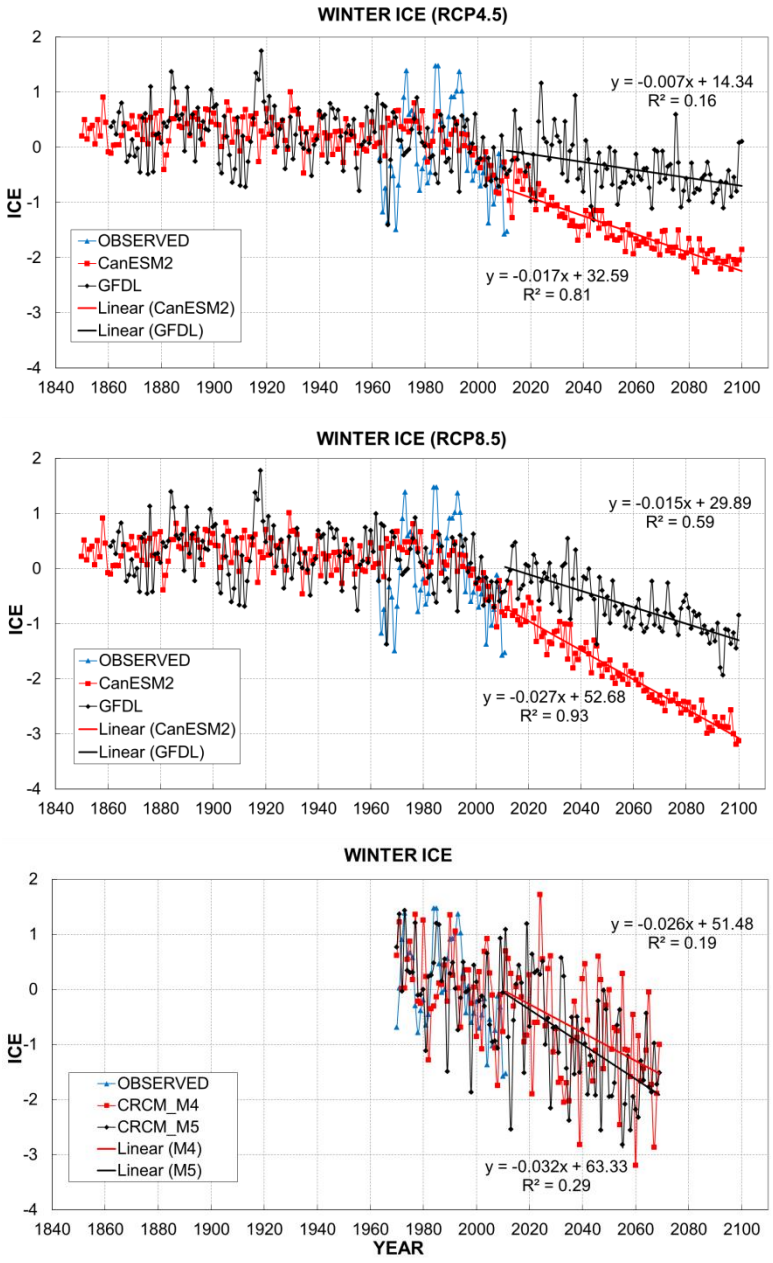

Figure 6-9 Reconstructed sea ice extent anomalies (SIE) ($\times 10^5$ km^2) off Labrador and Newfoundland based on the simulated winter air temperature anomalies at Cartwright. The air temperatures are the CanESM2 and GFDL-ESM2M output under RCP4.5 and RCP8.5 and the CRCM output under A1B. The straight lines are the linear fit to the SIE projections from 2011-2100. Note that years with SIE anomalies below -1.96 x 10^5 km^2 are ice-free.

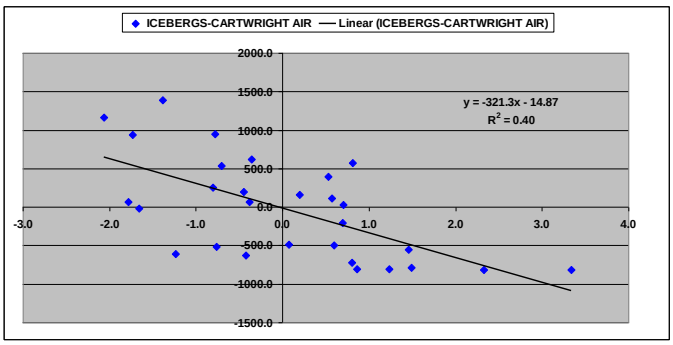

Figure 6-10 Scatter diagram between the observed number of icebergs anomalies at 48°N and the observed winter air temperature anomalies (°C) at Cartwright from 1983-2011. The line is the linear fit to the observations.

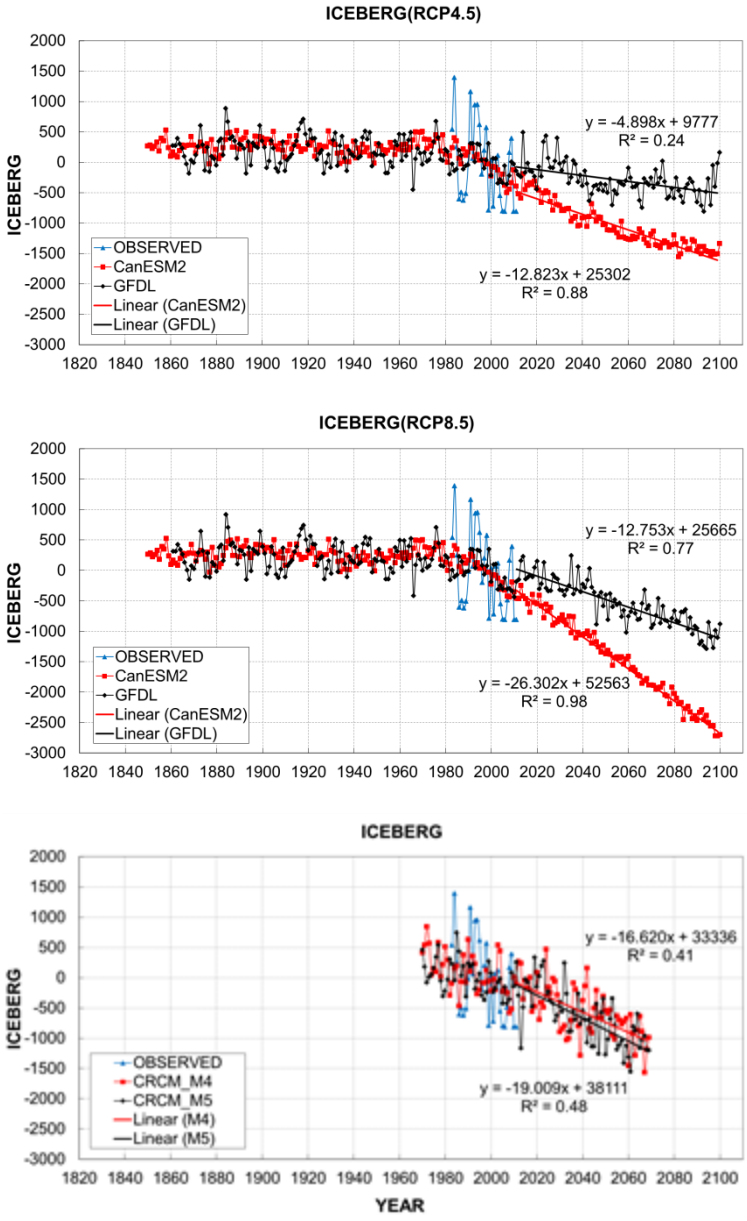

Figure 6-11 Reconstructed iceberg number anomalies at 48°N based on the simulated winter air temperature anomalies at Cartwright. The air temperatures are the CanESM2 and GFDL-ESM2M output under RCP4.5 and RCP8.5 and the CRCM output under A1B. The straight lines are the linear fit to the iceberg number projections from 2011-2100. Note that years with iceberg number anomalies below -813 are iceberg-free.

6.4 Conclusions

The preliminary empirical relationships identified in the Newfoundland and Labrador region demonstrate patterns that are consistent with expectations and the mechanisms involved in generating them. There is a strong link between air temperatures and SST (R^2 = 0.72) and sea ice extent (R^2 = 0.80) which reflects the strong interaction between these environmental metrics. A slightly weaker relationship exists between bottom temperature and air temperature at Cartwright (R^2 = 0.61). The weakening may be attributable partly to the time lag required for temperature variations to propagate from the surface to the bottom and partly to the influence of other processes that can affect conditions at the seafloor. The weak relationship between air temperature and the area of the CIL (R^2 = 0.47) may also reflect the time required and variables that affect intermediate water formation, the variability in ocean currents that can affect the CIL, and the underlying uncertainty in the estimation of the area of cold water and the coastal air

temperature station representativeness of the CIL water formation area. The influence of the air temperature on the iceberg melting (R^2 = 0.40) is, to a large degree, through its effects on the surface and subsurface water temperature and also on the extent of sea ice cover.

Using statistical relationships, we projected five physical oceanographic variables under RCPs 4.5 and 8.5, based on the projected air temperatures from two GCMs: CanESM2 and GFDL-ESM2M. Projections were also produced under the A1B emission scenario based on the projected air temperatures from the CRCM. The CRCM or CanESM2 air temperature at St. John's and Cartwright has stronger trends than the GFDL-ESM2M air temperature. In the next 50 years: the projected sea surface temperature increase at Station 27 ranges from 0.4 to 2.0°C; the projected bottom temperature increase over the Newfoundland and Labrador Shelf ranges from 0.4 to 2.1°C; the projected area of the cold intermediate layer decreases on the Flemish Cap (47°N) section from 2 to 10 km^2 (8-38% of the 1981-2010 mean); the projected sea ice extent decrease off Labrador and Newfoundland ranges from 0.3 to 1.6×10^5 km^2 (15-80%); and the decrease in the number of icebergs at 48°N off Newfoundland is in the range of 245 (30%) to 1315 (almost no icebergs at this latitude).

Although the three models predict differing magnitudes of change under the two RCPs and A1B scenario, they all project increases in environmental temperature throughout the Newfoundland and Labrador region over the next 50 years. Despite differences among models and scenarios, projections based on statistical downscaling indicate that conditions in this region will reach or move beyond the upper range of conditions that were observed over the course of past monitoring activities, possibly as early as 2040.

Despite differing levels of uncertainty in the statistical relationships that were to be used for projections, we note some important consistencies among variables, models, and representative concentration pathways. In many instances, there are differences between models and RCPs but these are generally small relative to the magnitude of the underlying residual error. In particular, the results produced, based on CanESM2 RCP4.5 and CRCM A1B output, are in good agreement. In nearly all instances, projections using CanESM2 demonstrate more pronounced changes than those obtained from GFDL-ESM2M, and, as a result, the likelihood of projected changes exceeding the range of past observations or moving beyond the underlying residual error differs substantially between the two models. Under most circumstances, projections from CanESM2 exceed the range of past observations (and the residual error) under the more conservative RCP4.5. In contrast, projections using GFDL-ESM2M seldom exceed the range of past observations or residual error under either RCP, although they tend to remain close to past extremes (high for temperature; low for areas) for most of the period beyond 2040. It is further cautioned that the statistical relationships established are from historical data and may not hold for the future and that there are large uncertainties in the projected air temperatures by the two GCMs and the CRCM. Therefore improved coupled models are needed.

6.5 Acknowledgment

The work has been funded by the Aquatic Climate Change and Adaptation Service Program (ACCASP) of Fisheries and Oceans Canada. We thank Augustine van der Baaren and John

Loder for providing the CanESM2 and GFDL-ESM2M model output, Lanli Guo for providing the CRCM model output, and Ingrid Peterson for providing the NL Shelf sea ice extent data. John Loder and Peter Galbraith provided review comments.

6.6 References

Brickman, D., B. DeTracey, Z. Long, L. Guo and W. Perrie. 2013. Analyses of CRCM output for climate changes in surface air temperature and wind. Ch. 12 (p. 173-184) *In:* This report.

Chassé, J., W. Perrie, Z. Long, D. Brickman, L. Guo, and M. Moriyasu. 2011. Modelling the vfuture climate of the Gulf of St. Lawrence and Scotian Shelf; an application to snow crab habitat. 45th CMOS Congress, Victoria, BC.

Deser, C., M. Holland, G. Reverdin, and M. Timlin. 2002. Decadal varations in Labrador Sea ice and North Atlantic sea surface temperatures. *J. Geophys. Res.*, 107, doi: 10.1029/2000JC000683.

Galbraith. P.S., D. Hebert, E. Colbourne and R. Pettipas. 2013. Trends and variability in eastern Canada sub-surface ocean temperatures and implications for sea ice. Ch. 5 (p. 57-72) *In:* This report.

Guo, L., W. Perrie, Z. Long, J. Chassé, Y. Zhang, and A. Huang. 2013. Dynamical downscaling over the Gulf of St. Lawrence using the Canadian Regional Climate Model. *Atmos.-Ocean*, 51(3), 265-283, doi: 10.1080/07055900.2013.798778.

Han, G., K. Ohashi, N. Chen, P. G. Myers, N. Nunes, and J. Fischer. 2010. Decline and partial rebound of the Labrador Current 1993-2004: Monitoring ocean currents from altimetric and CTD data. *J. Geophys. Res.*, 115, C12012, doi: 10.1029/2009JC006091.

Hurrell, J. W. 1995. Decadal trends in the North Atlantic Oscillation: regional temperatures and precipitation. *Science, 269*, 676-679.

Loder, J. W., B. D. Petrie, and G. Gawarkiewicz. 1998. The coastal ocean off northeastern North America: a large-scale view, Ch. 5 *In:* The Global Coastal Ocean: Regional Studies and Synthesis. *The Sea*, Vol. 11 [K. H. Brink and A. R. Robinson (Eds.)], John Wiley & Sons, Inc., 105-133.

Loder, J. W. and A. van der Baaren. 2013. Climate change projections for the Northwest Atlantic from six CMIP5 Earth System Models. Can. Tech.. Rep. Hydrogr. Ocean. Sci. 286: xiv + 112p. http://www.dfo-mpo.gc.ca/library/349550.pdf

Loder, J.W., Z. Wang and J. Morrison. 2013. Projected air temperature changes for Canada from eight NARCCAP model combinations. Ch. 11 (p. 151-172) *In:* This report.

7 Interannual-to-decadal variations of the Labrador Current

Guoqi Han *, Nancy Chen and Zhimin Ma

Fisheries and Oceans Canada, Northwest Atlantic Fisheries Centre
P.O. Box 5667, St. John's, Newfoundland and Labrador A1C 5X1

* Correspondence: Guoqi.Han@dfo-mpo.gc.ca

Suggested Citation:
Han, G., N. Chen and Z. Ma. 2013. Interannual-to-decadal variations of the Labrador Current. Ch.7 (p. 85-94) *In:* Aspects of climate change in the Northwest Atlantic off Canada [Loder, J.W., G. Han, P.S. Galbraith, J. Chassé and A. van der Baaren (Eds.)]. Can. Tech. Rep. Fish. Aquat. Sci. 3045: x + 190 p.

Abstract

The alongshore coherence of the Labrador Current off Atlantic Canada on the interannual-to-decadal scales has long been a puzzling question. We have used satellite altimetry data to study climatic variability of the North Atlantic subpolar gyre and the Labrador Current over 1992-2011. The subpolar surface gyre has notable quasi-decadal oscillations, well correlated with the winter North Atlantic Oscillation (NAO) index at zero lag (correlation coefficient r=0.77). It has also been declining in the past two decades. Though the declining trend is statistically significant at the 99% confidence level, it may be part of multi-decadal variability. The proxy Labrador Current transport has two distinct regimes, positively (r=0.46, with the transport lagging by one year) and negatively (r=-0.31, at zero lag) correlated with the winter NAO index in the north (the Labrador Slope) and in the south (the Scotian Slope), respectively. The transports over the Labrador Slope and the Scotian Slope are out of phase (r=-0.49); while those over the Labrador Slope and the northeast Newfoundland Slope are in phase (r=0.80). The proxy Labrador Current transport declines at 0.3-0.5 Sv/decade (1 Sv = 10^6 m^3/s) over the Labrador Slope and increases at 0.1-0.3 Sv/decade over the Scotian Slope. The interannual-to-decadal variability of the Labrador Current transport is comparable to the seasonal variability in magnitude, much smaller than the mean transport over the Labrador Slope, and comparable to or even dominant over the mean transport over the Scotian Slope.

7.1 Introduction

Physical oceanographic variables off Atlantic Canada exhibit significant climate-scale (interannual, decadal, and secular) changes, and are subject to strong influences of the North Atlantic subpolar gyre and the Labrador Current (Loder *et al.*, 1998). Studies (Han and Tang, 2001; Häkkinen and Rhines, 2004; Han *et al.*, 2010) have shown the weakening of the Labrador Current off Labrador and the North Atlantic subpolar gyre as a whole in the 1990s. They all indicated that the weakening over that period is related to the abrupt change of the atmospheric variability in the North Atlantic, whose dominant mode is the well-known North Atlantic Oscillation (NAO) (Hurrell, 1995).

The Labrador Current continues equatorward along the Newfoundland Slope and extends onto the Scotian Slope (Loder *et al.*, 1998; Han, 2011), with its impacts reaching further south in some years (Han, 2002; Smith *et al.*, 2012). Satellite observations indicate significant interannual variability of the Labrador Current over the Newfoundland Slope (Han, 2006) and over the Scotian Slope (Han, 2007). Some distinct and interconnected patterns for the coastal sea level (Han, 2002; Han, 2004b) and temperature and salinity (Petrie, 2007) have been found off Atlantic Canada. It was found that the Labrador Current had significant loss to the deep ocean before reaching the Tail of the Grand Banks at 55°W (Bower *et al.*, 2009; Han *et al.*, 2012). Nevertheless, the phase change of the Labrador Current from the north to the south has not been clear, due to the lack of the long-term current measurements.

The advent of satellite altimetry has provided new opportunity for estimating surface geostrophic currents. Efforts have been made to examine seasonal and interannual variations of the Labrador Current at selected transects from satellite altimetry only (Han, 2004a; Han and Li, 2008) or from the integration of satellite altimetry and *in situ* hydrographic data (Han and Tang, 1999; 2001; Han, 2007; Han *et al.*, 2010). Here we use along-track and gridded satellite altimetry data over 1993 to 2011 to investigate interannual variability and secular changes of the Labrador Current and the subpolar gyre over the past two decades. Our objective is to gain insights about the alongshore changes of the Labrador Current on the interannual scale and its linkages with the subpolar gyre and the NAO.

7.2 Data and Method

We have used weekly merged sea surface height anomalies from AVISO (Archiving Validation and Interpretation of Satellites Oceanographic data, http://www.aviso.oceanobs.com/en/altimetry/index.html). The AVISO dataset for 1992-2011 is an objectively mapped product of TOPEX/Poseidon/Jason-1 (T/P/J), ERS-1, ERS-2, Geosat-Follow-on and Envisat altimeter data, with a 1/3° Mercator projection grid (Ducet at al., 2000). All standard corrections were made to account for wet troposphere, dry troposphere, and ionosphere delays; inverted-barometer responses; sea state bias; and ocean, solid earth, and pole tides. Empirical orthogonal function (EOF) analysis is carried out to extract dominant modes.

We have also used along-track sea surface height anomalies for 1992-2011, including TOPEX/Poseidon, Jason-1, and Jason-2. The satellites repeat their ground track every 9.9156 days. The along-track data are used to derive the cross-track geostrophic current anomalies. The upper-layer volume transport anomalies are calculated by assuming a depth–invariant current structure in the top 200-m layer. The altimetry-based transport anomalies for the top 200 m layer are added onto a model-based long-term mean transport (Han *et al.*, 2008) to construct the proxy Labrador Current transport at selected transects (Fig. 7-1). The depth of 200 m is chosen in a somewhat arbitrary manner, to approximately match the seasonal transport anomalies to observational estimates.

The horizontal extent over which to calculate the Labrador Current transport is chosen based on model climatological mean current features (Han *et al.*, 2008; Han and Loder, 2003; Hannah *et al.*, 2001). The 3000 m isobath is approximately the boundary between the equatorward and poleward flows over the Newfoundland Slope (Han *et al.*, 2008); while the boundary is located

along the 2000 m isobath over the Scotian Slope (Han and Loder, 2003; Hannah *et al.*, 2001). Therefore, the offshore extent is chosen to be the 3000 m isobath for the Newfoundland and Labrador Slope as in Han and Li (2008) and the 2000 m isobath for the Scotian Slope as in Han (2004a).

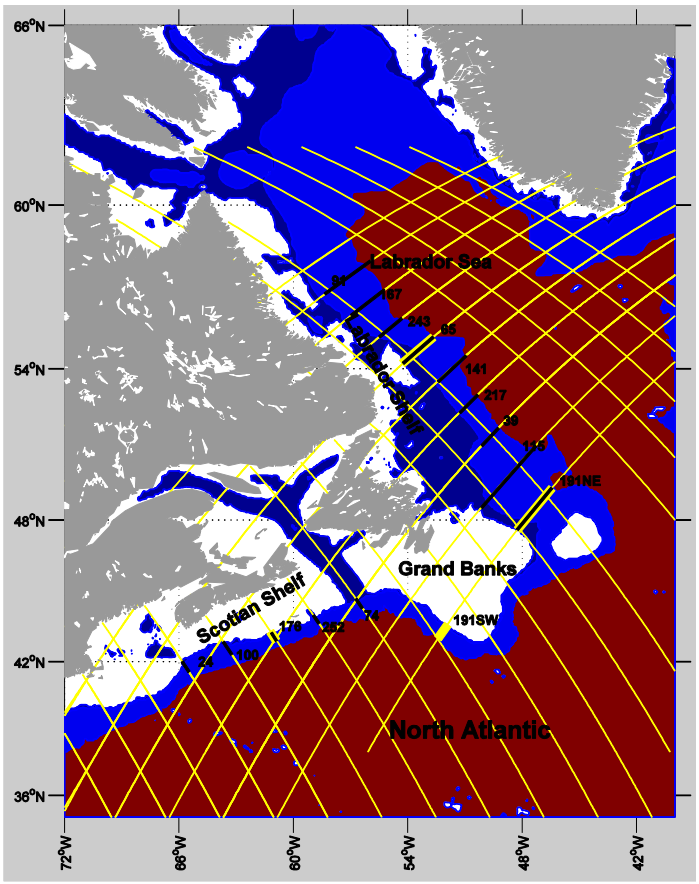

Figure 7-1 Map showing the Northwest Atlantic bottom topography (white: <200 m, blue: 200 to 3000 m, red: > 3000 m) and satellite altimetry ground tracks (yellow curves). The thick highlighted segments are transects where the Labrador Current transport is calculated.

The p-values associated with correlation coefficients and linear trends are calculated without accounting for autocorrelation in the time series. In some cases, the p-values may be larger if the autocorrelation is considered.

7.3 Results

The surface subpolar gyre

The spatial pattern of the first EOF mode represents the subpolar (see surface depression) and subtropical (sea surface dome) gyres at the surface (Fig. 7-2). It accounts for 14% of the total variance. The time series of the first mode shows notable quasi-decadal variability, strong in the early 1990s, around 2000, and in the late 2000s. The annual means of the time series are well correlated with the winter NAO (Fig. 7-3) at zero lag (correlation coefficient r=0.77, p-value p=0.00), implying a fast and primarily barotropic response of the subpolar gyre to the atmospheric forcing (Han *et al.*, 2010). The second highest correlation occurs if the NAO is set to advance the EOF time series by five years (r=0.52, p=0.03). The first mode also indicates that

the subpolar depression became shallower, implying a decline of the subpolar gyre. The decline is statistically significant at the 99% confidence level. If the linear trends of the NAO and first-mode EOF time series are removed the zero-lag correlation coefficient is 0.73 (p=0.00). Due to the short data length, it is difficult from the above to conclude if the apparent decline of the transport over the period is a long-term trend or associated with multi-decadal variability. Recent modelling studies indicate the latter is the likely case, in response to a weakening NAO (Xu *et al.*, 2013; Wang *et al.*, 2013).

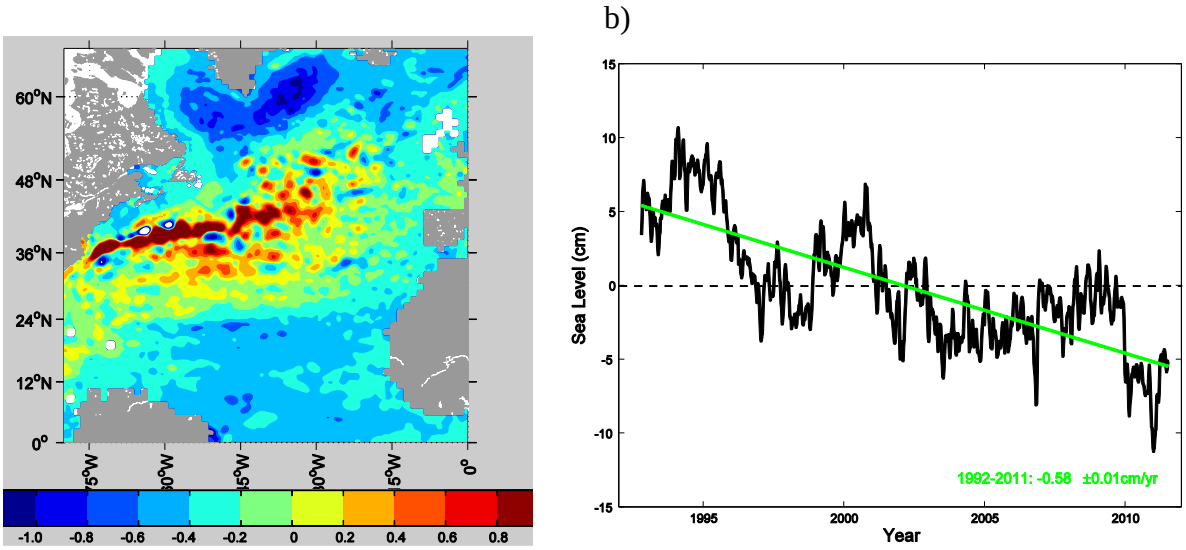

Figure 7-2 The first EOF mode of the altimetric sea surface height anomalies: (a) spatial pattern, and (b) temporal pattern. The first mode accounts for 14% of the total variance.

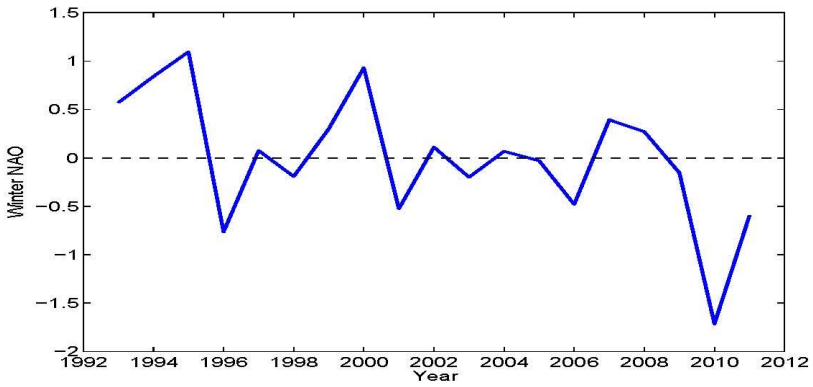

Figure 7-3 The winter (J-M) NAO index.

The Labrador Current transport

The proxy Labrador Current transport shows that the mean Labrador Current decreases equatorward (Fig. 7-4). The most significant loss of the Labrador Current transport is between the central Labrador Slope and the southwestern Grand Banks Slope.

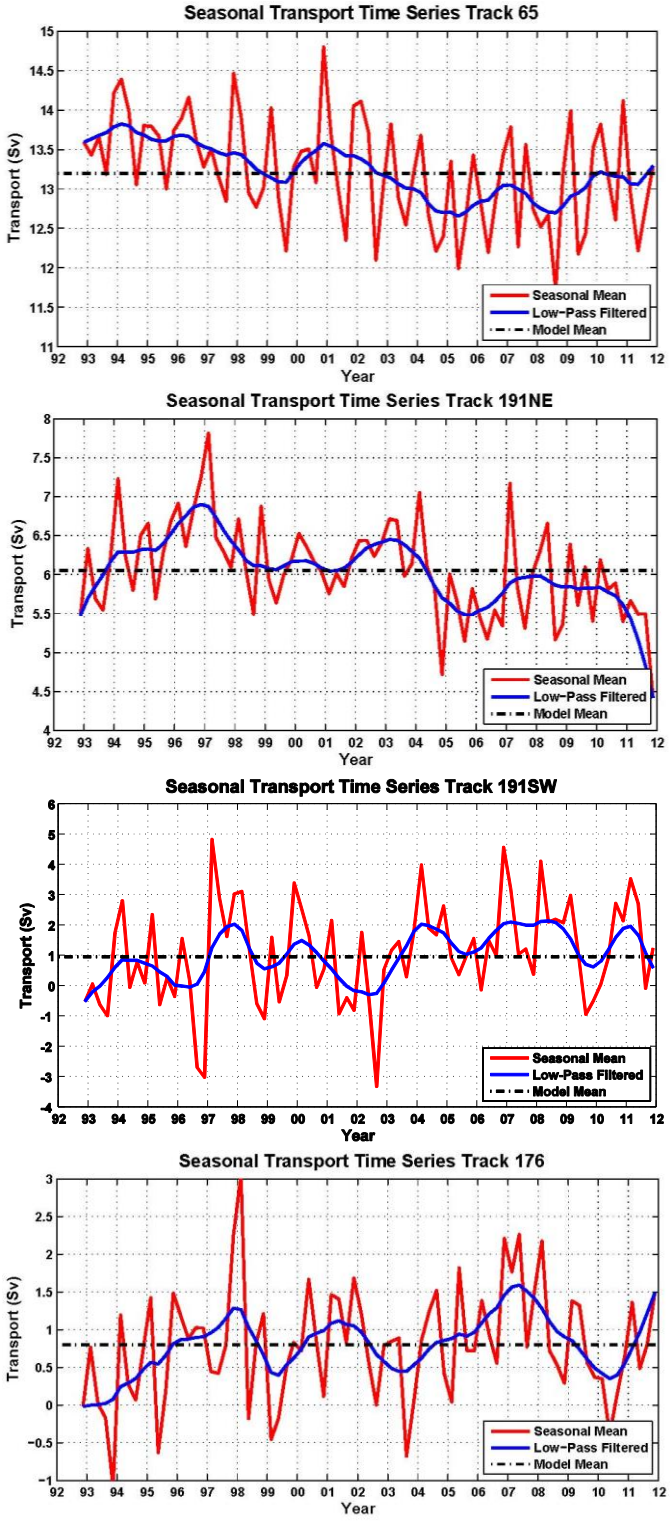

Figure 7-4 Labrador Current transport indices (positive equatorward) across the selected transects: the central Labrador Slope (Track 065), the northeastern Grand Bank Slope (Track 191NE), the southwestern Grand Bank Slope (Track 191SW), and the central Scotian Slope (Track 176). See Fig. 7-1 for locations (thick yellow segment).

There is considerable interannual variability of the Labrador Current transport at the four transects. The interannual variability is comparable to the seasonal one in magnitude, much smaller than the mean transport over the Labrador Slope, and comparable to or even dominant over the mean transport over the Scotian Slope. The transport seems to be declining at track 65, 191ne, increasing at track 176; while that at track 191sw is predominated by the interannual variability with no discernible trend. The decline of the transport from the early to late 1990s at track 065 is consistent with previous findings (Han and Tang, 2001; Han *et al.*, 2010). After a brief and partial rebound, the transport declined further to the lowest in the mid 2000s. In contrast, the transport at track 176 was strengthened in general from the early to late 1990s as shown in Han (2007), and reached its highest value in the mid 2000s on the quasi-decadal time scale.

It seems that the response of the local transports at these transects to the NAO is not always the same as that of the subpolar and subtropical gyres as a whole (see Section 7.1). The correlation coefficients between the annual-mean filtered transports across the four transects (from track 65, 191ne, 191sw, to 176) and the winter NAO index are 0.31 (p=0.20), 0.29 (p=0.22), -0.07 (p=0.78) and -0.09 (p=0.68), respectively. The transport correlation coefficient is 0.76 (p=0.00) between track 65 and 191ne; in contrast the value is -0.33 (p=0.17) between track 65 and 176. These results suggest that the temporal pattern over the Labrador Slope is coherent with that over the northeastern Newfoundland Slope, but not with that over the Scotian Slope (track 176).

However, the estimated transports for individual tracks may be significantly influenced by meanders and eddies pinched off from the Gulf Stream and the North Atlantic Current (Han, 2004a). Thus we have carried out EOF analyses of the filtered transports for the Labrador Slope and for the Scotian Slope. For the Labrador Slope, the first mode (accounting for 78% of the total variance) reveals a coherent spatial pattern. The temporal pattern indicates significant interannual variability with a declining trend (Fig. 7-5) The correlation coefficients between the annual means of the first-mode time series and the winter NAO index are 0.38 (p=0.11), 0.54 (p=0.02), and 0.43 (p=0.08) with the former lagging by zero, one and two years, respectively. For the northeastern Newfoundland Slope, the correlation coefficient between the annual means of the first-mode (accounting for 83% of the total variance) time series and the winter NAO index is highest (0.49, p=0.05) with the former lagging by two years. The correlation coefficient (0.80, p=0.00) between the first-mode time series over the two regions is highest at the zero lag. For the Scotian Slope, the first mode (accounting for 80% of the total variance) also reveals a coherent spatial pattern (Fig. 7-6). The temporal pattern indicates notable interannual variability with an increasing trend. The correlation coefficients between the first-mode time series and the winter NAO index are -0.31 (p=0.20), -0.24 (p=0.33), and -0.10 (p=0.70) with the former lagging by zero, one and two years, respectively. In addition, the correlation coefficients between the first-mode time series over the two regions are -0.49 (p=0.03), -0.44 (p=0.07), and -0.42 (p=0.09) with the Scotian Slope lagging by zero, one and two years, respectively. Therefore, it seems that the Labrador Current has two distinct regimes north and south of the Grand Banks. Its transport has a strong positive correlation with the winter NAO index in the north and a weak negative correlation in the south.

The present results also indicate a decline of the Labrador Current transport over the Labrador Slope (Fig. 7-5) and an increase over the Scotian Slope (Fig. 7-6). The decline rate is estimated

to be 0.3-0.5 Sv/decade (p=0.00) and the increase rate is 0.1-0.3 Sv/decade (p=0.03). Similar to the declining trend of the basin-scale subpolar and subtropical gyres in Section 7.1, these regional trends of the Labrador Current are likely associated with the multi-decadal variability, instead of long-term changes.

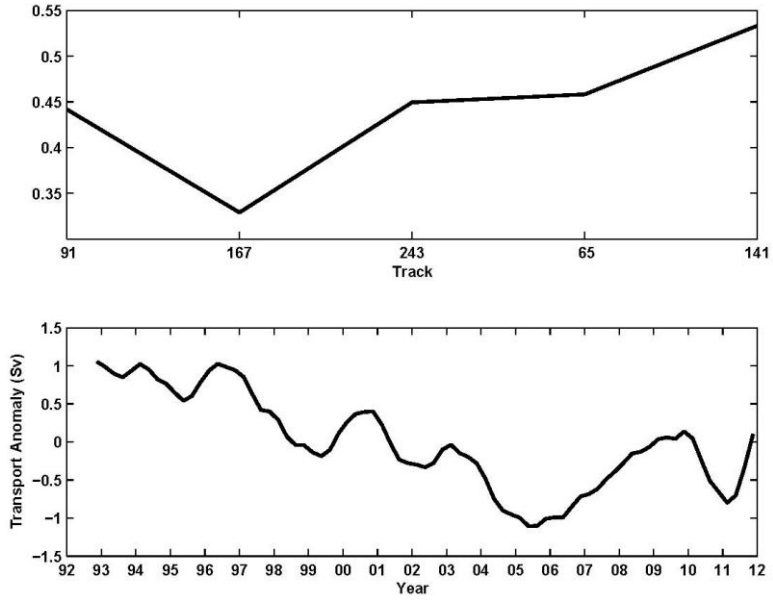

Figure 7-5 The first EOF mode of the Labrador Current transport anomalies over the Labrador Slope: (a) spatial pattern, and (b) temporal pattern. The first mode accounts for 78% of the total variance. See Fig. 7-1 for the track location (black segment).

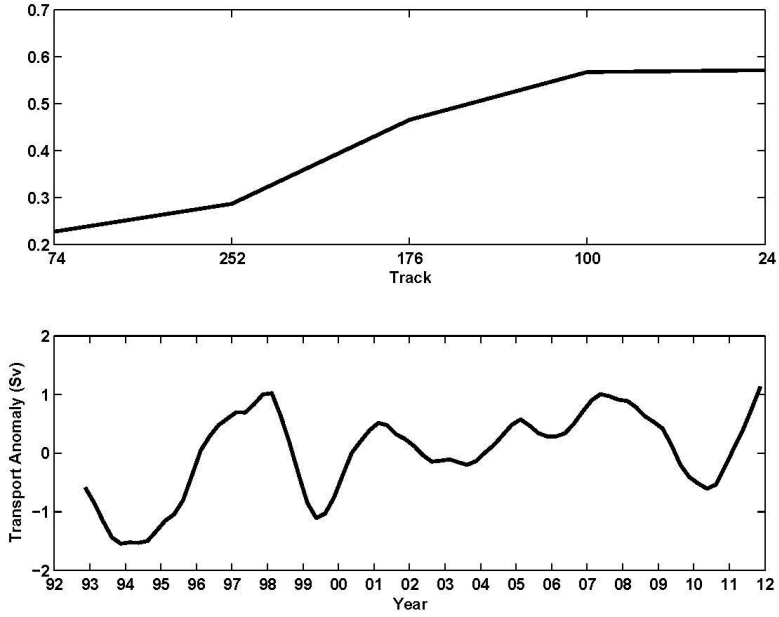

Figure 7-6 The first EOF mode of the Labrador Current transport anomalies over the Scotian Slope: (a) spatial pattern, and (b) temporal pattern. The first mode accounts for 80% of the total variance. See Fig. 7-1 for the track location (black segment).

7.4 Conclusion and Discussion

The present study has four findings:

1. The subpolar surface gyre has been declining (significant at the 99% confidence level) in the past two decades, with notable quasi-decadal oscillations that are positively correlated with the winter NAO. The decline of the transport over the period is likely associated with multi-decadal variability, instead of a long-term trend (Xu *et al.*, 2013; Wang *et al.*, 2013).
2. The Labrador Current transport is positively correlated with the winter NAO index in the north and negatively in the south, with the Grand Banks slope being a transitional zone.
3. The proxy Labrador Current transport declines at 0.3-0.5 Sv/decade (p=0.00) over the Labrador Slope and increases at 0.1-0.3 Sv/decade over the Scotian Slope (p=0.03).
4. The interannual variability of the proxy Labrador Current transport is comparable to the seasonal variability in magnitude, much smaller than the mean over the Labrador Slope, and comparable to or even dominant over the mean over the Scotian Slope.

The spatially varying (nearly out of phase from the Labrador Slope to the Scotian Slope) response of the Labrador Current to the large-scale atmospheric variability may represent the manifestation of the large scale oceanic variability. The Labrador Sea circulation is intensified associated with the enhanced deep convection when the winter NAO is highly positive (Häkkinen and Rhines, 2004; Han *et al.*, 2010). The frontal analysis data based on satellite observations indicated that the Gulf Stream off Nova Scotia was in a more northern position (Drinkwater *et al.*, 1994; Han, 2007) when the winter NAO was positive. It seems to suggest a tighter and more intense subpolar gyre and an expanded subtropical gyre in the horizontal during the years with an intensified NAO. The spatially varying relationship of the Labrador Current transport with the NAO supports Petrie's (2007) finding on the Canadian Atlantic shelf temperature and salinity and is consistent with Marsh *et al.*'s (1999) finding on cold shelf waters off the northeastern United States in response to the NAO

Over 1992-2011 as the NAO weakened in general, the Labrador Current in the north became weaker in strength but extended farther equatorward, well beyond the Tail of the Grand Banks and reaching the Scotian Slope. Alternatively viewed, the southward shift of the Gulf Stream allowed the penetration of the Labrador Current into the Scotian Slope.

7.5 Acknowledgement

This work was funded by the Aquatic Climate Change and Adaptation Service Program (ACCASP) of Fisheries and Oceans Canada. Eugene Colbourne, Charles Hannah and John Loder provided comments and suggestions.

7.6 References

Bower, A., M. Lozier, S. Gary, and C. Böning. 2009. Interior pathways of the North Atlantic meridional overturning circulation. *Nature*, 459 (7244), 243-247, doi: 10.1038/nature07979.

Drinkwater, K. F., R. A. Myers, R. G. Pettipas, and T. L. Wright. 1994. Climatic data for the northwest Atlantic: The position of the shelf/slope front and the northern boundary of the Gulf Stream between 50°W and 75°W, 1973-1992. Can. Data Rep. Fish. Ocean Sci. 12, iv + 103 p.

Ducet N., P.Y. Le Traon, and G. Reverdin (2000), Global high resolution mapping of ocean circulation from TOPEX/Poseidon and ERS-1 and -2, *J. Geophys. Res.*, 105, 19477-19498.

Häkkinen, S. and P.B. Rhines. 2004. Decline of subpolar North Atlantic circulation during the 1990s, *Science*, 304, 555-559.

Han, G. 2002. Interannual sea level variability in the Scotia-Maine region in the 1990s. *Can. J. Remote Sensing*, 28(4), 581-587.

Han G. 2004a. TOPEX/Poseidon-Jason comparison and combination off Nova Scotia, *Mar. Geodesy*, 27, 577-595.

Han, G. 2004b. Sea level and surface current variability in the Gulf of St. Lawrence from satellite altimetry. *Int. J. Remote Sensing*, 25, 5069-5088.

Han, G. 2006. Low-frequency variability of sea level and currents off Newfoundland. *Adv. Space Res.*, 38, 2141-2161.

Han, G. 2007. Satellite observations of seasonal and interannual changes of sea level and currents over the Scotian Slope. *J. Phys. Oceanogr*., 37, 1051-1065.

Han, G. 2011. Mean dynamic topography and surface circulation in the western Labrador Sea and Newfoundland offshore: satellite observations and ocean modelling, *Int. J. Remote Sensing*, 32, 5381-5391.

Han G. and J. Li. 2008. Sea level and geostrophic current features from tandem TOPEX/Poseidon-Jason data in the Newfoundland offshore. *Int. J. Remote Sensing*, 29(1), 265-280.

Han G. and J.W. Loder. 2003. Three-dimensional seasonal-mean circulation and hydrography over the eastern Scotian Shelf, *J. Geophys. Res.*, 108, 3136, doi:10.1029/2002JC001463

Han G. and C. Tang, 1999. Velocity and transport of the Labrador Current determined from altimetric and hydrographic data. *J. Geophys. Res.*, 104(C8), 18,047-18,057.

Han, G. and C. L. Tang. 2001. Interannual variations of volume transport in the western Labrador Sea based on TOPEX/Poseidon and WOCE data. *J. Phys. Oceanogr*., 31, 199-211.

Han G., Z. Lu, Z. Wang, J. Helbig, N. Chen, and B. deYoung. 2008. Seasonal variability of the Labrador Current and shelf circulation off Newfoundland. *J. Geophys. Res.*, 113, C10013, doi:10.1029/2007JC004376.

Han, G., K. Ohashi, N. Chen, P. G. Myers, N. Nunes, and J. Fischer. 2010. Decline and partial rebound of the Labrador Current 1993–2004: Monitoring ocean currents from altimetric and conductivity-temperature-depth data. *J. Geophys. Res.*, 115, C12012, doi:10.1029/2009JC006091.

Hannah, C. G., J. Shore, J. W. Loder, and C. E. Naimie. 2001, Seasonal circulation on the western and central Scotian Shelf. *J. Phys. Oceanogr.*, 31, 591-615.

Hurrell, J. W. 1995. Decadal trends in the North Atlantic Oscillation: regional temperatures and precipitation. *Science*, 269, 676-679.

Loder, J. W., B. D. Petrie, and G. Gawarkiewicz. 1998. The coastal ocean off northeastern North America: a large-scale view, Ch. 5 *In:* The Global Coastal Ocean: Regional Studies and Synthesis. In [K. H. Brink and A. R. Robinson (Eds.)], *The Sea*, Vol. 11, John Wiley & Sons, Inc., p. 105-133.

Marsh, R., B. Petrie, C.R. Weidman, R.R. Dickson, J.W. Loder, C.G. Hannah, K. Frank and K. Drinkwater. 1999. The 1882 tilefish kill - a cold event in shelf waters off the north-eastern United States? *Fish. Oceanogr.*, 8, 39-49.

Petrie, B. 2007. Does the North Atlantic Oscillation affect hydrographic properties on the Canadian Atlantic continental shelf? *Atmos.-Ocean.*, 45, 141-151.

Smith, P. C., N. R. Pettigrew, P. Yeats, D. W. Townsend, and G. Han. 2012. Regime shift in the Gulf of Maine. *In*: Advancing an ecosystem approach in the Gulf of Maine. [R. K. Stephenson, J. H. Annala, J. A. Runge, and M. Hall-Arber (Eds.)]. Amer. Fish. Soc. Symposium 79, Bethesda, Maryland.

Wang, Z., Y. Lu, F. Dupont, J. W. Loder, C. Hannah and D. G. Wright. 2013. Variability of sea surface height and circulation in the North Atlantic: forcing mechanisms and linkages. *Progr. Oceanogr.* (in press).

Xu, X., H. E. Hurlburt, W. J. Schmitz Jr., R. Zantopp, J. Fischer and P. J. Hogan. 2013. On the currents and transports connected with the atlantic meridional overturning circulation in the subpolar North Atlantic. *J. Geophys. Res.,* doi:10.1002/jgrc.20065.

8 Sea levels and storm surges in the Gulf of St. Lawrence and its vicinity

Zhigang Xu *, Denis Lefaivre, and Michel Beaulieu

Fisheries and Oceans Canada, Maurice Lamontagne Institute
P.O. Box 1000, Mont-Joli, Québec, G5H 3Z4

* Correspondence: Zhigang.Xu@dfo-mpo.gc.ca

Suggested Citation:
Xu, Z., D. Lefaivre and M. Beaulieu. 2013. Sea levels and storm surges in the Gulf of St. Lawrence and its vicinity. Ch.8 (p. 95-112) *In:* Aspects of climate change in the Northwest Atlantic off Canada [Loder, J.W., G. Han, P.S. Galbraith, J. Chassé and A. van der Baaren (Eds.)]. Can. Tech. Rep. Fish. Aquat. Sci. 3045: x + 190 p.

Abstract

Historical long-term tidal gauge data, from the Gulf of St. Lawrence and its vicinity, are analyzed for changes in annual-mean sea level, sea level climatological seasonal cycles, and extreme storm surges. The analyses show different long-term trends in annual mean sea level in two different parts of the region: rising trends at rates of 24 to 32 cm/century at sites in the southeast part of the Gulf and falling trends at rates of 3 to 6 cm/century at sites in its northwest part. The climatological monthly mean sea levels exhibit strong seasonal cycles with amplitudes varying from 6 cm at Charlottetown to 15 cm at Lauzon.

Extreme value analyses (EVA) are performed on sea level data from five tidal gauges where there are long records (Lauzon, Rimouski, Charlottetown, Halifax, and St. John's). Return period curves for different sizes of storm surges are obtained by using least squares fits to the annual maxima of storm surges of the past 90 years at these sites. To investigate if the past climate has resulted in any changes in the return periods of certain sizes of storm surges, the 90-year data are also divided into three tri-decade periods, and the same EVA is performed for each period. The results show that some sites exhibit a progressive shortening in the return periods of the extreme storm surges while other sites do not show such a trend.

8.1 Introduction

Sea level changes are largely caused by tides, oceans currents and atmospheric temperature, winds, and pressures. Therefore historical tidal gauge data may store valuable information about past climate change and their analyses may contribute to projections of future changes including extreme storm surges. As a contribution to DFO[6]'s Atlantic ACCASP[7] trends and projections summary, and as a continuation of our other sea level related projects supported by OURANOS[8]

[6] Department of Fisheries and Oceans Canada
[7] Aquatic Climate Change Adaptation Services Program (ACCASP)
[8] http://www.ouranos.ca/en/

Consortium, MSP[9], and MTQ[10], we analyzed tidal gauge data from the Estuary and Gulf of St. Lawrence and the Canadian Atlantic coast. Here we report the results of our analyses on three aspects of sea level variability: long-term changes of the annual means, variations of climatological monthly mean sea levels, and extreme storm surge events. The first two parts of this report are updated from a presentation by Xu *et al.* (2006) made at a UNESCO workshop on sea level rise and variability. Their conclusions remain the same, qualitatively, but are updated quantitatively with tidal gauge data to the end of 2012. The last part is largely a new addition due to DFO's Atlantic ACCASP summary. For complementary information on past and future sea level changes and surges, see McCulloch et al (2002), Bernier *et al.* (2007), Han *et al.* (2013) and Zhai *et al.* (2013).

8.2 Spatial Pattern of Annual Mean Sea Level Changes

The annual mean data are obtained by first dividing the available tidal gauge records (which may span over decades or over a century) into yearly periods, and then applying a tidal harmonic analysis to each period. We used t_tide (Pawlowicz *et al.*, 2002) for the harmonic analyses, the output of which includes the mean sea levels.

Figure 8-1 shows spatial variations of annual mean sea levels in the Estuary and Gulf of St. Lawrence and its vicinities. There are two types of long-term trends as indicated by the thumbnail plots inserted in the map: in the southeast of the map, the annual sea levels exhibit a relative (relative to the seabed) rising trend, represented by stations of Charlottetown (PEI), Halifax (NS), and St. John's (NF), with rates of increase of 31.1, 31.6, and 23.6 cm/century, respectively. In the northwest of the map, the annual mean sea level shows a relative falling trend, represented by Lauzon (QC), Rimouski/Pointe-au-Pere[11] (QC), and Harrington Harbour (QC), with rates being -5.3, -3.1, and -5.7 cm/century. Figures 8-2 and 8-3 are magnified views of the thumbnails with details of the regression analyses for the inferred mean sea level change rates. Error bars for 95% confidence intervals are included.

Among the thumbnail plots in Figure 8-1, we have also included a plot to show the mean sea level trend observed at Churchill (MB), whose location is outside and northwest of the map. We include this station because it illustrates the background of regional post-glacial isostatic adjustment affecting the Estuary and Gulf of St. Lawrence. A large area of land around Hudson Bay has been undergoing the post-glacial rebound process. This results in the mean sea level relatively decreasing rapidly at a rate of 94.0 cm/century. According to Henton *et al.* (2006), the Estuary and the north shore of the Gulf of St. Lawrence are at the wedging-out boundary of the rebound region, where the land uplift changes to land subsidence. This explains why there co-exist two types of mean sea level trends: the sea level rising due to global warming is offset at the sites where the land undergoes uplift, and is augmented at the places where the land subsides.

[9] Le Ministère de la Sécurité publique du Québec

[10] Le Ministère des Transports du Québec

[11] The tidal gauge at Pointe-au-Père functioned from 1897 to 1983 and afterward was relocated to Rimouski, which is about 10 km away. In this report, we treat them as one station and refer to it as Rimouski or Rimouski/Pointe-au-Pere.

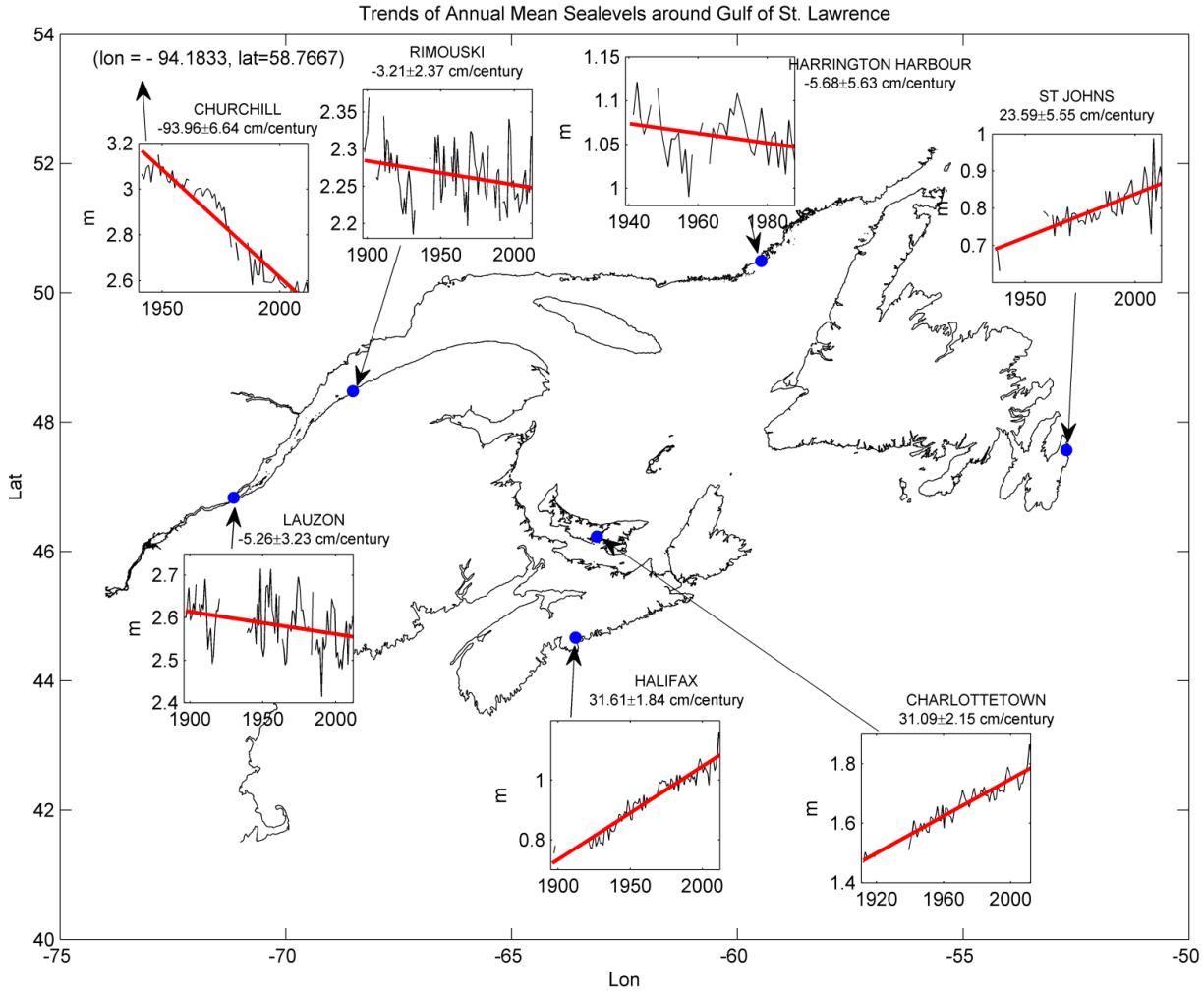

Figure 8-1 Spatial distribution of the long term trends in the annual mean sea level changes (updated from Xu *et al.*, 2006). Both trends of relative sea level rising and falling co-exist in the region, which is in a transition zone from the post-glacial land rebound to subsidence. The rising global sea level is offset/augmented by the regional land rebound/subsidence. The thumbnail insert for Churchill indicates the intensity of the land rebound northwest of the region.

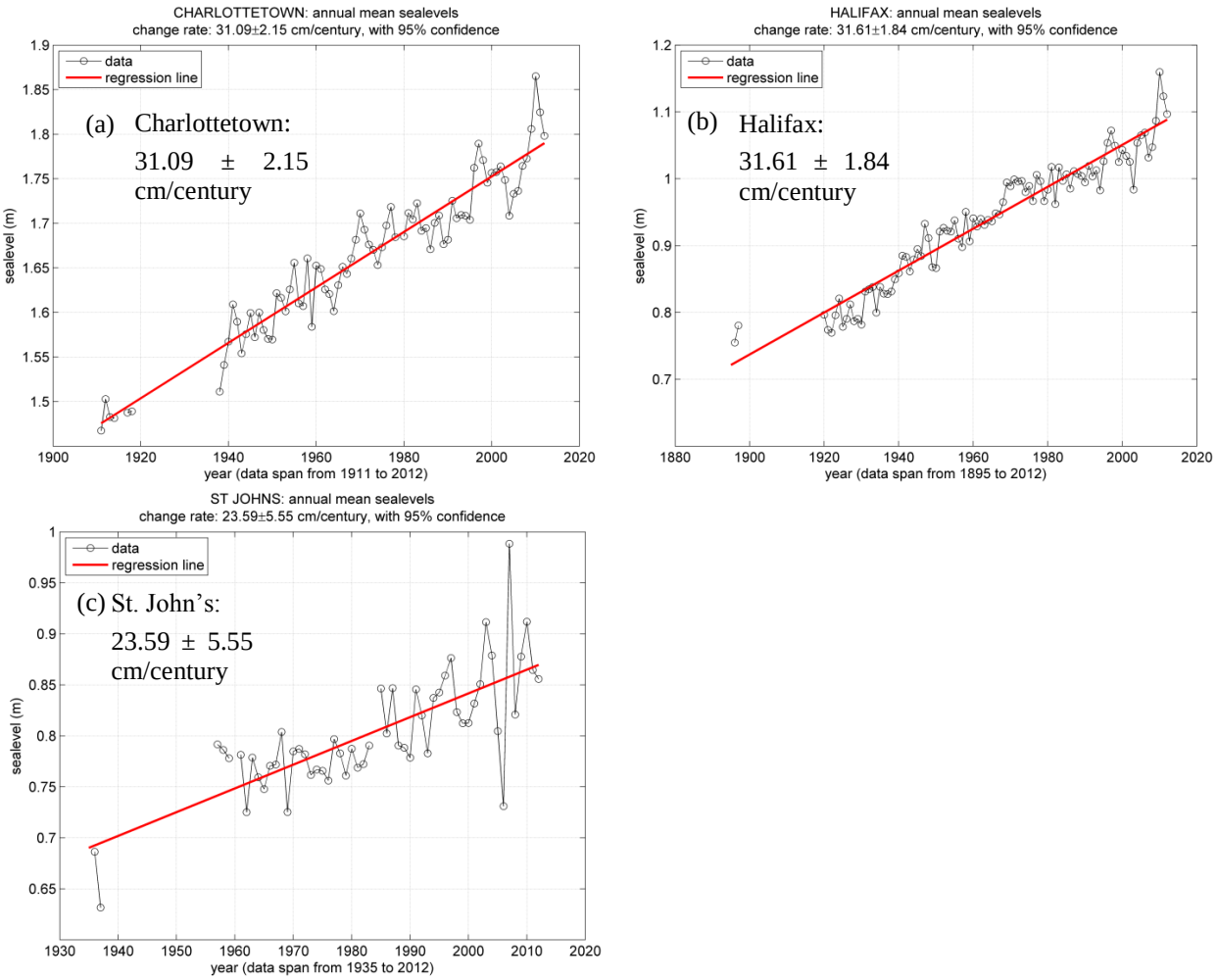

Figure 8-2 Three example sites showing relative sea level rise with regression analyses details. The rising global sea level is augmented by the subsiding seabed at these sites.

According to Aarup *et al.* (2010), the global sea level rise has been at a rate of 17 cm/century before 1993 and over 30 cm/century after 1993. The local seabed rise must have been at rates between 20 to 30 cm/century along the Estuary and the north shore of the gulf, and the subsidence rates of 6 to 16 cm/century before 1993. This inference is largely consistent with the uplift in the contour map shown by Henton *et al.* (2006) based on the Canadian Base Network monitoring data. McCulloch *et al* (2002) reported a rate of 32 cm/century of the relative mean sea level rise in Charlottetown. Our number for the same place is consistent with theirs.

Wolf *et al.* (2006) reported that the relative mean sea level at Churchill fell at a rate of 97.2 ± 2.6 cm/century based on their analyses of tidal gauge data from 1940 to 2001. Our estimated falling rate is a bit lower than theirs, which is perhaps due to the different lengths of data used, but their estimate is within the confidence interval of ours (our data length is 11 years longer, up to the end of 2012). Wolf *et al.* (2006) also reported, based on Global Positioning System (GPS) data from 1996 to 2001, that the land at Churchill is rising at a rate of 114.0 cm/century, while Mazzotti *et al.* (2011) have more recently estimated the rate to be in the 104-108 cm/century

range using GPS data from 1996 to 2010. Mazzotti *et al.* (2011) also found land rise rates exceeding 50 cm/century at other GPS sites in the continental interior around Hudson Bay, reflecting the large continental rebound associated with post-glacial isostatic adustment in the interior of northern North America (and extending to the northwestern Gulf of St. Lawrence).

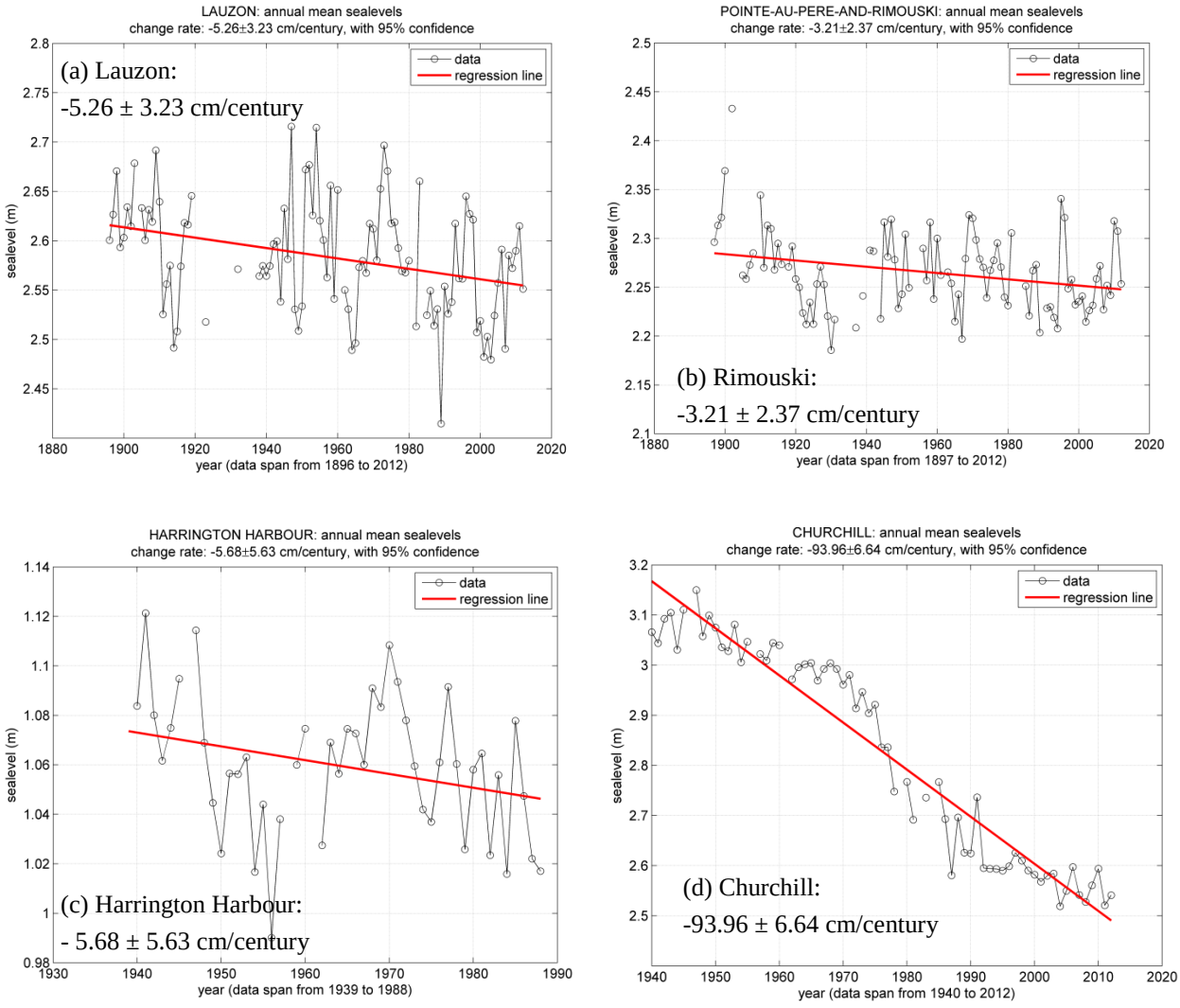

Figure 8-3 Four example sites showing relatively falling sea levels with regression analyses details. The Churchill station illustrates that a large area of land around Hudson Bay has been undergoing post-glacial rebound. Stations at Lauzon, Rimouski/Pointe-au-Père, and Harrington Harbour are at the wedging-out edge of the rebound area, and the rising seabed there offsets the rising global sea level, resulting in weak relatively falling sea levels.

8.3 Climatological Seasonal Variations

In the literature, the topic of mean sea levels often focuses on changes in their annual means. However in our investigation, we have also noticed that the seasonal mean sea levels, when averaged climatologically over the same months, exhibit a strong seasonal variation in the Estuary and Gulf of St. Lawrence. The seasonal oscillations may not affect the net annual means, however, they will matter when storm surges occur. A storm surge will be more disastrous when it occurs during a high seasonal mean sea level than low. From this point of view, we think it is worthwhile to document what we have found on the climatological seasonal variations. Information on the climatological seasonal variation of sea level elsewhere off Atlantic Canada may be found in Han *et al.* (2002).

We investigated the climatological seasonal variations for three sites, Lauzon, Rimouski (Pointe-au-Père), and Charlottetown, where there exists a century or more of data. We divided the data (i.e. residual water levels after removal of tides) into decadal periods. We then averaged all the data from the same months to result in 12 averages that represent the climatological monthly means for each of the decadal periods. The means are shown in Figure 8-4. Strong seasonal oscillations are evident and persist through all the decades. The oscillation amplitudes are near 15 cm at the head of the Estuary but decrease to 6 cm at Rimouski and Charlottetown. The oscillations between Lauzon and Charlottetown are evidently of opposite phase, whereas the phase of the oscillations in Rimouski (Pointe-au-Père) is somewhere in-between.

We cross-examined the meteorological records at the same or nearby sites in an attempt to seek causes for such seasonal variability. Figure 8-5 shows that there are also seasonal variations in the air pressures and they vary more or less in an opposite phase to those in the sea levels. This is the inverse barometer effect. The seasonal variations in the atmospheric pressures can account for 34%, 26%, and 12% of the variances of the mean sea levels at Lauzon, Rimouski, and Charlottetown, respectively. From the head of the Estuary to the tail of the gulf, the inverse barometer effect appears to decrease.

While we have clearly documented the strong seasonality in the mean sea levels, our explanation for its being caused by the inverse barometer effect is just a preliminary attempt. There may be other factors accounting for the seasonal variations in the mean sea levels. For example, the freshwater runoff in May/June due to ice/snow melt can also contribute to the peaks in the oscillations seen at Lauzon. Further pursuit of the causes is beyond the scope of this report.

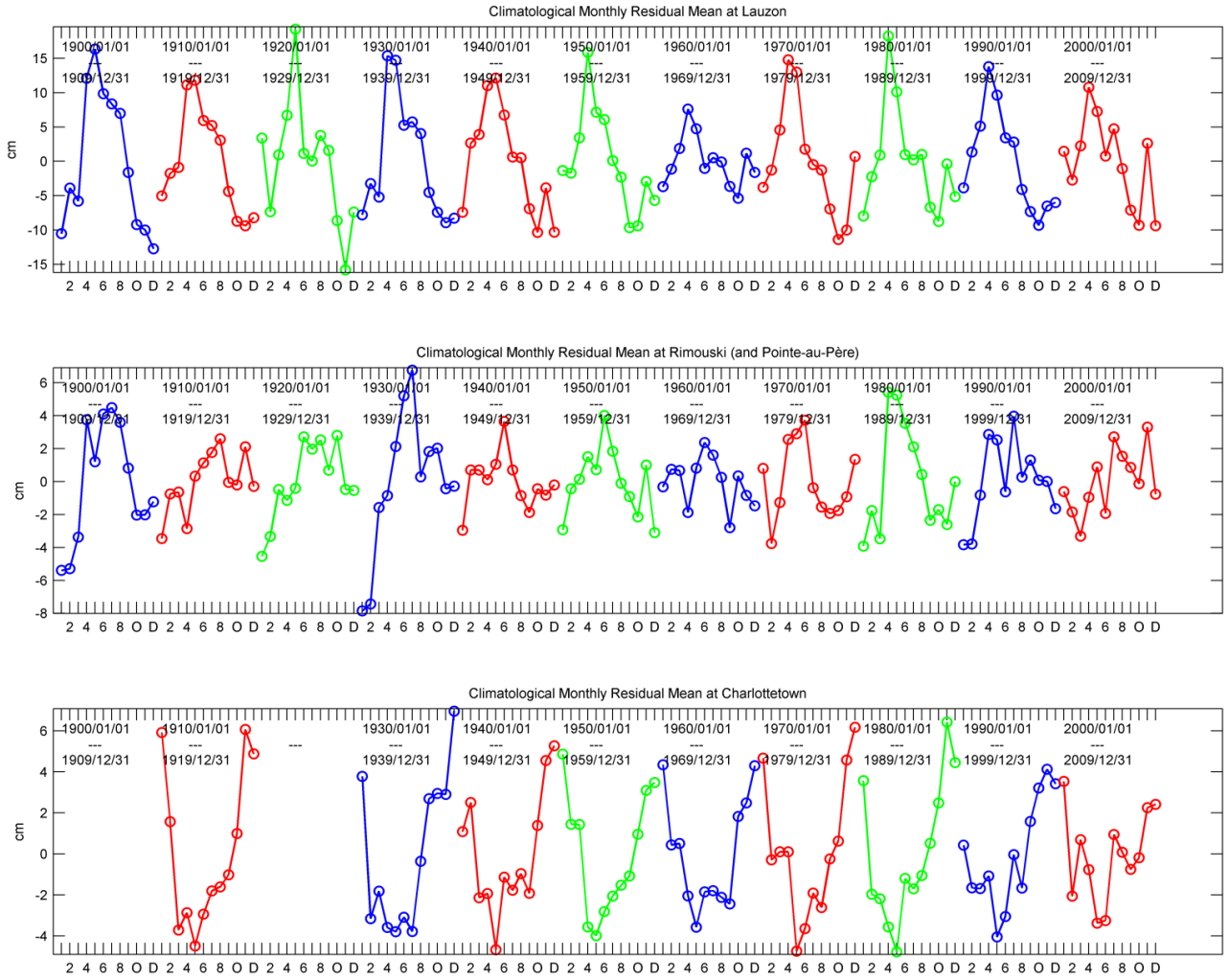

Figure 8-4 Climatological seasonal variations in the mean sea levels at Lauzon, Rimouski, and Charlottetown. For clarity, only even months are indicated by single-character numbers or letters.

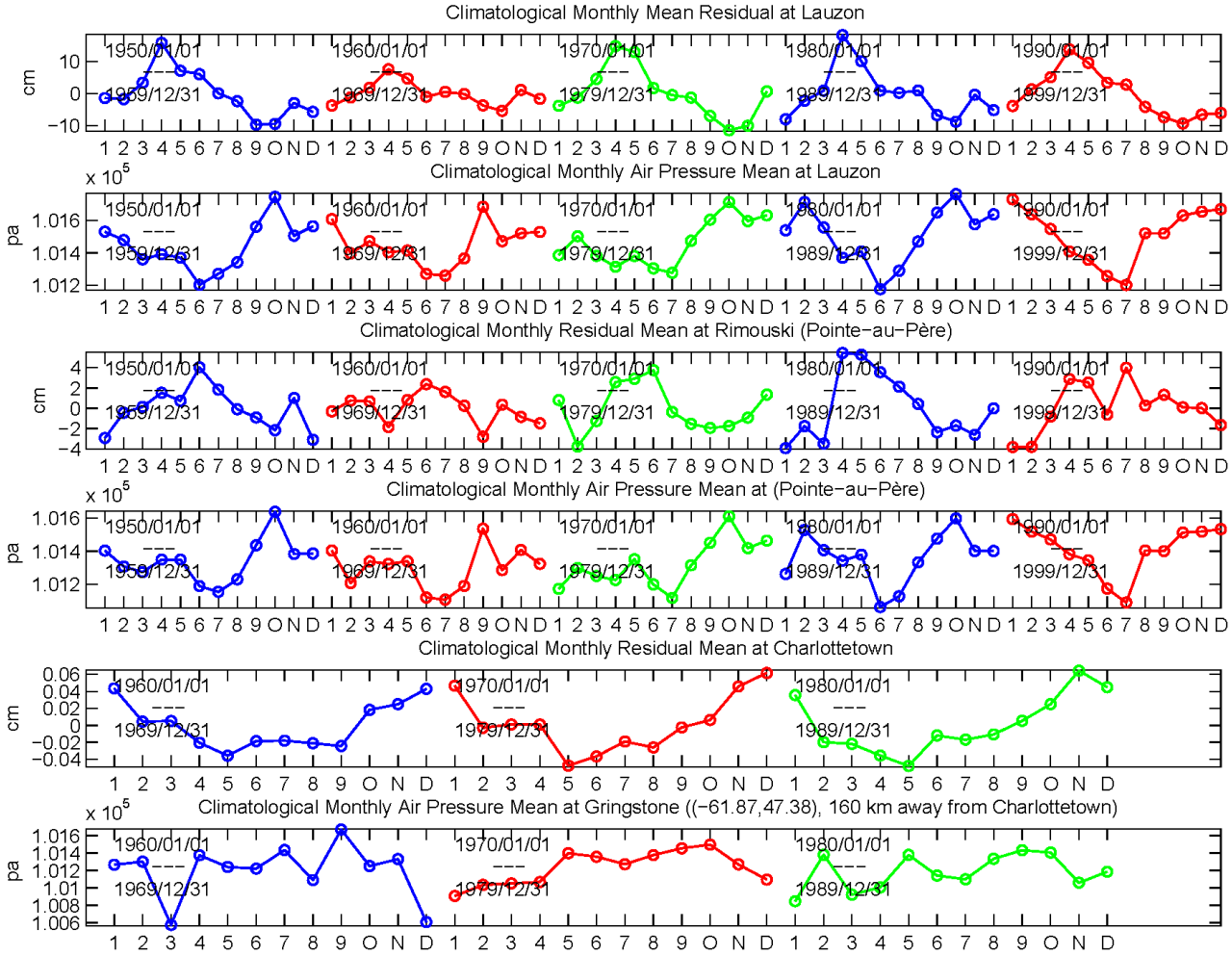

Figure 8-5 Climatological monthly means of sea levels and air pressures are aligned for three sites. The top two panels are for Lauzon, the middle two panels are for Rimouski, and the bottom two panels are for Charlottetown. Seasonal variations in the air pressures are also evident and so are their inverse barometric relations with the mean sea levels. For clarity, single-character numbers or letters are used to indicate the climatological months.

8.4 Extreme Storm Surges

We investigated the occurrence of extreme sea level events (storm surges) to see if the past climate has resulted in a shortening of the return periods of storm surges in Quebec and Maritime regions. Five long-term tidal gauges are selected for this purpose. They are Lauzon, Rimouski, Charlottetown, Halifax, and St. John's. Sea level data from the past 90 years, i.e. from 1922/01/01 to 2011/12/31, are analyzed. The 90 years of data are analyzed as a whole, as well as for three tri-decades, in order to identify any changes in the return periods of certain sizes of storm surges. The three tri-decades are 1922-1951, 1952-1981, and 1982-2011. Except for Halifax, all the other stations have big data gaps in the first tri-decade. A tri-decade is a popular choice as a basic period in climate modeling community and we carry it over here.

The residual water levels (after filtering out tides and annual mean components) are analyzed for the storm surge recurrence frequencies (or their inverse, the return periods). More specifically, the annual maxima of the residuals are used in the recurrence analysis with the extreme value theory of Gumbel (1954, 1958). According to Gumbel's theory, the annual maxima obey a double exponential distribution:

$$\Phi = e^{-e^{-\alpha(x-\mu)}} \qquad (8.1)$$

where Φ stands for the probability of an annual maximum not exceeding the level of x, α, and μ which are the scale and location parameters and can be determined by the data. Taking the log function twice on (8.1) results in a simple liner relationship

$$-\log(-\log\Phi) = \alpha(x-\mu) \qquad (8.2)$$

which says that on a properly scaled paper (i.e. Gumbel probability paper), the theoretical distribution is a straight line around which the observed data should be distributed. Thus, to estimate the scale and location parameters, we use (8.2) as a regression model to fit the data pairs that can be derived from the annual maxima data as follows:

Let

$$x_1, x_2, \cdots, x_m, \cdots, x_n \qquad (8.3)$$

denote the annual maxima arranged in ascending order, then

$$\Phi_m = \frac{m}{n+1}, \quad m = 1, 2, \cdots, n \qquad (8.4)$$

The results for the five stations are shown in Figures 8-6 to 8-10. Each of these figures has three panels: the top panels show the residual time series with color dots to show when the annual maxima occurred, and how many and how large they are in each of the tri-decades; the middle panel shows the results of EVA performed over the three tri-decades; and the bottom panel shows the EVA results for the entire 90 years. Three colors are used to distinguish the different tri-decades: blue for the first tri-decade, green for the second, and the red for the last. The thick straight lines are produced by a least square fit and the accompanying thin lines outline the confidence zone. Readers who wish to know the details on how to construct the confidence zone are referred to Gumbel (1954) lectures about the control curve. The confidence zone means that

two of three data points are expected to fall within this zone if we could repeat the experiment with the same conditions. The bullets in the figures show the data points.

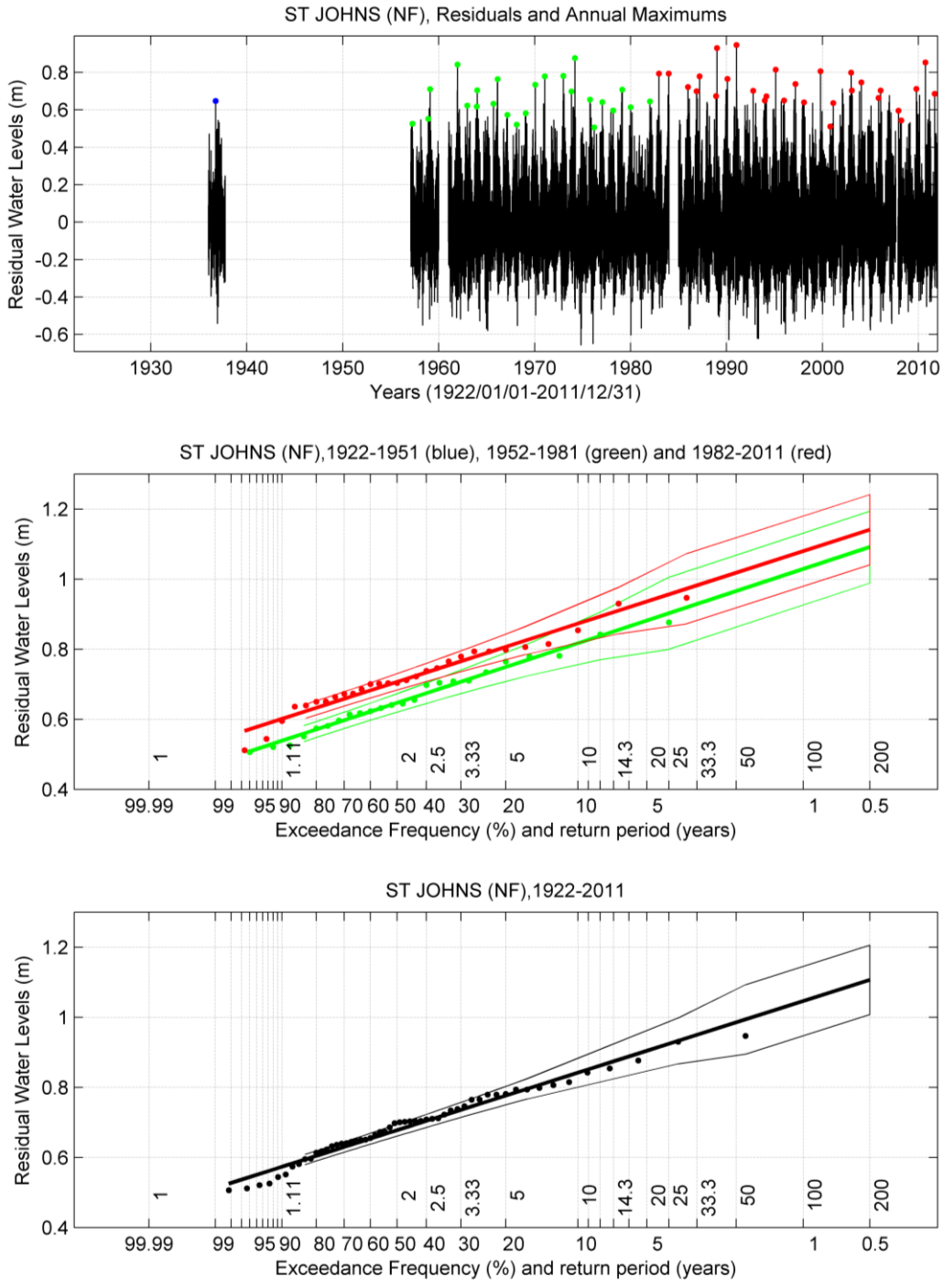

Figure 8-6 Storm surges and their return periods for St. John's (NF). Top panel is the residual time series with color dots indicating the annual maxima. The middle panel shows the results of Gumbel's EVA of the second and third tri-decades (the first tri-decade has too few annual maxima to perform an EVA). The bottom panel shows the result of the EVA using the entire 90 years of data as one data period.

A hypothesis that drove this investigation is that if the past climate had progressively produced more storms from one tri-decade to the next, we should see a progressive shortening of the return periods for a given size of surge. Support for this assumption by the EVA results varies from station to station. It seems to be best supported at St. John's (NF). In Figure 8-6, we see that storm surges with the same return periods in the last tri-decade become systematically higher than those in the second tri-decade. The red lines are significantly shifted above the green lines. If we focus on a storm surge of 0.8 m, we can find that the return periods of the storm surge have been shortened from 10 years to 5 years. As a cross-reference, looking at the top panel and counting the red and green dots equal to or above 0.8 m, we get 5 red dots and 2 green dots. This site has only one annual maximum for its first tri-decade, leaving us nothing to say about this period. With only two tri-decades of data, we have to be cautious in accepting our findings. The trend we see now might be altered if we could add another tri-decade of data. This caution may grow when we look at the results from the other sites.

The results for Charlottetown, Figure 8-7 do not show a significant difference between the second tri-decade and the third one, but they do show a significant shortening in the return period from the first tri-decade to the rest. The storm surges of the same size took much longer to re-occur in the first tri-decade. For example, a 1 m surge used to take 10 years to re-occur before 1952 but took less than 5 years in the second and third tri-decades. However, please note that the first tri-decade has only half the number of data points of those in the other tri-decades. We do not know whether this conclusion would still hold if the dataset of the first tri-decade were more complete.

Shown in Figure 8-8, the results for Halifax do not show a significant difference among the 3 tri-decades. The data points of the different colors all fall into the same confidence zone except for a red dot that represents a 1.5 m surge. This is the largest one in the 90- year history of the Halifax data and corresponds to Hurricane Juan which made landfall in Halifax on 2003/09/29. Another big event happened in the mid-1930s. Without these two big events, the EVA results for the 3 tri-decades would look more similar. It is these two big events that tilt up the best fit straight lines in red and in blue from the one in green towards the low frequency end.

Figure 8-9 is for Rimouski (and Pointe-au-Père). The results of this site show a progressive shortening of the return periods from the first tri-decade to the last one. The shortening is significant from the first tri-decade to the second one, but not so from the second one to the third. This site has about equally long data points in each of the tri-decades.

The results for Lauzon are shown in Figure 8-10. There are more big events in the second tri-decade than in the others (you can count the dots in different colors above or equal to 2 m in the first panel). The return periods in the second tri-decade became significantly shorter than in the others. The biggest one happened in 1971, with a size of 2.8 m. Again, caution should be taken in interpreting these results because the number of data points in the first tri-decade is only about half of the other two tri-decades.

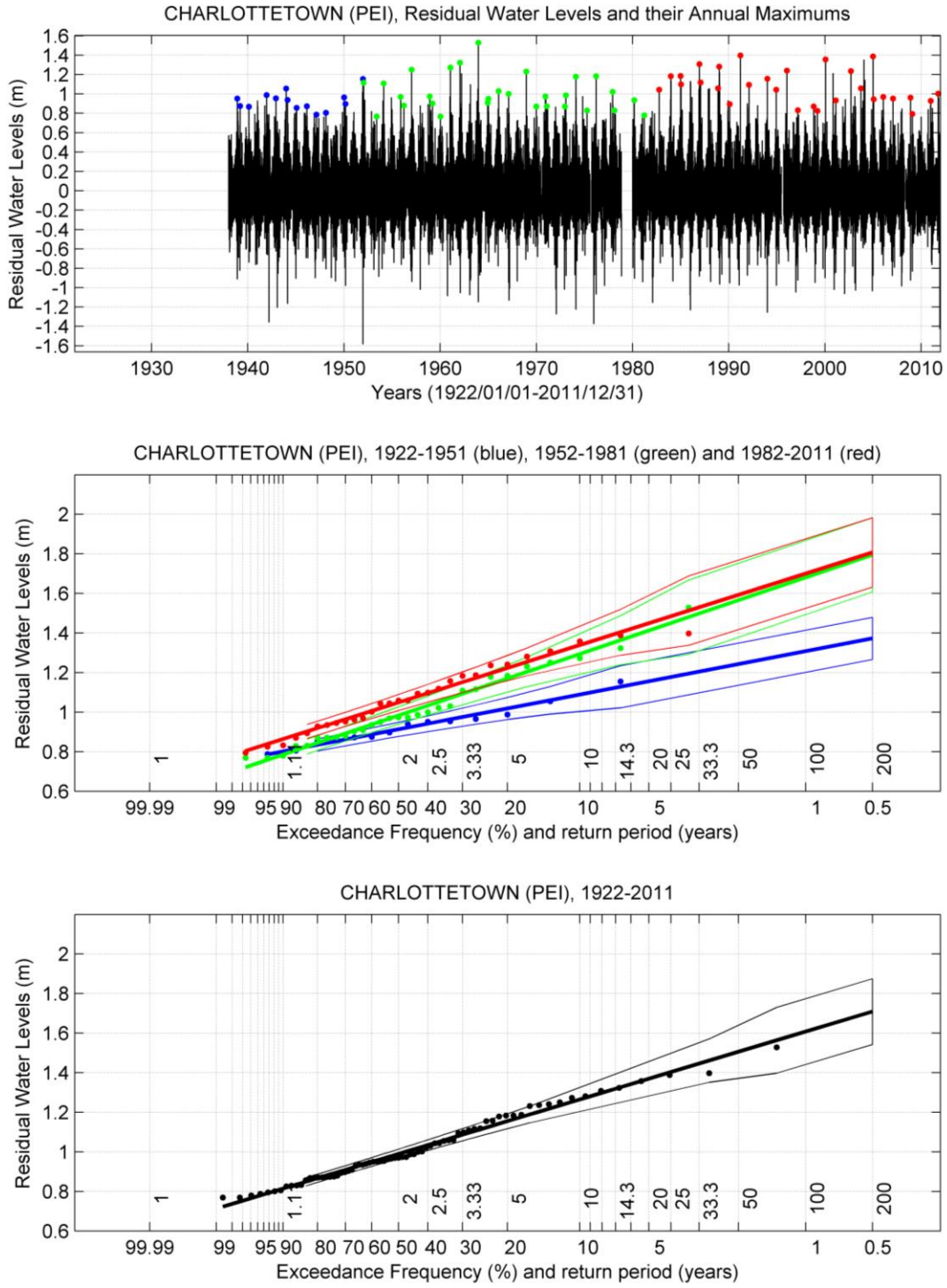

Figure 8-7 Storm surges and their return periods for Charlottetown (PEI).

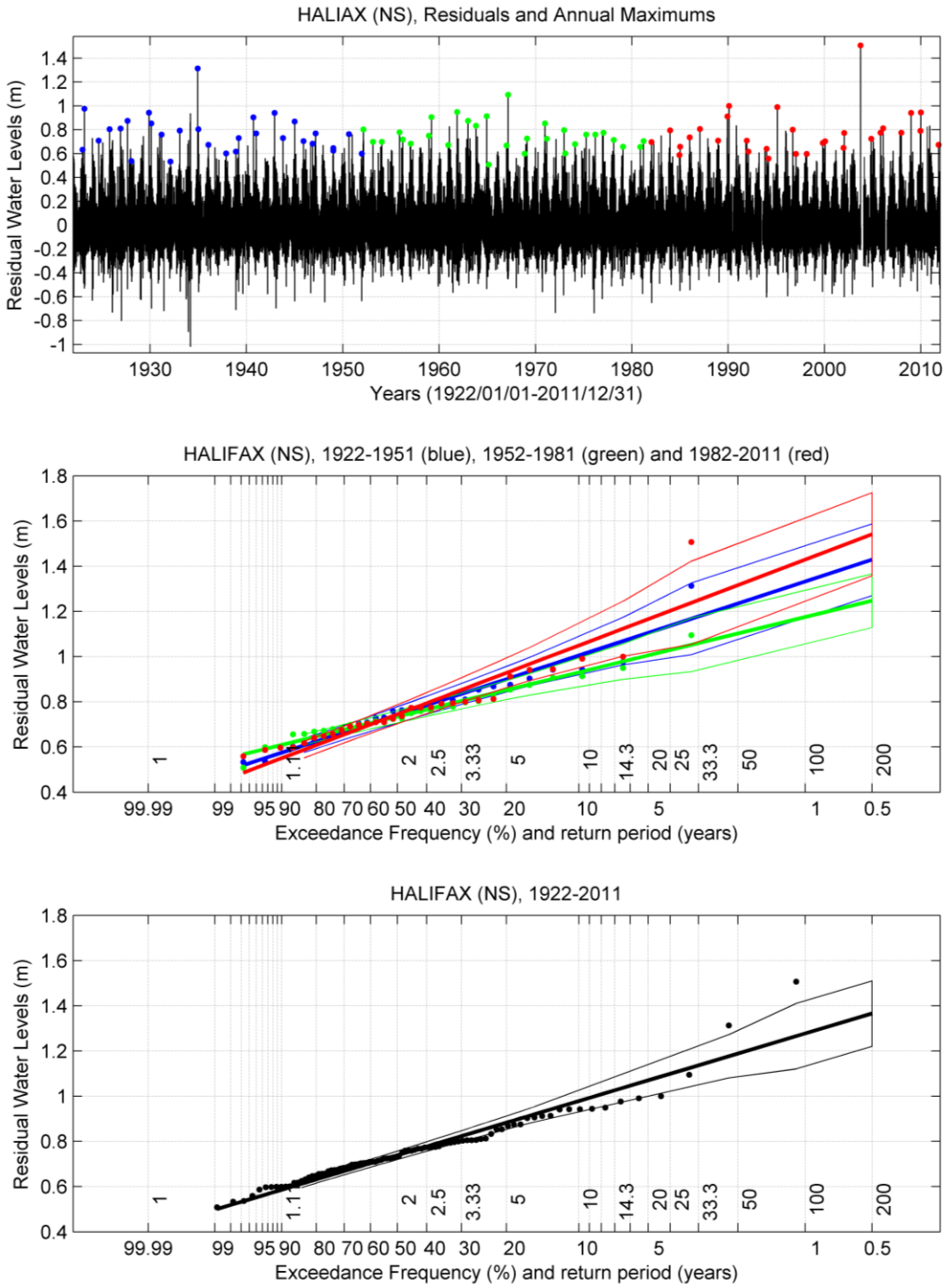

Figure 8-8 Storm surges and their return periods for Halifax (NS).

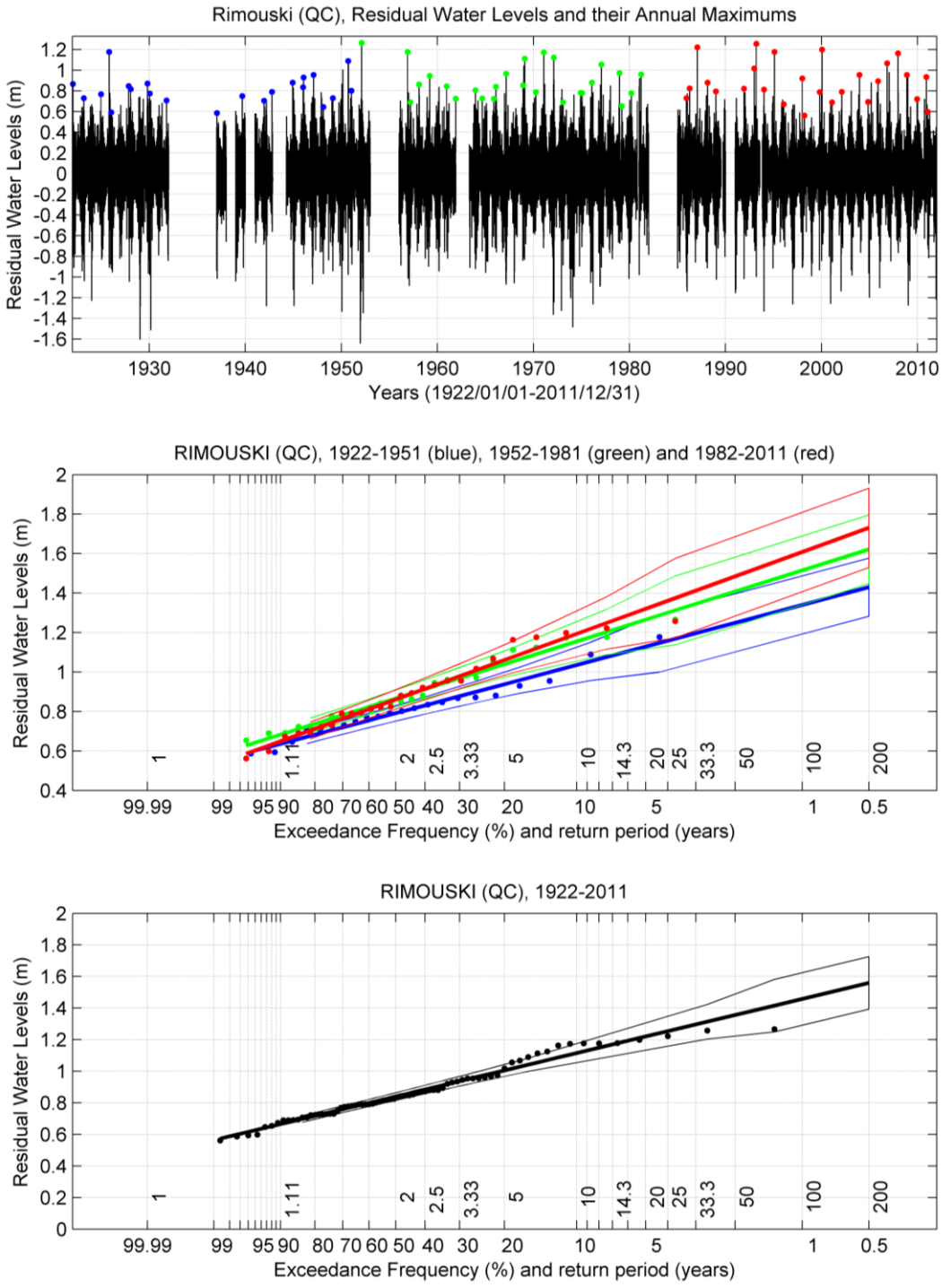

Figure 8-9 Storm surges and their return periods for Rimouski (QC).

The findings on the changes of the recurrence frequencies of extreme sea level events are very site dependent. It seems there is no universal picture applicable to the whole region, from the head of the St. Lawrence Estuary in Quebec to the coasts of Newfoundland and Nova Scotia. In retrospect, this should not be surprising given that low pressure centers are generally not large

enough to cover Lauzon and St. John's at the same time and that different storms have different tracks. In analyzing storm surge recurrences, the storm track is a big random factor. Although site specific, the result for each site is still valuable. It gives us an important statistical summary of what has happened in the past and what will be the reasonable expectation for potentially harmful storm surges in the future.

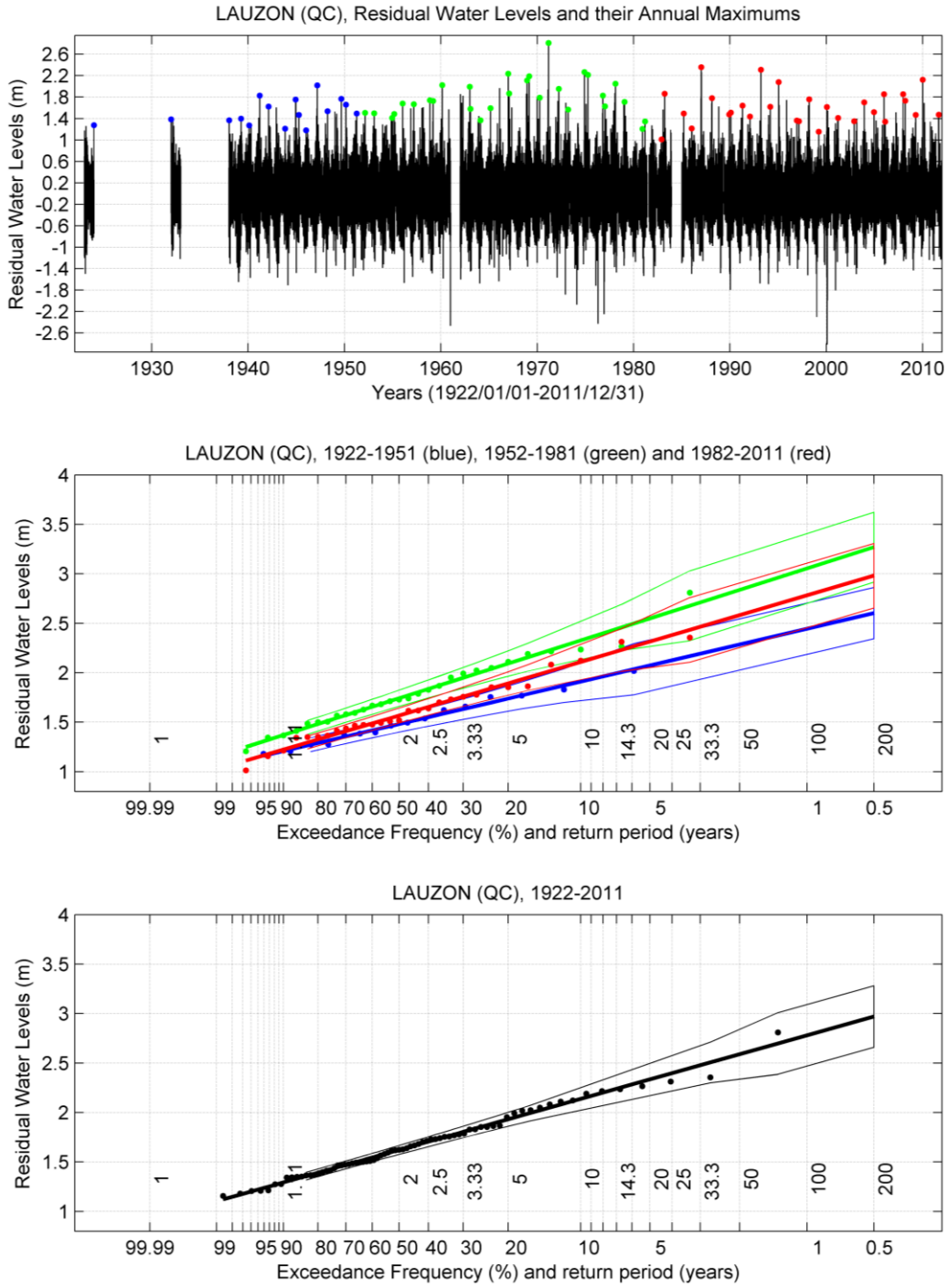

Figure 8-10 Storm surges and their return periods for Lauzon (QC).

We have also performed EVA over the entire 90 years to yield overall indications of recurrence frequencies of storm surges, as shown on the bottom panels in Figures 8-6 to 8-10. Constrained by the 90 years of data, these curves should give fairly reliable indications of the recurrence frequencies of storm surges to be superimposed on the mean sea levels. Note that the water levels shown in in Figures 8-6 to 8-10 are all relative to the local mean sea levels which, in turn, are relative to the local chart datum. Thus we cannot simply compare the same sizes of storm surges across different sites. For example, a 1 m storm surge is a rare event in St. John's; it only happens once in 50 years, on average, and may mean a significant threat to the local community. In contrast, a 1 m storm surge in Lauzon is a yearly event and may mean nothing to the local people. Therefore, to draw a comparison among different sites, in a meaningful way, we must compare the storm sizes for a given recurrence frequency (instead of comparing recurrence frequencies for a given storm size). Shown in Table 8-1 is such a comparison: sizes of storm surges with an expected return period of 50 years at the five sites:

Table 8-1 Sizes of storm surges at the five sites with an expected 50-year return period. The numbers indicating the water levels are all relative to the local mean sea levels, which, in turn, are relative to the local chart datum.

St. John's	Charlottetown	Halifax	Rimouski	Lauzon
0.98 m	1.51 m	1.19 m	1.35 m	2.59 m

8.5 Summary

We analyzed the historical tidal gauge data, from as early as 1896 to as late as the end of 2012, from the Estuary/Gulf of St. Lawrence and vicinity and documented the results in terms of three aspects of the sea level changes: the long term trends in the annual mean sea level changes, the climatological seasonal cyclic variations, and the return periods of storm surges. Although we also interpreted the results to some degree, we chose to clearly report what the data say as the main purpose of this document, leaving more profound interpretation as open questions for further research.

There exist two types of long-term trends in the annual mean seal level changes in the region: the rising relative sea level and the falling relative sea level (Fig. 8-1). The rising type is exemplified by the stations of Charlottetown, Halifax, and St. John's (Fig. 8-2), with rising rates, respectively, being 31.1±2.2, 31.6±1.8, and 23.6±5.6 cm/century. The falling type is illustrated by the stations of Lauzon, Rimouski, and Harrington Harbour (Fig. 8-3), with falling rates being 5.3±3.2, 3.2±2.4, and 5.7±5.6 cm/century, respectively. The uncertainties have 95% confidence. The Estuary and part of the north shore of the Gulf of St. Lawrence are at the wedging-out edge of a large area of post-glacial rebound. To the northwest of this edge, a large area of land around Hudson Bay has been uplifting since the last glacial period. To the southeast of the edge, the land (or the seabed) has been subsiding (Henton *et al.*, 2006). The rising global sea level is offset at the sites where the local land is uplifting and is augmented at the places where the local land is subsiding. To illustrate the post-glacial rebound background, we have included Churchill on Hudson Bay, where the sea level has been strongly falling, relative to the seabed, at a rate of 94.0±6.6 cm/century (Fig. 8-3).

The sea levels in the Estuary and Gulf of St. Lawrence also clearly exhibit climatological seasonal cyclic variations (Fig. 8-4). The amplitudes of the seasonal variations are from 15 cm at Lauzon to 6 cm at Charlottetown. We have partially attributed the seasonal variation to the same variation in the atmospheric pressures with the inverse barometer effect, but there could be other causal factors. The seasonal variation matters due to the hazardous nature of storm surges. A storm surge will cause more damage when it arrives during a high mean sea level season than during a low one.

We analyzed return periods for different sizes of storm surges with Gumbel's (1954, 1958) extreme value theorem for two purposes: one was to investigate if the past climate had resulted in a progressive shortening in the return periods for a given size of storm surge, and the other was to provide an overall indication of the return periods. Five permanent tidal gauges with long data records were chosen. For the first purpose, we grouped the data into three tri-decades, and performed the EVA for each one. The tri-decadal approach did not lead us to conclusively support the progressive shortening in the return periods from one decade to next. While the result for St. John's seems to show a progressive shortening trend, the results for the other stations could not clearly lend such support. Regardless of whether the results are supportive or not, however, we think it is worthwhile to conduct such an investigation. For our second objective, we performed the EVA on the whole data record and presented the results in the third panels of Figures 8-6 to 8-10. With the constraint of data only 90 years long, these curves give us a good statistical summary for the past storm surges at each site and may serve as a good projection for future storm surges if we assume that future storminess remains the same. Of course, whether or not future storminess will remain the same is an open question intrinsically under the topic of climate change. Currently we are proposing another project in which we will convert the global climate model solutions for the coming decades, or even the coming century, to water level time series for our points of interest. With such time series, we can perform the same type of EVA and better project future storm surges.

8.6 Acknowledgement

This study was funded by DFO's Atlantic ACCASP T&P project and benefited from our other relevant studies that were supported and funded by the OURANOS Consortium, the MPQ, and the MTQ. We thank our DFO colleagues: John Loder, Guoqi Han, and Blair Greenan for their internal review of our report.

8.7 References

Aarup, T., J A. Church, W. Wilson, W. Stanley, and L. Philip. 2010. Sea-level Rise and Variability: A summary for policy makers, Intergovernmental Oceanographic Commission (IOC); United Nations Educational, Scientific and Cultural Organization (UNESCO), 8 p. http://unesdoc.unesco.org/images/0018/001893/189369e.pdf

Bernier, N., K.R. Thompson, J. Ou and H. Ritchie. 2007. Mapping the return periods of extreme sea levels: allowing for short sea level records, seasonality and climate change. *Glob. Planetary Change* 57, 139-150.

Gumbel, E. 1954. Statistical Theory of Extreme Values and Some Practical Applications. National Bureau of Standards Applied Mathematics Series 33, U. S. Govt. Print. Office, 51 p.

Gumbel, E. 1958. Statistics of Extremes. Columbia University Press, New York and London.

Han G., C.L. Tang and P.C. Smith, 2002. Annual variations of sea surface elevations and currents over the Scotian Shelf and Slope, *J. Phys. Oceanogr.*, 32, 1794-1810.

Han, G., Z. Ma, J. Loder, H. Bao and A. van der Baaren. 2013. Mean sea level trends in the Northwest Atlantic: Historical estimates and future projections. Ch. 9 (p. 113-126) *In:* This report.

Henton, J., M. Craymer, R. Ferland, H. Dragert, S. Mazzotti, and D. Forbes. 2006. Crustal motion and deformation monitoring of the Canadian landmass. *Geomatica*, 60(2), 151-164.

Mazzotti, S., A. Lambert, J. Henton, T. S. James, and N. Courtier. 2011. Absolute gravity calibration of GPS velocities and glacial isostatic adjustment in mid-continent North America. *Geophys. Res. Lett.*, 38, L24311, doi:10.1029/2011GL049846.

McCulloch, M.M., D.L. Forbes, R.W. Shaw and the CCAF A041 Scientific Team. 2002. Coastal impacts of climate change and sea-level rise on Prince Edward Island: Synthesis report. Geological Survey of Canada Open File 4261. doi:10.4095/213246.

Pawlowicz, R., B. Beardsley, and S. Lentz. 2002. Classical tidal harmonic analysis including error estimates in MATLAB using T_TIDE. *Computers & Geosciences*, 28 (8), 929-937.

Wolf, D., V. Klemann, J. Wünsch and F.-P. Zhang. 2006. A reanalysis and reinterpretation of geodetic and geological evidence of Glacial-Isostatic Adjustment in the Churchill region, Hudson Bay. *Surveys in Geophysics*, 27, 19-61.

Xu, Z., J. Saucier, and D. Lefaivre. 2006. Water level variations in the Estuary and Gulf of St. Lawrence. Poster, UNESCO IOC workshop on sea level rise and variability, Paris.

Zhai, L., B. Greenan, J. Hunter, T.S. James and G. Han. 2013. Estimating sea-level allowances for Atlantic Canada under conditions of uncertain sea-level rise. Can. Tech. Rep. Hydrogr. Ocean Sci. 283: v + 40 p. http://www.dfo-mpo.gc.ca/Library/349546.pdf

9 Mean sea level trends in the Northwest Atlantic: Historical estimates and future projections.

Guoqi Han [1 *], Zhimin Ma [1,2], John Loder [3], Huizhi Bao [1] and Augustine van der Baaren [4]

[1] Fisheries and Oceans Canada, Northwest Atlantic Fisheries Centre
P.O. Box 5667, St. John's, Newfoundland and Labrador A1C 5X1

[2] Memorial University of Newfoundland
St. John's, Newfoundland and Labrador

[3] Fisheries and Oceans Canada, Bedford Institute of Oceanography
Dartmouth, Nova Scotia

[4] Wolfville, Nova Scotia

* Correspondence: Guoqi.Han@dfo-mpo.gc.ca

Suggested Citation:
Han, G., Z. Ma, J. Loder, H. Bao and A. van der Baaren. 2013. Mean sea level trends in the Northwest Atlantic: historical trends and future projections. Ch.7 (p. 113-126) *In:* Aspects of climate change in the Northwest Atlantic off Canada [Loder, J.W., G. Han, P.S. Galbraith, J. Chassé and A. van der Baaren (Eds.)]. Can. Tech. Rep. Fish. Aquat. Sci. 3045: x + 190 p.

Abstract

Mean sea level is one of the most important indicators for climate variability and change. In the Northwest Atlantic, mean relative sea level (RSL) is mainly influenced by ocean temperature and salinity changes, large-scale oceanic circulation, mountain glacier and ice-sheet melt, and glacial isostatic adjustment (GIA). Here we use tide-gauge data to examine recent trends in mean RSL, and then combine the sea level output of global climate models and a global land ice melt model with modelled and measured GIA effects to provide sea level projections. The mean RSL trend based on tide-gauge data shows large regional variations, from 2-4 cm/decade in the south (above the global mean RSL rise rate) to -2 cm/decade along the Labrador coast and between the northern coast of the Gulf of St. Lawrence and the St. Lawrence Estuary. This spatial difference can, to a significant degree, be attributed to vertical land motion. When the vertical land motion measured by the Global Positioning System is used, the projected mean RSL rise between 1986-2005 and 2046-2065 ranges from 20 to 40 cm along the Canadian Atlantic coast and is smaller along the Labrador coast, the northern coast of the Gulf of St. Lawrence, and the St. Lawrence Estuary. There are considerable uncertainties in the magnitude of the sea level projections associated with the ocean dynamic effect, the ice-sheet melt component, and the spatial structure of the GIA effect (mainly the vertical land motion). On the decadal time scale, it is projected that mean RSL will continue to rise at 3-4 cm/decade along many parts of the Canadian Atlantic coast and to fall or rise, with smaller magnitude, along the northern coast of the Gulf of St. Lawrence, the St. Lawrence Estuary, and Labrador, with uncertainties as much as or greater than the estimates.

9.1 Introduction

Sea level is one of the most important indicators for climate variability and change. It represents an integrated manifestation of the ocean's interior variability in response to forcings of oceanic, atmospheric, cryospheric, and terrestrial origins. Local sea-level changes can differ significantly from the global mean (Cazenave and Nerem, 2004).

Knowledge of sea level trends has come largely from tide-gauge data. The global mean sea level rise rate is estimated at 1.7±0.2 mm/yr over 1900-2009 (Church and White, 2011). Since the early 1990s, satellite altimetry has become vital in complementing the tide-gauge observations. The global mean sea level rise rate is estimated to be 3.2±0.4 mm/yr over the past two decades (Nerem *et al.,* 2010). It has been found that the mean sea level rise is thus far the major reason responsible for more frequent flooding in the world (UNESCO, 2010).

The Intergovernment Panel on Climate Change Fourth Assessment Report (IPCC AR4; Solomon *et al.*, 2007) used global Atmosphere-Ocean General Circulation Models (AOGCMs) to project global sea level rise in the 21st century. Under the medium-level A1B scenario from the Special Report on Emission Scenarios (SRES; Nakićenović, *et al.*, 2000), the projected global sea level rise in the 21st century is 0.21-0.48 m, and 0.20-0.61 m when the recent observational dynamic effect of ice sheet mass loss is considered (Meehl *et al.*, 2007). Like in the past, local sea level changes in the future may significantly differ from the global mean (Slangen *et al.*, 2012). Their projected local sea level changes vary from -3.91 to 0.79 m in the 21st century under SRES A1B, with a global mean of 0.47 m.

In the Northwest Atlantic, there is significant interannual sea level variability (Han, 2002; Han, 2004; Han, 2007), in addition to the seasonal cycle (Greatbatch *et al.*, 1990, Han *et al.*, 2002). The interannual sea level variability appears to be related to the dominant mode of atmospheric variability in the North Atlantic, the North Atlantic Oscillation (NAO) (Han, 2002). It is influenced by the large-scale ocean circulation (Han, 2002, 2007; Yin *et al.*, 2009; Sallenger Jr. *et al.*, 2012). The secular sea level change is not only influenced by ocean dynamic adjustment and land ice and ice-sheet melt in response to the present climate change, but also by the glacial isostatic adjustment (GIA) to the last glacial maximum (Han, 2004; Slangen *et al.*, 2012). The GIA causes vertical land motion and a change of the sea surface topography itself. Though the latter is small in general, the combination of both is the net GIA effect that contributes to the sea level measured by a tide gauge.

In this study, we combine historical tide-gauge data and global AOGCM output to analyse the past change and to project future trends of the mean relative sea level (RSL) in the Northwest Atlantic. For the RSL projections, we will focus on the changes in the next 50 years which are of particular interest in the Aquatic Climate Change Adaptation Services Program of Fisheries and Oceans Canada (DFO). The RSL is defined as the sea level relative to the local land, as measured by tide gauges, and thus influenced by the local land motion in the vertical. Complementary information of extreme sea level can be found in Xu *et al.* (2013) and Zhai *et al.* (2013)

9.2 Data and Methods

Tide-gauge data

Tide-gauge data along the Canadian Atlantic coast are collected by the Canadian Hydrographic Service. We use annual-mean sea level data at selected tide gauge stations (Fig. 9-1), obtained from DFO's Integrated Science Data Management (http://www.dfo-mpo.gc.ca/science/data-donnees/index-eng.html). Annual means are calculated from daily water level data, for years with more than 180 days of data. Annual-mean data for Boston and Portland, US are obtained from the Permanent Service for the Mean Sea Level (PSMSL, http://www.psmsl.org/). Linear trends (positive rising and negative falling) of the RSL and associated standard errors are derived from the tide-gauge data using a least squares fit.

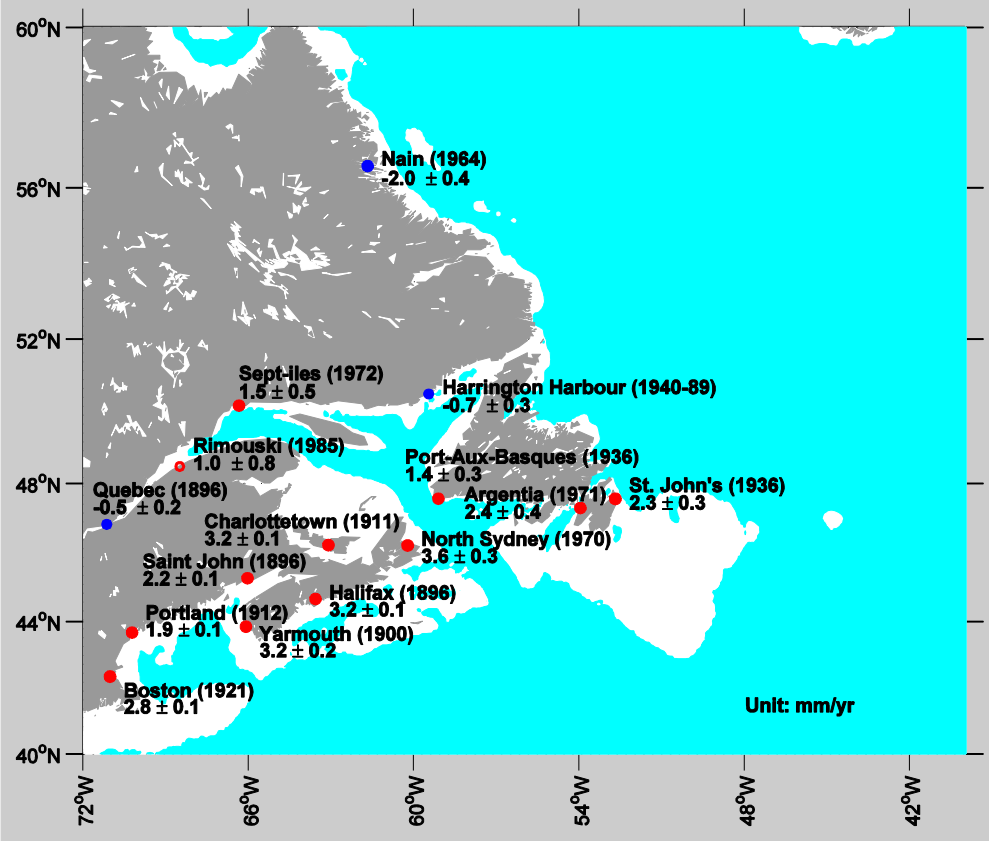

Figure 9-1 Rates of RSL change (positive depicted in red and negative in blue; different from zero at the 95% confidence level shown in solid dots and not different in open circles) and plus-minus one standard error based on tide-gauge measurements at selected tide-gauge stations. The values in the braces are the start years of the data (with the same end year of 2012 for all stations), except for Harrington Harbour that has both start and end years indicated. The statistical significance is inferred with the assumption of uncorrelated errors.

There are considerable differences in the duration of the tide-gauge record. We use the data from variable beginning years (shown in Fig. 9-1) to 2012. The record for Harrington Harbour is from 1940 to 1989. Measurements at a site 10 km away from Rimouski from 1897-1983 are also used to provide a longer-term perspective for Rimouski where the record began in 1985.

Glacial Isostatic Adjustment (GIA) model and data

The GIA has two effects on the RSL: the vertical land motion, and the resulting change in sea surface topography. The land subsidence (uplift) would on the one hand increase (decrease) the RSL but, on the other hand, decrease (increase) the gravity attraction and decrease (increase) the sea surface topography and thus the RSL.

We use the GIA model (ICE-5G, VM2) results of Peltier (2004). The model results include the present-day vertical land motion and the net RSL change associated with the GIA in a 1°×1° grid. We also use the vertical land motion derived from the Global Positioning System (GPS) (Craymer *et al.*, 2011; Sellar *et al.*, 2007). The GPS data are available at some of the tide-gauge sites. The average duration of the GPS data is about 10 years. Note that GPS data include any vertical land motion caused by other factors, in addition to the GIA.

Computation of RSL projections

We have considered the IPCC AR4 low (B1), medium (A1B), and medium-high (A2) SRES emission scenarios and the IPCC AR5 medium-low (RCP4.5) and medium-high (RCP8.5) Representative Concentration Pathways (RCPs) (Moss *et al.*, 2010). For regional RSL projections, we have summed different contributing components: the GIA, the land ice melt (including mountain glacier and Greenland and Antarctic ice sheets), and the ocean dynamic effects. For the GIA component, Peltier's (2004) model output of the net RSL change is first used, including the results for the vertical land motion and for the sea surface topography, respectively. Then the GPS-based vertical land motions, where available, are used for comparison at tide-gauge stations. For the land ice melt effect, we use Slangen *et al.*'s (2012) model output, with an assumption of linear evolution between 1980-1999 and 2090-2099. In addition, we use Slangen *et al.*'s (2012) A1B for RCP4.5 and A2 for RCP8.5, as a crude approximation. For the ocean dynamic effect, we used an ensemble average of 8 global AOGCMs for IPCC AR4 scenarios (Slangen *et al.*, 2012), with an assumption of linear evolution between 1980-1999 and 2090-2099. See Slangen *et al.*'s (2012) Table 2 for more details of the 8 global AOGCMs. An ensemble average of 2 global AOGCMs (CanESM2 and GFDL-ESM2M) is used for IPCC AR5 RCP4.5 and RCP8.5.

9.3 Historical Trends

Historical RSL change from tide-gauge data

There are significant spatial variations in the long-term mean RSL trend (Figs. 9-1 and 9-2). The RSL rates are 2-4 mm/yr at Nova Scotia (North Sydney, Halifax, Yarmouth), southern New Brunswick (Saint John), Prince Edward Island (Charlottetown), and Newfoundland (St. John's, Argentia, and Port-Aux-Basques) sites. In contrast, the RSL rate is -2 mm/yr at one Labrador site (Nain). Along the northern Gulf of St. Lawrence coast, the RSL rates vary from negative at Harrington Harbour to positive at Sept-Iles. The RSL rate at Quebec is small and negative, marginally different from zero at the 95% confidence level. The rate at Rimouski on the southern coast of the St. Lawrence Estuary is positive over 1985-2012, but not different from zero; while that at a nearby (about 10 km away) site is -0.4±0.2 (one standard error) mm/yr over 1897-1983, marginally different from zero. The above results suggest that the magnitude of the historical

long-term RSL trend is small along the northern Gulf of St. Lawrence and in the St. Lawrence Estuary.

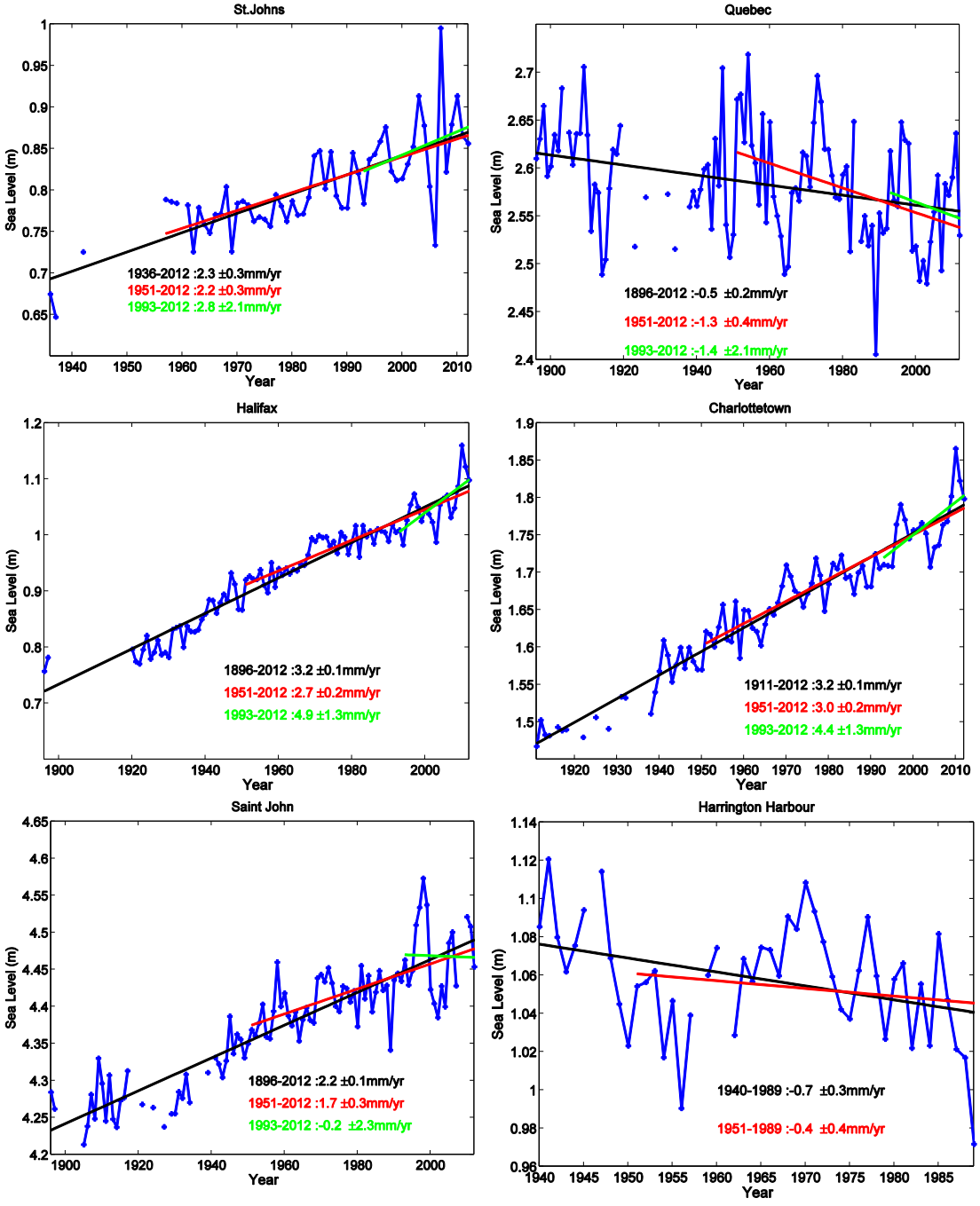

Figure 9-2 Annual-mean RSLs and linear fitting lines for selected time periods at selected tide-gauge stations along Atlantic Canada. Time periods and linear trends plus/minus one standard error are shown inside each panel.

There appears to be some suggestion of a recent acceleration of the sea level rise at some locations but there are large uncertainties (Fig. 9-2 and Table 9-1), e.g. Halifax and St. John's.

However, the statistical significance of the acceleration depends on the period and location, as reported by Sallenger Jr. *et al.* (2012). For example, the RSL trend of 2.8 mm/yr at St. John's over 1993-2012 is not different from zero at the 95% confidence level (Table 9-1).

Table 9-1 RSL rate (mm/yr or cm/decade) along the coast of the Atlantic Canada and the coast of the Gulf of St. Lawrence from tide-gauge data over 1993-2012. Vertical land motion rate plus/minus one standard deviation (mm/yr) along the Atlantic coast, from observations (GPS) and a model. The GPS data duration is about 10 years on average (Craymer *et al.*, 2011). The GIA model value is the average 250 years before and after the present.

Site	RSL Rate	GPS	GIA model
St. John's	2.8±2.1	0.1±0.0	-1.1
North Sydney	5.7±1.0	-1.2±0.6*	-2.0
Halifax	4.9±1.3	-0.7±0.6	-1.1
Yarmouth	5.7±1.0	0.0±0.6	-0.9
Saint John	-0.2±2.3	0.3±0.6	-0.8
Charlottetown	4.4±1.3	N/A	-1.9
Sept-Isle	-2.0±1.1	4.9±0.3	0.3
Rimouski	0.5±1.5	3.6±0.3	-1.1
Nain	-2.8±4.1**	4.6±0.1	1.0

*From a nearby site **Over 2002-2012

There are also evident interannual, decadal, and multidecadal variations (Fig. 9-2). For example, the annual-mean sea level at St. John's rose by about 0.3 m from 2005 to 2006, and then fell by about 0.2 m from 2006 to 2007. There is an indication of significant decadal to bi-decadal sea level fluctuations at Quebec. Due to the strong decadal and multi-decadal variability and the weak long-term RSL trend, the sign of the estimated trend is highly sensitive to the data period and duration in the St. Lawrence Estuary.

Effects of GIA

From Figures 9-3 and 9-4, the RSL change associated with GIA is dominated by the land subsidence (uplift) along the Canadian Atlantic coast. The change of the sea surface topography itself is relatively small. Over most areas of the Northwest Atlantic, Peltier's (2004) model indicates that the GIA results in land subsidence and RSL rise, but along the northern Gulf coast and the southern Labrador coast it indicates land uplift and RSL decrease.

We have compared Peltier's (2004) model results with the vertical land motion derived from the GPS-measurements (Craymer *et al.*, 2011; Sellar *et al.*, 2007). The average GPS rate along the Atlantic coast of Nova Scotia, New Brunswick, and Newfoundland is -0.3±0.6 (one standard deviation) mm/yr; while the model vertical land motion rate is -1.2 mm/yr (Table 9-1). There is poorer agreement along the northern coast of the Gulf of St. Lawrence, the St. Lawrence Estuary, and Labrador (Table 9-1), where the model average of 0.4 mm/yr significantly underestimates the average GPS uplift of 4.4±0.7 mm/yr.

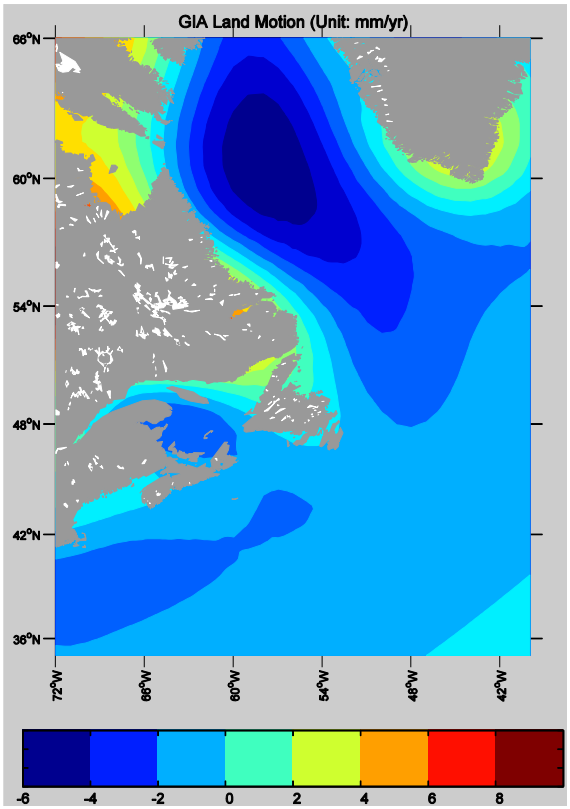

Figure 9-3 Rate of the vertical land motion due to GIA based on Peltier's (2004) model.

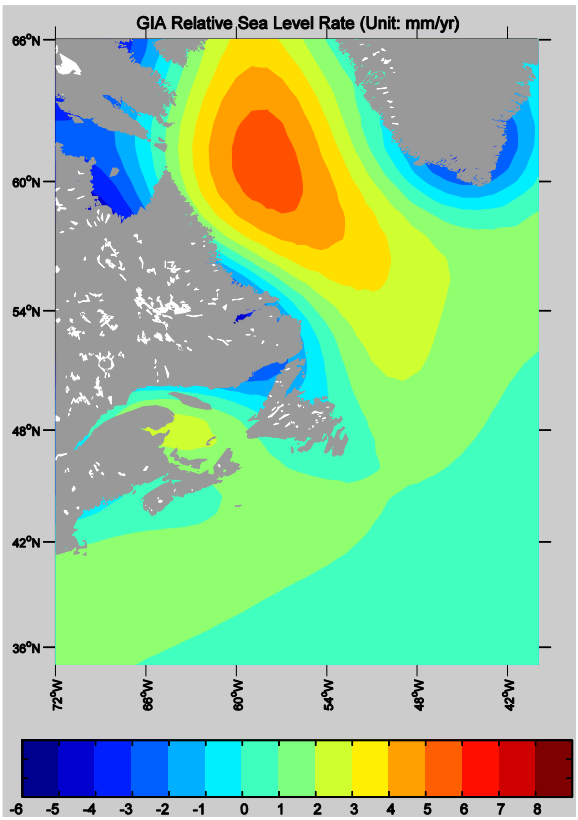

Figure 9-4 Rate of the RSL change due to GIA based on Peltier's (2004) model.

From Table 9-1 and Figure 9-1, it can be inferred that the spatial difference in the RSL trends observed by the tide gauges can, in part, be attributed to the vertical land motion, especially when the GPS data are used. For example, at Nain with a land uplift of 4.6 mm/yr, the RSL rate is -2 mm/yr and well below the global average of 1.7 mm/yr; while at Halifax with a land subsidence of 0.7 mm/yr the RSL rate is 3.2 mm/yr and above the global average. The difference of 5.2 mm/yr in the RSL trends between Halifax and Nain can be accounted for by the difference of 5.3 mm/yr in the GPS estimates of vertical land motion.

9.4 Projections of the mean RSL change

Slangen *et al.* (2012) projected a global mean RSL rise of 0.37±0.09, 0.47±0.11, and 0.55±0.17 m between 1980-1999 and 2090-2099 for B1, A1B, and A2, respectively. For A1B, the contributions on this century timescale by the steric height, mountain glaciers, Antarctic ice sheet, Greenland ice sheet, and GIA were 0.21±0.09, 0.17±0.04, 0.01±0.02, 0.08±0.02, and 0.004±0.003 m, respectively. They also indicated that the global mean RSL rise for A1B could be up to 1.02 m over the same period, in consideration of a faster increase of ice sheet mass loss than was estimated in IPCC AR4. For the land ice contribution, the IPCC AR4 projected a global mean of 0.08-0.15 m, while Slangen *et al.* (2012) projected 0.13-0.25 m. Although the projected RSL rise is also subject to the uncertainties in the GIA model, the GIA influence is smaller on the global scale.

On the century time scale, projected RSL changes in the Northwest Atlantic between 1980-1999 and 2090-2099, from Slangen *et al.* (2012) for A1B, are shown in Figure 9-5. The mean RSL rise under A1B is over 60 cm along the south and southeast coast of Newfoundland and along the coast of Nova Scotia, although the AOGCMs do not resolve the shelf topography well so there is additional uncertainty in the coastal values. The highest RSL rise appears to be along the south coast of the Gulf of St. Lawrence, over 80 cm. There is an indication that the RSL rise is smaller in the northeastern Gulf of St. Lawrence, off the northeastern Newfoundland coast, and off the Labrador coast which can, in part, be attributed to the land uplift in the GIA model (Fig. 9-3). In the case of accelerated ice sheet loss, the mean RSL rise around some parts of the Atlantic coast (Newfoundland and Nova Scotia) could be 1 m (Slangen *et al.*, 2012; their Fig. 9), an additional rise of 30-40 cm.

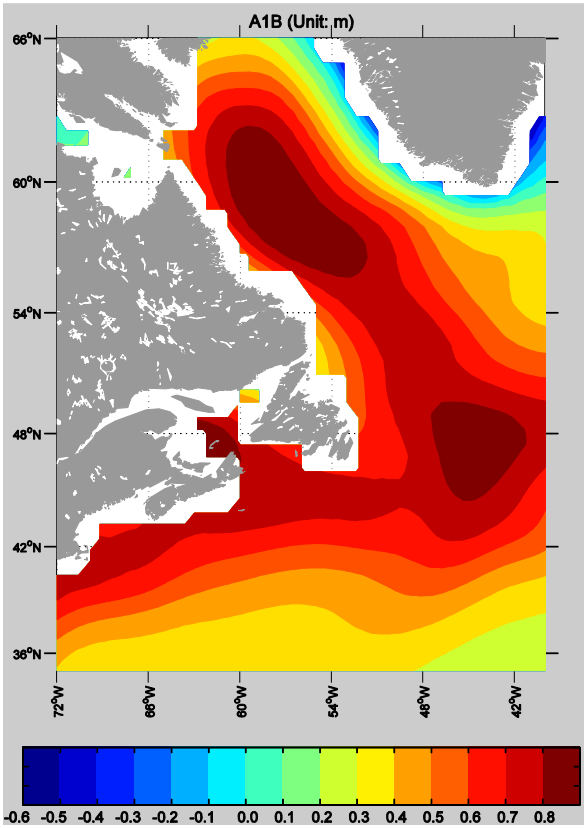

Figure 9-5 Ensemble mean total RSL change between 1980-1999 and 2090-2099 for A1B (Slangen *et al.*, 2012).

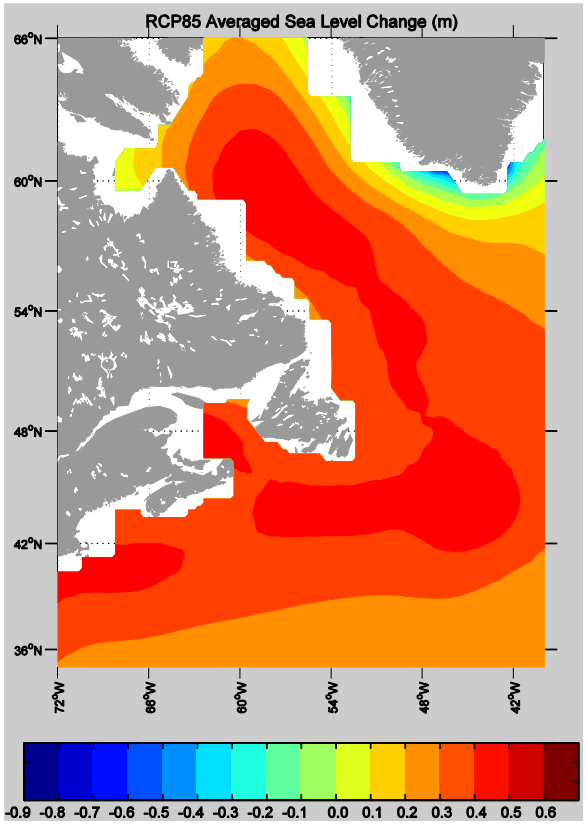

Figure 9-6 Projected sea level change between 1986-2005 and 2046-2065 under RCP 8.5, based on the two IPCC AR5 AOGCMs, Slangen *et al.*'s (2012) land ice model, and Peltier's (2004) GIA model.

On the half-century time scale, we first show rough estimates of the RSL rise in the Northwest Atlantic under IPCC AR5 RCP4.5 and RCP8.5 for 2046-2065, relative to 1986-2005. The estimates are produced by combining the average of the projected changes from CanESM2 and GFDL-ESM2M output with Slangen *et al.*'s (2012) land ice result and Peltier's (2004) GIA model effect on the RSL,. For RCP8.5 the projected mean RSL rise along the Canadian Atlantic coast is around 35-40 cm by 2046-65 (Fig. 9-6). For RCP4.5 (not shown), the projected rise over 60 years is about 25-35 cm. Note that the estimated values are subject to uncertainties in the models and in the method. For example, if the accelerated ice sheet loss is considered, the sea level rise could be 18-24 cm higher for the Newfoundland and Nova Scotia coast. The dynamic oceanographic component in the above estimates is from two IPCC AR5 models which differ from each other substantially (Loder and van der Baaren 2013). More AOGCM output should be used to produce the average. The model sea level results from IPCC AR4 AOGCMs also differ significantly (Slangen *et al.*, 2012)

At the tide-gauge stations, along the coast of Newfoundland, Nova Scotia, and New Brunswick, the GPS-based projections range from 28 to 35 cm under RCP8.5 (Table 9-2). They are about 5 cm smaller than the GIA model-based projections. In contrast, the projections with the land subsidence from the GIA model overestimate the RSL rise by about 28 cm along the Labrador coast, the northern coast of the Gulf of St. Lawrence, and the St. Lawrence Estuary. The projected sea level changes under RCP8.5 with the GPS-based vertical land motion are 7 and 6 cm at Sept-Iles and Rimouski, respectively. Off Labrador, the projected RSL increases 8 cm based on the GPS vertical land motion under RCP8.5. The projected RSL changes under RCP4.5 are 5 cm smaller on average than those under RCP8.5.

Table 9-2 Projected sea level change (cm) between 1986-2005 and 2046-2065 under RCPs 4.5 and 8.5 based on the two IPCC AR5 AOGCMs (CanESM2 and GFDL-ESM2M), Slangen *et al.*'s (2012) land ice model, and Peltier's (2004) GIA effect on the RSL (column "Model"). Also shown are projections under IPCC A2 SRES based on the 8 IPCC AR4 AOGCMs from Slangen *et al.* (2012) (column "Model"). Where available Peltier's vertical land motion is replaced with the GPS data (Craymer *et al.*, 2011) (column "GPS").

Site	RCP4.5		RCP8.5		A2	
	Model	GPS	Model	GPS	Model	GPS
St. John's	30	22	35	28	29	22
North Sydney	35	30	40	35	41	36
Halifax	33	30	37	35	34	32
Yarmouth	32	27	36	31	31	26
Saint John	31	24	36	28	31	25
Charlottetown	36	N/A	41	N/A	43	N/A
Sept-isle	30	3	35	7	42	14
Rimouski	29	1	34	6	51	23
Nain	24	3	29	8	22	0

Figure 9-7 shows the projected total RSL changes at selected tide-gauge sites between 1986-2005 and 2046-2065 under RCP8.5, and the contributions by ocean dynamics based on the two IPCC

AR5 AOGCMs, by the land ice melt based on Slangen *et al.*'s (2012) land ice model, and by the GIA with the land motion based on Craymer's (2011) GPS data. Overall, the ocean dynamical effect is the dominant factor for the RSL rise along the Canadian east coast. The land ice melt contributes about 10 cm to the RSL rise except at Nain where the land-ice contribution is negligible. The effect of the vertical land uplift is large at Nain, Sept-Iles, and Rimouski, significantly reducing the sea level rise due to present and future global warming.

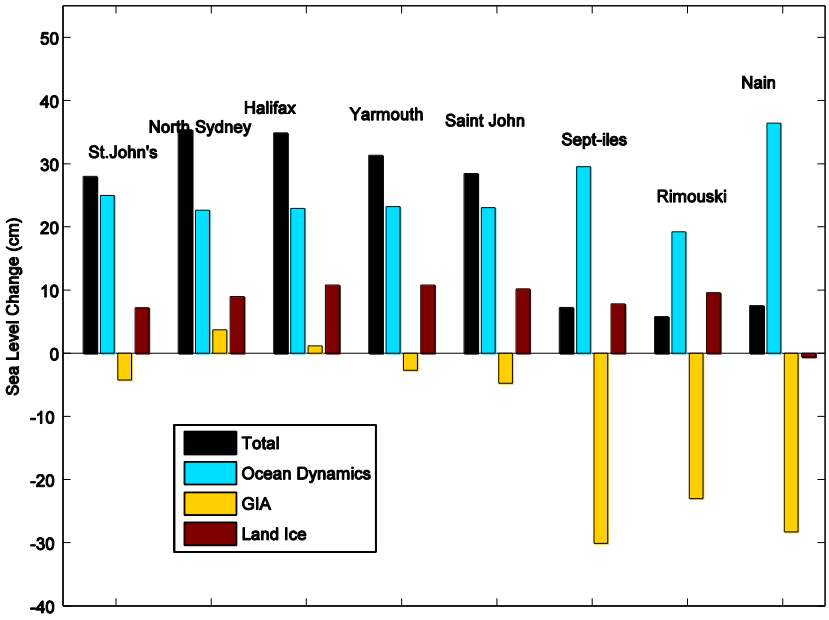

Figure 9-7 Projected total RSL change between 1986-2005 and 2046-2065 under RCP 8.5, and the contributions by ocean dynamics based on the two IPCC AR5 AOGCMs, by the GIA with the land motion from Craymer's (2011) GPS data, and by the land ice melt based on Slangen *et al.*'s (2012) land ice model. Note that the GIA component also includes any vertical land motion caused by other potential factors, in addition to the GIA.

Sea level projections under IPCC AR4 A2 are also derived based on the 8 IPCC AR4 global AOGCMs (Slangen *et al.*, 2012) for the period from 1986-2005 to 2046-2065 (Fig. 9-8, Table 9-2). The AR4 results are generally consistent with the present projections using the AR5 global AOGCMs. For example, the GPS-based projections range from 22 to 36 cm under A2 along the coast of Newfoundland, Nova Scotia, and New Brunswick, comparable to the RCP8.5 range of 28 to 35 cm. Nevertheless, there is significantly greater or smaller magnitude at certain sites. For example, the projected RSL rise based on the AR4 models is 7 and 17 cm greater at Sept-Iles and Rimouski, and about 8 cm smaller at Nain (Table 9-2). The results under A1B (not shown) are nearly the same as those under A2, and are about 5 cm greater than those under B1 (not shown).

On the decadal time scale, it is reasonable to expect that the RSL trends will be comparable to long-term historical values, but with large uncertainties due to interannual-decadal variability (Fig. 9-2). If we linearly scale down the 60-year projections in Tables 9-2, the projected mean relative sea level rise will vary from 0 to 6 cm in the next decade, depending on locations. To summarize, it is likely that the mean relative sea level will continue to rise at 3-4 cm/decade along the coast of Newfoundland, Prince Edward Island, Nova Scotia, and New Brunswick, and

to rise or fall at smaller magnitude elsewhere with the uncertainties as much as or greater than the estimates.

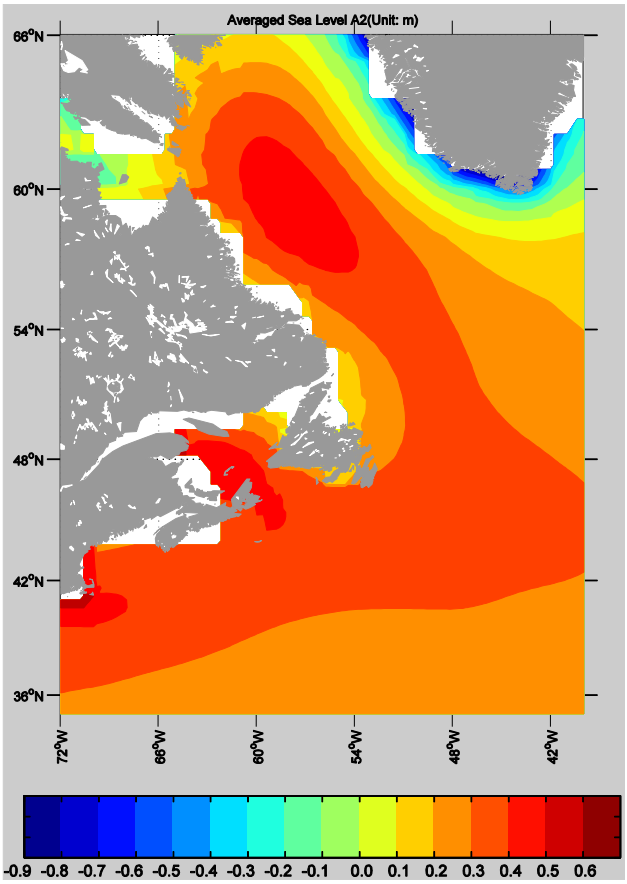

Figure 9-8 Projected sea level change between 1986-2005 and 2046-2065 under A2, based on the 8 IPCC AR4 AOGCMs, Slangen *et al.*'s (2012) land ice model, and Peltier's (2004) GIA model.

9.5 Conclusions

We have used tide gauge data to investigate the historical mean RSL change in the Northwest Atlantic. Results from different sources that account for ocean-atmosphere interaction (from global AOGCMs), GIA effects (mainly the vertical land motion from model or GPS observations), and land ice melt effects (model) are combined to generate RSL projections.

The coastal RSL change in the past shows significant regional variations, from 2-4 mm/yr along the coast of Newfoundland, Prince Edward Island, Nova Scotia, and New Brunswick (above the global mean RSL rise rate) to -2 mm/yr along the Labrador coast and between the northern coast of the Gulf of St. Lawrence and the St. Lawrence Estuary. The vertical land motion associated with GIA is an important contributor to this spatial difference of sea level changes in Atlantic Canada. Peltier's (2004) GIA model has a moderate mean bias of -0.9 mm/yr relative to the GPS vertical land motion along the coast of Nova Scotia and New Brunswick but differs significantly from it (a mean bias of 4.0 mm/yr) along the St. Lawrence Estuary, the northern coast of the Gulf of St. Lawrence, and Labrador. The difference in the GPS vertical land motion can account, to a significant degree, for that in the RSL trends between tide-gauge stations.

The projected RSL rise between 1986-2005 and 2046-2065, adjusted for the GPS-measured vertical land subsidence or uplift, is about 20-40 cm along the Canadian Atlantic coast, with smaller or even no rise at some locations along Labrador, the northern coast of the Gulf of St. Lawrence, and along the St. Lawrence Estuary. There are considerable uncertainties associated with the coastal sea level projections, especially within the ocean dynamic effect and the ice-sheet melt component. On the decadal time scale, it is likely that the mean RSL will continue to rise at 3-4 cm/decade along the coast of Newfoundland, Prince Edward Island, Nova Scotia, and New Brunswick, and to rise or fall with smaller magnitude elsewhere with the uncertainties as much as or greater than the estimates.

The present global AOGCMs are too coarse in their spatial resolution to sufficiently account for the regional difference in the ocean dynamical contribution to the sea level rise, especially in the St. Lawrence Estuary. Therefore, regional atmosphere-ocean climate models with an active ocean component with sufficient spatial resolution are needed to provide sea level projections along the Canadian Atlantic coast. Besides, long-term GPS data and improved GIA models are needed for accurate spatial structure of the GIA effect. Close attention should also be paid to the latest advances on the contribution of the ice sheet melt so that the best available estimates can be incorporated in the projection for this potentially large but highly uncertain factor (Pfeffer *et al.*, 2008). Given the large uncertainty associated with future regional sea level rise estimates, it is warranted to establish regional and local sea level rise scenarios for coastal planning, risk assessment, and adaptation strategy (Parris *et al.*, 2012).

9.6 Acknowledgment

The work has been funded by the Aquatic Climate Change and Adaptation Services Program (ACCASP) of Fisheries and Oceans Canada. We thank Aimée Slangen for providing the IPCC AR4 AOGCM and land ice melt results and Michael Craymer for providing the GPS data. Li Zhai, Blair Greenan, and Eugene Colbourne provided internal reviews.

9.7 References

Cazenave, A. and R. S. Nerem. 2004. Present-day sea level change: observations and causes. *Rev. Geophys*., 42 (RG3001).

Church, J. A. and N. J. White. 2011. Sea-level rise from the late 19th to the early 21st century, *Surv. Geophys.*, 32, 585-602.

Craymer, M. R., J. Henton, M. Piraszewski, and E. Lapelle. 2011. An updated GPS velocity field for Canada. *EOS Transactions*, AGU, 92(51), Fall Meeting Supplement, Abstract G21A-0793.

Greatbatch, R. J., B. deYoung, A. Goulding, and J. Craig. 1990. On the influence of local and North Atlantic wind forcing on the seasonal variation of sea level on the Newfoundland and Labrador Shelf, *J. Geophys. Res.*, 95, 5279-5289.

Han, G. 2002. Interannual sea level variations in the Scotia-Maine region in the 1990s, *Can. J. Remote Sensing*, 28, 581-587.

Han, G. 2004. Sea level and surface current variability in the Gulf of St. Lawrence from satellite altimetry. *Int. J. Remote Sensing*, 25, 5069-5088.

Han, G. 2007. Satellite observations of seasonal and interannual changes of sea level and currents over the Scotian Slope. *J. Phys. Oceanogr*., 37, 1051-1065.

Han, G., C. L. Tang, and P. C. Smith. 2002. Annual variations of sea surface elevations and currents over the Scotian Shelf and Slope. *J. Phys. Oceanogr.*, 32, 1794-1810.

Loder, J.W. and A. van der Baaren. 2013. Climate change projections for the Northwest Atlantic from six CMIP5 Earth System Models. Can. Tech. Rep. Hydrogr. Ocean Sci. 286: xiv + 112 p. http://www.dfo-mpo.gc.ca/library/349550.pdf

Meehl, G. A., T. F. Stocker, W. D. Collins, P. Friedlingstein, A. T. Gaye, J. M. Gregory, A. Kitoh, R. Knutti, J. M. Murphy, A. Noda, S. C. B. Raper, I. G. Watterson, A. J. Weaver, and Z.-C. Zhao. 2007. Global Climate Projections. In: *Climate Change 2007: The Physical Science Basis. Contribution of Working Group I to the Fourth Assessment Report of the Intergovernmental Panel on Climate Change* [Solomon, S., D. Qin, M. Manning, Z. Chen, M. Marquis, K. B. Averyt, M. Tignor, and H. L. Miller (Eds.)]. Cambridge University Press. http://www.ipcc.ch/publications_and_data/ar4/wg1/en/ch10.html

Moss, R. H., J. A. Edmonds, K. A. Hibbard, M. R. Manning, S. K. Rose, D. P. van Vuuren, T. R. Carter, S. Emori, M. Kainuma, T. Kram, G. A. Meehl, J. F. B. Mitchell, N. Nakićenović, K. Riahi, S. J. Smith, R. J. Stouffer, A. M. Thomson, J. P. Weyant, and T. J. Wilbanks 2010. The next generation of scenarios for climate change research and assessment. *Nature*, 463, 747-756, doi: 10.1038/nature08823

Nakićenović, N., J. Alcamo, G. Davis, B. de Vries, J. Fenhann, S. Gaffin, K. Gregory, A. Grubler, T.Y. Jung, T. Kram, E. L. La Rovere, L. Michaelis, S. Mori, T. Morita, W. Pepper, H. Pitcher, L. Price, K. Riahi, A. Roehrl, H.-H. Rogner, A. Sankovski, M. Schlesinger, P. Shukla, S. Smith, R. Swart, S. van Rooijen, N. Victor, and Z. Dadi. 2000. *IPCC Special Report on Emissions Scenarios*, Cambridge, U. K. and New York: Cambridge University Press, 599 pp.

Nerem, R. S., D. Chambers, C. Choe, and G. T. Mitchum. 2010. Estimating Mean Sea Level Change from the TOPEX and Jason Altimeter Missions. *Mar. Geodesy*, 33(1), Supp. 1, 435.

Parris, A., P. Bromirski, V. Burkett, D. Cayan, M. Culver, J. Hall, R. Horton, K. Knuuti, R. Moss, J. Obeysekera, A. Sallenger, and J. Weiss. 2012. Global sea level rise scenarios for the US National Climate Assessment. NOAA Tech Memo OAR CPO-1, 37 pp.

Peltier, W. 2004. Global glacial isostasy and the surface of the ice-age earth: the ICE-5G (VM2) model and GRACE. *Ann. Rev Earth Planet Sci.*, 32, 111-149.

Pfeffer, W. T., J. T. Harper, and S. O'Neel. 2008. Kinematic constraints on glacier contributions to 21st century sea-level rise. *Science*, 321, 1340-1343.

Sallenger Jr., A. H., K. S. Doran, and P. A. Howd. 2012. Hotspot of accelerated sea-level rise on the Atlantic coast of North America. *Nature Climate*, 2, 884–888, doi: 10.1038/NCLIMATE1597.

Sellar, G. F., S. Stein, T. H. Dixon, M. Craymer, T. S. James, S. Mazzotti, and R. K. Dokka. 2007. Observation of glacial isostatic adjustment in "stable" North America with GPS. *Geophys. Res. Lett.*, 34(2), L02306.

Slangen, A. B. A., C. A. Katsman, R. S. W. van de Wal, L. L. A. Vermeersen and R. E. M Riva. 2012. Towards regional projections of twenty-first century sea-level change based on IPCC SRES scenarios. *Climate Dynamics*, 38(5-6), 1191-1209, doi: 10.1007/s00382-011-1057-6.

Solomon, S., D. Qin, M. Manning, R. B. Alley, T. Berntsen, N. L. Bindoff, Z. Chen, A. Chidthaisong, J. M. Gregory, G. C. Hegerl, M. Heimann, B. Hewitson, B. J. Hoskins, F. Joos, J. Jouzel, V. Kattsov, U. Lohmann, T. Matsuno, M. Molina, N. Nicholls, J. Overpeck, G. Raga, V. Ramaswamy, J. Ren, M. Rusticucci, R. Somerville, T. F. Stocker, P. Whetton, R. A. Wood, and D. Wratt. 2007. Technical Summary. In: *Climate Change 2007: The Physical Science Basis. Contribution of Working Group I to the Fourth Assessment Report of the Intergovernmental Panel on Climate Change* [Solomon, S., D. Qin, M. Manning, Z. Chen, M. Marquis, K. B. Averyt, M. Tignor, and H. L. Miller (Eds.)]. Cambridge University Press, Cambridge, United Kingdom and New York, NY, USA.
http://www.ipcc.ch/publications_and_data/ar4/wg1/en/contents.html

UNESCO/ICO, 2010. Sea-level rise and variability – a summary for policy makers. IOC/BRO/2010/5, France.

Xu, Z., D. Lefaivre and M. Beaulieu. 2013. Sea levels and storm surges in the Gulf of St. Lawrence and its vicinity. Ch. 8 (p. 95-112) *In:* This report.

Yin, J., M. E. Schlesinger, and R. J. Stouffer. 2009. Model projections of rapid sea-level rise on the northeast coast of the United States. *Nature Geosci.*, 2, 262-266.

Zhai, L., B. Greenan, J. Hunter, T.S. James and G. Han. 2013. Estimating sea-level allowancesfor Atlantic Canada under conditions of uncertain sea-level rise. Can. Tech. Rep. Hydrogr. Ocean Sci. 283: v + 40 p. http://www.dfo-mpo.gc.ca/Library/349546.pdf

10 Temporal trends in nutrient concentrations in the northwest Atlantic basin

Pierre Pepin [1]*, Gary L. Maillet [1], Diane Lavoie [2], and Catherine Johnson [3]

[1] Fisheries and Oceans Canada, Northwest Atlantic Fisheries Centre
P.O. Box 5667, St. John's, Newfoundland and Labrador A1C 5X1

[2] Fisheries and Oceans Canada, Maurice Lamontagne Institute
Mont-Joli, Québec

[3] Fisheries and Oceans Canada, Bedford Institute of Oceanography
Dartmouth, Nova Scotia

*correspondence: Pierre.Pepin@dfo-mpo.gc.ca

Suggested Citation:
Pepin, P., G.L. Maillet, D. Lavoie and C. Johnson. 2013. Temporal trends in nutrient concentrations in the northwest Atlantic basin. Ch. 10 (p. 127-150) *In:* Aspects of climate change in the Northwest Atlantic off Canada [Loder, J.W., G. Han, P.S. Galbraith, J. Chassé and A. van der Baaren (Eds.)]. Can. Tech. Rep. Fish. Aquat. Sci. 3045: x + 190 p.

Abstract

We summarize the average and range of variability in nitrate, silicate, and phosphate concentrations, as well as long term trends (1960 – present), for the western North Atlantic basin, from the Labrador Sea to the Gulf of Maine. Our assessment was based on a survey of the BioChem archive of biological and chemical data of Fisheries and Oceans Canada, and the World Ocean Database (WOD) established by the International Oceanographic Commission (IOC). Our objective was to provide advice concerning the current state and long term changes of nutrient concentrations in waters off Canada's east coast. The eastern Labrador Sea and Central Scotian Shelf had significant long term declines in all macro-nutrients whereas most parts of the Gulf of St. Lawrence demonstrated notable increases in nutrient concentrations since the early 1970s. The western Labrador Sea saw an increase in silicate concentrations coupled with notable declines in nitrate, and, to a lesser extent, phosphate levels. We noted the opposite pattern in most parts of the Gulf of Maine and Bay of Fundy. Other areas generally demonstrated weak trends that were variable among macro-nutrients. Short term trends (1990 – present) were highly variable among areas. Overall, we did not find a highly consistent pattern of change in the northwest Atlantic basin. When coupled with the uncertainty in predicting future changes in regional circulation patterns based on AOGCMs, the most optimistic short and long term expectations of nutrient concentrations are that conditions may remain in the current "below average" state or that nutrient availability may decline, depending on the influx from the deep basin and the influx of water from the Labrador Current. Future model trends (next 50 years) indicate a general decrease in both the upper and lower layers for the Atlantic Northwest region, although there are spatial differences in the degree and direction of change.

10.1 Introduction

Harrison and Li (2007) and Yeats *et al.* (2010) summarized the trends in nutrient concentrations on the Labrador Shelf (1965-2009), Labrador Sea (1991-2009), and Scotian Shelf (1974-2009). They noted declines in silicate and phosphate concentrations, as well as in the relative departures from the Redfield ratio (N:Si:P – 16:16:1), which can indicate a decrease in transport of water from the Arctic or a decrease in the concentrations of silicate and phosphate in Arctic waters. Yeats *et al.* (2010) concluded that "the importance of Arctic source waters and the relatively larger decreases for silicate and phosphate than for nitrate all indicate that decreases in near-surface nutrient concentrations in the Arctic are responsible for the observed trends in preformed nutrients" in all Labrador Basin deep waters they considered (Danish Strait overflow water and Iceland-Scotland overflow water, which contribute to the Northeast Atlantic deep water; Arctic surface water outflow from both the West Greenland Current and the Baffin Island Current, which contribute to forming Labrador Sea water).

Declines in nutrient concentrations in the Northwest Atlantic can have significant consequences on the productivity of the region, particularly when coupled with the increasing stratification that has been associated with the trend toward higher temperatures and lower salinity (e.g. Hebert, 2013). If these trends persist under anticipated environmental conditions associated with climate change, ecosystem production potential may be severely impacted through changes in biogeochemical processes and trophic relationships in areas where nutrient, rather than light, limitation currently controls productivity.

In this report, we summarize the average and range of variability in nutrient concentrations, as well as long term trends (1960 – present), based on a survey of the BioChem archive of biological and chemical data of Fisheries and Oceans Canada, and the World Ocean Database (WOD) established by the International Oceanographic Commission (IOC). The purpose is to provide advice concerning the current state and long term changes of nutrient concentrations in waters of the continental shelf from northern Labrador to the Gulf of Maine, along with the Estuary and Gulf of St. Lawrence, as well as the Labrador Sea, as part of the Aquatic Climate Change Adaptation Services Program. This program aims to undertake a risk assessment of Fisheries and Oceans' ability to fulfil its mandate under emerging impacts of climate change. This report represents a contribution to the review of Trends and Projections activities of Science Branch.

10.2 Data and Methods

Geo-referenced nutrient concentrations (mmol m^{-3}) were gathered from BioChem (Fisheries and Oceans) and the World Ocean Database (International Oceanographic Commission). Observations were included only if the essential metadata (date, location, depth) were available. Data were grouped into a number of geographic areas (polygons) that aimed to separate the information into representative areas and sub-areas of well-identified eco-regions (Fig. 10-1). Data from the upper 50 m of the water column were excluded from consideration because of the strong seasonality associated with phytoplankton production that could result in biased estimates of long term trends in nutrient concentrations if sampling was uneven among years. This resulted

in a significant loss of information that might have been avoided if more time had been available for the analyses. The remaining data were binned into upper (50 – 100 m) and lower (100 – bottom or 400 m) layers. Preliminary investigations had demonstrated limited evidence of seasonal variations in nutrient concentrations in these layers.

The variables included nitrate + nitrite (NO_3^- + NO_2^-), silicate (SiO_4^{4-}) and phosphate (PO_4^{3-}) concentrations derived using a variety of analytical methods that were not distinguished in our analyses. Note that nitrite represents only 1-2% of the fixed nitrogen in the upper and lower layers, which leads us to refer to fixed nitrogen macro-nutrients as nitrate henceforth. For ocean waters, nitrate and silicate concentrations in excess of 30 mmol m^{-3} were excluded from our analyses whereas a threshold of 60 mmol m^{-3} was applied to data from the Estuary and Gulf of St. Lawrence. Phosphate concentrations were within expected ranges for all regions. In addition, we estimated the excess silicate (Si – N) and excess phosphate (P – N/16) that could be useful water mass indicators.

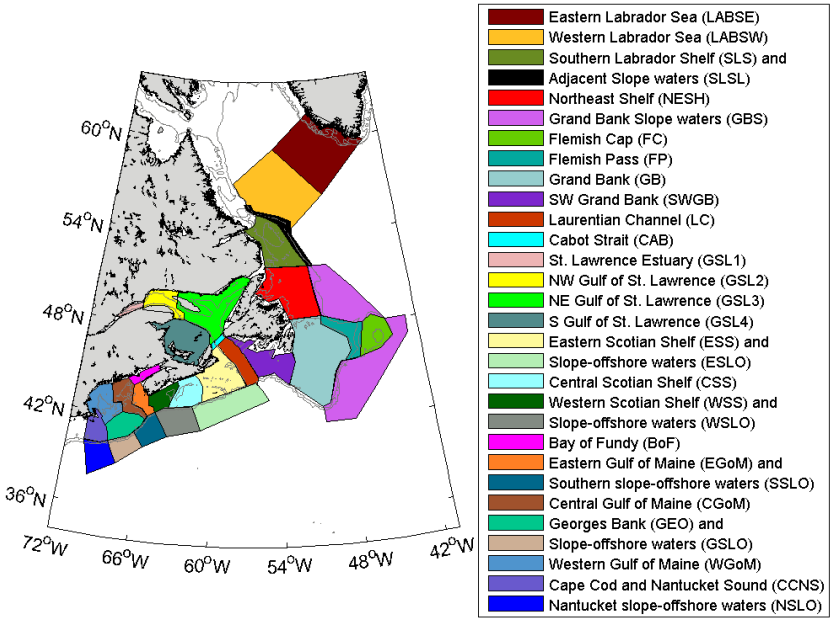

Figure 10-1 Map of study area with outline of polygons used to group data into representative subareas of major eco-regions.

Data density (observations per year) varied greatly among areas and significant gaps in coverage were apparent, particularly during the 1960s and parts of the late 1980s and early 1990s. There were few data prior to 1965 and all data prior to that year were excluded because of concerns about reliability. The introduction of the Atlantic Zone Monitoring Program in 1999, or a few years earlier in some areas, resulted in significant improvements in coverage, quality, and consistency. Quality control and assurance flags, when available, were not considered because of difficulties in interpreting standards and their application among the different sources.

The first step in the analysis was to estimate the overall arithmetic mean, standard deviation, and 10^{th} and 90^{th} percentiles of all available data for each variable, polygon and depth interval for the entire time series of available data in order to describe the general state and variability among polygons.

The annual anomaly for each variable was calculated according to:

$A_i = \frac{\overline{X}_i - \overline{X}}{\sigma}$ where A_i is the annual anomaly, $\overline{X}_i$ is the annual average concentration, $\overline{X}$ is the overall average of annual averages for the entire time series for each area and depth interval, and σ is the standard deviation of the time series of annual averages. We chose not to define a standard reference period (e.g. 1971 – 2000) that could serve as a basis for comparison among areas because of significant variations in data density and gaps among the polygons. Anomalies were used to effectively visualize periods of high (positive anomalies) and low (negative anomalies) average nutrient concentrations.

Short (1990-2010) and long term (over the entire time period over which data were available for each region) trends for each area were evaluated using Spearman's rank correlation (r_s). This provides a measure of the monotonic change in nutrient concentrations over time. The procedure avoids interpolating over extended gaps by simply ranking anomalies relative to year based on data availability rather than assuming linear constancy over time that would be assumed by using Pearson's correlation coefficient (r).

10.3 Results

Nitrate

Nitrate concentrations in the upper layer (50 – 100 m) were highest in the estuarine portion of the Gulf of St. Lawrence (GSL1, GSL2) and in the western Labrador Sea (LABSW, SLSL, GBS, FC) and lowest on the Grand Bank (GB, SWGB), the Laurentian Channel (LC, CAB), Eastern Scotian Shelf (ESS) and the slope area off Georges Bank (GEO) (Fig. 10-2). Spatial trends were apparent across the zone with a positive gradient in nitrate concentration from the Cabot Strait-Laurentian Channel down to the western Gulf of Maine. Areas on the Scotian Shelf tend to have higher average nitrate concentrations than the Newfoundland Shelf but concentrations are slightly lower than for areas in the Gulf of Maine. Areas with high average concentrations tend to have higher standard deviations, although the association is weak (r = 0.47). Nitrate concentrations in the lower layer (100 – 400 m) were higher than those in the upper water column (Fig. 10-3). The differences were most pronounced in areas in, and in proximity to, the Gulf of St. Lawrence, where average nitrate concentrations were higher by 8 to 11 mmol m^{-3}. The vertical gradient in average nitrate concentrations between upper and lower layer was generally greater from the Gulf of St. Lawrence to the Gulf of Maine than in the area from Labrador Sea to the Flemish Cap.

For areas where data were available in the 1980s, upper layer (50 – 100 m) nitrate concentrations in most areas have declined since the start of that period (Fig. 10-4). Areas in the Labrador Sea and adjacent shelf have also shown decreases in nitrate concentrations since the 1990s. Short (1999 – present) and long term trends are often consistent within regions, with the eastern (LABSE; r_s = -0.71 and -0.70) and western (LABSW; r_s = -0.45 and -0.50) Labrador Sea, and central Scotian Shelf (CSS; r_s = -0.67 and -0.66) all experiencing substantial declines in upper layer nitrate concentrations during the period with available data (Fig. 10-4). Moderate long and short term declines (-0.45 < r_s < -0.3) are also apparent on the Grand Bank (GB), eastern Gulf of Maine (EGoM), northern Gulf of St. Lawrence (GSL2-3), and Central Gulf of Maine (CGoM) as

well as a short term decline on the eastern Scotian Shelf (ESS; r_s = -0.66). The St. Lawrence Estuary (GSL1; r_s = 0.50) and western Gulf of Maine (WGoM; r_s = 0.47) both exhibited long term increases in upper layer nitrate concentration. Other areas demonstrated only weak short term trends.

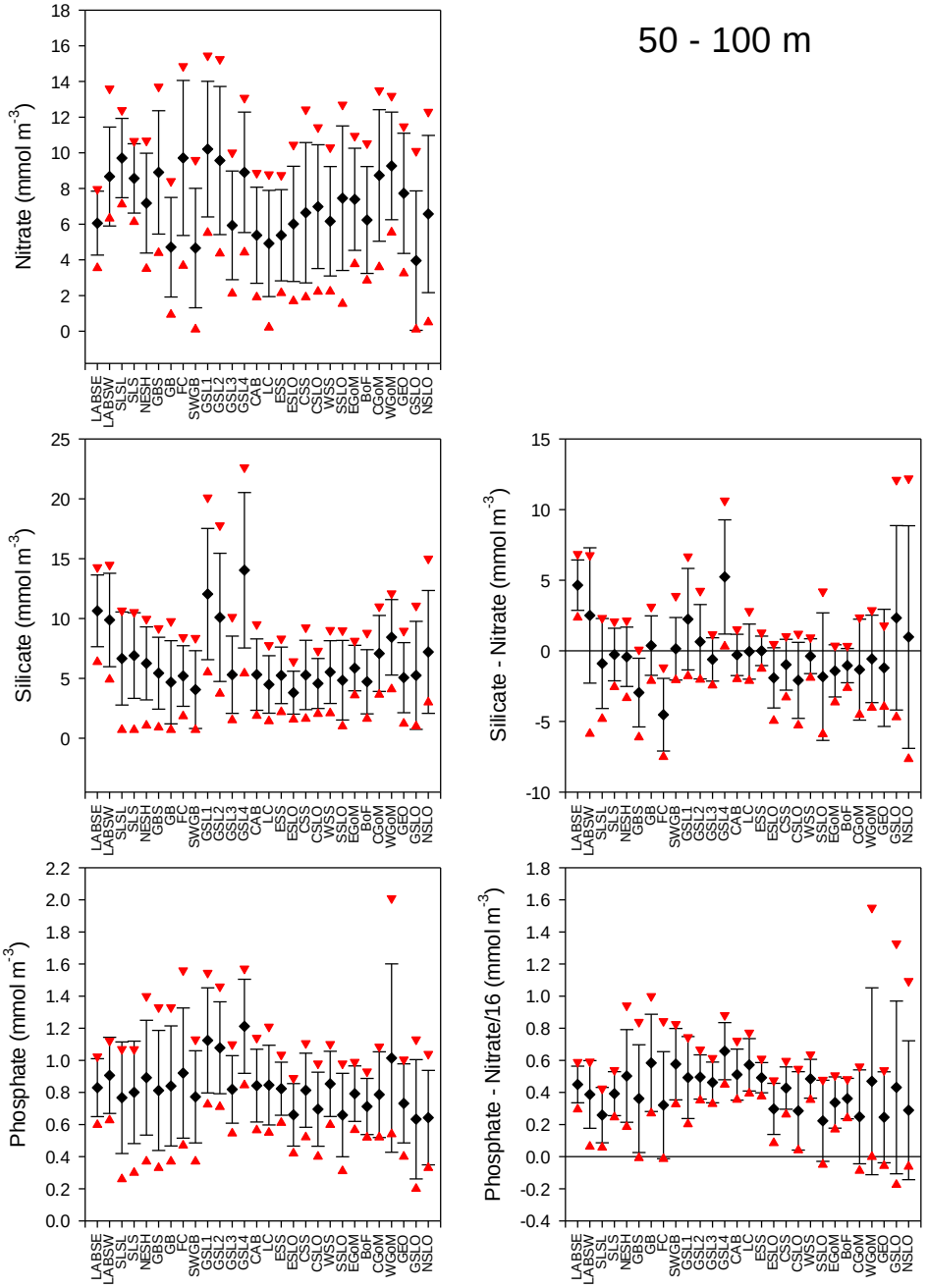

Figure 10-2 Descriptive statistics (overall mean, black symbol; standard deviation, black lines; 10th and 90th percentiles, red triangles) of nitrate concentrations in the upper (50 – 100 m) water column all the observations for all geographic areas.

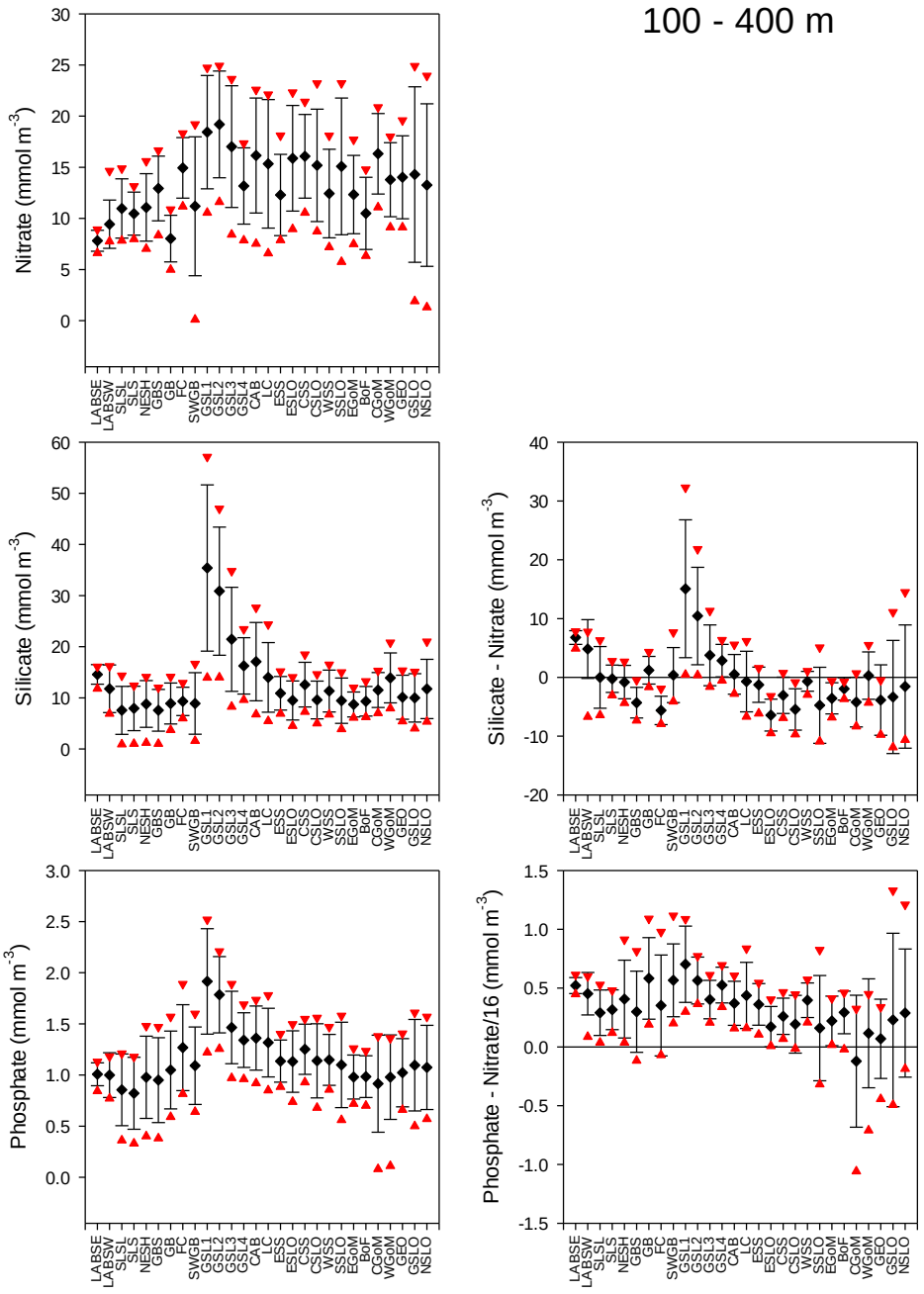

Figure 10-3 Descriptive statistics (overall mean, black symbol; standard deviation, black lines; 10th and 90th percentiles, red triangles) of nitrate concentrations in the lower (100 – 400 m) water column all the observations for all geographic areas.

The declines in nitrate concentration in the eastern and western Labrador Sea have been more pronounced in the lower layer (100 – 400 m) and somewhat less pronounced on the eastern (ESS) and central Scotian Shelf (CSS) (Fig. 10-5). Although the overall long term trend in areas within the Gulf of St. Lawrence indicated a general increase in nitrate concentrations relative to the early-1970s, we note that increasing short term trends in nitrate concentration in the lower

layer occurred only in the northeastern (GSL3) and southern Gulf of St. Lawrence (r_s = 0.46 and 0.51, respectively).

The availability of nitrate data on the Newfoundland Shelf and adjacent areas was limited until the 1990s whereas data provided good coverage of the Gulf of St. Lawrence, Scotian Shelf, and Gulf of Maine back to the 1970s (Figs. 10-4 and 10-5). Nitrate concentrations were well below average on the Scotian Shelf and Gulf of Maine in the early 1970s, whereas they were well above average during the second half of the decade and into the early 1980s. Nitrate levels in the Gulf of St. Lawrence have shown a trend toward increased concentrations, particularly in the deep layer, throughout the period for which data are available, but the overall variability around the long term average has been modest and relatively less pronounced than in the areas south of the Laurentian Channel. . There has been limited short term variability on the Newfoundland Shelf and in the Labrador Sea but the overall trend has been toward decreasing nitrate concentrations. The only exception to this occurred on the southern Labrador Shelf where concentrations appear to have increased slightly over the entire length of the time series (r_s = 0.27 in upper layer and 0.11 in lower layer).

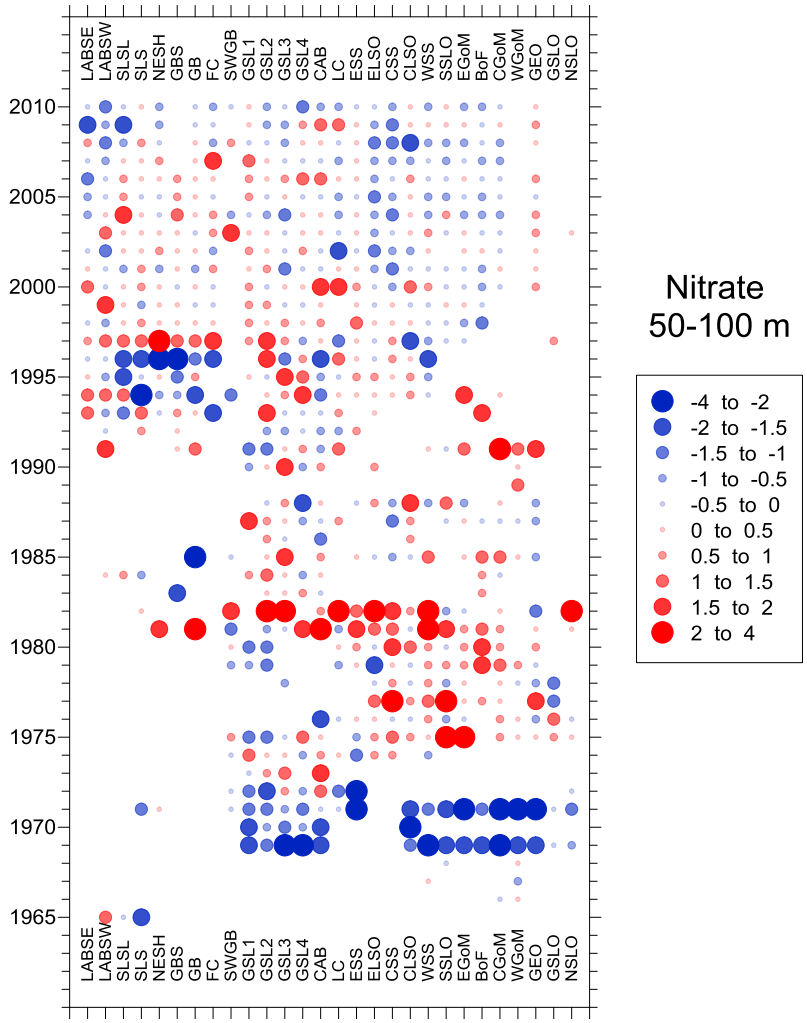

Figure 10-4 Annual standardized anomalies of average regional nitrate concentrations in the upper (50 – 100 m) water column 1965 – 2010. Blue symbols represent values below the long term average for each region; red symbols represent values above the long term average. The size of the symbols reflects the magnitude of the departure of that year's average (in terms of the standard deviation of the time series of annual averages) from the long term average for the region.

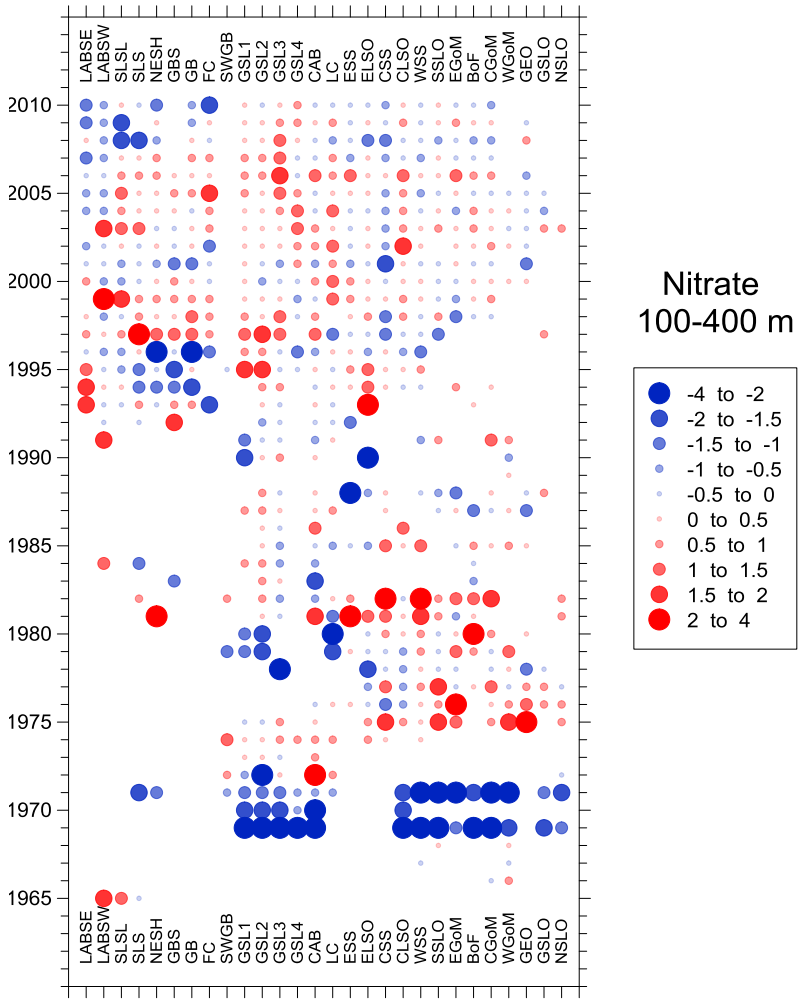

Figure 10-5 Annual standardized anomalies of average regional nitrate concentrations in the lower (100 – 400 m) water column 1965 – 2010. Blue symbols represent values below the long term average for each region; red symbols represent values above the long term average. The size of the symbols reflects the magnitude of the departure of that year's average (in terms of the standard deviation of the time series of annual averages) from the long term average for the region.

Silicate

Average silicate concentrations in the upper layer are generally lower or equal to those of nitrate, with the exception of the St. Lawrence Estuary (GSL1), northwest Gulf (GSL2) and southern Gulf (GSL4), Labrador Sea (LABSW, LABSE), NSO, and NGO, where concentrations are 10 – 70% greater than nitrates and highly variable (Figs. 10-2 and 10-3). Average silicate concentrations are 68% of nitrate concentrations on Georges Bank and 76% of nitrate concentrations on most of the Newfoundland Shelf and adjacent slopes, whereas they are generally above 80% in all other areas. The contrast between silicate and nitrate concentrations in the lower layer is similar to the upper layer in most areas, except in the Gulf of Lawrence (GSL1 – 4) and Cabot Strait (CAB) where average silicate concentrations can be twice those of nitrates (Figs. 10-2 and 10-3). A weak positive gradient in the 50 – 100 m silicate concentration extended from the Cabot Strait to the Gulf of Maine, in contrast to a more pronounced gradient from the southwest Grand Bank to the Labrador Sea. We also noted a strong positive gradient for the deep layer from the Cabot Strait through the Gulf of St. Lawrence into the upper estuary.

Anomaly plots (Figs. 10-6 and 10-7) of silicate concentrations demonstrate similar overall patterns of variation in the upper and lower layers. Considerable variability occurred during the early parts of the time series, and this pattern may be partly the result of a limited number of observations available in a given year and partly caused by differences in the analytical approaches used to estimate nutrient concentrations.

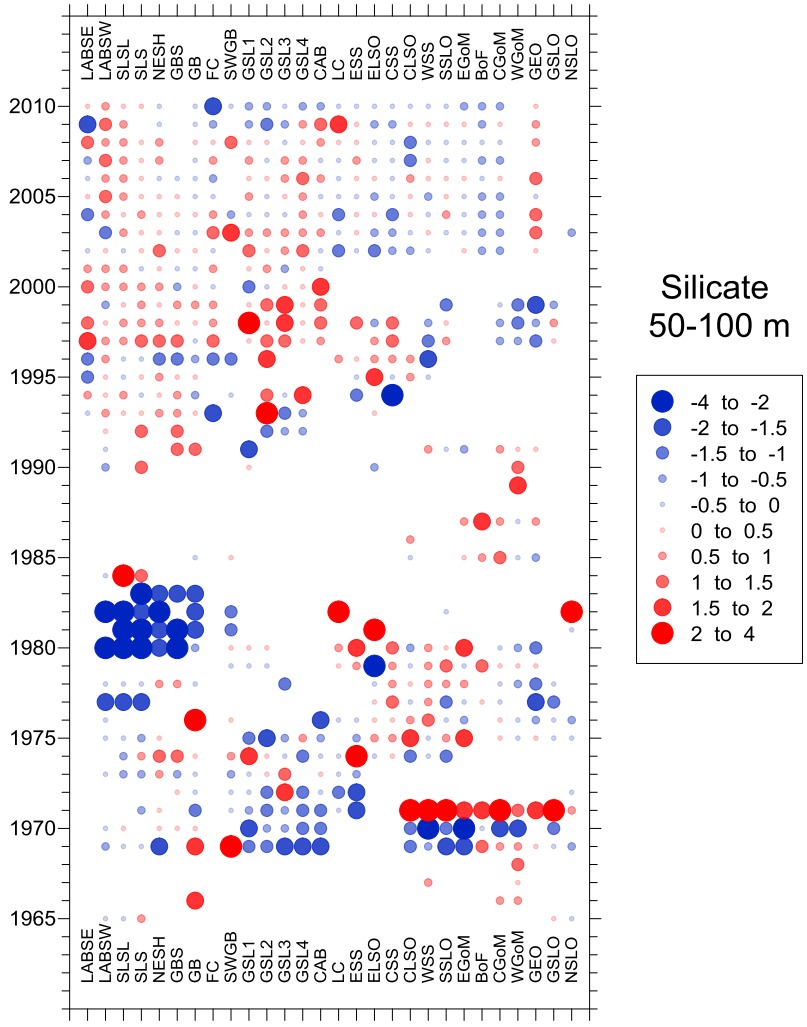

Figure 10-6 Annual standardized anomalies of average regional silicate concentrations in the upper (50 – 100 m) water column 1965 – 2010. Blue symbols represent values below the long term average for each region; red symbols represent values above the long term average. The size of the symbols reflects the magnitude of the departure of that year's average (in terms of the standard deviation of the time series of annual averages) from the long term average for the region.

Areas on the Scotian Shelf had large negative anomalies in silicate concentrations in the early 1970s followed by a period with pronounced and persistent positive anomalies in the latter half of the 1970s; the overall long term trend on the central Scotian Shelf (CSS) points toward a decline in silicate concentrations (r_s = -0.53) whereas the eastern Scotian Shelf (ESS) showed an increase (r_s = 0.39). Silicate concentrations were below normal in the Gulf of St. Lawrence in the early 1970s but the trend after that was toward a general increase in concentrations until the early to mid-1990s, particularly in the upper layer, after which the short term fluctuations are highly variable among different parts of the Gulf. There were substantial negative anomalies across the Newfoundland Shelf in the early 1980s but we have to question the reliability of the data

available for this period. Even with the exclusion of the observations from 1980 − 1984, positive anomalies in silicate concentrations have dominated in areas off Newfoundland during the 1990s. Notable positive short term trends occurred in the western Labrador Sea (LABSW; r_s = 0.64 in upper layer and 0.74 in lower layer) and Labrador slope (SLSL; r_s = 0.43, lower layer). There has also been a short term trend toward increasing silicate concentrations in both upper and lower layers on the eastern Scotian Shelf (ESS; r_s =0.37 and 0.33) but the trends on the central (CSS) and western (WSS) Scotian Shelf have been weak. Negative or near average anomalies were frequent on the Gulf of Maine during the 1990s and 2000s and indicative of lower concentrations than in the 1970s. Interannual variations have been relatively small throughout the Northwest Atlantic basin since the start of the AZMP. Most anomalies are less than ±1 standard deviation, with the most recent observations (2008 − 2010) below the long term average for most areas.

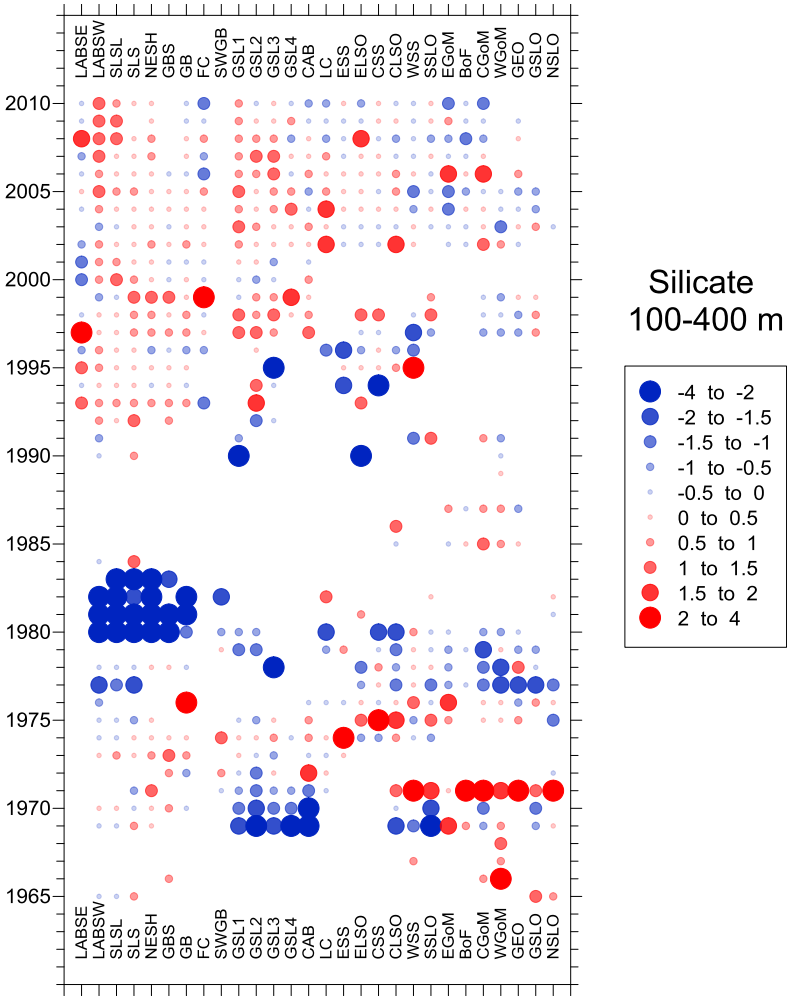

Figure 10-7 Annual standardized anomalies of average regional silicate concentrations in the lower (100 – 400 m) water column 1965 – 2010. Blue symbols represent values below the long term average for each region; red symbols represent values above the long term average. The size of the symbols reflects the magnitude of the departure of that year's average (in terms of the standard deviation of the time series of annual averages) from the long term average for the region

Phosphate

Regional variations in average phosphate concentrations demonstrated some similarities with those of nitrate and silicate but also some distinctions (Figs. 10-2 and 10-3). Phosphate levels in the upper layer (50 – 100 m) of the Labrador Sea and adjacent shelves were similar although variability increased from north to south. Phosphate concentrations were higher throughout most of the Gulf of St. Lawrence than in other parts of the Atlantic Basin, with the exception of the northern Gulf (GSL3), but the relative difference was less than for silicate. Phosphate concentrations on the eastern Scotian Shelf were similar to those off Newfoundland and average concentrations declined progressively toward the Gulf of Maine. Variations in phosphate concentrations in the lower layer (100 – 400 m) were more pronounced than in the upper layer. Average concentrations increased slightly from north to south along the Newfoundland Shelf. The highest concentrations were found in the St. Lawrence Estuary, approximately twice those found in the Labrador Sea, and they declined toward the Cabot Strait and the eastern Scotian Shelf, beyond which concentrations continued a moderate decline toward the Gulf of Maine. Southern slope waters (NSLO, GSLO) had slightly higher average phosphate concentrations relative to Georges Bank and the Gulf of Maine.

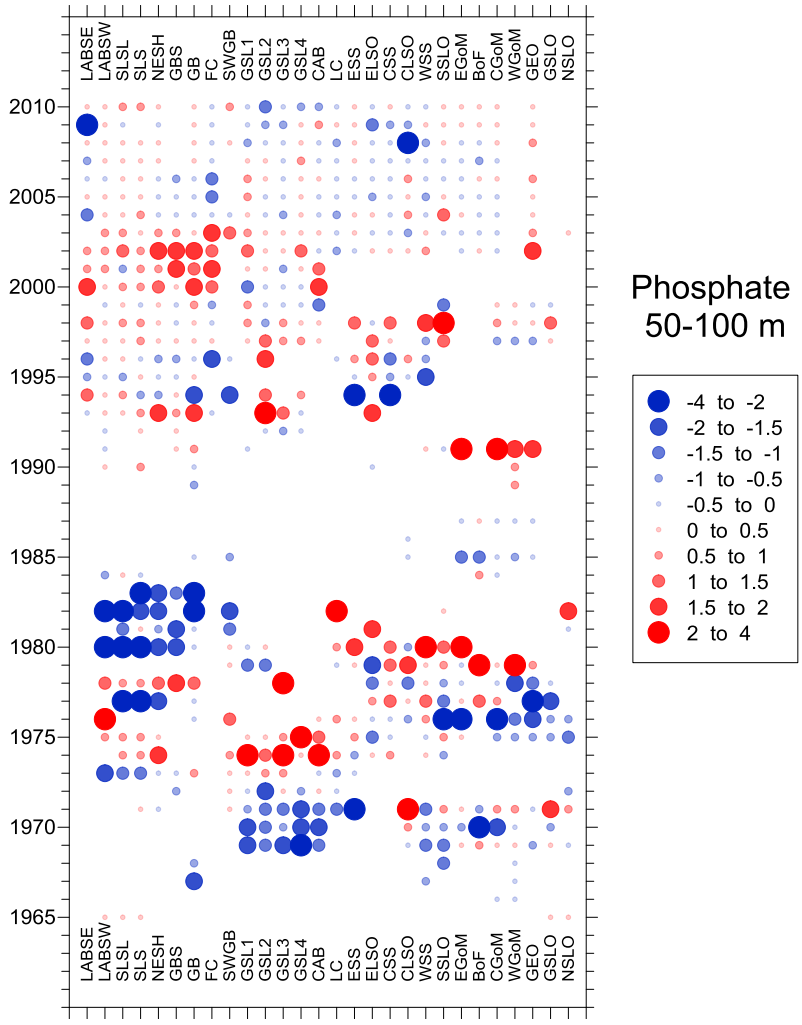

Figure 10-8 Annual standardized anomalies of average regional phosphate concentrations in the upper (50 – 100 m) water column 1965 – 2010. Blue symbols represent values below the long term average for each region; red symbols represent values above the long term average. The size of the symbols reflects the magnitude of the departure of that year's average (in terms of the standard deviation of the time series of annual averages) from the long term average for the region.

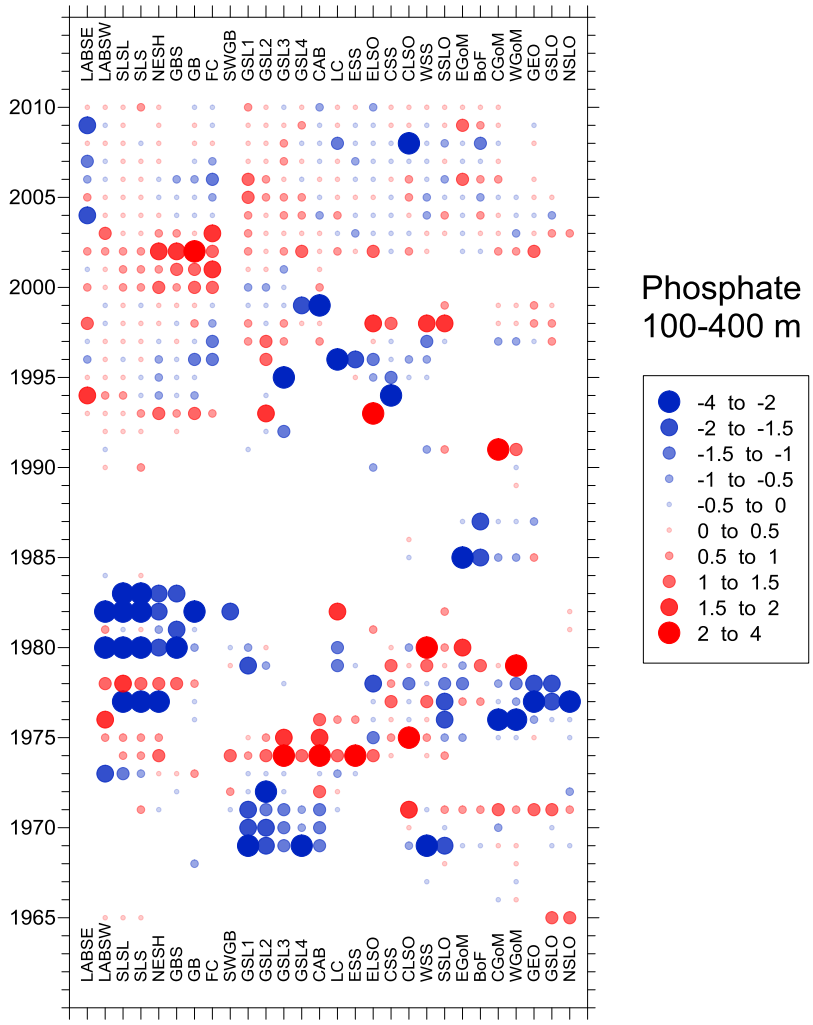

Figure 10-9 Annual standardized anomalies of average regional phosphate concentrations in the lower (100 – 400 m) water column 1965 – 2010. Blue symbols represent values below the long term average for each region; red symbols represent values above the long term average. The size of the symbols reflects the magnitude of the departure of that year's average (in terms of the standard deviation of the time series of annual averages) from the long term average for the region.

Most of the time series extend back to 1965, with notable gaps in the late-1960s and early-1970s and in much of the 1980s for most areas (Figs 10-8 and 10-9). Patterns of variation in phosphate concentrations have been dominated by relatively short term variations (decadal and shorter) and are similar in both the upper and lower layers. There has been a general decline in phosphate concentrations in both the upper and lower layers in the eastern Labrador Sea (LABSE; r_s = -0.29) since 1993 but this has not been matched in the western Labrador Sea (LABSW). Areas off Newfoundland (SLS, SLSL, NESH, GB, GBS) had large negative anomalies between 1977 and 1983, with short term fluctuations from negative to positive anomalies starting in the mid-1990s until present. The Gulf of St. Lawrence was characterized by large negative anomalies in the early 1970s followed by high positive anomalies in 1974-1975. There has been a general decline in concentrations from the early 1990s to the present in the upper layer of GSL1 – 4 (r_s = -0.09 to -0.55) but concentrations have shown a small increase in the lower layer of all four areas recently. As in the Gulf of St. Lawrence, phosphate concentrations on the Scotian Shelf were low in the early 1970s, increased until 1980, were at low levels in the early 1990s, with a sharp increase in 1997 but have remained just below the long term average since 2000. Recent trends have shown increases in the upper layer on the eastern and central Scotian Shelf (ESS; r_s = 0.31, CSS; r_s =

0.30) and in the deep layer on the central and western Shelf (CSS; r_s = 0.54, and WSS; r_s = 0.26). Conditions in the Bay of Fundy/Gulf of Maine areas were similar to those on the Scotian Shelf throughout the 1970s; positive anomalies persisted into the late 1980s and conditions have been near the long term average throughout much of the most recent decade.

Variations in excess nutrient ([Si – N] (Figs. 10-10 and 10-11), [P – (N/16)] (Figs. 10-12 and 10-13) are dominated by short term (< decadal) clusters in the anomalies but generally demonstrate similarities between the two layers. There were major gaps in the time series, with almost no information prior to 1990 off Newfoundland, few data throughout the 1980s, and very limited information prior to 1970.

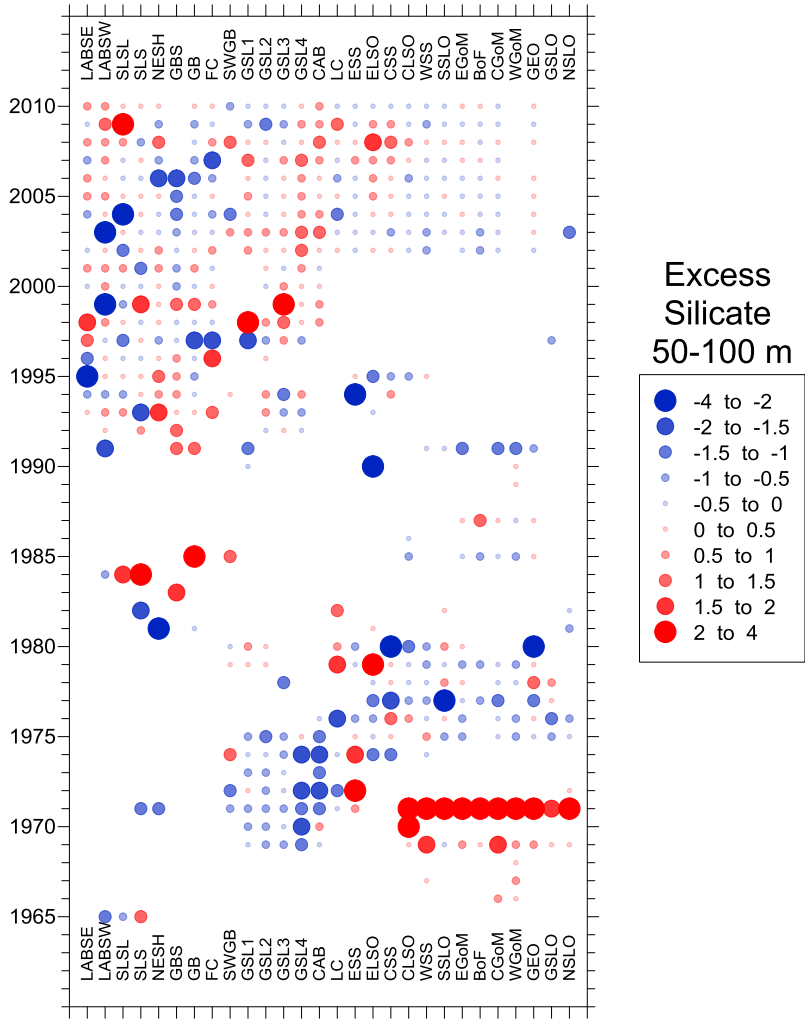

Figure 10-10 Annual standardized anomalies of average regional excess silicate concentrations (Si – N) in the upper (50 – 100 m) water column 1965 – 2010. Blue symbols represent values below the long term average for each region; red symbols represent values above the long term average. The size of the symbols reflects the magnitude of the departure of that year's average (in terms of the standard deviation of the time series of annual averages) from the long term average for the region.

Silicate concentrations in waters of the eastern (LABSE) and western Labrador Sea (LABSW) have nearly always been in excess of the Redfield ratio relative to nitrogen (N:Si = 1:1) but the southern Labrador Shelf Slope waters (SLSL) have demonstrated states in which silicate concentrations have been above (excess; N<Si) and below (depletion, N>Si) the Redfield ratio (Figs. 10-2 and 10-3). Since 2005, excess silicate levels have been increasing in the Labrador

Sea (LABSW, LABSE) whereas the high anomalies on the Labrador Slope (SLSL) indicate that silicate concentrations exceed the Redfield ratio whereas prior to that time we note a high occurrence of silicate depletion (i.e. below the Redfield ratio). There is considerable year-to-year variability in the signal for this region, likely indicative of the influence of short term variations in sea ice melt or Arctic water inflow. In contrast, positive anomalies of excess silicate were more frequent on the Grand Bank (GB, GBS) and adjacent areas prior to 2000, after which silicate appears to be more consistently depleted. High excess phosphate concentrations were apparent throughout the region during 2000 – 2002, with the strongest and most persistent signal on the Newfoundland Shelf (NESH, GB, GBS, and FC). There is evidence of more positive anomalies in 2008 – 2010 in the western Labrador Sea, but these are not apparent on either the Labrador or Newfoundland continental shelves.

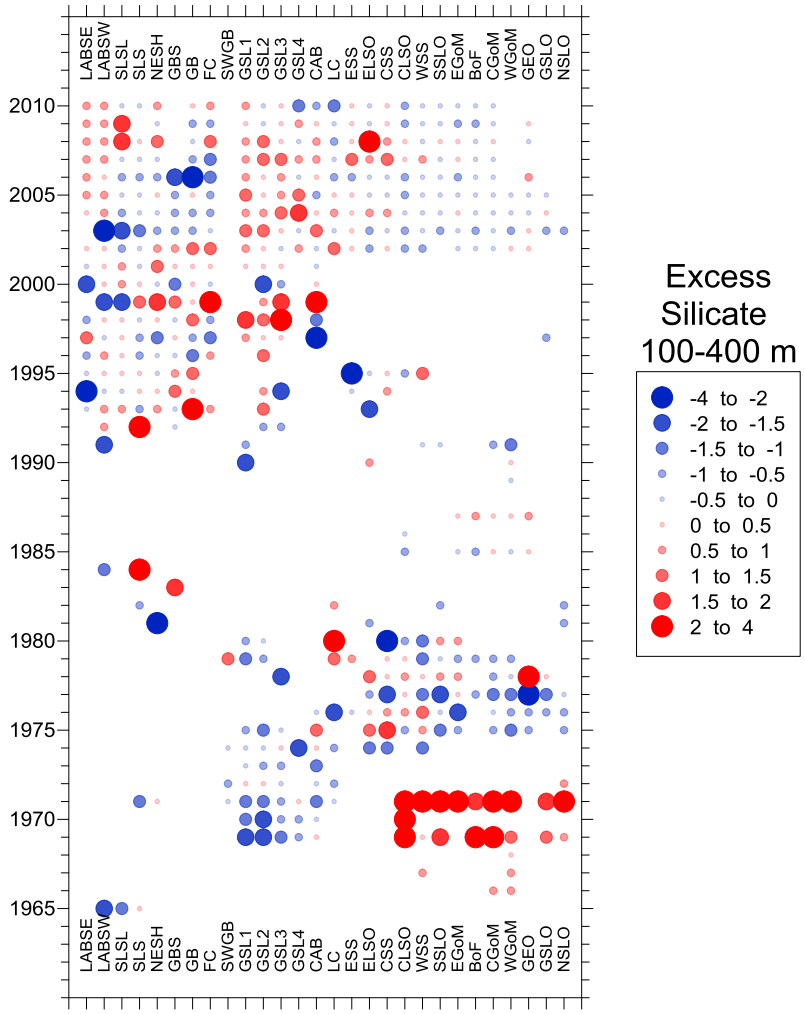

Figure 10-11 Annual standardized anomalies of average regional excess silicate concentrations (Si – N) in the lower (100 – 400 m) water column 1965 – 2010. Blue symbols represent values below the long term average for each region; red symbols represent values above the long term average. The size of the symbols reflects the magnitude of the departure of that year's average (in terms of the standard deviation of the time series of annual averages) from the long term average for the region.

In the Gulf of St. Lawrence, negative anomalies in the excess levels of silicate were predominant in the 1970s whereas the 1990s and 2000s have seen generally above average concentrations of excess silicate. Excess phosphate anomaly values generally did not exhibit the long term trends

apparent for silicate except in the Estuary where the patterns were consistent between variables. Fluctuations from low levels of excess phosphate in the early 1970s to high levels in the mid-1970s were apparent throughout much of the Gulf of St. Lawrence with no clear pattern of variation from the 1990s onward.

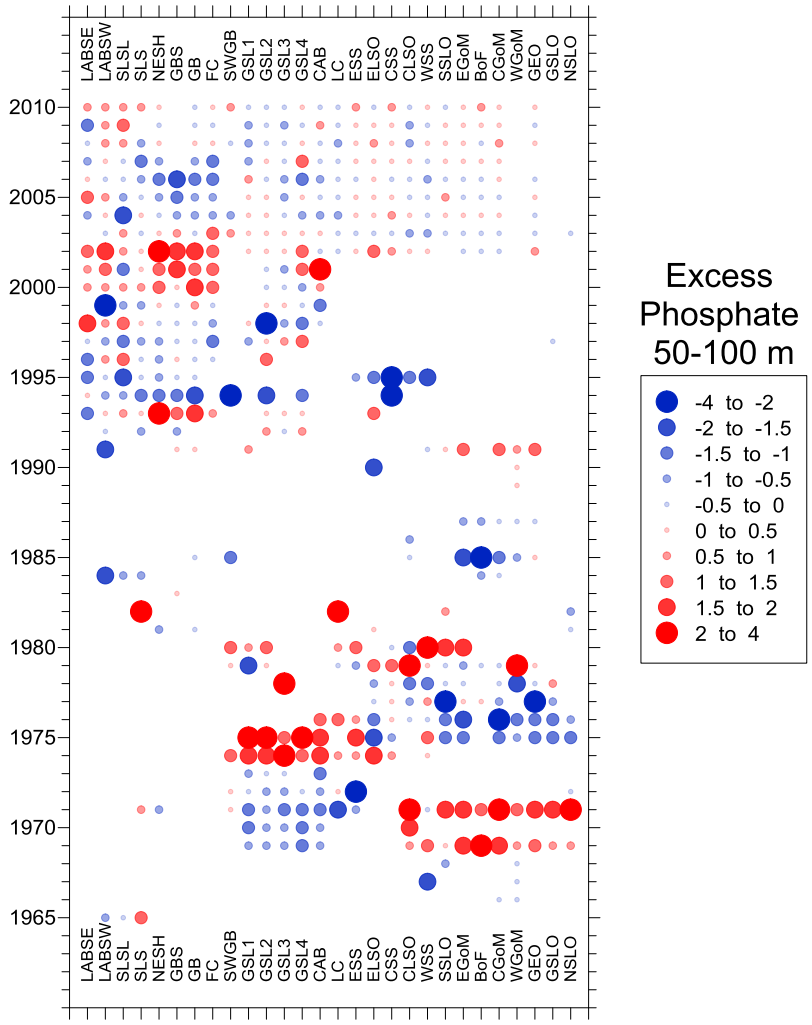

Figure 10-12 Annual standardized anomalies of average regional excess phosphate concentrations (P – N/16) in the upper (50 – 100 m) water column 1965 – 2010. Blue symbols represent values below the long term average for each region; red symbols represent values above the long term average. The size of the symbols reflects the magnitude of the departure of that year's average (in terms of the standard deviation of the time series of annual averages) from the long term average for the region.

Data for the Scotian Shelf and Gulf of Maine proved to have significant gaps that limited our ability to identify long term patterns of variation. There appears to have been greater overall levels of variability in excess nutrient concentrations in the 1970s than in more recent times. We note a high occurrence of high levels of excess silicate and phosphate concentrations in the late-1960s, and considerable spatial variability of positive and negative anomalies during the late-1970s from the eastern Scotian Shelf to Georges Bank. There has been very little variability in excess nutrient concentrations between 2000 and 2010, although significant positive anomalies occurred in the areas of the eastern and central Scotian Shelf in 2007 – 2008.

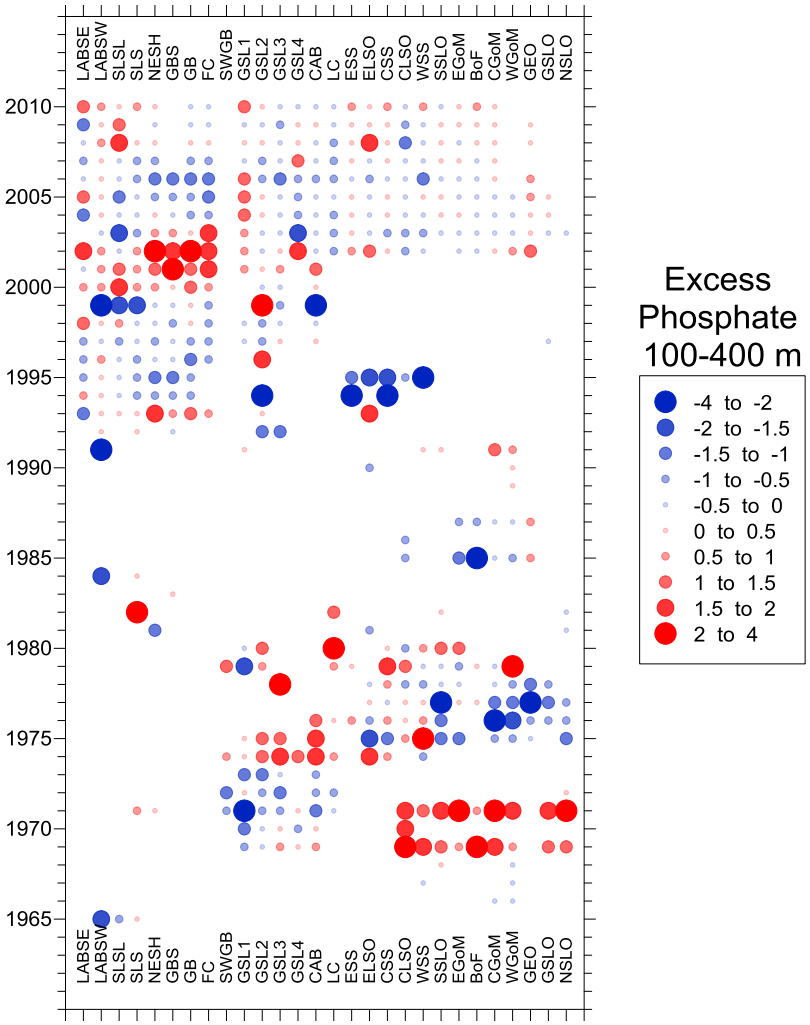

Figure 10-13 Annual standardized anomalies of average regional excess phosphate concentrations (P –N/16) in the lower (100 – 400 m) water column 1965 – 2010. Blue symbols represent values below the long term average for each region; red symbols represent values above the long term average. The size of the symbols reflects the magnitude of the departure of that year's average (in terms of the standard deviation of the time series of annual averages) from the long term average for the region.

10.4 Discussion

The approach applied in this assessment of the patterns of variations of nutrient concentrations since the mid-1960s has been constrained by the short term requirements of the Department in developing the Risk Assessment for the Climate Change Adaptation Program. Exclusion of data from the surface layer resulted in the reduction of more than 50% of the observations gathered from various data sources, because a large proportion of nutrient collections have been linked to studies of phytoplankton dynamics. A more comprehensive approach might have derived regional monthly or seasonal climatological average vertical profiles, possibly linked to harmonic analyses of seasonal cycles, from which anomalies could have been derived. In all likelihood, such an approach would have been possible only in a limited portion of the Northwest Atlantic because the density of observations would have been insufficient for numerically demanding statistical methods. This would also have been limited by the important gap in data that occurred during the 1980s and early 1990s throughout much of the basin. Consequently, we

consider that our assessment provides a consistent approach that is applicable to a broad geographic region that most likely highlights the major patterns of variation over time.

Long term variations in nutrient concentrations can be categorized based on three broad regions: Newfoundland Shelf/ Labrador Sea (NSLS), Gulf of St. Lawrence (GSL), and Scotian Shelf/Gulf of Maine (SSGoM). There are spatial differences within regions that will be addressed when noteworthy. The NSLS is directly influenced by Arctic outflow coming from the Denmark, Davis and Hudson Straits, whereas outflow from the St. Lawrence River and deep inflow through Cabot Strait are the primary influence on the GSL, and the SSGoM is influenced indirectly by both the Labrador Current and the outflow from the GSL as well as by intrusions of Slope water and Gulf Stream meanders. The different influences were reflected in the overall variability and in the trends identified in each region.

To extract the essential trends in the data, for whatever period was available for the different regions, we performed a principal component analysis of the long term trends in nutrient concentration anomalies based on the Spearman rank correlation values from the upper and lower layers for nitrate, silicate and phosphate. We chose to carry out this procedure because of the high degree of variability in the patterns of variation among regions and macro-nutrients. The first two principal components explained 47% (PC1) and 27% (PC2) of the variance in correlations. All nutrients, in both upper and lower layers, loaded negatively on PC1 (Fig. 10-14). Trends in nitrate and phosphate had negative loadings on PC2 whereas trends in silicate loaded positively. Overall, the trends in nitrate/phosphate versus silicate were nearly orthogonal.

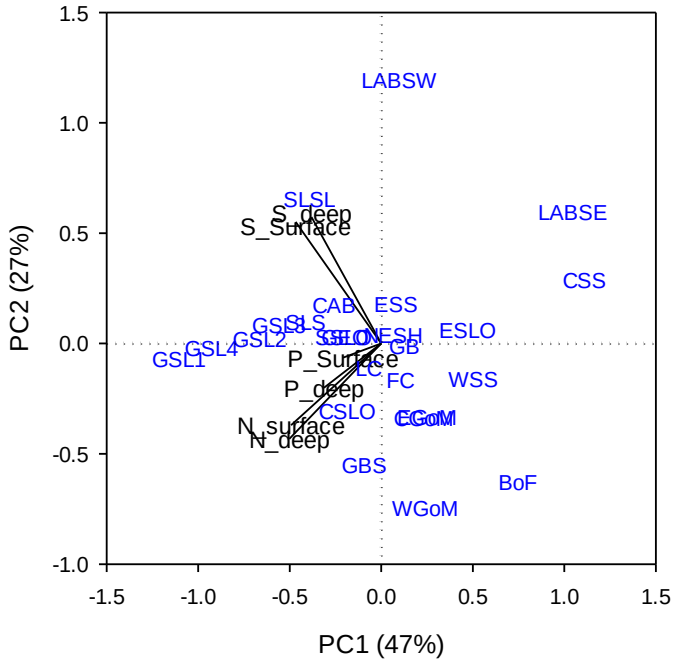

Figure 10-14 Loading of long term trends, based on Spearman rank correlations, of anomalies in nitrate (N), silicate (S), and phosphate (P) concentrations from upper (surface) and lower (deep) layers in relation to the first (PC1) and second (PC2) principal component.

The central Scotian Shelf and eastern Labrador Sea, which had declining trends in all nutrient concentrations, were at positive extreme of PC1 whereas regions of the Gulf of St. Lawrence, in which we note substantial increases in nutrient concentrations since the early 1970s, tended to

have negative loadings on PC1. Because most regions demonstrated variations among nutrients in their overall long term trends, their loading on PC1 tended to be small relative to the extremes. The western Labrador Sea, which has seen an increase in silicate concentrations but a decline in nitrate levels, loaded positively on PC2 whereas areas in the Gulf of Maine and the Bay of Fundy, which have seen declines in silicate concentrations with increases in either nitrate and phosphate concentrations, loaded negatively on PC2.

There are few nitrate data in the NSLS region prior to 1990. The available observations indicate high concentrations in the 1980s and in 1997, but overall, concentrations have been relatively stable throughout the region, with the exception of the AR7W line (LABSW, LABSE) where there appears to have been a decline in nitrate concentration over the last two decades.

The availability of nutrient data in the NSLS region was unbalanced, with few nitrate data prior to 1990, whereas there appear to have been more data detailing silicate and phosphate concentrations during 1965-1985. It should be noted, however, that the high occurrence of extremely low silicate and phosphate concentrations during this period ($\leq$ 3 s.d. from long-term average for each area) raises concerns about the overall accuracy of these observations and suggests that we should discount their influence on the assessment of long term trends. Overall, it is difficult to identify a persistent long term trend in this region. There appears to have been a consistent decline in nutrient concentrations in the Labrador Sea, as noted in previous analyses (Harrison and Li, 2007; Yeats *et al.*, 2010), but otherwise the patterns of variation suggest that decadal scale fluctuations dominate in these data. The patterns are not necessarily consistent among nutrients and depth layers, with a modest decline in nitrate levels, a period of high silicate concentrations in the late 1990s which was followed by a period of elevated phosphate levels in the early 2000s, indicative of the influence of different water masses on the region.

It is important to note that we have found some significant departures from the conclusions of Harrison and Li (2007) and Yeats *et al.* (2010) who each noted a decline in the amounts of excess silicate and phosphate on the Labrador Shelf and in other parts of the basin. The results reported here did not find significant declines in these variables, although we did note declines in nitrate and silicate concentrations in the eastern Labrador Sea but an increase in silicate levels in the western Labrador Sea. We note that Yeats *et al.* (2010) set a threshold depth of 60 m in their analysis of surface waters whereas we chose 50 m, which could have resulted in greater influence of nutrient depletion by phytoplankton, but the anomalies are generally similar in the deeper layer. The results are therefore puzzling and will require further investigation as to how the additional data collected in this study could have yielded such different conclusions when we were able to achieve results similar to those of Yeats *et al.* (2010) for the central Scotian Shelf. Most observations of nitrate:phosphate levels, however, appear to be within the expected range based on Jones *et al.*'s (1998) definition of "pure" Atlantic and Pacific waters (Fig. 10-15). The potential for methodological or collection biases may not be insignificant, which warrants further consideration.

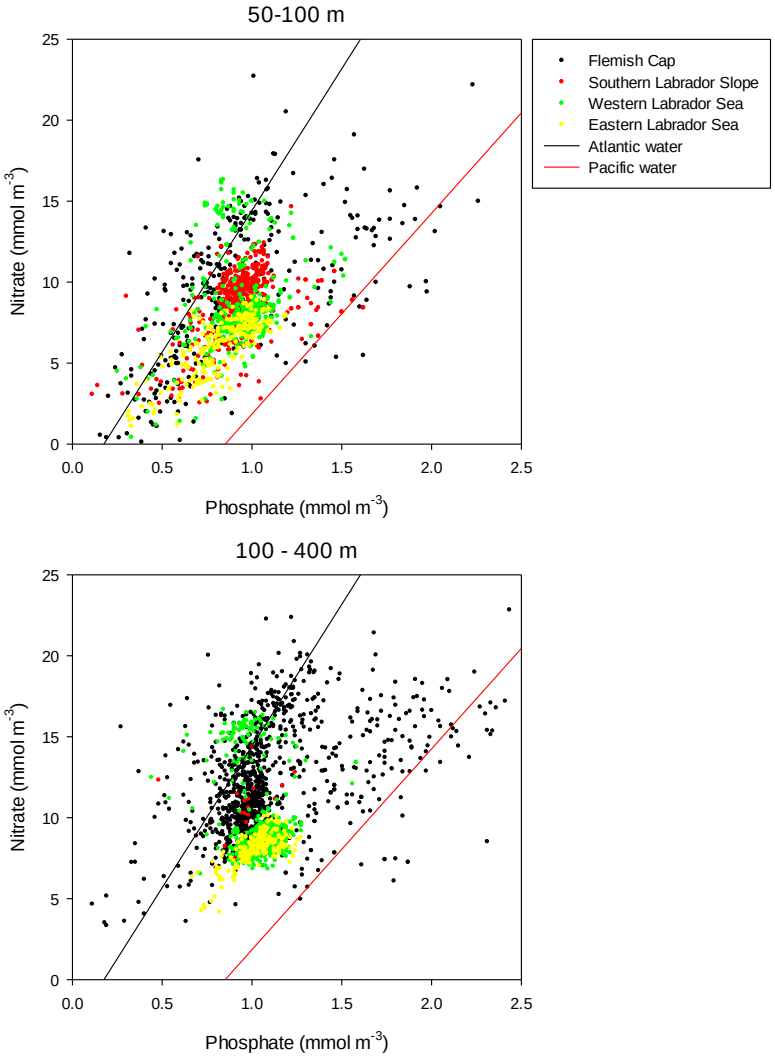

Figure 10-15 Nitrate-to-phosphate relationship for data from the upper (50 – 100 m) and lower (100 – 400 m) layers in the Eastern (E Lab Sea) and Western (W Lab Sea) Labrador Sea as well as the Labrador Shelf (SLS) and Flemish Cap (FC) areas. The black and red lines represent the nitrate-to-phosphate relation-ships of "pure" Atlantic and Pacific source waters described by Jones *et al.* (1998).

Changes in absolute and relative nutrient concentrations could affect phytoplankton community structure and regional productivity, as Harrison and Li (2007) note the occurrence of both nitrate and silicate limitation in different parts of the Labrador Sea. Nitrogen limitation appears to be confined to the Labrador Shelf whereas silicate limitation occurs throughout the region but more likely in the central basin (Harrison and Li, 2007). Higher phosphate levels, which might result from greater influx of modified Pacific waters through Arctic outflow, could also favour increased production by cyanobacteria, which would result in greater nitrogen fixation in the Labrador Sea (Yamamoto-Kawai *et al.*, 2006). We note, however, that our analysis has not found strong evidence of long term or decade long changes in nutrient concentrations that are consistent with those expected with increased outflow of Arctic waters of Pacific origin. Increases in phosphate concentrations have generally lasted only a few years, which may be suggestive of pulsed influx of such water masses but are not indicative of a steady change during the last twenty years.

The Gulf of St. Lawrence has been affected by inputs from large urban and agricultural areas located around the Great Lakes and along tributaries of the St. Lawrence River. Nitrate

concentrations revealed decadal scale patterns of variations, with periods of highs and lows alternating depending on the specific area of the Gulf being considered, with a relatively persistent decline to values below the long term average in the upper layer (50 – 100 m) since the mid-1990s and a general increase in the long term average for the lower layer (100 – bottom) for all three macro-nutrients. A substantial data gap throughout most of the 1980s for silicate and phosphate contributes to some uncertainty about the trend, but the broad differences appear to be robust and based on accurate information. The consistent increasing trend in the deep layer for both short and longer time scales is most likely the result of increased remineralisation of organic matter at the bottom as a result of an increase in bottom water temperature (Genovesi *et al.*, 2011). In addition to these factors, changes in upstream river flow (Galbraith *et al.*, 2012) and pumping of nutrients into the upper layer from the Laurentian Channel head will likely affect nutrient concentrations in this region. It is unclear at present how these factors may be contributing to the long term and future trends identified for this region. We can be assured that population density upstream of the GSL will continue to increase during the coming decades, so we can expect some increase in the input of nutrients associated with societal needs, although how these may be moderated through increased use of sewage treatment facilities needs to be explored. Atmosphere-Ocean General Circulation Models (AOGCMs) and Regional Climate Models (RCMs) indicate a more substantial increase in precipitation in northern Canada relative to the southern portions of the country that drain into the GSL. Greater runoff would increase the flux of nutrient from rivers, and increase stratification as well, which would in turn reduce nutrient pumping from deep water. The net effect on regional productivity would depend on the concentration of nutrients in fresh versus ocean waters.

Despite a notable contrast in nutrient concentrations on the Scotian Shelf during the 1970s and 1980s relative to the most recent decade, we have noted limited variability in nitrate, silicate or phosphate levels during the last two decades. Recently, concentrations of all nutrients have generally been below average but the low level of variability in an area that is influenced by many current systems is somewhat puzzling particularly in the light of recent increased variability in integrated ocean temperature (Hebert *et al.*, 2012). Furthermore, despite a significant influence of outflow from the Gulf of St. Lawrence to water mass characteristics on the Scotian Shelf, we found limited evidence of significant export of high nitrate and silicate concentrations from that source. Warmer water masses to the south and east of the region tend to have similar or lower nitrate and silicate concentrations to those on the adjacent shelf areas although we note that average silicate and phosphate concentrations in warm slope waters tend to be slightly lower than on the shelf whereas the opposite is true for nitrate (Figs. 10-2 and 10-3).

When coupled with the uncertainty in predicting future changes in regional circulation patterns based on AOGCMs, the most optimistic short and long term expectations of nutrient concentrations are that conditions may remain in the current “below average” state or that nutrient availability may decline, depending on the influx from the deep basin and the influx of water from the Labrador Current. GCMs simulations of historical nitrate levels are generally consistent with the trends presented in this report (from 3 or 4 models out of 5, Lavoie *et al.*, 2013). Future model trends (next 50 years) indicate a general decrease in both the upper and lower layers for the Atlantic Northwest region, although there are spatial differences in the degree and direction of change. The multi-model ensemble averages range between -0.4 to -1 mmol N m^{-3} over the next 50 years.

Analytical issues

Data were insufficient to comment on possible trends in nutrient concentrations in areas north of the AR7W line, which provides most of the data for the Labrador Sea. This places limits on our ability to infer possible changes in nutrient concentrations caused by alterations in the state of different sources waters coming from the Canadian Archipelago. Ancillary temperature-salinity data could have served to further identify variations in water masses, but there were insufficient resources at this time to obtain the required data in order to complete those analyses.

Upper and lower layers were limited to data from 50 – 100 m and 100 – 400 m, respectively. As noted previously, the 50 m boundary for the upper layer may have resulted in some influence of nutrient depletion by phytoplankton on the perceived patterns of variation in some regions. Similarly, our choice of 400 m as the bottom boundary for the lower layer could have included Oceanic water, which has higher nitrate concentrations than shelf or slope waters, introducing some errors to regional patterns of variation, particularly in slope areas. Patterns of variations of nutrient anomalies in upper and lower layers were generally positively correlated for all macro-nutrients for all regions where there were >10 observations for both depth strata (Fig. 10-16). There was a very strong inverse relationship of the anomalies in phosphate concentrations in the upper and lower layers on the eastern Scotian Shelf based on Pearson correlation coefficient (r = -0.68). Weak (r < 0.4) relationships in nitrate anomalies between layers were also apparent for the Laurentian Channel, the southern Gulf of St. Lawrence, the slope waters off the eastern Scotian Shelf and Georges Bank. In the case of silicate anomalies, weak or inverse relationships were apparent in the eastern Labrador Sea, Laurentian Channel, and eastern Gulf of Maine. Based on the generally positive relationships in anomalies between depth strata, we suggest that the potential uncertainty in the overall trends in macro-nutrient concentrations caused by either depletion or vertical transport was probably minimal for most of the western Atlantic basin.

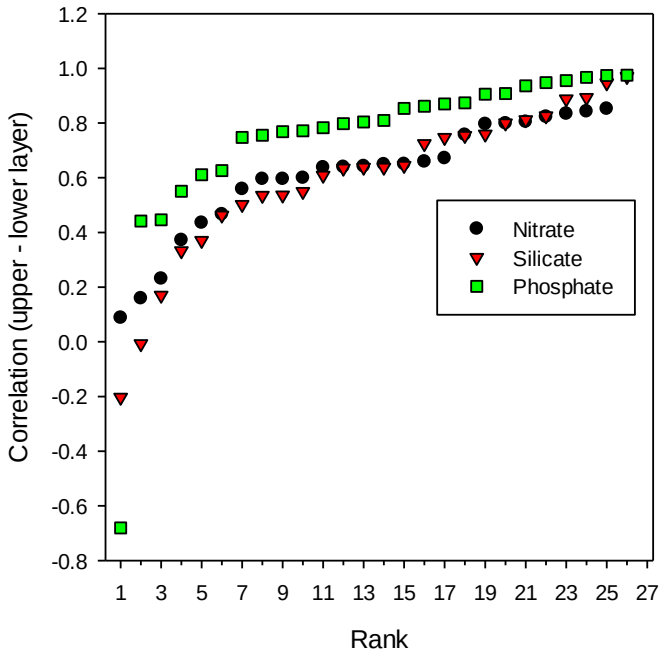

Figure 10-16 Cumulative rank order of Pearson correlation coefficient values between macro-nutrient anomalies in the upper (50 – 100 m) and lower (100 – 400 m) layers from the 26 regions considered in this analysis (1965 – 2010). The information illustrates how in the majority of instances, variations in the concentration of each nutrient in the upper and lower layers are correlated. Significance levels are not provided because the number of observations varied among regions. The median numbers of observations for nitrate, silicate and phosphate anomalies were 27, 23, and 22 respectively.

As we indicated previously, it is important to note that we have found some significant departures from the conclusions of Harrison and Li (2007) and Yeats *et al.* (2010) who each noted a decline in the amounts of excess silicate and phosphate on the Labrador Shelf. Data for both these studies were derived from a seasonally consistent observation program along the AR7W line across the Labrador Sea. The data considered in our analysis included additional data collected as part of the Atlantic Zone Monitoring Program but from a different time of year (mostly late July). Although we did not identify strong seasonal signals in the data for each depth strata, subtle seasonal differences may have contributed to the dissimilarities among the studies, particularly in a case where inferences were based on relatively few sampling locations within the polygons used in our analysis. Subtle seasonal signals, particularly when confounded with differences in the number of years from different data sources, present a significant obstacle in the identification of long term trends based on average annual anomalies when the magnitude of variation in the latter is considerably less than the inherent variability found in the original observations. Spatial patterns of variation within regions also add to the uncertainty.

The analytical difficulties faced in this assessment could have been reduced considerably had the collection of comprehensive observations from consistent long term monitoring programs been undertaken earlier, as soon as Fisheries and Oceans Canada, its predecessors and collaborative agencies were mandated by Canadians to provide stewardship of the Oceans surrounding Canada. The concentrations and flux of macro-nutrients represent key components of marine ecosystems that determine the overall production potential, and thereby fishery yields, in each region and sub-basin. Uncertainties in seasonal and inter-annual variations caused by limited or inconsistent observation programs weaken our ability to infer or project the magnitude or constancy of trends that may be occurring in a changing environment. The requirements and objectives of the Aquatic Climate Change Adaptation Services Program point to the necessity for continued and comprehensive observation programs throughout the Atlantic basin, as well as other ocean and freshwater basins, in order to provide the Department with sound advice about current and anticipated changes in aquatic ecosystems.

Despite some potential limitations that may have affected some inferences derived from our analyses, we reiterate that our assessment provides a consistent approach that is applicable to a broad geographic region that most likely highlights the major patterns of variation over time.

10.5 Acknowledgements

Comments from Glen Harrison and Phil Yeats helped clarify some of the issues in the interpretation of our findings. Jennifer Holden provided invaluable technical support in the completion of our analysis.

10.6 References

Galbraith, P. S., J. Chassé, D. Gilbert, P. Larouche, D. Brickman, B. Pettigrew, L. Devine, A. Gosselin, R. G. Pettipas, and C. Lafleur. 2012. Physical oceanographic conditions in the Gulf of St. Lawrence in 2011. Can. Sci. Advis. Sec. Res. Doc. 2012/023, iii + 85 p. http://www.dfo-mpo.gc.ca/Csas-sccs/publications/resdocs-docrech/2012/2012_023-eng.pdf

Genovesi, L., A. deVernal, B. Thidodeau, C. Hillaire-Marcel, A. Mucci, and D. Gilbert. 2011. Recent changes in bottom water oxygenation and temperature in the Gulf of St. Lawrence: Micropaleotological and geochemical evidence. *Limnol. Oceanogr.*, 56,1319-1329.

Harrison W. G., and K.W. Li. 2007. Phytoplankton growth and regulation in the Labrador Sea: Light and nutrient limitation. *J. Northw. Atlant. Fish. Org.* 39, 71-82.

Hebert, D. 2013. Trends in temperature, salinity, and stratification in the upper ocean for different regions of the Atlantic Canadian shelf. Ch. 3 (p. 33-42) *In:* This report.

Hebert, D., R. Pettipas, and B. Petrie. 2012. Meteorological, sea ice and physical oceanographic conditions on the Scotian Shelf and in the Gulf of Maine during 2011. Can. Sci. Advis. Sec. Res. Doc. 2012/055: vi + 43 p. http://www.dfo-mpo.gc.ca/Csas-sccs/publications/resdocs-docrech/2012/2012_055-eng.pdf

Jones, E. P., L. G Anderson, and J. H. Swift. 1998. Distribution of Atlantic and Pacific waters in the upper Arctic Ocean: Implications for circulation. *Geophys. Res. Lett*., 25, 765-768.

Lavoie, D., N. Lambert, S. Ben Mustapha and A. van der Baaren. 2013. Projections of future physical and biogeochemical conditions in the Northwest Atlantic from CMIP5 Global Climate Models. Can. Tech. Rep. Hydrogr. Ocean Sci. 285: xiv + 156 pp. http://www.dfo-mpo.gc.ca/Library/349066.pdf

Yamamoto-Kawai, M., E. Carmack, and F. McLaughlin. 2006. Nitrogen balance and Arctic throughflow. *Nature*, 443, 43.

Yeats, P, S. Ryan, and W. G. Harrison. 2010. Temporal trends in nutrient and oxygen concentrations in the Labrador Sea and on the Scotian Shelf. Atlantic Zone Monitoring Program Bulletin, 9, 23-27. http://www.meds-sdmm.dfo-mpo.gc.ca/isdm-gdsi/azmp-pmza/docs/bulletin_9_05.pdf

10.7 Appendix: Risk Analysis

This section outlines key anticipated impacts, for 10 and 50 year time frames, of the patterns of variation in macro-nutrient concentrations based on past trends in the Atlantic basin. The analysis provides a qualitative assessment of the potential impacts of climate change on ecosystem processes based on expert evaluation of quantitative analysis of past events and forecasted changes in environmental conditions. Impact on the ecosystem identifies the magnitude of change; the probability of occurrence provides a measure of the likelihood of the impact taking place; and uncertainty of the analysis provides a sense of the quality of the information on which the projected impacts are based. L: low; M: moderate; H: high.

Impact from analysis (10 year)	Impact	Proba-bility	Uncer-tainty	Spatial extent
Labrador Sea – decline in phytoplankton-limiting nutrients (silicate, nitrate)	M	H	M	Patterns may differ on shelves vs. deep basin area
Labrador Sea – increased outflow of Pacific water that may enhance nitrogen fixation by cyanobacteria	M	M	M	Impact likely to be greater in western Labrador Sea
Scotian Shelf – decline in phytoplankton-limiting nutrients (silicate, nitrate)	M	M	L	Impact likely greatest on ESS and CSS based on current trends
Gulf of St. Lawrence – changes in nutrient input from Great Lakes and Quebec drainage basin areas. Role of climate change versus other anthropogenic impacts are unclear because of uncertainties in the relative contribution of the two factors in the future	M	H	M	Likely to have greater impact in the northwest and southern Gulf
Combined effects of changes in nutrient concentrations and increased stratification	M	H	M	

Impact from analysis (50 year)	Impact	Proba-bility	Uncer-tainty	Spatial extent
Labrador Sea – decline in phytoplankton-limiting nutrients (silicate, nitrate)	M	H	L	Patterns may differ on shelves vs. deep basin area
Labrador Sea – increased outflow of Pacific water that may enhance nitrogen fixation by cyanobacteria	M	H	M	Impact likely to be greater in western Labrador Sea
Scotian Shelf – decline in phytoplankton-limiting nutrients (silicate, nitrate)	M	M	L	Impact likely greatest on ESS and CSS based on current trends
Gulf of St. Lawrence – changes in nutrient input from Great Lakes and Quebec drainage basin areas. Role of climate change versus other anthropogenic impacts are unclear because of uncertainties in the relative contribution of the two factors in the future	M	H	M	Likely to have greater impact in the northwest and southern Gulf
Combined effects of changes in nutrient concentrations and increased stratification	H	H	L	

11 Projected air temperature changes for Canada from eight NARCCAP model combinations.

John W. Loder [1] *, Zeliang Wang [1], and John Morrison [2]

[1] Fisheries and Oceans Canada, Bedford Institute of Oceanography
P.O. 1006, Dartmouth, Nova Scotia B2Y 4A2

[2] Vynx Design Inc. and Institute of Ocean Sciences
Sidney, British Columbia

*correspondence: John.Loder@dfo-mpo.gc.ca

Suggested Citation:
Loder, J.W., Z. Wang and J. Morrison. 2013. Projected air temperature changes for Canada from eight NARCCAP model combinations. Ch. 11 (p. 151-170) *In:* Aspects of climate change in the Northwest Atlantic off Canada [Loder, J.W., G. Han, P.S. Galbraith, J. Chassé and A. van der Baaren (Eds.)]. Can. Tech. Rep. Fish. Aquat. Sci. 3045: x + 190 p.

Abstract

Projected monthly climate changes in surface air temperature between the tri-decades 1971-2000 and 2041-2070 are examined in an ensemble of eight combinations of Atmosphere-Ocean General Circulation Models (AOGCMs) and Regional Climate Models (RCMs), for the A2 emissions scenario. The model projections were obtained from the North American Regional Climate Change Assessment Program (NARCCAP), and involved three AOGCMs from CMIP3 and six RCMs. The seasonal evolution of the change patterns over Canada are influenced strongly by a broad area of "Arctic amplification" centered over northern Canada in winter and, to a lesser degree, by a mid-latitude continental-interior area of amplified changes in summer. The annual cycle of the changes is examined in ten areas in eastern Canada and five areas elsewhere in Canada. The ensemble-mean changes are positive in all areas and all months, but the spread of the projected changes is generally comparable to the magnitude of the ensemble-mean changes. This points to uncertainty in the projected changes and the need for caution in using the results from particular RCM+AOGCM combinations. Over the Atlantic Large Aquatic Basin, the projected changes are largest in winter, but there is also greater uncertainty in winter, apparently related to deficiencies in the representation of sea ice in the AOGCMs.

11.1 Introduction

Surface air temperature strongly affects atmosphere-ice-ocean-terrestrial interactions as well as human populations. It is an important indicator of anthropogenic climate change because of its inherent relation to warming of Earth's climate system, the relatively large spatial scales of its variability (e.g. compared to precipitation or winds), and its relative ease of measurement. Consequently, surface air temperature is one of the most discussed climate variables in observational and model studies.

Surface air temperature was the lead climate variable discussed in the Global Climate Projections (Meehl *et al.*, 2007) and the Regional Climate Projections (Christensen *et al.*, 2007) chapters of the Fourth Assessment Report (AR4) of the Intergovernmental Panel on Climate Change (IPCC). The projections were primarily based on the ensemble statistics of the Multi-Model Dataset (MMD) arising from Phase 3 of the Climate Model Intercomparison Project (CMIP3) of the Program for Climate Model Diagnosis and Interpretation (PCMDI). It is widely recognized that, with their typical horizontal resolution of 2-4° (Randall *et al.*, 2007), the Atmosphere-Ocean General Circulation models (AOGCMs) used in CMIP3 were not able to resolve the influences of land-ocean boundaries, mountains and lakes, and atmospheric phenomena on scales of a couple of hundred km and less. Consequently, there has been substantial ongoing activity in the climate science community in the area of "downscaling" of climate change projections from AOGCMs. In particular, there has been a major effort in the development and use of Regional Climate Models (RCMs) to dynamically downscale the projections of AOGCMs, with the largest set of currently-available results coming from the downscaling of CMIP3 models.

For North America, the largest downscaling activity has been carried out by the North American Regional Climate Change Assessment Program (NARCCAP; Mearns *et al.*, 2009, 2012, 2013; http://www.earthsystemgrid.org/project/NARCCAP.html). NARCCAP is a collaborative effort by multiple institutions. Using six different RCMs, the project aimed to systematically downscale projections from four different CMIP3 AOGCMs for the A2 emissions scenario (Nakićenović *et al.*, 2000). With the model-ensemble results of the projections phase of NARCCAP only recently starting to become available (e.g. Bukovsky, 2012; Mearns *et al.*, 2012, 2013; de Elía *et al.*, 2013; Di Luca *et al.*, 2013), it is timely that they be given some consideration in the development of projections for the ACCASP Large Aquatic Basin (LAB) assessments and adaptation work. It will be some time before a comparable ensemble of RCM+AOGCM projections will be available from the models being used in the IPCC's Fifth Assessment Report (AR5). Most of the RCM projections used in Canadian climate change and impacts assessments in recent years have come from CMIP3 AOGCMs, generally using only one or two AOGCMs (e.g. CCCSN http://www.cccsn.ec.gc.ca/?page=main; OURANOS http://www.ouranos.ca/en/; PCIC http://www.pacificclimate.org/resources/publications; Long *et al.*, 2009; Guo *et al.*, 2013).

It should be cautioned that, in addition to not using the latest AOGCM projections, the projections from RCM+AOGCM downscaling have limitations. In particular, the RCMs used in NARCCAP do not have active ice or ocean components, which implies that their representation of ice and ocean influences in the coupled climate system is not much better than in the AOGCMs used to force them. In addition, the NARCCAP simulations do not involve "bias" adjustments to partly compensate for the deviations of the ocean in the historical AOGCM simulations from observations (as generally used in downscaling over ocean regions, e.g. Guo *et al.*, 2013). These issues are of particular significance to the Atlantic LAB. Thus, like other model projections for regional climate change, the NARCCAP projections should be used in conjunction with other available information on climate change and future projections. For the Atlantic LAB assessment, other important information sources for future air temperature changes include the downscaled projections from a smaller set of CMIP3 RCM+AOGCM combinations which include a crude ocean bias adjustment (Guo *et al.*, 2013; Brickman *et al.*, 2013), and the projections from AR5 AOGCMs (Loder and van der Baaren, 2013).

The objectives of this report are to provide indications of the magnitude and range of the projected air temperature changes for various parts of Canada in the simulations available from NARCCAP, for consideration in the ACCASP climate change assessments (DFO, 2013a, 2013b, 2013c; Steiner *et al.*, 2013) for the Atlantic, Inland Freshwater and Arctic LABs on the 50-Year time scale. The primary focus is on the Atlantic LAB but more limited information is also provided for all Canada and for areas relevant to the Inland Freshwater and Arctic LABs. The report is not intended to be a definitive or comprehensive presentation of NARCCAP results; rather, the reader is referred to the many publications on the individual NARCCAP models and on their ensemble statistics (e.g. Bukovsky, 2012; de Elía *et al.*, 2013; Di Luca *et al.*, 2013; Mearns *et al.*, 2013). The present report will provide information from eight RCM+AOGCM combinations, whereas nine RCM+AOGCM combinations and other simulations are considered in the more in-depth study by de Elía *et al.* (2013).

The models and methods are briefly summarized in Section 11.2. Following the natural sequence of proceeding from larger to smaller scale, cursory results are presented for Canada in Section 11.3, followed by more detailed results for eastern Canada and the Atlantic LAB in Section 11.4. A brief summary is in Section 11.5.

11.2 Models and Methodology

NARCCAP considers four AOGCMs from CMIP3 as forcings, and six RCMs in the downscaling. In this report, we present results from the downscaling involving three of the AOGCMs and six RCMs. All fields used in our computations were downloaded from the NARCCAP website (http://www.narccap.ucar.edu/data/index.html).

The three AOGCMs that we used were:

- the Canadian Climate Centre Coupled General Circulation Model version 3 (CGCM3; Scinocca and McFarlane, 2004; Flato, 2010)
- the US NCAR (National Centre for Atmospheric Research) Community Climate System Model (CCSM2; Collins *et al.*, 2006)
- the US Geophysical Fluid Dynamics Laboratory Climate Model version 2.1 (GFDL CM2.1; GFDL Global Atmospheric Model Development Team, 2004).

The six RCMs were:

- the Canadian RCM from Ouranos (CRCM; Caya and Laprise, 1999; Music and Caya, 2007)
- the fifth generation Pennsylvania State University–National Center for Atmospheric Research (NCAR) Mesoscale Model (MM5I; Grell *et al.*, 1994)
- the U.K. Met Office Hadley Centre's regional climate model version 3 (HRM3; Jones *et al.*, 2003)
- the US NCAR Regional Climate Model version 3 (RegCM3 or RCM3; Giorgi *et al.*, 1993a,b; Pal *et al.*, 2000, 2007)
- the Scripps Experimental Climate Prediction Center (ECPC) Regional Spectral Model (ECP2; Juang *et al.*,1997)
- the U.S. Weather Research and Forecasting model (WRFG; Skamarock *et al.*, 2005).

We present results from Phase II of NARCCAP in which the lateral and lower boundary conditions for the RCM simulations were taken from the AOGCMs for 30 years of the past climate (1971-2000) in their 20C3M simulations, and 30 years of a future climate (2041–2070) in their simulations for the SRES A2 scenario (Mearns *et al.*, 2012). The different RCM simulations were for a similar North American domain with a grid size of ~50 km and with output saved at 3-hr intervals. The domain extends from northern Mexico to the southern part of the Canadian Arctic Archipelago (CAA), and ~1000 km offshore into the NE Pacific and NW Atlantic (except off Alaska and Newfoundland where it is less). Note that the 70-year offset of the above simulation periods is only an approximation to the ACCASP 50-Year time scale with some of the projected changes probably having already occurred. However, since recent greenhouse gas emissions have been greater than in the A2 scenario (Peters *et al.*, 2013), overestimation of the time offset should be partly offset by underestimation of the emissions.

The specific RCM+AOGCM combinations considered here are listed in Table 11-1. This choice was based on ready availability of the datasets at the time of the analyses.

Table 11-1 The eight RCM+AOGCM combinations used in this report are indicated in the appropriate cells of this table of RCMs (rows) and AOGCMs (columns).

RCM	**AOGCM**		
	CCSM2	**CGCM3**	**GFDL CM2.1**
CRCM	CRCM+CCSM	CRCM+CGCM	
ECP2			ECP2+GFDL
HRM3			HRM3+GFDL
MM5I	MM5I+CCSM		
RCM3		RCM3+CGCM	RCM3+GFDL
WRFG		WRFG+CGCM	

For each model combination and 30-year period, data were averaged to provide tri-decadal means for each month of the year at each gridpoint. Then the monthly climate change (over 70 years) for each model combination and gridpoint was computed as the difference between the tri-decadal mean for the future period and the past period. Ensemble statistics (mean, minimum, maximum, spread between the minimum and maximum, and standard deviation about the mean) were computed for each gridpoint, for the ensemble of eight RCM+AOGCM combinations.

The areal-averaged monthly climate change for each model combination was computed by arithmetic averaging the changes at all gridpoints within selected latitude-longitude boxes, and then ensemble statistics were computed. It should be emphasized that the boxes are only crude approximations to the areas indicated, chosen to provide an indication of the ensemble-mean climate change and the spread among the change estimates from the individual model combinations (rather than firm projections).

11.3 Projected Changes for Canada

Figure 11-1 shows the spatial patterns of the ensemble-mean monthly climate changes for Canada. Figure 11-2 shows the spread among the monthly climate changes from the eight RCM+AOGCM combinations. It can be seen that the winter maximum over northern Canada, commonly referred to as "Arctic amplification" (e.g. Serreze and Barry, 2011), evolves in the NARCCAP ensemble from a weak maximum centered over the southern CAA in September and October, to a much broader and more intense maximum in December and January that is centered further south (but still in northern Canada). Peak magnitudes then occur over Hudson Bay and, to a lesser degree, over the northern Labrador Sea. These features are present in all but one (RCM3+GFDL) of the eight model combinations considered here. De Elía *et al.* (2013) indicate that decreases in sea-ice cover, depth, and fraction contribute to these local maxima (see their Figure 6), but they do not discuss the reliability of the sea ice projections in the models. The winter amplification weakens as the Pacific, Atlantic, and Arctic coasts and the continental US boundary are approached, with the exception of its extension into the Labrador Sea.

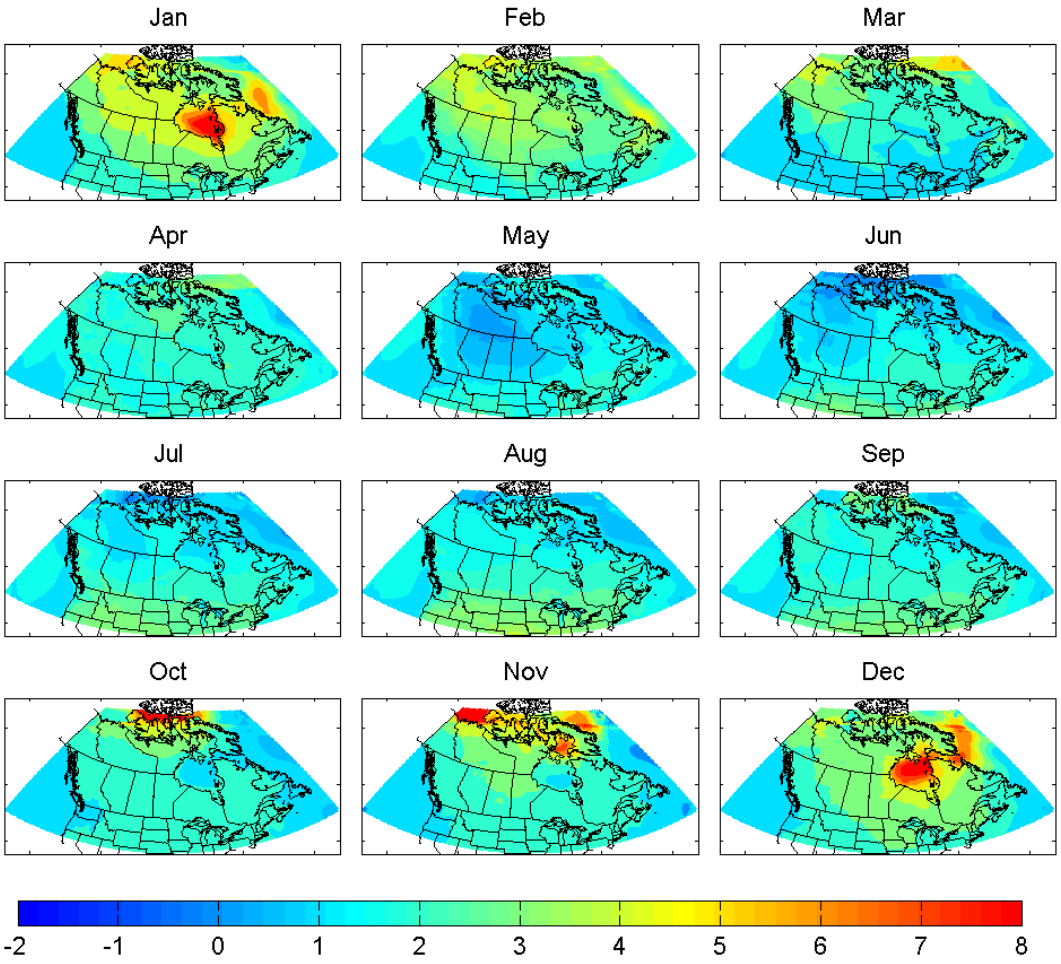

Figure 11-1 Ensemble-mean monthly climate changes in surface air temperature (°C) for Canada from the tri-decade 1971-2000 to the tri-decade 2041-2070, from eight NARCCAP AOGCM+RCM combinations. Note that the colour bar does not cover the full range (-0.5 to +10.8°C) of the temperature changes.

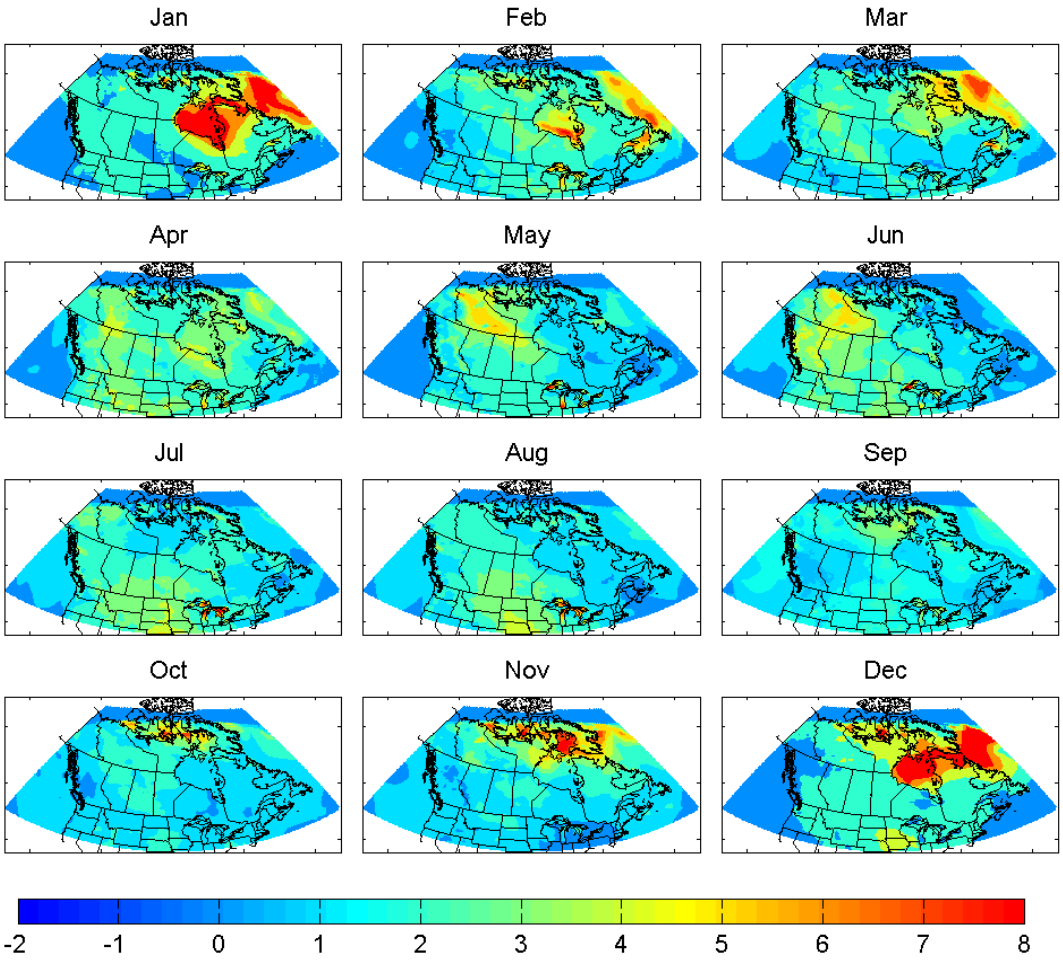

Figure 11-2 The spread (or range) of the monthly climate changes in surface air temperature (°C) for Canada from the tri-decade 1971-2000 to the tri-decade 2041-2070, among the eight NARCCAP RCM+AOGCM combinations. Note that the colour bar does not cover the full range (0 to +14.8°C) of the spread.

The seasonal pattern of the climate changes (Fig. 11-1) includes a second but weaker maximum which peaks in July and August and is centered over the continental interior in the latitude range of 30-40^{o}N. This maximum is delineated better in displays of temperature change over the entire continent such as those in Figure 7 of de Elía *et al.* (2013). In the ensemble mean pattern, it extends weakly into southern Canada in the continental interior while, in individual models, it can also extend into the southern parts of Atlantic and Pacific Canada.

While the above winter and summer "amplification" areas appear to be recurrent features of climate model projections, their magnitude and detailed spatial pattern vary substantially among models. The seasonal and spatial patterns, and the approximate magnitudes, of the spread of the projected changes from the eight NARCCAP combinations (Fig. 11-2) show a striking similarity to those of the ensemble-mean change. In other words, the spread of the projected changes about their ensemble means is comparable in magnitude to the means, and in some areas larger than the means (see later for more on this). This reflects the various uncertainties associated with the

AOGCMs and RCMs used in the climate change simulations, and with internal variability in the coupled climate system (e.g. Deser *et al.*, 2012; Mearns *et al.*, 2012, 2013).

The magnitude of the projected climate changes from the different model combinations can be better seen in scatterplots of the spatially-averaged monthly changes for particular areas of interest, starting with the five areas outside of the Atlantic LAB shown in Figure 11-3. The Prairies, and greater Lake Winnipeg and Great Lakes regions are chosen to provide input to the ACCASP assessment for the Freshwater LAB, the CAA area for input to the assessment for the Arctic LAB, and northern North America (NAMnorth) as a broader reference. This spatial averaging smooths features that are the size of particular lakes that can be expected to depend on the RCMs' representation of lake interactions and are beyond the scope of this summary.

Figure 11-4 shows the annual cycles of the monthly temperature changes in these five areas in each of the eight model combinations, and the annual cycle of the ensemble-mean changes in each area. The ensemble-mean annual cycle of the changes, the monthly spread (maximum minus minimum), and standard deviation (about the ensemble mean) for each area are shown in Figure 11-5.

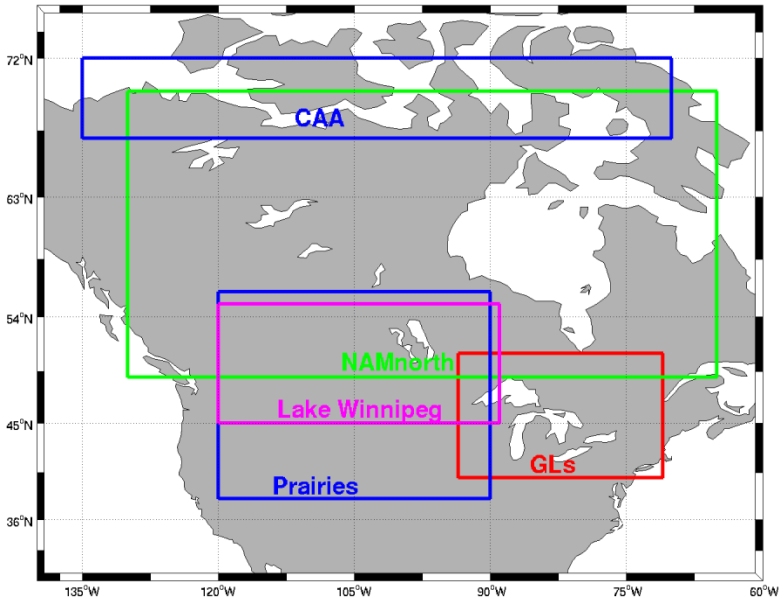

Figure 11-3 The five latitude-longitude boxes used to approximate areas of Canada in the annual-cycle computations displayed in Figs. 11-4 and 11-5. The areas are: the southern part of the Canadian Arctic Archipelago (CAA; 67-72°N, 70-135°W); the northern part of North America (NAMnorth; 49-70°N, 65-130°W); the Prairies (38-56°N, 90-120°W); the greater Lake Winnipeg region (45-55°N, 89-120°W); and the Great Lakes region (GLs; 40-51°N, 71-93.5°W).

A seasonal variation of the changes is apparent in all five areas (Figs. 11-4 and 11-5). Its amplitude is largest in the NAMnorth and CAA areas where the largest change (~4°C for the ensemble mean) occurs in late fall and winter consistent with the Arctic amplification. There is a noticeable shift in the timing of the fall-winter maximum between these two areas, also consistent with the seasonal progression of the area of Arctic amplification described earlier, with the peak changes occurring in late fall (November) in the CAA and in winter (January) in the broader NAMnorth area. The smallest climate changes (~1°C for the ensemble mean) occur in spring (April-May).

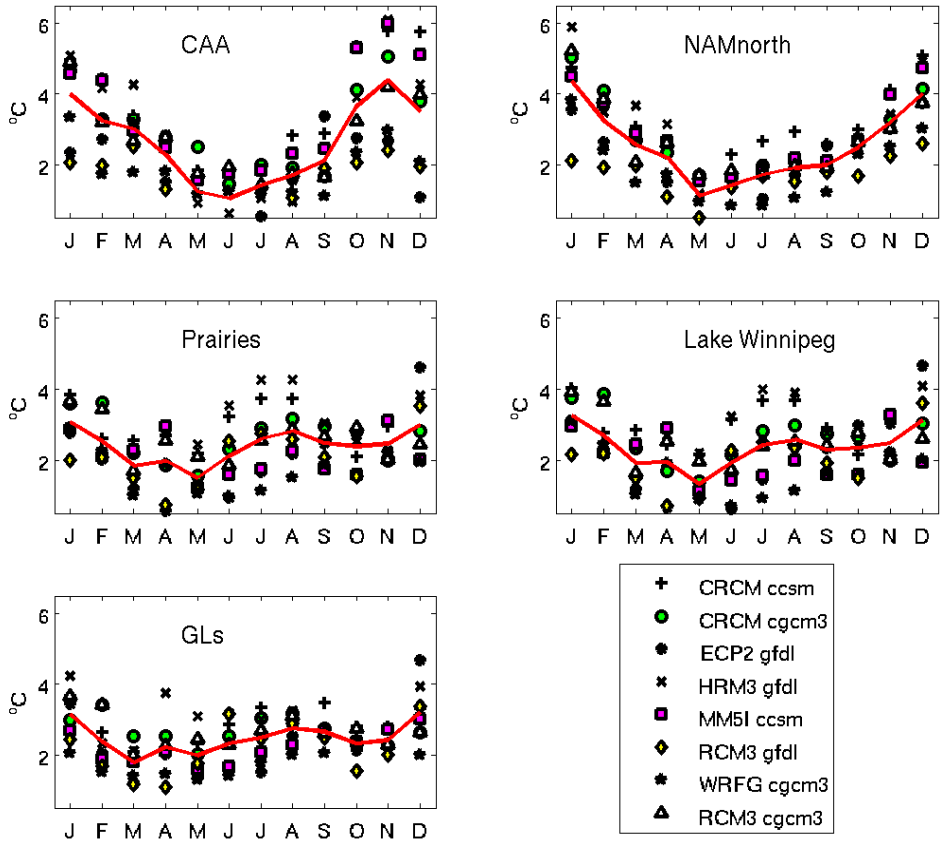

Figure 11-4 The monthly climate changes in surface air temperature between the tri-decades 1971-2000 and 2041-2070 in five areas of interest (see Fig. 11-3) from each of the eight NARCCAP model combinations (different symbols). The ensemble-mean annual cycles are also shown in red.

In the other three areas which are more inland and mid-latitude, there are indications of two seasonal peaks in the projected changes: one in winter (December-January, of ~3°C for the ensemble mean) consistent with a contribution from Arctic amplification, and the second in summer (July-August, of ~2.5-3°C) consistent with a contribution from the mid-latitude interior maximum. The seasonal minimum of the changes in these areas (of ~1.5-2°C) occurs during March-May, with some indications of a slightly larger magnitude and earlier occurrence than in the two more northern areas.

While the range of the projected changes from the different models is generally of similar magnitude to the ensemble-mean changes (Fig. 11-5) and, in particular, is generally larger in spring-summer than the amplitude of the summer ensemble-mean maximum, the seasonal changes in many of the individual models (Fig. 11-4) follow the qualitative annual cycle. These findings point to the potential value of considering the evolution of the two seasonal areas of maximum change when interpreting the seasonality of the air temperature change in particular areas.

Finally, while it is not the objective of this examination to evaluate the different NARCCAP model combinations, some comments can be made from Figure 11-4. For the largest area considered (NAMnorth), RCM3+GFDL projects the smallest change in six of the months

(generally fall and winter), and CRCM+CCSM projects the largest change in five of the months (with the largest change in June-August). The projected changes for NAMnorth from the combination of Canadian models (CRCM+CGCM), which is used most commonly in Canada (e.g. OURANOS; Long *et al.*, 2009; Perrie *et al.*, 2010; Guo *et al.*, 2013), are generally close to the ensemble-mean changes except in January and February when they are higher by nearly 1°C.

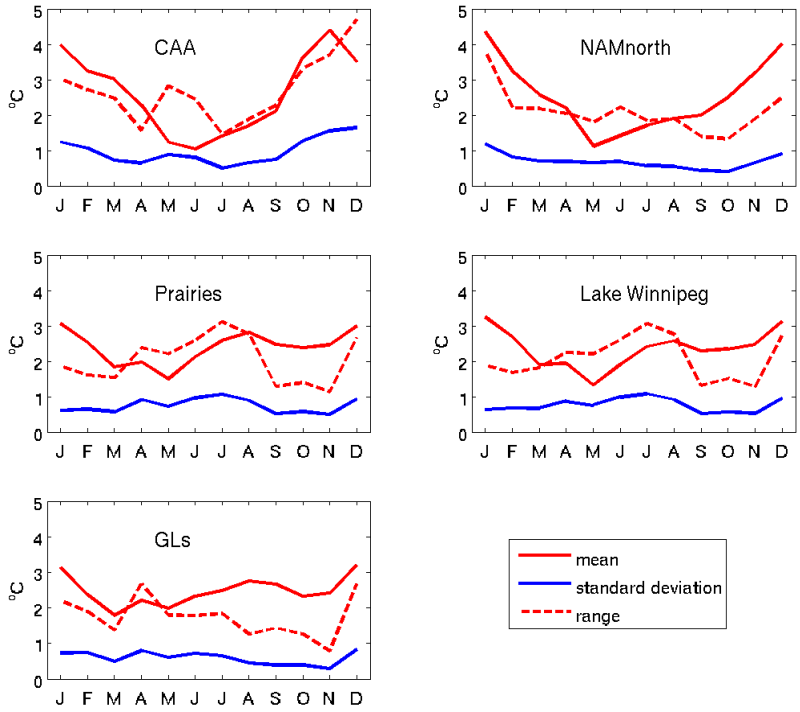

Figure 11-5 The annual cycles of the ensemble statistics of the monthly climate changes in surface air temperature between the tri-decades 1971-2000 and 2041-2070 in five areas of interest (Fig. 11-3), in the eight NARCCAP model combinations. The ensemble means are indicated by the solid red curves, the spreads by the dashed red curves and the standard deviations by the solid blue curves.

11.4 Projected Changes for the Atlantic LAB

The spatial patterns of the ensemble-mean monthly climate changes in eastern Canada are shown in Figure 11-6, and of the spread among the monthly climate changes from the eight NARCCAP model combinations are in Figure 11-7. The northeastern corner of the domain in these displays is near the outer boundary of the RCM domains and/or in the "sponge" zones of the domains. These zones are the edge regions where boundary conditions from the AOGCM are blended with those from the RCM. Therefore, the results in Baffin Bay should not be taken as meaningful and those in Davis Strait should be interpreted with caution. The abrupt offsets in the mean changes in Figure 11-6 reflect the different extent of different RCMs.

Figure 11-6 indicates that "Arctic" amplification (in eastern Canada) in this NARCCAP ensemble-mean pattern starts in September-October in CAA waters west of Baffin Island (Gulf of Bothnia and Foxe Basin), and expands and shifts to Hudson Bay and Hudson Strait in

December and January. In parallel, another area of amplified warming develops in southwestern Davis Strait in November, and expands and shifts to the northwestern Labrador Sea in December and January. In December, Hudson Strait links these areas but in the preceding and succeeding months, the areas are distinct. This pattern is evident in seven of the eight model combinations (with RCM3+GFDL the exception). Considering the delineation of the amplification features by the land-ocean boundary, especially the Labrador Sea feature, it seems natural to explore a relation to changes in sea ice as their origin, as suggested by de Elía *et al.* (2013). A possible explanation is that the amplified air temperature changes are related to a delayed future return of sea ice cover in the fall in these areas, with fall ice cover in the past period resulting in cooler overlying air temperature and delayed/reduced ice cover in the future period resulting in warmer air temperatures. If this is indeed the explanation for these features in the models, then any overestimation of the spatial and temporal extent of the ice cover in the past period would logically be a factor in the development of these amplified air temperatures in the future. Because the sea ice extent in the Labrador Sea is overestimated by CGCM3 (Loder *et al.*, 2010), and by versions of CGCM3 (CanESM2) and GFDL (GFDL-ESM2M) used in CMIP5 (Loder and van der Baaren, 2013), the spatial structure and seasonal extent of these areas of winter amplification in eastern Canada in the NARCCAP ensemble appear to be unreliable.

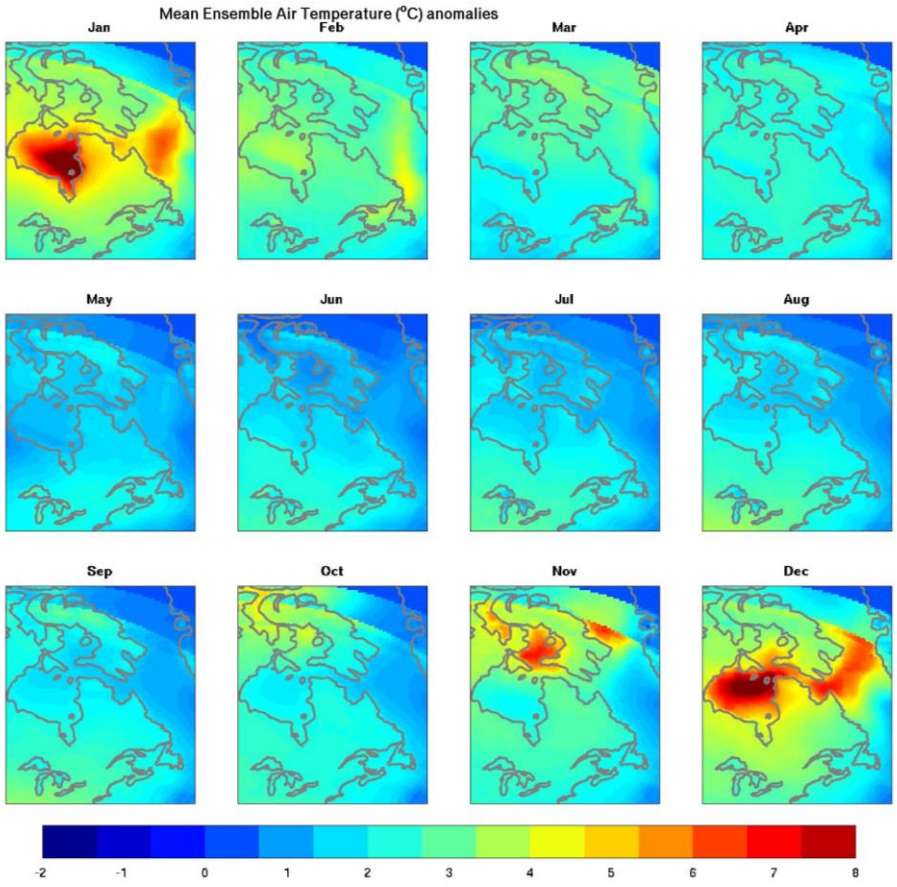

Figure 11-6 Ensemble-mean monthly changes in surface air temperature (°C) for eastern Canada from the tri-decade 1971-2000 to the tri-decade 2041-2070, from eight NARCCAP model combinations.

The ensemble-mean pattern (Fig. 11-6) indicates that the northern area of winter amplification extends into the northern half of the Atlantic LAB, and, weakly, into the land areas of its southern part, except for Newfoundland. It also indicates that summer amplification in the mid-latitude continental interior extends weakly into the southwestern part of the LAB (also see Fig. 11-1).

Figures 11-6 and 11-7 indicate that the spread of the projected changes in eastern Canada from the eight models actually exceeds the ensemble-mean change in most areas and months. This suggests greater uncertainty in the projected climate changes in air temperature for eastern Canada, than in the areas considered in Section 11.3.

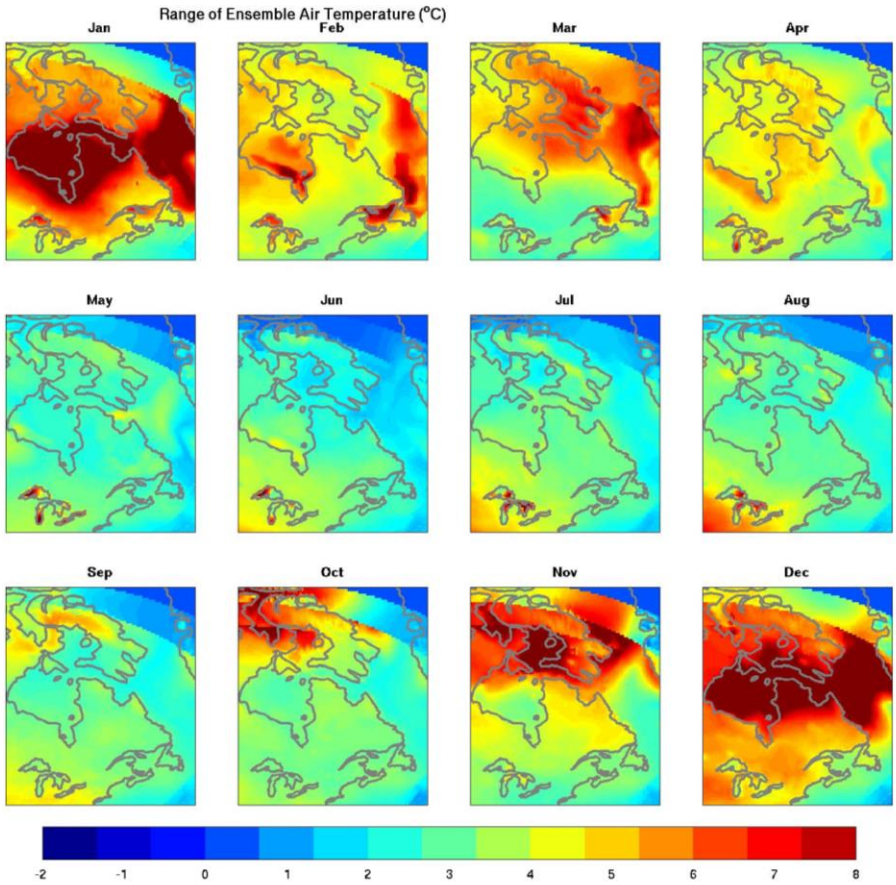

Figure 11-7 The spread (or range) of the monthly climate changes in air temperature (°C) for eastern Canada from 1971-2000 to 2041-2070, among the eight NARCCAP model combinations.

We next consider the magnitude of the projected climate changes from the various model combinations in ten particular areas of interest in the Atlantic LAB, approximated by the latitude-longitude boxes in Figure 11-8. Two of the areas are the northern (NA-LAB) and southern (SA-LAB) parts of the Atlantic LAB, which include about half land and half ocean. Four of the others primarily cover land: Northern Labrador and Quebec (NLQ), Eastern Quebec and Southern Labrador (EQ-SL), Newfoundland (Nfld), and the Maritimes (Mar). The remaining four primarily cover ocean: the Northern Labrador Shelf (NLS), the Northeast Newfoundland

Shelf and the Southern Labrador Shelf (NENS-SLS), the Gulf of St. Lawrence (GLS), and the Scotian Shelf and Gulf of Maine (SS-GoM).

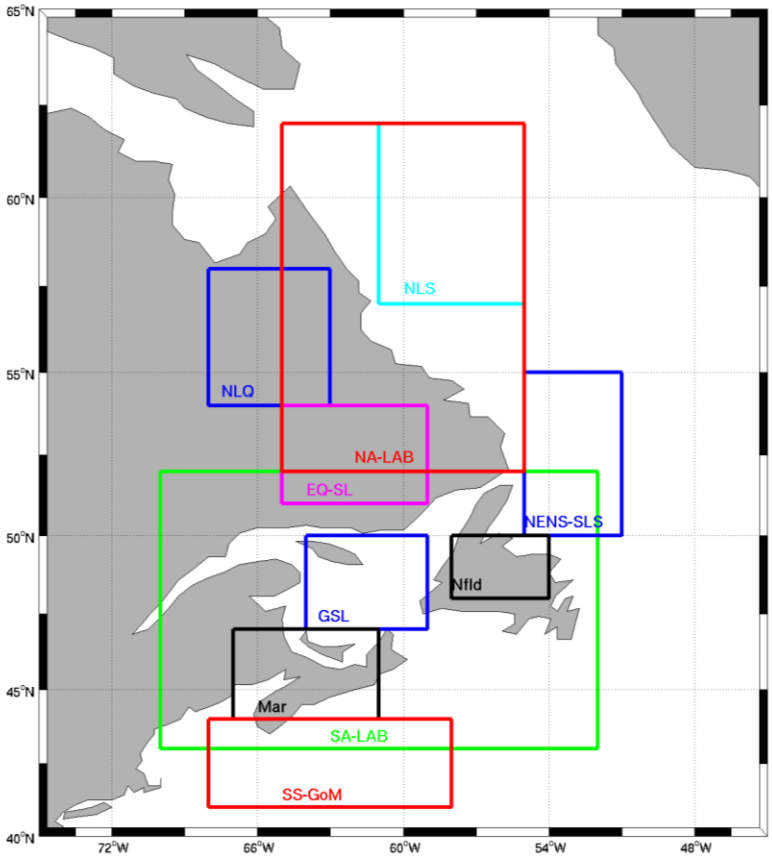

Figure 11-8 The latitude-longitude boxes used to approximate ten areas of the Atlantic LAB in the annual-cycle computations displayed in Figs. 11-9 and 11-10. The latitude and longitude ranges of the areas (see text for expanded names) are as follows: SA-LAB: 43-52°N, 52-70°W; NA-LAB: 52-62°N, 55-65°W; NLQ: 54-58°N, 63-68°W; EQ-SL: 51-54°N, 59-65°W; Nfld: 48-50°N, 54-58°W; and Mar: 44-47 °N, 61-67 °W.

Table 11-2 shows the seasonally-averaged ensemble statistics for the northern and southern parts of the LAB that indicate the magnitudes and scatter of the changes. The seasonal-mean change is largest (4°C) in the northern part in winter and smallest (1.4°C) in the southern part in summer, reflecting the winter amplification discussed above. The seasonal variation in the changes in the southern part is much smaller. The largest change (2.7°C) is in winter, while changes in other seasons are ~2°C and are not likely to be statistically significant for this broad area. The spread shows a somewhat similar pattern to the seasonal means (as expected based on Figs 11-6 and 11-7). In the northern part, the largest spread (~5°C) is in winter and the smallest (1.3°C) in summer, while, in the southern part, the extreme spreads are during these same seasons but smaller in magnitude (particularly in winter). Table 11-2 also shows the ratio of the ensemble-mean change to two standard deviations (SDs) as an indication of the statistical significance of the changes in view of the inter-model variability (e.g. spread). This ratio is greater than 1 in all seasons in both areas. It points to some robustness of the ensemble-mean changes. The ratio is substantially larger (by >70%) in the southern part than the northern part in all seasons, reflecting greater uncertainty of the projected changes in the northern part. If the RCM3+GFDL model

were excluded from the ensemble as an outlier, then the uncertainty in the northern part in winter would be reduced more than in the southern part.

Table 11-2 Ensemble statistics of the seasonal climate changes in surface air temperature (°C) in the Northern (NA-LAB) and Southern (SA-LAB) Atlantic LAB. The seasons are taken as three-months periods, starting with December-February for winter. The Ratio, defined as the Mean divided by two standard deviations (SDs), provides an indication of the significance or robustness of the projected changes considering inter-model variability.

	Winter: Dec-Feb					
	Mean	**Min**	**Max**	**SD**	**Spread**	**Ratio**
NA-LAB	4	1.1	6.3	1.8	5.2	1.1
SA-LAB	2.7	1.5	3.6	0.7	2.1	1.9
	Spring: Mar-May					
NA-LAB	1.9	0.8	3.5	0.9	2.7	1.1
SA-LAB	2	1.4	2.6	0.4	1.2	2.5
	Summer: Jun-Aug					
NA-LAB	1.4	0.8	2.1	0.5	1.3	1.4
SA-LAB	1.9	1.3	2.4	0.4	1.1	2.4
	Fall: Sept-Nov					
NA-LAB	1.6	1	2.8	0.7	1.8	1.1
SA-LAB	2	1.5	2.8	0.5	1.3	2.0

Figure 11-9 shows the monthly temperature changes in the ten areas from the eight models and their ensemble statistics are in Figure 11-10. The anomalously small changes in RCM3+GFDL in winter in the northern areas are immediately apparent, and the estimates from this model in winter are at the spread's low end in the southern areas as well. The largest spread among the other models occurs on the NLS in March, the NENS-SLS in January and February, and in the GSL in February. Because sea ice is an observed feature of these areas in these months, we speculate that this spread may be related to the different representations of sea ice in the models. The spreads in these months and areas are also amplified relative to the mean changes, as is apparent in Figure 11-10. The spreads are smaller than the ensemble means in all months in the SA-LAB, particularly in the Maritimes and SS-GoM areas, and more so than in the other areas considered within and outside (Fig. 11-5) the Atlantic LAB (except, perhaps, the Great Lakes).

While the magnitude of the seasonal variations in the Atlantic LAB areas in the NARCCAP ensemble depends to some extent on whether the RCM3+GFDL estimate is included, there are clear indications of a seasonal variation with a maximum in winter (December, January, or February) in all areas except for the Maritimes and SS-GoM. There is no clear seasonal variation in the latter areas but there is a weak hint of slight maxima in winter and summer, consistent with the winter northern and summer mid-latitude amplifications. It is also noteworthy that the occurrence of a winter maximum in some of the other mid-latitude areas (e.g. Nfld, GSL, and EQ-SL) is heavily influenced by the estimates from just two models, specifically the two (CRCM+CCSM, MM5I+CCSM) with forcing by CCSM. This discussion illustrates well the

differences among the projected air temperature changes for the Atlantic LAB from different RCM + AOGCM combinations and the need to be cautious in the use of only one or two models (or model combinations) for downscaling climate change projections.

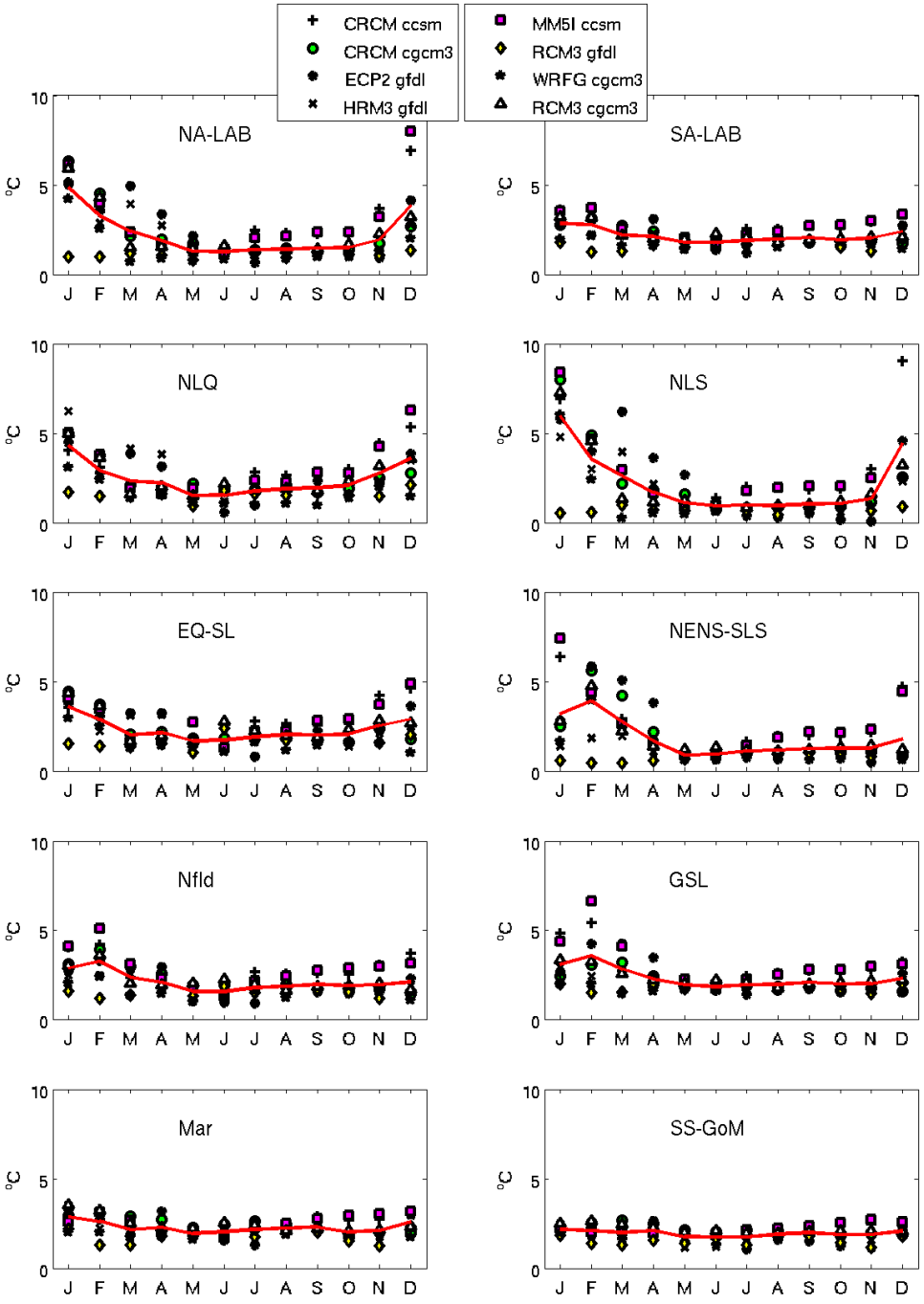

Figure 11-9 The monthly climate changes in surface air temperature between the tri-decades 1971-2000 and 2041-2070 in ten areas of interest (Fig. 11-8) in the Atlantic LAB, from each of the eight NARCCAP model combinations (different symbols). The ensemble-mean annual cycle in each area is in red.

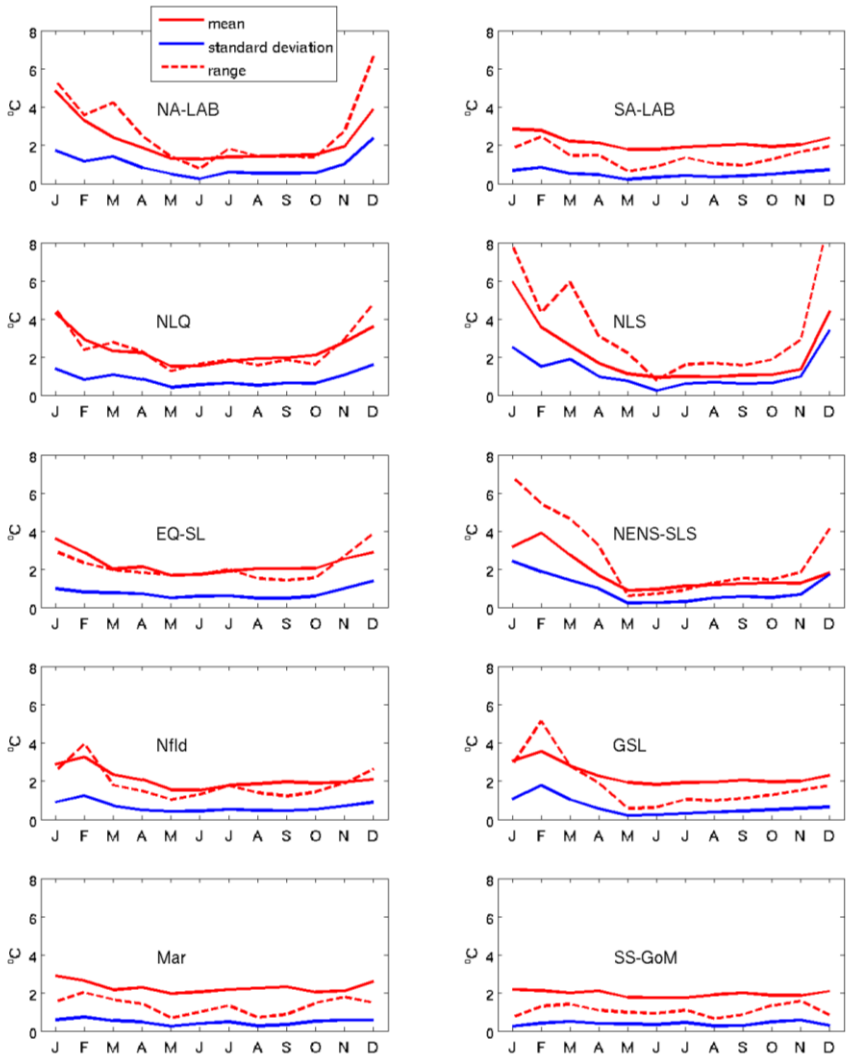

Figure 11-10 Annual cycles of the ensemble statistics of the monthly climate changes in surface air temperature shown in Fig. 11-9, for the ten areas of interest (Fig. 11-8) in the Atlantic LAB (different panels). Ensemble means are indicated by the solid red curves, spreads by the dashed red curves, and standard deviations by the solid blue curves.

11.5 Summary and Conclusions

The displays and statistics presented here provide indications of the magnitudes, spatial patterns, seasonality, and uncertainties in the projected climate changes in surface air temperature over Canada between 1971-2000 and 2041-2070 in a subset of NARCCAP model combinations, but they do not provide firm estimates of the changes or quantitative measures of the uncertainties. It should be re-emphasized that, in addition to being only one-third of the potential model combinations under consideration in NARCCAP, the eight model combinations used here were chosen because of the availability of their outputs, rather than critical evaluation of the models.

The generally strong similarity among the spatial patterns and annual cycles of the temperature changes in the model combinations suggests that many of the qualitative features of the changes are meaningful representations of the climate dynamics affecting air temperature over most of

Canada. However, the spread in the magnitude of the projected changes among the different model combinations is generally comparable to the ensemble mean of the changes, such that there is considerable uncertainty in the magnitude of the changes. Nevertheless, there is a clear indication of increased air temperatures in all seasons in the parts of Canada covered by the NARCCAP RCM domains although the CAA and the NW Atlantic off Canada are only partly covered. In addition, in the southern part of the Atlantic LAB, the ensemble means exceed two standard deviations of the inter-model variability pointing to statistically significant changes.

A prominent feature of the seasonal variation of the changes is an area of amplified temperature increase over northern Canada in winter which is commonly referred to as Arctic amplification (e.g. Serreze and Barry, 2011). In the NARCCAP models, this feature develops in fall over the southern CAA and reaches peak extent and magnitude in winter when it is centered over Hudson Bay. This contributes to a winter maximum in the ensemble-mean temperature increases in all areas examined except the Maritimes and SS-GoM, with magnitudes (over 70 years) ranging from ~3°C over the continental interior (e.g. Great Lakes and Prairies) and southern part of the Atlantic LAB (e.g. GSL and Nfld, but excluding Mar and SS-GoM) to 4-5°C in more northern areas. However, the wide spread in the magnitudes of the projected winter change among the individual model combinations, particularly in the Hudson Bay and LSS regions, raises questions about how well the models are representing atmosphere-ice-ocean interactions in these regions and whether differences among the models are related to inadequacies in model dynamics and/or resolution. Arctic amplification is considered to be related to ice and snow cover feedbacks to the atmosphere (Serreze *et al.*, 2009; Serreze and Barry, 2011) and there is the potential that the contribution from sea ice variability in eastern Canada may be contaminated by deficiencies in the representation of atmosphere-ice-ocean interactions. However, the NARCCAP RCM+AOGCM combinations might represent the contribution to amplification from the effects of snow cover over land well.

A second prominent feature of the seasonal variation, also previously identified in AOGCM (e.g. Meehl *et al.*, 2007) and RCM (e.g. de Elía *et al.*, 2013) simulations, is an area of amplified increase over the interior continent at mid-latitudes in summer. This feature, centered over the northern U.S. in the NARCCAP simulations, contributes to a second seasonal maximum (of ~3°C) over the southern interior of Canada (e.g. Great Lakes and Prairies) in summer, with a weak effect on southwestern parts of the Atlantic LAB. The seasonal minima in the ensemble-mean changes generally are in the 1-2°C range and occur in spring or summer.

The largest ensemble-mean seasonal changes occur in winter in the northern part of the Atlantic LAB. However, the ratio of the ensemble-mean change to two standard deviations of the individual member changes is actually smallest in winter and spring in the LAB's northern part. This ratio is more than twice as large in the southern part of the LAB in spring and summer than in the northern part in winter and spring. This points to the projected changes in the southern part of the LAB being more statistically robust than the larger projected changes in the LAB's northern part.

The comparable magnitudes of the ensemble-mean changes and the inter-model spread about these means in much of eastern Canada are similar to those found recently in an examination of the projected air temperature changes in an ensemble of six Earth System Models (ESMs) used

in AR5 (Loder and van der Baaren, 2013). That study also found substantial differences between model representation of ocean temperature, salinity, and sea ice in the NW Atlantic and observations, and among the projected changes in the different ESMs. Collectively, these two studies point to difficulties in obtaining reliable projections of atmospheric, ice, and oceanographic variables in the NW Atlantic off Canada and in the CAA and Hudson Bay regions. Improvements in the ice and ocean components of climate models are needed in these areas, which, with appropriate coupling with atmospheric models and validation against observations, should lead to improved representations and projections of various atmospheric, ice, and ocean variables in these regions.

11.6 Acknowledgements

We wish to thank the North American Regional Climate Change Assessment Program (NARCCAP) and its participants for making available the data used in this report. NARCCAP is funded by the National Science Foundation, the U.S. Department of Energy, the National Oceanic and Atmospheric Administration, and the U.S. Environmental Protection Agency Office of Research and Development. We also thank Mike Foreman for his contributions to the acquisition of the data, and Joël Chassé, Mike Foreman, Anne Frigon, Zhenxia Long, and Will Perrie for helpful discussions and/or internal review comments.

11.7 References

Brickman, D., B. DeTracey, Z. Long, L. Guo, and W. Perrie. 2013. Analyses of CRCM output for emergence times of climate changes in air temperature and wind speed. Ch. 12 (p. 173-184) *In:* This report.

Bukovsky, M. S. 2012. Temperature trends in the NARCCAP regional climate models. *J. Clim.*, 25(11), 3985–3991.

Caya, D. and R. Laprise. 1999. A semi-Lagrangian semi-implicit regional climate model: The Canadian RCM. *Mon. Wea. Rev.*, 127, 341–362.

Christensen, J. H., B. Hewitson, A. Busuioc, A. Chen, X. Gao, I. Held, R. Jones, R. K. Kolli, W.-T. Kwon, R. Laprise, V. Magaña Rueda, L. Mearns, C. G. Menéndez, J. Räisänen, A. Rinke, A. Sarr, and P. Whetton, 2007. Regional Climate Projections. In: *Climate Change 2007: The Physical Science Basis. Contribution of Working Group I to the Fourth Assessment Report of the Intergovernmental Panel on Climate Change* [Solomon, S., D. Qin, M. Manning, Z. Chen, M. Marquis, K. B. Averyt, M. Tignor, and H.L. Miller (eds.)]. Cambridge University Press. http://www.ipcc.ch/publications_and_data/ar4/wg1/en/ch11.html

Collins W., C. M. Bitz, M. L. Blackmon, G. B. Bonan, C. S. Bretherton, J. A. Carton, P. Chang, S. Doney, J. J. Hack, T. B. Henderson, J. T. Kiehl, W. G. Large, D. S. McKenna, B. D. Santer, and R. D. Smith. 2006. The community climate system model version 3 (ccsm3). *J. Clim.*, 19, 2122–2143.

DFO. 2013a. Risk-based assessment of climate change impacts and risks on the biological resources and infrastructure within Fisheries and Oceans Canada's mandate – Atlantic Large

Aquatic Basin. Fisheries and Oceans Canada, Can. Sci. Sec. Sci. Resp. 2012/044. 40 p. http://www.dfo-mpo.gc.ca/csas-sccs/Publications/ScR-RS/2012/2012_044-eng.html.

DFO. 2013b. Risk-based assessment of climate change impacts and risks on the biological systems and infrastructure within Fisheries and Oceans Canada's mandate - Freshwater Large Aquatic Basin. DFO Can. Sci. Advis. Sec. Sci. Resp. 2013/011, 43 p. http://www.dfo-mpo.gc.ca/csas-sccs/Publications/ScR-RS/2013/2013_011-eng.html

DFO. 2013c. Risk-based assessment of climate change impacts and risks on the biological resources and infrastructure within Fisheries and Oceans Canada's mandate – Arctic Large Aquatic Basin, Fisheries and Oceans Canada, Can. Sci. Sec. Sci. Resp. 2012/042, 39 p. http://www.dfo-mpo.gc.ca/csas-sccs/Publications/ScR-RS/2012/2012_042-eng.html

de Elía, R., S. Biner, and A. Frigon. 2013. Interannual variability and expected regional climate change over North America. *Clim. Dyn.*, 41(5-6), 1245-1267, doi:10.1007/s00382-013-1717-9.

Deser, C., A. Phillips, V. Bourdette, and H. Teng. 2012. Uncertainty in climate change projections: the role of uncertainty. *Clim. Dyn.*, 38, 527–546, doi: 10.1007/s00382-010-0977-x.

Di Luca, A., R. de Elía, and R. Laprise. 2013. Potential for added value in temperature simulated by high-resolution nested RCMs in present climate and in the climate change signal. *Clim. Dyn.*, 40, 443–464, doi:10.1007/s00382-012-1384-2.

Flato, G. M. 2010. The third generation Coupled Global Climate Model (CGCM3). Environment Canada Canadian Centre for Climate Modelling and Analysis. http://www.ec.gc.ca/ccmac-cccma/default.asp?lang=En&n=1299529F-1

GFDL Global Atmospheric Model Development Team. 2004. The new GFDL global atmospheric and land model AM2-LM2: Evaluation with prescribed SST simulations. *J. Climate*, 17, 4641–4673.

Giorgi, F., M. R. Marinucci, and G. T. Bates. 1993a. Development of a second-generation regional climate model (RegCM2). Part I: Boundary-layer and radiative transfer processes. *Mon. Wea. Rev.*, 121, 2794–2813.

Giorgi, F., M. R. Marinucci, G. de Canio, and G. T. Bates. 1993b. Development of a second-generation regional climate model (RegCM2). Part II: Convective processes and assimilation of lateral boundary conditions. *Mon. Wea. Rev.*, 121, 2814–2832.

Grell, G., J. Dudhia, and D. R. Stauffer. 1994. A description of the fifth generation Penn State/NCAR Mesoscale Model (MM5). NCAR Tech. Note NCAR/TN-398+STR, 121 p. http://opensky.library.ucar.edu/collections/TECH-NOTE-000-000-000-214

Guo, L., W. Perrie, Z. Long, J. Chassé, Y. Zhang, and A. Huang. 2013. Dynamical downscaling over the Gulf of St. Lawrence using the Canadian Regional Climate Model. *Atmos.-Ocean*, 51(3), 265-283, doi: 10.1080/07055900.2013.798778

Jones, R., D. Hassell, D. Hudson, S. Wilson, G. Jenkins, and J. Mitchell. 2003. Generating high resolution climate change scenarios using PRECIS. UNDP National Communications Unit Workbook, 34 pp. http://www.uncclearn.org/sites/www.uncclearn.org/files/inventory/UNDP17.pdf

Juang, H., S. Hong, and M. Kanamitsu. 1997. The NMC nested regional spectral model: An update. *Bull. Amer. Meteor. Soc.*, 78, 2125–2143.

Loder, J. W., A. van der Baaren, B. Petrie, and I. Yashayaev. 2010. Projecting ocean climate change in the NW Atlantic. 44th Annual CMOS Congress, Ottawa. https://www1.cmos.ca/abstracts/abstract_print_view.asp?absId=4090.

Loder, J. W. and A. van der Baaren. 2013. Climate change projections for the Northwest Atlantic from six CMIP5 Earth System Models. Can. Tech. Rep. Hydrogr. Ocean Sci. 286: xiv + 112 p. http://www.dfo-mpo.gc.ca/library/349550.pdf

Long, Z., W. Perrie, J. Gyakum, R. Laprise, and D. Caya. 2009. Scenario changes in the climatology of winter midlatitude cyclone activity over eastern North and the Northwest Atlantic. *J. Geophys. Res.*, 114, D12111, doi: 10.1029/2008JD010869.

Mearns, L. O., W. J. Gutowski, R. Jones, R. Leung, S. McGinnis, A. M. B. Nunes, and Y. Qian. 2009. A regional climate change assessment program for North America. *EOS, Trans. Amer. Geophys. Union*, 90: 311, doi:10.1029/2009EO360002.

Mearns, L. O., R. Arritt, S. Biner, M.S. Bukovsky, S. McGinnis, S. Sain, D. Caya, J. Correia, D. Flory, W. Gutowski, E. S. Takle, R. Jones, R. Leung, W. Moufouma-Okia, L. McDaniel, A. M. B. Nunes, Y. Qian, J. Roads, L. Sloan, and M. Snyder. 2012. The North American Regional Climate Change Assessment Program: Overview of Phase I Results. *Bull. Amer. Meteor. Soc*., 93. 1337–1362.

Mearns, L. O., S. Sain, L. R. Leung, M. S. Bukovsky, S. McGinnis, S. Biner, D. Caya, R. W. Arritt, W. Gutowski, E. Takle, M. Snyder, R. G. Jones, A. M. B. Nunes, S. Tucker, D. Herzmann, L. McDaniel, and L. Sloan. 2013. Climate change projections of the North American Regional Climate Change Assessment Program (NARCCAP). *Climatic Change*, 120, 965–975, doi: 10.1007/s10584-013-08.

Meehl, G. A., T. F. Stocker, W. D. Collins, P. Friedlingstein, A. T. Gaye, J. M. Gregory, A. Kitoh, R. Knutti, J. M. Murphy, A. Noda, S. C. B. Raper, I. G. Watterson, A. J. Weaver, and Z.-C. Zhao. 2007. Global Climate Projections. In: *Climate Change 2007: The Physical Science Basis. Contribution of Working Group I to the Fourth Assessment Report of the Intergovernmental Panel on Climate Change* [Solomon, S., D. Qin, M. Manning, Z. Chen, M. Marquis, K. B. Averyt, M. Tignor and H. L. Miller (Eds.)]. Cambridge University Press. http://www.ipcc.ch/publications_and_data/ar4/wg1/en/ch10.html

Music B. and D. Caya. 2007. Evaluation of the hydrological cycle over the Mississippi river basin as simulated by the Canadian regional climate model (CRCM). *J Hydrometeor*., 8(5), 969–988. doi: 10.1175/JHM627.1.

Nakićenović, N., J. Alcamo, G. Davis, B. de Vries, J. Fenhann, S. Gaffin, K. Gregory, A. Grubler, T. Y. Jung, T. Kram, E. L. La Rovere, L. Michaelis, S. Mori, T. Morita, W. Pepper, H.

Pitcher, L. Price, K. Riahi, A. Roehrl, H.-H. Rogner, A. Sankovski, M. Schlesinger, P. Shukla, S. Smith, R. Swart, S. van Rooijen, N. Victor, and Z. Dadi. 2000. *IPCC Special Report on Emissions Scenarios*, Cambridge University Press. http://www.grida.no/publications/other/ipcc_sr/.

Pal, J. S., E. E. Small, and E. A. B. Eltahir. 2000. Simulation of regional-scale water and energy budgets: Representation of subgrid cloud and precipitation processes within RegCM. *J. Geophys. Res.*, 105(D24), 29579–29594.

Pal, J. S., F. Giogi, X. Bi, N. Elguindi, F. Solmon, X. Gao, S. A. Rauscher, R. Francisco, A. Zakey, J. Winter, M. Ashfaq, F.S. Syed, J.L. Bell, N.S. Diffenbaugh, A. Konare, D. Martinez, R.P. da Rocha, L.S. Sloan, and A.L. Steiner. 2007. Regional climate modeling for the developing world: The ICTP RegCM3 and RegCNET. *Bull. Amer. Meteor. Soc.*, 88, 1395–1409.

Perrie, W., Y. Yao, and W. Zhang. 2010. On the impacts of climate change on midlatitude northwest Atlantic land-falling cyclones. *J. Geophys. Res.*, 115, D23110, doi:10.1029/2009JD013535.

Peters, G. P., R. M. Andrew, T. Boden, J. G. Canadell, P. Ciais, C. Le Quéré, G. Marland, M. R. Raupach, and C. Wilson. 2013. The challenge to keep global warming below 2°C. *Nature Climate Change*, 3: 4-6, doi:10.1038/nclimate1783.

Randall, D. A., R. A. Wood, S. Bony, R. Colman, T. Fichefet, J. Fyfe, V. Kattsov, A. Pitman, J. Shukla, J. Srinivasan, R. J. Stouffer, A. Sumi, and K. E. Taylor. 2007. Climate Models and Their Evaluation. In: *Climate Change 2007: The Physical Science Basis. Contribution of Working Group I to the Fourth Assessment Report of the Intergovernmental Panel on Climate Change* [Solomon, S., D. Qin, M. Manning, Z. Chen, M. Marquis, K. B. Averyt, M. Tignor, and H. L. Miller (Eds.)]. Cambridge University Press, New York, NY, USA. http://www.ipcc.ch/publications_and_data/ar4/wg1/en/ch8.html

Scinocca, J. F. and N. A. McFarlane. 2004. The variability of modeled tropical precipitation. *J. Atmos. Sci.*, 61, 1993–2015.

Serreze, M. C., A. P. Barrett, J. C. Stroeve, D. M. Kindig, and M. M. Holland. 2009. The emergence of surface-based Arctic amplification. *Cryosphere*, 3, 11–19.

Serreze, M. C. and R. G. Barry. 2011. Processes and impacts of Arctic amplification: A research synthesis, *Global Planet. Change*, 77, 85–96, doi:10.1016/j.gloplacha.2011.03.004.

Skamarock, W. C., J. B. Klemp, J. Dudhia, D. O. Gill, D. M. Barker, W. Wang, and J. G. Powers. 2005. A description of the Advanced Research WRF version 2. NCAR Tech. Note NCAR/TN-468+STR, 88 p. http://www.mmm.ucar.edu/wrf/users/docs/arw_v2.pdf

Steiner, N., K. Azetsu-Scott, P. Galbraith, J. Hamilton, K. Hedges, X. Hu, M.Y. Janjua, N. Lambert, P. Larouche, D. Lavoie, J. Loder, H. Melling, A. Merzouk, P.G. Myers, W. Perrie, I. Peterson. R. Pettipas, M. Scarratt, T. Sou, M. Starr, R.F. Tallmann and A. van der Baaren. 2013. Climate change assessment in the Arctic Basin, Part 1: Trends and projections – A contribution to the Aquatic Climate Change Adaptation Services Program. Can. Tech. Rep. Fish. Aquat. Sci. 3042: xv + 163 p. http://www.dfo-mpo.gc.ca/library/350169.pdf

12 Analyses of CRCM output for climate changes in surface air temperature and wind

David Brickman *, Brendan DeTracey, Zhenxia Long, Lanli Guo, and William Perrie

Fisheries and Oceans Canada, Bedford Institute of Oceanography
P.O. Box 1006, Dartmouth, Nova Scotia B2Y 4A2

*correspondence: David.Brickman@dfo-mpo.gc.ca

Suggested Citation:
Brickman, D., B. DeTracey, Z. Long, L. Guo and W. Perrie. 2013. Analyses of CRCM output for climate changes in surface air temperature and wind. Ch. 12 (p. 171-182) *In:* Aspects of climate change in the Northwest Atlantic off Canada [Loder, J.W., G. Han, P.S. Galbraith, J. Chassé and A. van der Baaren (Eds.)]. Can. Tech. Rep. Fish. Aquat. Sci. 3045: x + 190 p.

Abstract

This document summarizes analyses of atmospheric model data from current and future climate simulations using the Canadian Regional Climate Model (CRCM) atmospheric downscaling model. Three members of future climate scenario A1B were available for analysis on two domains – a high resolution Atlantic Canada domain and selected locations on a larger North Atlantic domain. The data analyzed were daily averaged surface air temperature (T_{AIR}) and surface wind variables for the period 1970-2069. Calculations included emergence times (the time at which the mean value is greater than 2 standard deviations from its current climate value) and trend analyses. The average change in T_{AIR} for coastal stations is predicted to be about 2.5°C. Typical emergence times are about 40 years (from 1995), with longest times on the Newfoundland-Labrador shelves (~60 yr). On a seasonal basis, emergence times tend to be longest for winter (60-70 yr) and shortest for summer (40-50 yr) indicating that the effects of global warming will be felt sooner during the warmer time of year. For wind direction and speed no trends were observed. Rather, for wind field metrics the variability within bi-decades was found to be much greater than the variability between bi-decades.

12.1 Introduction

Three members of the AR4 SRES A1B future climate scenario (Solomon *et al.*, 2007), downscaled from the Canadian Global Climate Model (CGCM) version 3.1 using the CRCM and the technique developed by (Guo *et al.*, 2013), were available for analysis – M3, M4 and M5 on two domains. On the "Atlantic Canada" domain (Fig. 12-1; model resolution of 30 km), all model grid points were analyzed for all 3 scenario members. On a larger "North Atlantic" domain (model resolution of 45 km) only data extracted for 13 representative locations, for scenarios M4 and M5, were available. These stations are: Iqaluit, Bravo, Nain, Cartwright, Natashquan, Quebec City, Mont Joli, Charlottetown, St. John's, Halifax, Sable Island, Boston, and Fredericton. Of the above, only Iqaluit, Bravo, and Nain are outside the Atlantic Canada domain. Although the data from the duplicate stations are not identical, to keep our analyses as simple as possible, we chose to ignore the duplicate data from the larger domain.

The data analyzed are daily averaged surface air temperature (T_{AIR}) and surface wind variables for the period 1970-2069. Other variables were not analyzed. The analyses presented herein focus on the 13 stations with the complete domain coverage used to provide a sense of regional patterns.

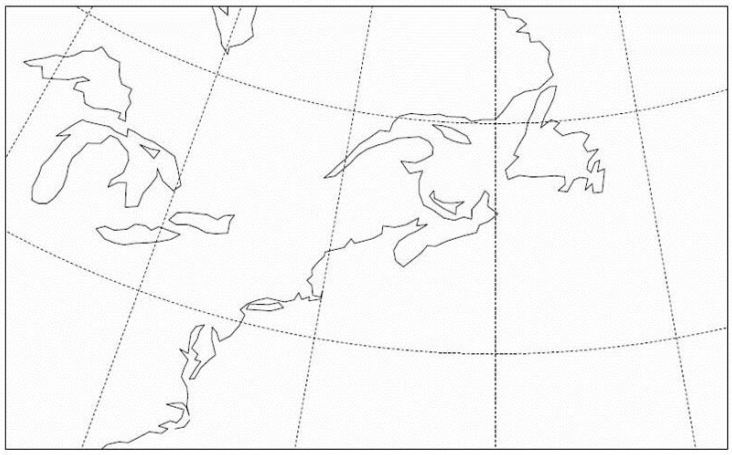

Figure 12-1 CRCM Atlantic Canada domain.

The basic goal of the analyses is to compare future climate predictions with the current model climate. For these purposes, the current climate is defined as the 20 year period from 1985-2004 (where periods are defined as Jan. 1 of the first year to Dec. 31 of the last year).

Emergence Time

The idea of emergence time for a variable derives from the premise that climate change involves a directed trend (usually increasing) for a variable that is superimposed upon "natural climate variability" (Hawkins and Sutton, 2012). The signal of interest is considered to "emerge" at a time interval when its time-dependent mean value is greater than 2 standard deviations (STDs) from its current climate value (Fig. 12-2).

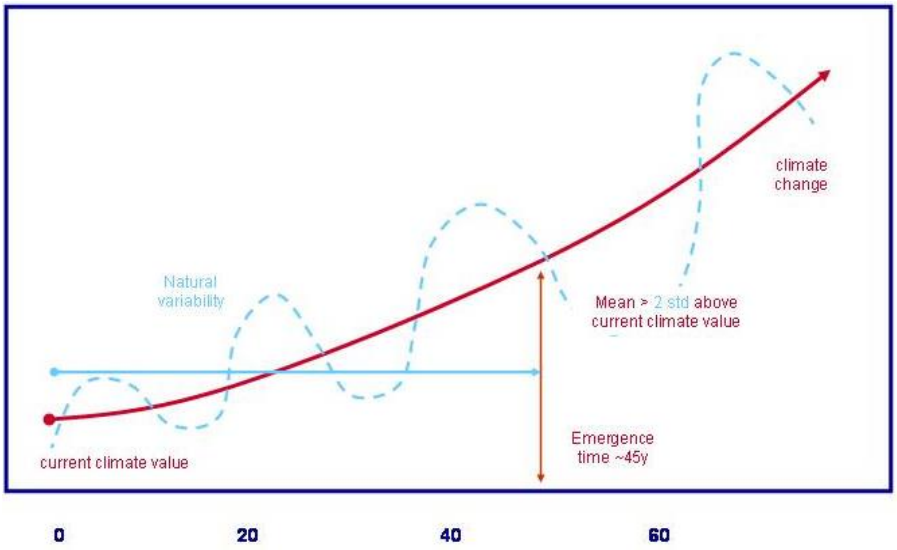

Figure 12-2 Illustration of emergence time, with the climate varable on the vertical axis and years on the horizontal axis. In the near-term (10-20 years), signals due to natural climate variability can mask the climate change signal.

Emergence times were computed for T_{AIR} only as no significant directed trend was observed for the wind speed variables. Calculations based on annually averaged and seasonally averaged T_{AIR} are presented.

Bi-decadal Changes

Changes in air temperature (T_{AIR}), wind speed (W_{SPD}), and wind direction (W_{DIR}) were computed for 3 bi-decadal periods (2005-2024, 2025-2044, 2045-2064) and compared to the current climate (1985-2004). Statistics computed were annual and seasonal mean T_{AIR}, W_{SPD}, and W_{DIR}, plus STDs. For wind speed, extreme event probabilities (W_{FX}) were also computed and (expressed as the expected number of days per year that the daily average wind speed exceeds some value (see explanation below).

12.2 Methodology

Time Series Averaging

At each location, and for each member, the daily data were first averaged to produce 100-year time series of annual means and of seasonal means, removing intra-annual variability. Seasons are defined as calendar seasons (winter is January-March, spring is April-June, etc.). The resulting time series were the starting point for all following calculations, except extreme wind probability.

Bi-decadal Time Series

For each time series, the mean and STDs of T_{AIR}, W_{SPD}, and W_{DIR} were calculated for the four bi-decadal periods indicated above. Ensemble statistics were produced by calculating the mean and STD of all scenario members per bi-decadal period.

Emergence Time Calculation: (T_{AIR} only)

The mean and STD were calculated for the "present climate", defined as the years 1985-2004. A quadratic, with a fixed point defined at 1995 (the present climate mean) was fit to the time series (Fig. 12-3). The emergence time was defined as the point at which the fitted quadratic for forecast climate emerges from the present climate envelope, defined as two STDs from the present climate mean. Also computed from the quadratic fit was the 75 year change in air temperature. The emergence time was calculated for the entire spatial domain, as was the "change in T_{AIR}".

Wind Statistics

Wind speed (W_{SPD}) is the magnitude of the wind vector with *u* and *v* components. The mean STD for wind speed were calculated by the standard formulae for scalar time series.

The mean wind direction $\overline{W}_{DIR}$ was calculated from $\overline{W}_{DIR} = \arg \vec{r}$ where

$$\vec{r} = \frac{1}{N} \sum_{n=1,N} \frac{\vec{W}_n}{\left\| \vec{W}_n \right\|}$$

i.e. the argument of the vector average of the normalized wind vector. $\vec{W}_n = u_n + iv_n$ is the complex number representation of the wind vector. The wind direction STD is given by $\sigma_{W_{DIR}} = \sqrt{2(1-R)}$, R defined as $R = \|\vec{r}\|$ (for more details see Fisher, 1995). After its calculation, mean wind direction was converted from mathematical to standard meteorological convention (degrees clockwise from north) and is the direction from which the wind blows.

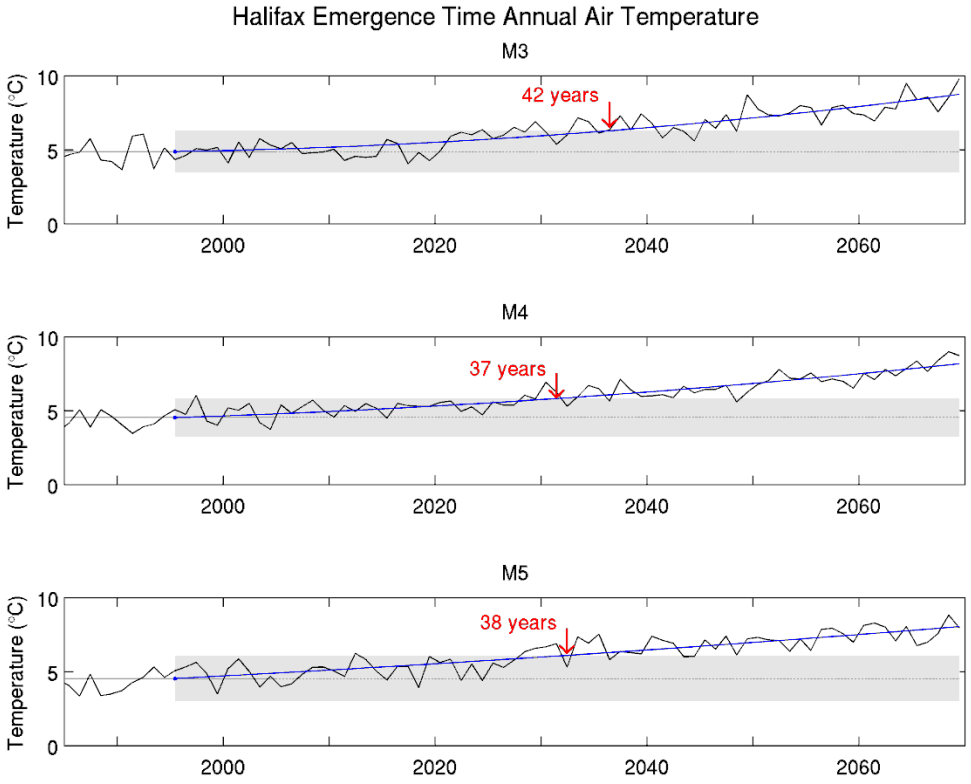

Figure 12-3 Example of emergence time calculation for Halifax for M3 (top), M4 (middle), M5 (bottom).

Extreme Wind Probability:

The "extreme wind" threshold value W_{th} is defined by:

$$0.95 = \int_0^{W_{th}} P(W_{SPD})dW_{SPD}$$

where $P(W_{SPD})$ is the probability distribution function (PDF) of the wind speed. Extreme wind events were arbitrarily defined as those in the top 5% of the cumulative probability distribution (CDF) of the population (Fig. 12-4). The population was the concatenation, over all locations, of the present climate daily mean wind speed time series. $P(W_{SPD})$ was estimated as the normalized histogram of this population, with bin widths of 1 m/s. Coincidentally, the threshold value was the same for all members, 13 m/s.

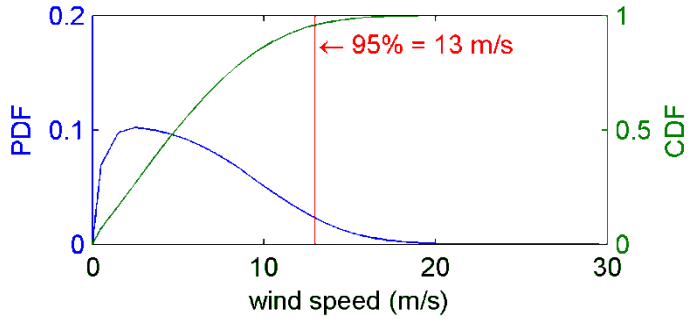

Figure 12-4 PDF and CDF of wind speed for the Atlantic domain, for the present climate (1985-2004). Example is from M3.

F_{WX} is the frequency of extreme wind events, expressed as the number of days per year for which the daily mean wind speed, at a given location, exceeds the wind threshold W_{th}. It is calculated as F_{WX} = 365 × (1-CDF(W_{th})). A bootstrap method was used to estimate error bounds on this calculation and implemented as follows. A histogram of wind speed was generated for a given location, member, and bi-decadal period. The histogram was randomly sampled to produce a simulated annual time series of daily wind speed. The number of days per year exceeding the wind threshold was then counted. The calculation was repeated 100,000 times allowing calculation of the standard deviation of F_{WX} .

12.3 Results, Discussion and Conclusions

Analyses have been carried out for the cases indicated in Table 12-1. Results are presented and briefly discussed in the following subsections. Recall that all calculations were done for the 13 stations, plus the complete CRCM Atlantic domain for the 3 A1B climate scenario members. Seasonal calculations are available for the bi-decadal analyses but are not presented here. Additional figures and tables are contained in the Appendix.

Table 12-1 Summary of presented calculations.

Calculation	Variable	Annual / Seasonal
emergence time	T_{AIR}	Y/Y
bi-decadal mean + STD	T_{AIR}, W_{SPD}, W_{DIR}	Y/N
bi-decadal extreme event probability	W_{SPD}	Y/N

Emergence Times

Annual and seasonal emergence times for the 13 stations are shown in Table 12-2. Typical emergence times are about 40 years (from 1995) with a suggestion that they are shortest for oceanic station Sable Island (Fig. 12-5). Spatially (Fig. 12-6), emergence times are longer on the Newfoundland-Labrador shelves (~60 yr), and tend to be shorter over the oceans than over land in the west and southwest part of the domain. On a seasonal basis, emergence times tend to be longest for winter (60-70 yr) and shortest for summer (40-50 yr) indicating that the effects of global warming will be felt sooner during the warmer time of year.

Table 12-2 Annual and seasonal emergence times, in years, for T_{AIR}. The dashes denote calculations for which emergence times do not exist in the 1970-2069 time frame.

		Annual	Winter	Spring	Summer	Autumn
IQALUIT	ENSEMBLE	52 ± 1	-	68 ± 0	62 ± 2	66 ± 0
	M4	51	-	68	60	-
	M5	52	-	-	63	66
NAIN	ENSEMBLE	41 ± 3	56 ± 6	65 ± 0	53 ± 12	71 ± 0
	M4	39	52	65	44	71
	M5	43	60	-	61	-
CARTWRIGHT	ENSEMBLE	51 ± 3	71 ± 0	-	62 ± 3	60 ± 0
	M3	48	-	-	65	60
	M4	53	-	-	59	-
	M5	51	71	-	63	-
BRAVO	ENSEMBLE	50 ± 0	62 ± 0	-	69 ± 0	-
	M4	50	62	-	69	-
	M5	-	-	-	-	-
NATASHQUAN	ENSEMBLE	42 ± 5	68 ± 4	57 ± 4	48 ± 6	56 ± 6
	M3	42	71	53	54	53
	M4	46	70	61	43	63
	M5	37	63	57	48	53
QUEBEC	ENSEMBLE	40 ± 2	64 ± 10	63 ± 7	47 ± 6	59 ± 10
	M3	40	73	70	48	58
	M4	42	64	57	41	69
	M5	39	54	63	52	49
MONT JOLI	ENSEMBLE	38 ± 2	59 ± 8	55 ± 5	47 ± 7	48 ± 4
	M3	39	66	57	50	47
	M4	40	62	49	39	53
	M5	36	50	58	51	45
CHARLOTTETOWN	ENSEMBLE	41 ± 1	57 ± 9	55 ± 2	48 ± 9	49 ± 5
	M3	42	64	57	45	44
	M4	41	60	55	41	53
	M5	40	47	53	58	50
ST. JOHN'S	ENSEMBLE	44 ± 2	62 ± 7	60 ± 9	53 ± 3	62 ± 9
	M3	45	68	-	55	59
	M4	42	63	53	49	72
	M5	46	55	66	54	56
HALIFAX	ENSEMBLE	39 ± 3	58 ± 10	47 ± 5	44 ± 9	48 ± 5
	M3	42	64	52	45	44
	M4	37	63	43	35	53
	M5	38	47	45	52	48
SABLE ISLAND	ENSEMBLE	31 ± 9	40 ± 12	42 ± 8	35 ± 11	39 ± 4
	M3	41	53	51	47	44
	M4	25	36	37	26	36
	M5	28	30	38	33	38
BOSTON	ENSEMBLE	40 ± 5	67 ± 4	51 ± 2	46 ± 6	54 ± 6
	M3	44	71	53	51	49
	M4	40	66	49	40	60
	M5	35	63	50	46	52
FREDERICTON	ENSEMBLE	43 ± 2	64 ± 6	55 ± 2	48 ± 7	51 ± 5
	M3	43	67	53	49	49
	M4	44	68	54	40	57
	M5	41	57	57	54	48

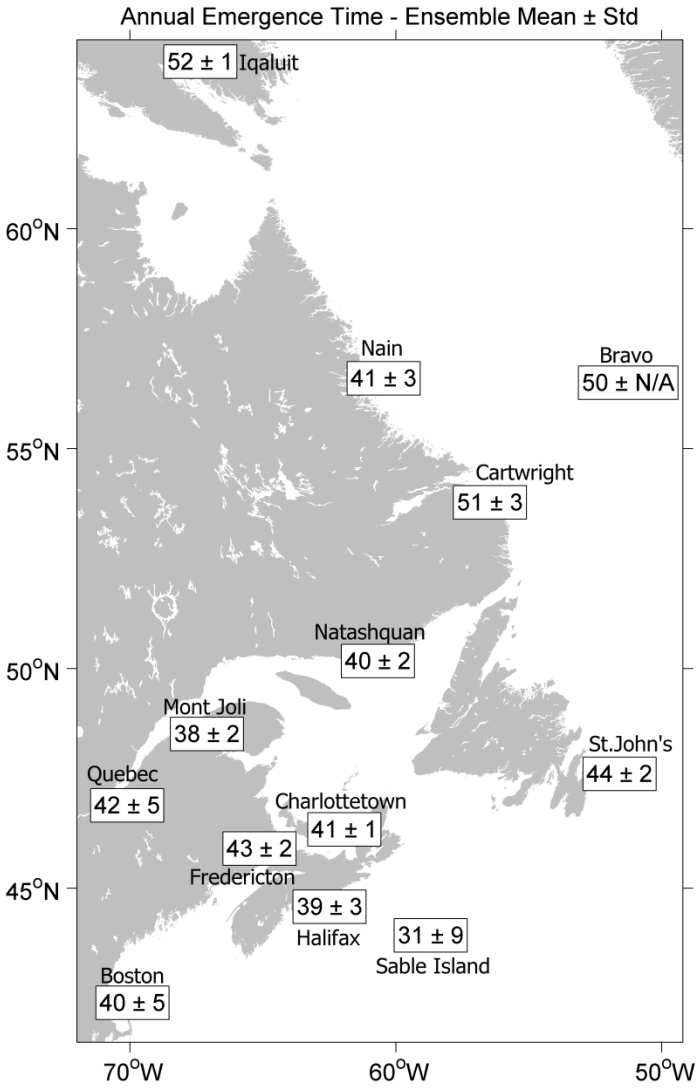

Figure 12-5 Ensemble mean emergence times (years from 1995), plus STD, for the 13 stations. N/A denotes no STD calculation due to insufficient data.

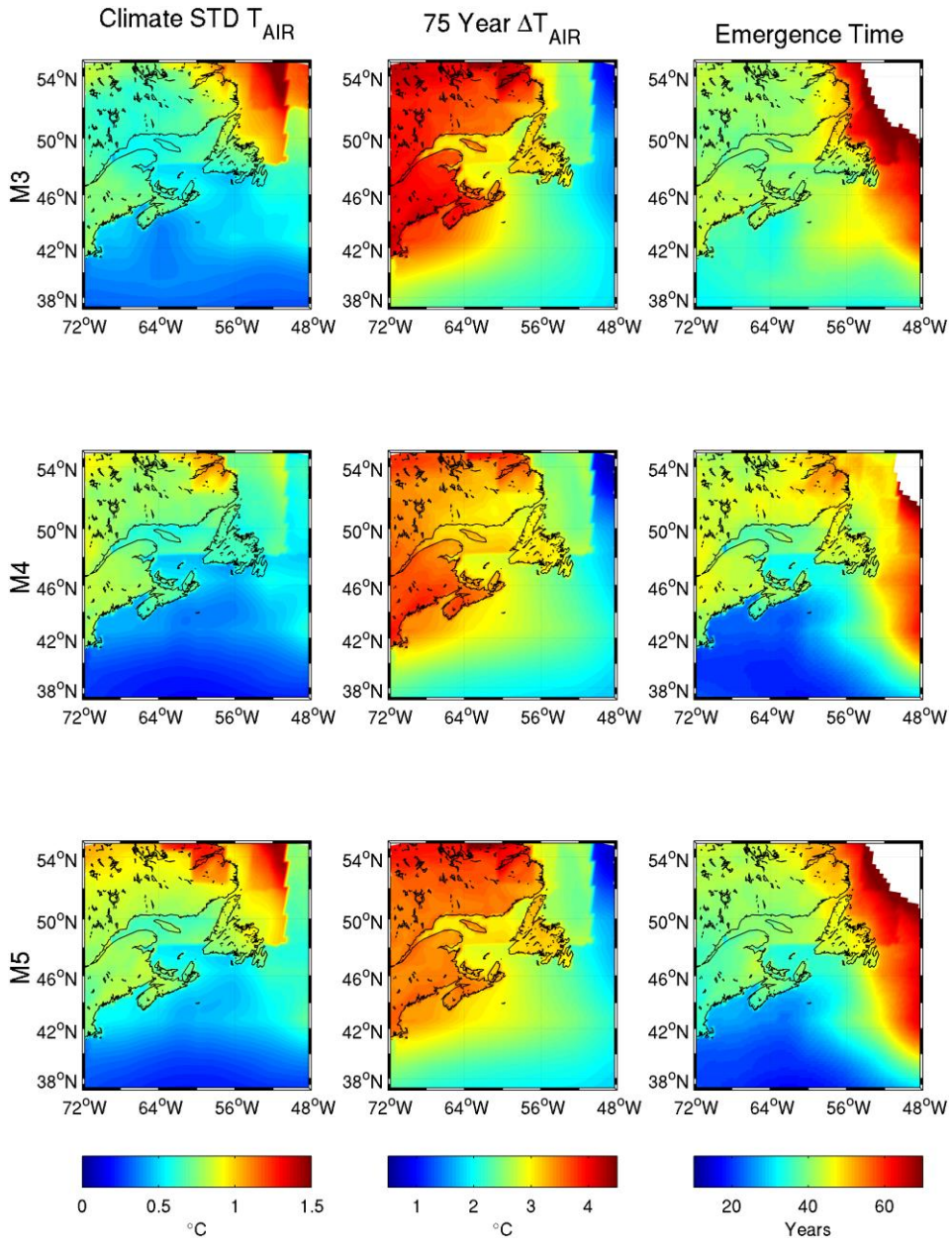

Figure 12-6 Results of analyses for annual T_{AIR} over the Atlantic domain: STD for present climate (left column). Change in T_{AIR} from 1995 to 2069 (middle column). Emergence times for T_{AIR} (right column). Each field plotted for climate scenario members M3 (top row), M4 (middle row), M5 (bottom row). Discontinuities, due to the low resolution of the sea ice used in downscaling, are clearly visible.

Changes in Air Temperature

The bi-decadal air temperature changes (see Appendix) reflect the emergence time calculations, showing monotonic increases for all decades and stations. The exception is ocean weather station Bravo whose trend is more variable, particularly during 2005-2024. The ensemble mean increases (difference of 2045-2064 and 1985-2004 bi-decades) for the 13 stations are shown in Table 12-3.

Table 12-3 Increase in bi-decadal mean air temperature (°C) between 1985-2004 and 2045-2064.

Iqaluit	***Bravo***	***Nain***	***Cartwright***	***Natashquan***	***Quebec City***	***Mont Joli***
3.4	1.5	3.0	2.6	2.5	2.6	2.7
Charlottetown	***St. John's***	***Halifax***	***Sable Island***	***Boston***	***Fredericton***	
2.5	2.1	2.6	2.1	2.7	2.7	

Bi-decadal Changes in Wind Field Properties

In general, no obvious patterns were found in the model wind field data (see Appendixs). For the annual mean wind speed there is a weak suggestion of a latitudinal gradient whereby the wind speed increases (in the future) for the higher latitude stations (Iqaluit, Nain, Cartwright: 0.1-0.3 m/s), and decreases (in the future) for lower latitude stations (Sable Island, Boston, Fredericton: 0.1-0.2 m/s).

For wind direction, the majority of the stations show a tendency toward a clockwise turning of the wind in the future, but these changes are so slight (typically a few degrees) that it is difficult to imagine that this would have a significant effect. Regarding wind speed extreme events, values range from 2-3 days-per-year (Mont-Joli) to about 40 days-per-year (Bravo), but, again, no trends are observed. Note that for the wind speed and direction the variability ***within*** bi-decades is much greater than the variability ***between*** bi-decades – which is not true for air temperature where emergence times do exist.

12.4 Acknowledgements

Internal review comments were provided by Joël Chassé, John Loder, Youyu Lu and Zeliang Wang.

12.5 References

Fisher, N. I. 1995. *Statistical Analysis of Circular Data*, revised edition, Cambridge University Press.

Guo, L., W. Perrie, Z. Long, J. Chassé, Y. Zhang, and A. Huang. 2013. Dynamical downscaling over the Gulf of St. Lawrence using the Canadian Regional Climate Model, *Atmos.-Ocean*, 51, doi: 10.1080/07055900.2013.798778.

Hawkins, E. and R. Sutton. 2012. Time of emergence of climate signals, *Geophys. Lett.*, 39, L01702, doi: 10.1029/2011GL050087.

Solomon, S., D. Qin, M. Manning, R. B. Alley, T. Berntsen, N. L. Bindoff, Z. Chen, A. Chidthaisong, J. M. Gregory, G. C. Hegerl, M. Heimann, B. Hewitson, B. J. Hoskins, F. Joos, J. Jouzel, V. Kattsov, U. Lohmann, T. Matsuno, M. Molina, N. Nicholls, J. Overpeck, G. Raga, V. Ramaswamy, J. Ren, M. Rusticucci, R. Somerville, T. F. Stocker, P. Whetton, R. A. Wood, and D. Wratt (2007). Technical Summary. In: *Climate Change 2007: The Physical Science Basis. Contribution of Working Group I to the Fourth Assessment Report of the Intergovernmental Panel on Climate Change* [Solomon, S., D. Qin, M. Manning, Z. Chen, M. Marquis, K. B. Averyt, M. Tignor, and H. L. Miller (Eds.)]. Cambridge University Press, Cambridge, United Kingdom and New York, NY, USA
http://www.ipcc.ch/publications_and_data/ar4/wg1/en/contents.html

12.6 Appendix: Bi-decadal Statistics

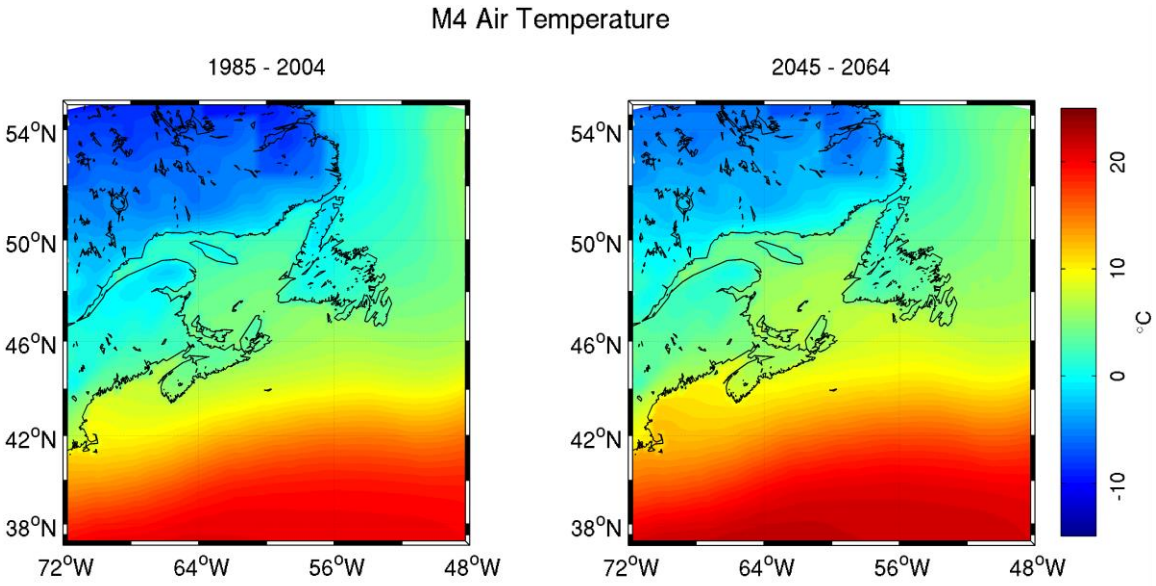

Figure 12-7 Plots of spatial patterns of bi-decadal mean air temperature (T_{AIR}) for scenario member M4. Only the first and last bi-decades are shown. Spatial patterns for other bi-decades and members are similar.

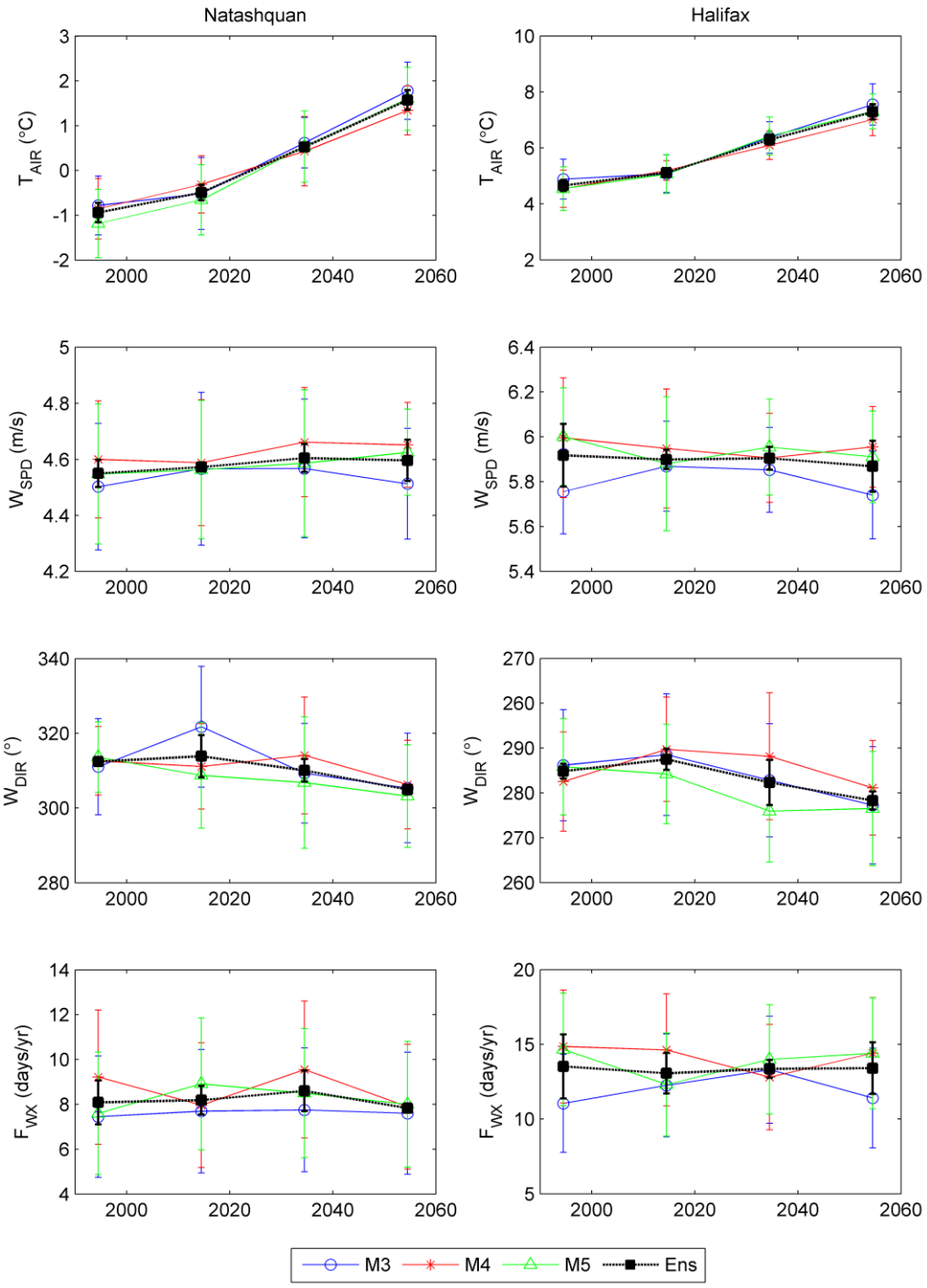

Figure 12-8 Illustrative plots, for the Natashquan and Halifax stations, of bi-decadal mean air temperature (T_{AIR}), wind speed (W_{SPD}), wind direction (W_{DIR}) and annual frequency of extreme wind (F_{WX}) for scenario members M3, M4, M5, and the ensemble mean (Ens). Error bars indicate ± one STD. The ensemble STD is that of the three members, to illustrate the spread between members.

Table 12-4 Bi-decadal ensemble mean air temperature (T_{AIR}), wind speed (W_{SPD}), wind direction (W_{DIR}) and annual frequency of extreme wind (F_{WX}) for the 13 stations. Error indicates ± one STD.

Iqaluit	**1985 – 2004**	**2045 – 2064**
T_{AIR} (°C)	-16.0 ± 1.3	-12.6 ± 1.2
W_{SPD} (m/s)	3.2 ± 0.3	3.4 ± 0.3
W_{DIR} (°)	34 ± 38	31 ± 43
F_{WX} (days/yr)	5.7 ± 2.4	7.5 ± 2.8
Cartwright	**1985 – 2004**	**2045 – 2064**
T_{AIR} (°C)	-6.2 ± 1.2	-3.6 ± 1.1
W_{SPD} (m/s)	4.0 ± 0.2	4.1 ± 0.2
W_{DIR} (°)	306 ± 8	302 ± 10
F_{WX} (days/yr)	6.2 ± 2.5	5.6 ± 2.4
Natashquan	**1985 – 2004**	**2045 – 2064**
T_{AIR} (°C)	-0.9 ± 0.8	1.6 ± 0.6
W_{SPD} (m/s)	4.6 ± 0.2	4.6 ± 0.2
W_{DIR} (°)	312 ± 11	305 ± 14
F_{WX} (days/yr)	8.1 ± 3.0	7.8 ± 2.8
Mont Joli	**1985 – 2004**	**2045 – 2064**
T_{AIR} (°C)	0.2 ± 0.7	2.9 ± 0.7
W_{SPD} (m/s)	4.1 ± 0.2	4.2 ± 0.2
W_{DIR} (°)	265 ± 5	263 ± 6
F_{WX} (days/yr)	2.1 ± 1.5	2.2 ± 1.6
St.John's	**1985 – 2004**	**2045 – 2064**
T_{AIR} (°C)	3.5 ± 0.7	5.6 ± 0.6
W_{SPD} (m/s)	7.1 ± 0.3	7.2 ± 0.3
W_{DIR} (°)	269 ± 6	269 ± 5
F_{WX} (days/yr)	29.2 ± 5.6	30.2 ± 5.5
Sable Island	**1985 – 2004**	**2045 – 2064**
T_{AIR} (°C)	8.7 ± 0.5	10.8 ± 0.5
W_{SPD} (m/s)	7.7 ± 0.3	7.5 ± 0.3
W_{DIR} (°)	274 ± 5	273 ± 5
F_{WX} (days/yr)	34.1 ± 6.1	30.9 ± 6.1
Fredericton	**1985 – 2004**	**2045 – 2064**
T_{AIR} (°C)	2.3 ± 0.8	5.0 ± 0.8
W_{SPD} (m/s)	5.5 ± 0.3	5.5 ± 0.2
W_{DIR} (°)	280 ± 5	277 ± 6
F_{WX} (days/yr)	8.9 ± 3.1	8.4 ± 2.9

Nain	**1985 – 2004**	**2045 – 2064**
T_{AIR} (°C)	-9.6 ± 1.0	-6.6 ± 0.9
W_{SPD}(m/s)	5.3 ± 0.4	5.7 ± 0.3
W_{DIR} (°)	308 ± 7	303 ± 8
F_{WX} (days/yr)	20.5 ± 6.0	23.7 ± 6.0
Bravo	**1985 – 2004**	**2045 – 2064**
T_{AIR} (°C)	-0.7 ± 1.0	0.8 ± 1.4
W_{SPD} (m/s)	6.9 ± 0.4	6.7 ± 0.4
W_{DIR} (°)	311 ± 18	309 ± 22
F_{WX} (days/yr)	40.7 ± 6.0	39.4 ± 6.0
Quebec	**1985 – 2004**	**2045 – 2064**
T_{AIR} (°C)	0.0 ± 0.8	2.6 ± 0.8
W_{SPD} (m/s)	4.9 ± 0.2	4.9 ± 0.2
W_{DIR} (°)	270 ± 5	267 ± 6
F_{WX} (days/yr)	5.4 ± 2.4	5.3 ± 2.3
Charlottetown	**1985 – 2004**	**2045 – 2064**
T_{AIR} (°C)	3.4 ± 0.7	5.9 ± 0.6
W_{SPD} (m/s)	5.8 ± 0.3	5.8 ± 0.2
W_{DIR} (°)	274 ± 6	272 ± 5
F_{WX} (days/yr)	13.2 ± 5.5	12.7 ± 5.5
Halifax	**1985 – 2004**	**2045 – 2064**
T_{AIR} (°C)	4.7 ± 0.8	7.3 ± 0.7
W_{SPD} (m/s)	5.9 ± 0.2	5.9 ± 0.2
W_{DIR} (°)	277 ± 6	274 ± 6
F_{WX} (days/yr)	13.5 ± 4.1	13.4 ± 3.8
Boston	**1985 – 2004**	**2045 – 2064**
T_{AIR} (°C)	7.1 ± 0.8	9.8 ± 0.9
W_{SPD} (m/s)	4.8 ± 0.2	4.8 ± 0.2
W_{DIR} (°)	280 ± 5	275 ± 8
F_{WX} (days/yr)	4.2 ± 2.2	4.5 ± 2.1

13 Impact of climate change on water temperatures for selected rivers in New Brunswick and potential implications on Atlantic salmon

Daniel Caissie *

Fisheries and Oceans Canada, Gulf Fisheries Centre
P.O. 5030, Moncton, New Brunswick E1C 9B6

* Correspondence: Daniel.Caissie@dfo-mpo.gc.ca

Suggested Citation:
Caissie, D. 2013. Impact of climate change on water temperatures for selected rivers in New Brunswick and potential implications on Atlantic salmon. Ch. 13 (p.183-190) *In:* Aspects of climate change in the Northwest Atlantic off Canada [Loder, J.W., G. Han, P.S. Galbraith, J. Chassé and A. van der Baaren (Eds.)]. Can. Tech. Rep. Fish. Aquat. Sci. 3045: x + 190 p.

Abstract

Water temperature is a key component of river ecosystems as it influences many physical, chemical and biological processes. River water temperature follows both annual and diel cycles which influence the growth rate as well as the distribution of fishes within rivers. High water temperature events have been shown to impact fishes, and in particular, salmonids. The present study deals with the potential impact of climate change on river water temperatures and salmon habitat for selected rivers in New Brunswick. Water temperature and air temperature are highly correlated, and as air temperature is projected to increase in eastern Canada by 2-6°C over the next 100 years, water temperature is also expected to increase as well. Increases in water temperature will very likely have an impact on river habitat, as some river temperatures are already reaching their upper lethal limit for some fish species (*e.g.*, Atlantic salmon - Miramichi River). Results showed that the duration and occurrence of high temperature events (daily water temperature exceeding 23°C) could increase significantly under climate change. An increase in water temperature would likely impact the frequency of salmon fishing closures as well as the socioeconomic well-being of the region.

13.1 Introduction

Water temperature influences many physical, chemical and biological processes in river systems, including the growth rate of many fish species and their distribution, habitat selection, behaviour, and survival at various life stages. Most aquatic species have a specific range of water temperatures that they can tolerate and high water temperatures can adversely affect fisheries resources by limiting their habitat or can even result in fish mortality (Huntsman, 1942). For instance, Lund *et al.* (2002) showed that high summer water temperatures exceeding 23°C can cause significant protein damage and induce a heat-shock response in juvenile salmonids.

Water temperature fluctuations can occur naturally or as a result of anthropogenic perturbations (*e.g.*, construction of reservoirs, deforestation, climate change, etc.). Among these, climate

change is of particular interest due to a high association between air and water temperatures (*e.g.*, Caissie *et al.*, 1998; Caissie *et al.* 2004; Caissie, 2006). As such, climate change will very likely have a significant impact on water temperature and aquatic resources in most rivers (Mohseni and Stefan, 2001; Schindler, 2001; Stefan *et al.*, 2001). The increase in river temperatures under climate change could potentially extirpate specific species of aquatic biota or dramatically modify their distribution and survival within river systems (Minns *et al.*, 1995). Studies have already pointed out that, in many parts of North America, fish are already experiencing their upper lethal limit in water temperatures (Sinokrot *et al.*, 1995; Eaton *et al.*, 1995). Some studies have suggested that a warmer climate will reduce the abundance of cold water fish species by as much as 50% in the United States (Eaton and Sheller, 1996). Other studies have shown that projected increases in water temperatures due to climate change could significantly affect the growth rate of juvenile Atlantic salmon (Swansburg *et al.*, 2004b).

Climate change studies related to river water temperature require long-term data which are seldom available, although a few studies have been found in the literature. For example, Langan *et al.* (2001) studied 30 years of water temperature data in the Girnock catchment (Scotland) and found no increases in mean annual water temperatures; however, winter and spring maximum temperatures increased by approximately 2°C. Webb and Nobilis (1997) analysed over 90 years of water temperature data from north-central Austria and showed no specific trends in water temperatures. Foreman *et al.* (2001) studied long-term trends in water temperatures from simulated historical temperatures and they noted an increase of 0.12°C per decade in British Columbia (1941-98). Another related study in British Columbia (Fraser River) showed that climate change could potentially alter the timing of peak flows as well as increase summer water temperatures by 2099 (Morrison *et al.*, 2002). According to that study, summer water temperatures are projected to increase by 1.9°C by the end of the century (compared to the baseline period 1961-1990).

In New Brunswick, studies have indicated that the air temperature is expected to increase between 2-6°C in the next 100 years (Swansburg *et al.*, 2004a; Turkkan *et al.*, 2011). Reports prepared for DFO's Aquatic Climate Change Adaptation Services Program (ACCASP) indicate that model projections of the summer increase in the Maritimes over the next 50-70 years are in the 2-4°C range (Loder and van der Baaren, 2013; Loder *et al.*, 2013). Such an increase in air temperature will likely translate into similar increases in river water temperature (see Galbraith and Larouche, 2013, for similar coupling of air and oceanic water temperatures). This brief report will outline important river water temperature characteristics as well as potential impacts of climate change on salmon angling closures due to increase in river temperatures.

13.2 River water temperature characteristics and modeling

To understand the thermal regime of rivers and its impact on aquatic biota, it is very important to describe the water temperature characteristics and corresponding cycles. These attributes are also important for modeling purposes. For instance, river water temperatures follow both annual and diel cycles. The diel cycle (variability over a 24 hour period) is generally described by a minimum water temperature early in the morning and a maximum temperature reached in late afternoon or early evening. The range of the diel variability can be significant depending on the size and location of the river; however, it typically varies between 1.5-6°C (Caissie *et al.*, 2013).

Smaller groundwater fed rivers and very large rivers experience less diel variability whereas wide and shallow rivers experience the largest diel variability. Rivers with large diel variability are those that generally reach the highest summer maximum water temperatures (Caissie *et al.*, 2013). The annual cycle determines the timing of high temperature events during the summer. This cycle follows a truncated sinusoidal function in mid-latitude rivers (*e.g.* rivers of eastern Canada; Caissie *et al.*, 1998; Caissie, 2006). Results for the Little Southwest Miramichi River, a site with over 20 years of data, are presented in Figure 13-1 as an example. The water temperature is generally close to 0°C throughout the winter followed by a departure from 0°C early April. The river water temperature increases until it reaches its climatology maximum on July 29. Thereafter, the river experiences a cooling period and typically reaches 0°C again in early December.

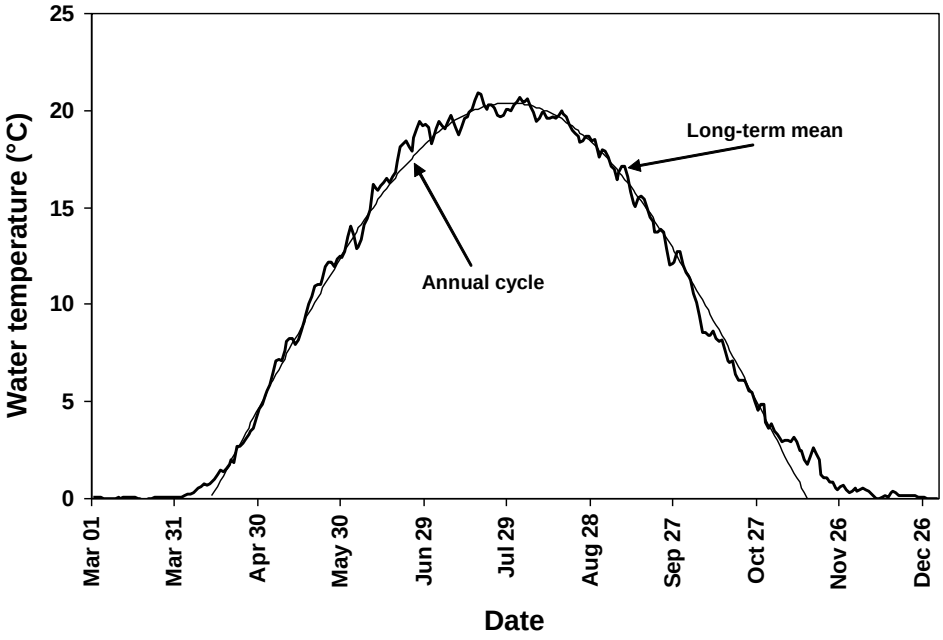

Figure 13-1 Long-term mean water temperatures for the Little Southwest Miramichi River (1992-2011, missing 1994) and annual cycle (truncated sinusoidal function).

The months of July and August are those with the highest monthly water temperatures and have similar air and water temperatures (Caissie *et al.*, 2013). From an aquatic habitat perspective, these two months are often used to represent summer water temperatures. For instance, water temperatures were analysed for 42 sites on the Miramichi and Restigouche rivers, and mean summer water temperatures were between 14°C and 22°C (Caissie *et al.*, 2013). The colder sites were mainly observed in headwater tributaries, whereas warmer temperature sites were generally observed in lower sections of the main-stem of rivers. This study also showed that the Miramichi River consisted mainly of warm temperature sites (mean = 19.4°C) compared to the Restigouche River which was generally colder (mean = 16.5°C). The two rivers also exhibited different maximum temperatures with the Miramichi maximum water temperature found between 27°C and 30°C and the Restigouche River between 24°C and 27°C. These results showed that under climate change, the Miramichi River can be expected to be more severely impacted, as water temperatures are already at the upper lethal limit for salmonids.

For many rivers there is a good linear relation between monthly (and summer) air temperature and water temperature (Caissie *et al.*, 2004). An example of such a relationship is presented for the Little Southwest Miramichi River (Fig. 13-2).

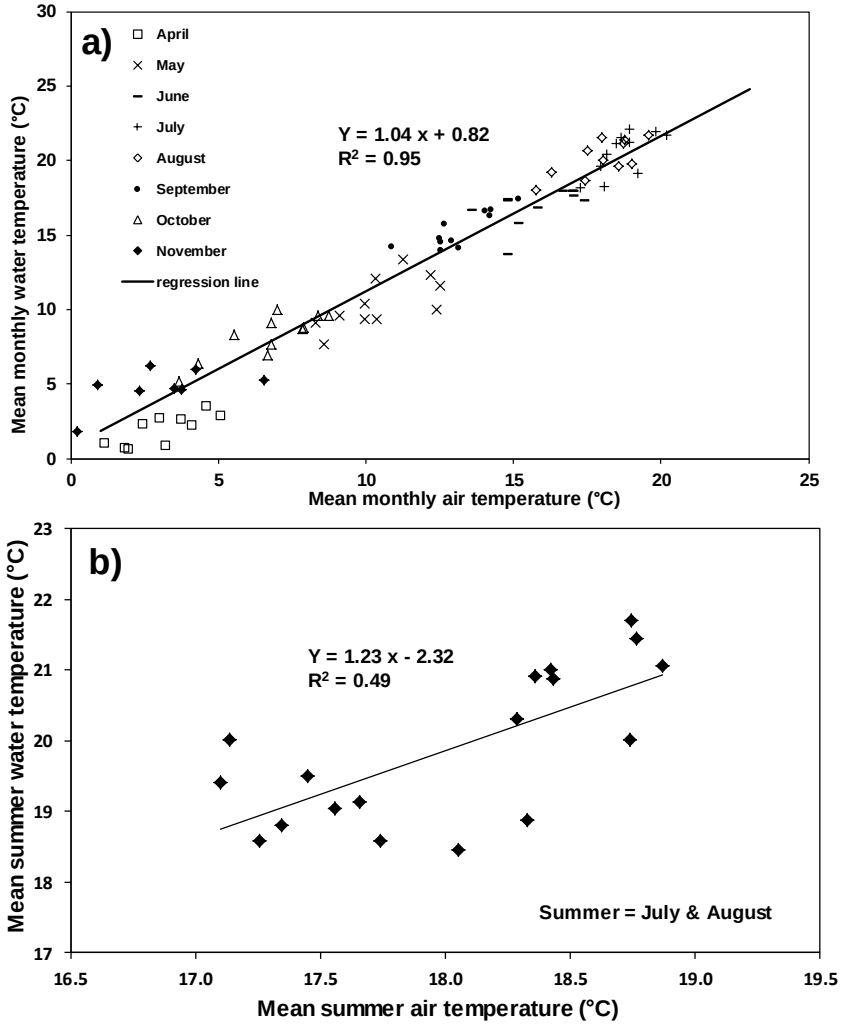

Figure 13-2 Relationship between the a) monthly and b) summer (July & August) air and water temperatures for the Little Southwest Miramichi River (1992-2011, missing 1994).

These results indicate that future increases in air temperature will likely result in increases in monthly river water temperatures. While the annual cycle is a large contributor to the specific regression relationship in Figure 13-2a, it can be seen from detailed examination of the observations for summer (July and August; Fig. 13-2b) that a similar relationship holds for interannual variations during the summer period.

13.3 Example of aquatic habitat implications

A study by Breau (2013) showed that both maximum and minimum water temperatures are important for Atlantic salmon during high temperature events. Water temperature must fall to

less than 20°C in order for the stressed salmon to recover, and these minimum temperatures generally occur at night. Accordingly, when studying management options for closing angling fisheries due to high temperature stress, these two thresholds (T_{max} of 23°C and T_{min} of 20°C) were used in the characterisation of both Miramichi and Restigouche rivers. As an example, the number of days in which T_{max} exceeded 23°C in the Little Southwest Miramichi River between 1992 and 2011 (missing data in 1994) ranged between 0 and 62 days (Fig. 13-3).

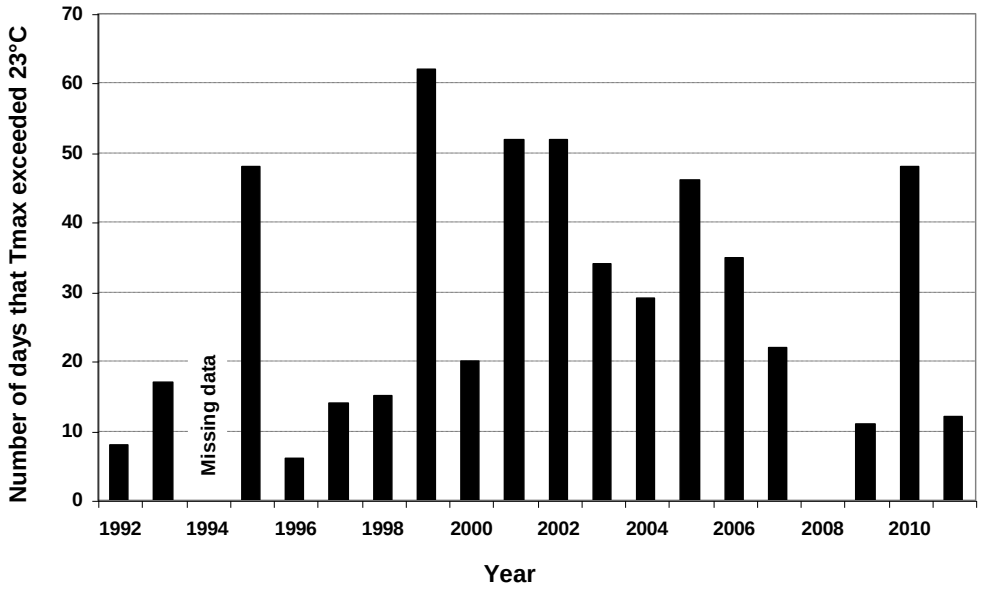

Figure 13-3 The number of days where T_{max} exceeded 23°C by year for the Little Southwest Miramichi River (1992-2011, missing 1994).

The year with the highest value was 1999; however, 1995, 2001, 2002, 2005 and 2010 all showed more than 45 days. The year 1998 had a relatively cold summer, as the summer water temperature did not exceed 23°C. During some high water temperature years (*e.g.* 1995, 1999 and 2010), salmon angling fisheries were actually closed due to high temperature stress. These closures have potentially important socioeconomic impacts within the Miramichi River region, as salmon fisheries are an important source of food (First Nation) and revenue (recreational fisheries).

A good relationship was also observed between the mean summer (July and August) water temperature and the number of days that T_{max} exceeded 23°C in the Little Southwest Miramichi River ($R^2 = 0.77$; Fig. 13-4). Results suggest that, under a future warmer climate, the number of stressful days would very likely increase as well. Under these conditions, high temperature events ($T_{max} > 23$°C) would likely be experienced sooner as well as later within the year (*e.g.* June and September). These results demonstrate the importance of protecting cold water streams and tributaries, as they contribute to the overall protection of the thermal regime. Moreover, cold water habitats may play an even greater role, as thermal refugia, under a future warmer climate.

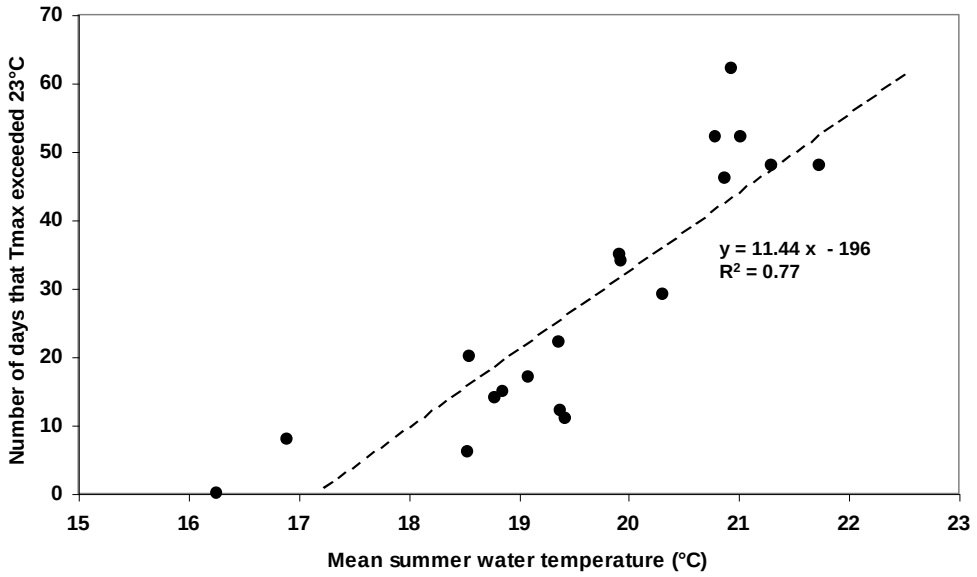

Figure 13-4 The number of days that T_{max} exceeded 23°C as a function of the mean summer water temperature for the Little Southwest Miramichi River (1992-2011, missing 1994).

13.4 Conclusions

Information presented in this study as well as data from the literature suggest that climate change will have a significant impact on the quality of river water, particularly on river water temperature. It is highly likely that the expected increase in air temperature in eastern Canada and the high level of association between air and river water temperatures will have an impact on some aquatic resources (*e.g.*, salmon). Both annual and diel cycles need to be considered when analysing river water temperature under climate change, as they are both important in determining maximum summer water temperatures. Some rivers are more impacted by high water temperature events (*e.g.*, Miramichi River) than others (*e.g.*, Restigouche River). From an aquatic habitat perspective and for fish, such as salmon, the maximum river water temperature is important; however, the duration and occurrence of high temperature events, particularly those exceeding 23°C (T_{max}), are equally important. Salmonids also need colder water temperature at night (water temperatures generally less than 20°C) to recover from high temperature stress. An increase in high temperature events would likely impact the frequency of salmon fishing closures as well as the socioeconomic welfare of the Miramichi River region.

13.5 Acknowledgements

Internal review comments were provided by Peter Galbraith, Jamie Gibson and John Loder.

13.6 References

Breau, C. 2013. Knowledge of fish physiology used to set water temperature thresholds for inseason closures of Atlantic salmon (Salmo salar) recreational fisheries. DFO Can. Sci. Advis. Sec. Res. Doc. 2012/163. iii + 24 p. http://www.dfo-mpo.gc.ca/Csas-sccs/publications/resdocs-docrech/2012/2012_163-eng.pdf

Caissie, D. 2006. The thermal regime of rivers: A review. *Freshwater Biol.* 51, 1389-1406.

Caissie, D., C. Breau, J. Hayward, and P. Cameron. 2013. Water temperature characteristics within the Miramichi and Restigouche rivers. DFO Can. Sci. Advis. Sec. Res. Doc. 2012/165. vi + 31 p. http://www.dfo-mpo.gc.ca/Csas-sccs/publications/resdocs-docrech/2012/2012_165-eng.pdf

Caissie, D., N. El-Jabi and A. St-Hilaire. 1998. Stochastic modelling of water temperature in a small stream using air to water relations. *Can. J. Civil Engineer.* 25, 250-260.

Caissie, D., A. St-Hilaire and N. El-Jabi. 2004. Prediction of water temperatures using regression and stochastic models. 57th Canadian Water Resources Association Annual Congress, June 16-18, 2004, Montreal, QC, 6 p.

Eaton, J.G., J.H. McCormick, H.G. Stefan and M. Hondzo. 1995. Extreme value analysis of a fish/temperature field database. *Ecological Engineering*, 4 (4), 289-305.

Eaton, J.G., and R.M. Scheller. 1996. Effects of climate warming on fish thermal habitat in streams of the United States. *Limnol. Oceanogr.* 41(5), 1109-1115.

Foreman, M.G.G., D.K. Lee, J. Morrison, S. MacDonald, D. Barnes and I.V. Williams. 2001. Simulation and retrospective analyses of Fraser watershed flows and temperatures. *Atmos.-Ocean* 39 (2), 89-105.

Galbraith, P.S. and P. Larouche. 2013. Trends and variability in air and sea surface temperatures in eastern Canada. Ch. 1 (p. 1-18) *In:* This report.

Huntsman, A.G., 1942. Death of salmon and trout with high temperature. *J. Fish. Res. Bd. Can.* 5 (5), 485–501.

Langan, S.J., L. Johnston, M.J. Donaghy, A.F. Youngson, D.W. Hay and C. Soulsby. 2001. Variation in river water temperatures in an upland stream over a 30-year period. *The Science of the Total Environment*, 265, 195-207.

Loder, J.W. and A. van der Baaren. 2013. Climate change projections for the Northwest Atlantic from six CMIP5 Earth System Models. Can. Tech. Rep. Hydrogr. Ocean Sci. 286: xiv + 112 p. http://www.dfo-mpo.gc.ca/library/349550.pdf

Loder, J.W., Z. Wang and J. Morrison. 2013. Projected air temperature changes for Canada from eight NARCCAP model combinations. Ch. 11 (p. 151-176) *In:* This report.

Lund, S.G., D. Caissie, R.A. Cunjak, M.M. Vijayan and B.L. Tufts. 2002. The effects of environmental heat stress on heat-shock mRNA and protein expression in Miramichi Atlantic salmon (Salmo salar) parr. *Can. J. Fish. Aquat. Sci.*, 59, 1553-1562.

Minns, C.K., R.G. Randall, E.M.P. Chadwick, J.E. Moore and R. Green. 1995. Potential impact of climate change on the habitat and production dynamics of juvenile Atlantic salmon (Salmo salar) in eastern Canada. *In:* R.J. Beamish [ed.], Climate change and northern fish population, Can. Spec. Publ. Fish. Aquat. Sci., 121, 699-708.

Mohseni, O., and H.G. Stefan. 2001. Water budgets of two watersheds in different climatic zones under projected climate warming. *Climate Change,* 49 (1-2), 77-104.

Morrison, J., M.C. Quick and M.G.G. Foreman. 2002. Climate change in the Fraser River watershed: flow and temperature projections. *J. Hydrol.,* 263, 230-244.

Schindler D.W. 2001. The cumulative effects of climate warming and other human stresses on Canadian freshwaters in the new millennium. *Can. J. Fish. Aquat. Sci.,* 58: 18-29.

Sinokrot, B.A., H.G. Stefan, J.H. McCormick and J.G. Eaton. 1995. Modeling of climate change effects on stream temperatures and fish habitats below dams and near groundwater inputs. *Climatic Change,* 30 (2), 181-200.

Stefan, H.G., X. Fang and J.G. Eaton. 2001. Simulated fish habitat changes in North American lakes in response to projected climate warming. *Trans. Amer. Fish. Soc.,* 130 (3), 459-477.

Swansburg, E., N. El-Jabi and D. Caissie. 2004a. Climate change in New Brunswick (Canada): statistical downscaling of local temperature, precipitation, and river discharge. Can. Tech. Rep. Fish. Aquat. Sci. 2544: 42p. http://www.dfo-mpo.gc.ca/Library/283189.pdf

Swansburg, E., N. El-Jabi, D. Caissie and G. Chaput. 2004b. Hydrometeorological trends in the Miramichi River, Canada: Implications for Atlantic salmon growth. *North American J. Fish. Management,* 24, 561–576.

Turkkan, N., N. El-Jabi and D. Caissie. 2011. Floods and droughts under different climate change scenarios in New Brunswick. Can. Tech. Rep. Fish. Aquat. Sci. 2928: xii + 55p. http://www.dfo-mpo.gc.ca/Library/343700.pdf

Webb, B.W., and F. Nobilis. 1997. A long-term perspective on the nature of the air-water temperature relationship: a case study. *Hydrological Processes,* 11 (2), 137-147.